2 TELIDON SYSTEM STUDY

FINAL REPORT

Indu
L
JU
JL
BIF

QUEEN
P
91
.C655
M668
1984
v.6

MCS MILLER COMMUNICATIONS SYSTEMS LTD.

COMMUNICATIONS CANADA
DEC 4 1986
LIBRARY - BIBLIOTHÈQUE

P91
.C655
M668
1984
V.6
[illegible]

TELIDON SYSTEM STUDY

FINAL REPORT

Industry Canada
LIBRARY
JUIL 20 1998
JUL
BIBLIOTHEQUE
Industrie Canada

Contract No: 1ST82-00710
MCS File No: 8342
DSS File No: DSS21ST.36100-2-4380
Date: July 27, 1984

Prepared by: K W Moreland R M Armstrong
K. W. Moreland, R. M. Armstrong

Approved by: R A Tiedemann
R. K. Tiedemann

SUBMITTED BY:

MCS MILLER COMMUNICATIONS SYSTEMS LTD.
300 Legget Drive,
Kanata, Ontario,
Canada K2K 1Y5

SCIENTIFIC AUTHORITY: Dr. M. Sablatash,
Communications Research Centre

COMMUNICATIONS CANADA
DEC 4 1986
BIBLIOTHÈQUE - LIBRARY

P
91
C655
M668
1984
v.6

DJ 5276130
DL 6880835

TABLE OF CONTENTS

1.0 INTRODUCTION 1

2.0 SUMMARY OF THE PERFORMANCE OF THE EXISTING SYSTEM 15

2.1 Review of The Existing Telidon System 15

2.2 Broadcast Television Multipath Channels 29

2.3 Simulated Performance of the Existing Telidon System 41

2.3.1 Evaluating the Effectiveness of the Error Protection Coding Presently Employed in Telidon 48

3.0 COMPARISON OF PULSE SHAPES 57

3.1 Introduction 57

3.2 Recommended Pulse Shape for Teletext 61

3.3 Pulse Shape Simulation Results 71

4.0 TELIDON SYSTEM PERFORMANCE WITH QUASI-SYNCHRONOUS DETECTION 99

4.1 Quasi-Synchronous Design Considerations 103

4.2 Simulation Approach For Quasi-Synchronous Detection 114

4.2.1 Simulation Model 118

4.2.2 Carrier Recovery Phase Error at Various Points in the Phase Extraction Process 122

4.3	Telidon System Performance With Quasi-Synchronous Carrier Recovery	127
5.0	EQUALIZATION FOR TELETEXT SYSTEMS	139
5.1	Overview	139
5.2	Implementation of a Linear Equalizer for the Simulation Program	155
5.3	Evaluating the Improvement Provided by Linear Equalization	160
6.0	ERROR PROTECTION CODING EVALUATION	171
6.1	The Codes	174
6.2	General Performance Characteristics	180
6.2.1	Performance of the Codes	180
6.2.2	Rejection/Corruption Tradeoff	188
6.2.3	Proposed Modification	192
6.2.4	Performance With Modification	193
6.3	Coding vs Equalization	197
6.4	Coding Conclusions	201
7.0	CONCLUSIONS	205
7.1	Improvements to Existing System	205
7.2	Areas For Further Work	209
7.3	Comments on Field Trial Measurements	211

REFERENCES		213
APPENDIX A	PERFORMANCE DEGRADATION ESTIMATES	219
APPENDIX B	CHANNEL CLASSIFICATION PROCEDURE	233
APPENDIX C	MODELLING THE QUASI-SYNCHRONOUS CARRIER RECOVERY ERROR	259
APPENDIX D	IMPLEMENTATION CONSIDERATIONS FOR TELETEXT EQUALIZATION	319
APPENDIX E	DETAILS OF THE SIMULATION PROGRAM EQUALIZER	335

1.0 INTRODUCTION

In the broadcast Telidon system, teletext data is inserted in the vertical blanking lines of commercial television broadcasts. While this makes use of previously unused television bandwidth and circumvents the need for developing an expensive distribution system, the television transmission system is not ideally suited for digital data transmission. This complicates the design of a reliable teletext receiver.

A simplified block diagram of the broadcast Telidon system is provided in Figure 1.1. Telidon data is transmitted during the vertical blanking interval of normal video programming. The Telidon data is stored in a computer database which is cyclically retransmitted. The data is encoding and subjected to baseband pulse shaping. The message signal to be transmitted , whether it be television video programming or teletext data, is then passed through a line inserter, which places a line sync pulse and colour burst in front of the message signal. The format of an inserted teletext line is shown in Figure 1.2. The signal is then passed to the broadcast equipment, which performs upconversion, IF filtering, zonal filtering, and power amplification. The amplitude response of an idealized transmitter IF filter is shown in Figure 1.1. The signal is then transmitted from a convenient transmitting antenna site over a VHF or UHF channel. The signal is then picked up by the television antenna of a customer, and processed by the television receiver. An idealized receiver IF characteristic is shown in Figure 1.1. The video output of the television receiver is processed by the teletext decoder, which converts picture description instructions into graphical images to be displayed on the customers television screen.

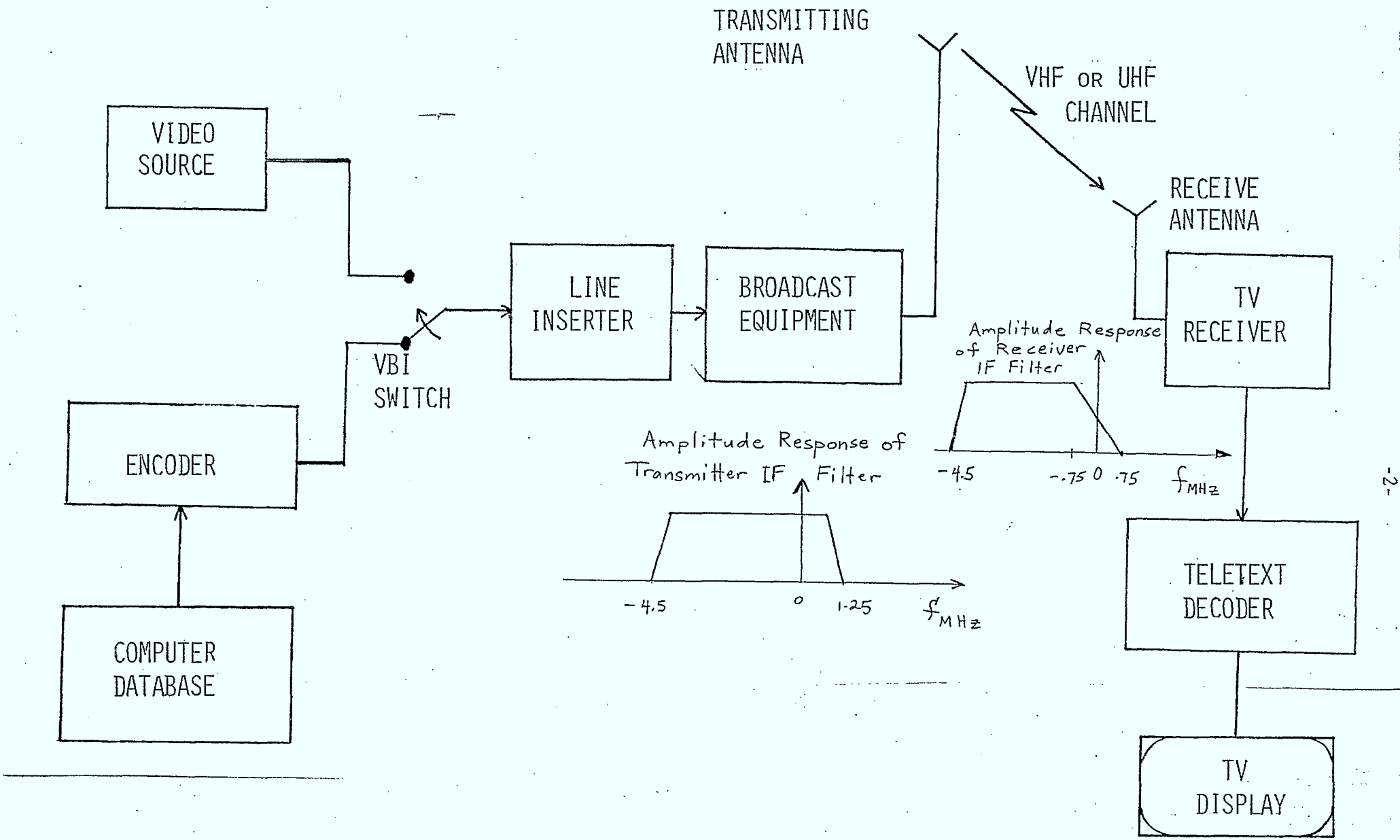

FIGURE 1.1: BROADCAST TELETEXT SYSTEM MODEL

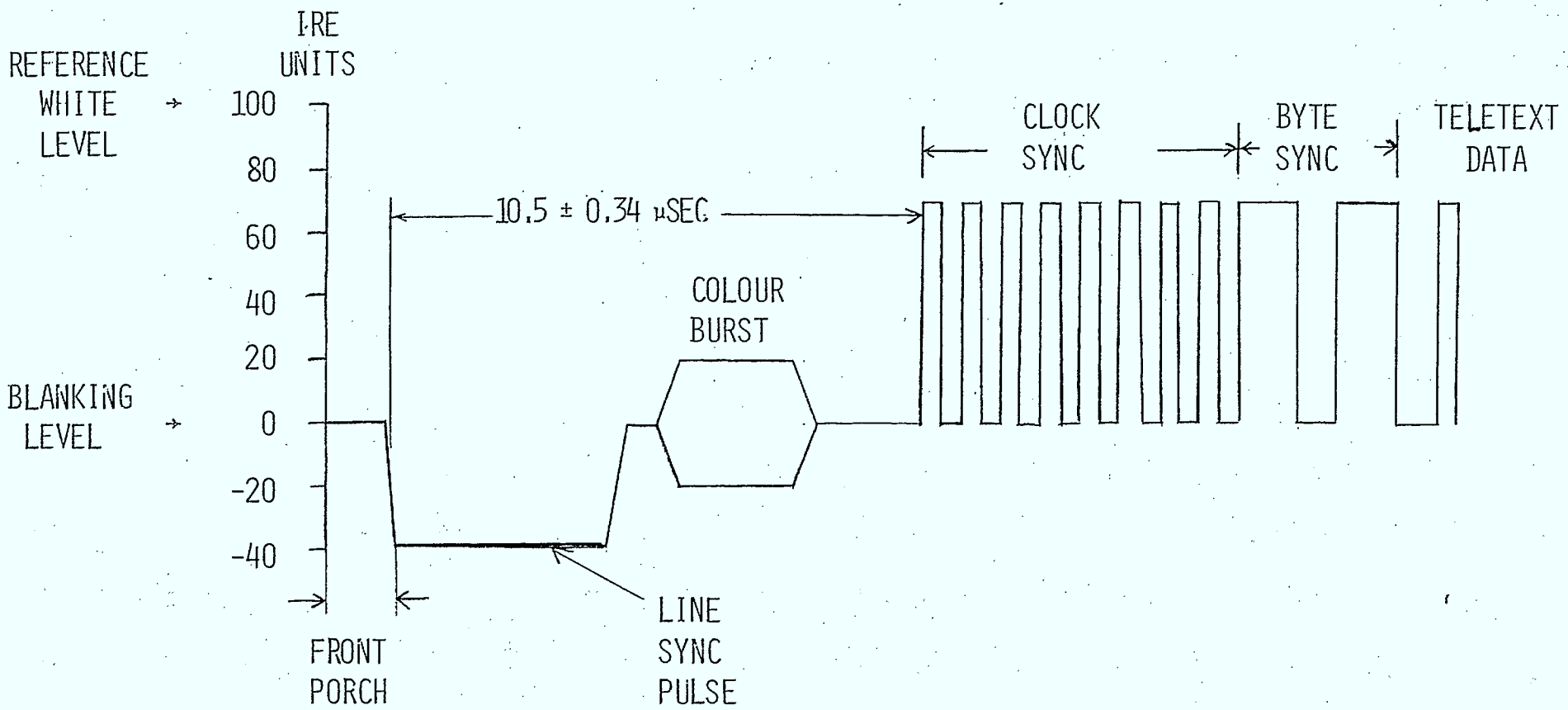

FIGURE 1.2: TELETEXT LINE FORMAT

At this point, it is worthwhile reviewing some of the aspects of the television transmission system which impact the performance of the broadcast Telidon system. The television transmission system is vestigial sideband in nature. Due to the asymmetrical nature of the transmitter and receiver filtering operations (see Figure 1.1), a quadrature component signal is generated. The quadrature component can often introduce unwanted distortion on the desired baseband video signal. This quadrature distortion can be generated in several ways including

- non-ideal receiver filter characteristics in the critical Nyquist slope region of the response,
- non-linear envelope or diode detectors,
- non-ideal carrier recovery in synchronous demodulators, and
- multipath propagation.

In older television sets, simple envelope or diode detectors are commonly used. These non-linear detectors introduce considerable quadrature distortion. Because of the opportunity to dramatically reduce the amount of quadrature distortion, the movement in recent years has been towards synchronous or coherent demodulation. Although it is possible, in theory, to completely eliminate quadrature distortion, to do so would require exact carrier regeneration and precise control on the amplitude and group delay responses of the receiver IF, especially in the critical Nyquist slope region of the response. In practice, most systems are non-ideal due to economic constraints which prohibit precise control of the receiver

response. Carrier regeneration at the receiver is made more difficult by the vestigial sideband nature of the receiver IF filter, which introduces incidental phase modulation on the transmitted carrier. Most current television receivers use what is referred to as "quasi-synchronous detection". That is, the carrier signal used for demodulation is derived from a relatively wideband carrier recovery loop. These detectors are susceptable to quadrature distortion, which is introduced by time varying carrier recovery phase errors. In theory, quasi-synchronous detectors can be improved by reducing the carrier recovery loop bandwidth, thereby approaching true synchronous demodulation. Unfortunately, non-ideal signal impairments such as transmitter and tuner generated incidental phase modulation place fundamental limits on economically achievable carrier recovery loop bandwidths.

For the broadcast Telidon system, the major consequence of the quadrature distortion introduced by carrier recovery phase offsets is increased intersymbol interference. A carrier recovery phase offset results in the superposition of the quadrature signal on the desired signal. The amplitude of the interfering quadrature component is proportional to $\sin \theta$, where θ is the phase offset. In practice, the pulse shape is chosen to ensure that, in the absence of phase distortion, the overall inphase transfer function satisfies, or nearly satisfies, Nyquist's criterion for no intersymbol interference. In general, the quadrature transfer function will not satisfy Nyquist's first criterion, because of the global asymmetry about f=0 [11]. As a result, the superposition of the quadrature component introduces intersymbol interference because it does not have the desired zero crossings.

When multipath propagation is present with vestigial sideband transmission, the inphase channel does not experience pure multipath channel but rather a superposition of the multipath channel operating on both the inphase and quadrature channels [25], [46]. Consequently, distortion due to multipath propagation can consist of two components; one from the "in phase" multipath channel and the other from the "quadrature" multipath channel.

For VHF and UHF channels in suburban and urban environments, multipath propagation is typically the limiting factor on the quality of an off-air video signal. When compared to the amplitude and group delay distortion caused by multipath, the amplitude and group delay distortion introduced by transmitter and receiver IF filters is relatively minor. In addition to introducing intersymbol interference, multipath severely degrades the synchronization of the teletext signal. It is these synchronization difficulties that have the most profound effect on performance of the Telidon system in multipath environments. This multipath sensitivity problem is briefly addressed below.

In the television transmission system, video signals are transmitted with a significant dc (carrier) component. This is evident in Figure 1.2, which shows the teletext signal format. This makes necessary the estimation of the teletext dc offset (commonly referred to as the slicing level), in addition to the extraction of a local sampling clock at the teletext receiver. However, the major problem with the television signal format is that it makes the system sensitive to multipath propagation. Most low cost

decoders estimate the slicing level during the two byte clock synchronization signal. It is apparent from Figure 1.2 that even relatively modest amounts of multipath can introduce significant offsets in the slicing level during the clock synchronization signal. This is because the signal level preceding the clock sync signal is appreciably different than the average level of the teletext data signal. The situation becomes even worse when the multipath channel spread is large enough that a delayed version of the line sync pulse or colour burst gets superimposed on the clock sync signal. Note that the sensitivity of the Telidon system to multipath is a direct consequence of the television transmission format. Sophisticated and complex measures are required to overcome these problems.

Another major restriction of the television transmission system for high speed data transmission is its limited bandwidth. The NTSC video bandwidth is 4.2 MHz. The Telidon transmission rate is 5.7272 Mbps, which happens to be 8/5 the colour burst frequency. Given the non-ideal nature of the channel and the bandwidth limitation, this is a relatively high data rate. The integrity of communications could be improved by lowering the data rate, which would result in reduced distortion and intersymbol interference. Since nine of the twenty-one vertical blanking interval lines are used for synchronization purposes, the maximum number of lines that can be used per field is twelve. This corresponds to a maximum throughput rate of 207.4 Kbps. It is apparent that one cannot achieve a very high throughput rate simply using previously unused television bandwidth (VBI transmission systems).

The above discussion has outlined some of the major weaknesses of the broadcast television channel as a data communications link. As we will see in this report, these factors have a significant impact on the form and complexity of the teletext receiver required for reliable operation in typical broadcast environments. The purpose of this report is to summarize the major achievements of the Telidon system study and to present performance simulation results of fundamental importance to future teletext decoder design.

One of the major objectives of the Telidon system study was to analyze and determine the performance of the existing Telidon system, making suggestions and recommendations for system improvements. To achieve this objective, a flexible software simulation program was developed to simulate the broadcast Telidon transmission system. A block diagram of the complex baseband simulation model is provided in Figure 1.3. No simulation details will be provided here. The interested reader is referred to the 'Software User's Guide' and references [11] and [36] for a detailed discussion. The operation principles of the peak detector slicing level decoder, presently used in the Telidon system, are discussed briefly in Section 2.1 and in detail in [11] and [36]. A separate and distinct error protection coding analysis program has been developed that can operate on error sequences generated by the Telidon performance simulation program and/or error sequences generated during field trial measurements.

Since error correction and detection coding is employed in the Telidon system, system performance depends on the output error statistics, not those at the input to the decoder. In certain circumstances, the output error

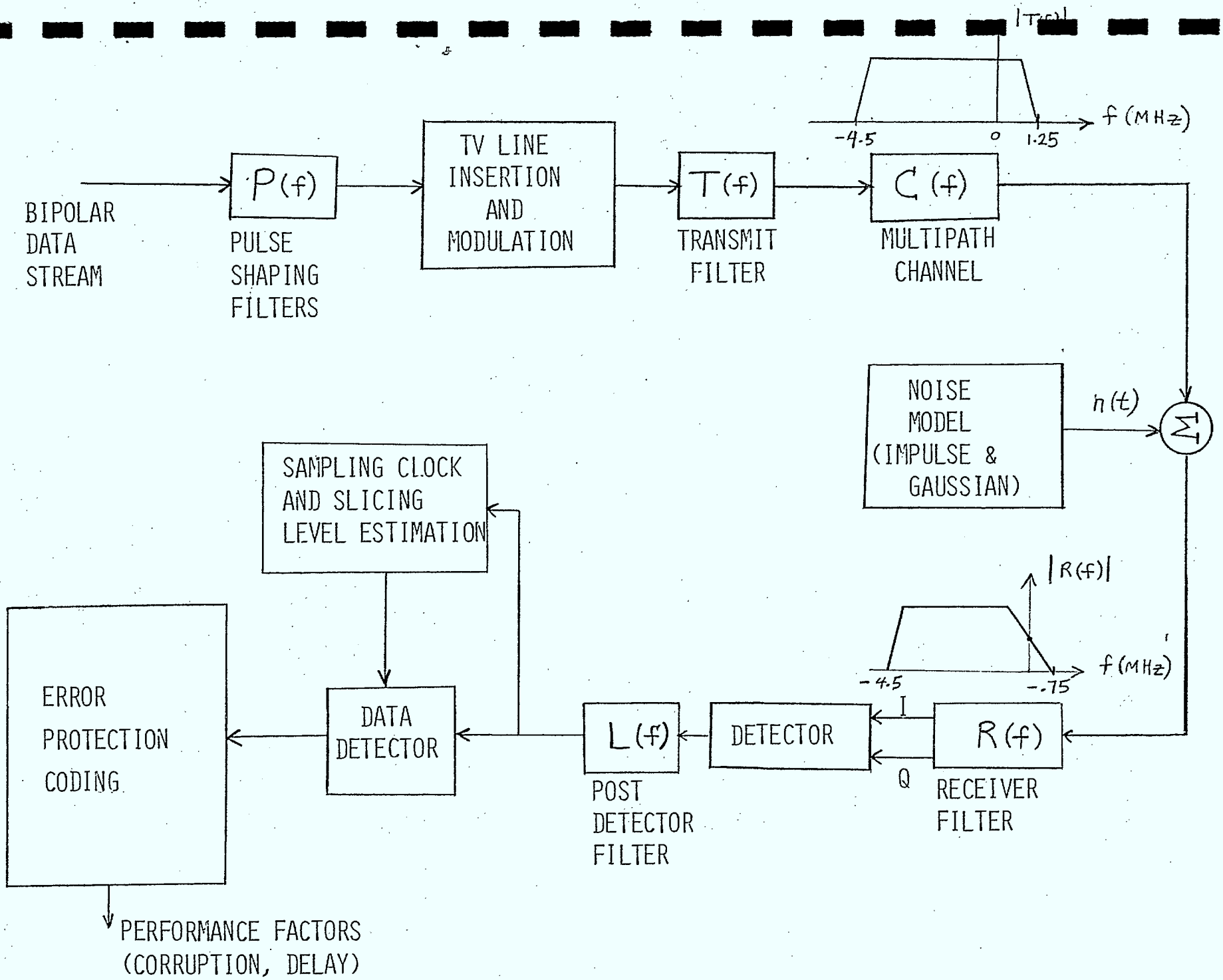

FIGURE 1.3: DATA TRANSMISSION MODEL

statistics can be adequately characterized by the average input bit error rate. Unfortunately, this is not the case for the Telidon system. This is because the error rate can vary considerably from burst to burst because of the sensitivity to slicing level errors. Furthermore, in impulse noise dominated urban environments, errors are likely to occur in bursts. Determining the grade of service of the Telidon system is complicated by the compact picture descriptor instructions (PDI's) used to describe graphical images, which make the severity of an error strongly dependent on its location. Ideally, system performance should be assessed with subjective testing. This would require implementing an entire decoder and transmitting actual Telidon pages, which would be a formidable task. Such a software simulation would be extremely computationally demanding and slow. To circumvent the need for a complete simulation, suitable performance indices such as the packet rejection rate (delay) and number of corrupting errors per standard image can be extracted from supplied error sequences. Subjective testing should be used to establish realistic thresholds for these quantities, and some feeling for the relative importance of delay and corruption.

One of the major accomplishments of the Telidon system study was the characterization of the broadcast television multipath environment. A theoretical multipath propagation model for suburban and urban environments was developed to gain insight into the nature of typical television multipath channels. The propagation model geometry is illustrated in Figure 1.4. An expression for the ratio of the scattered to direct field strength caused by a vertical dielectric slab (representative of the wall of a building) of thickness T, height H, and width W, forms the basis of the propagation model [46]. With the addition of a

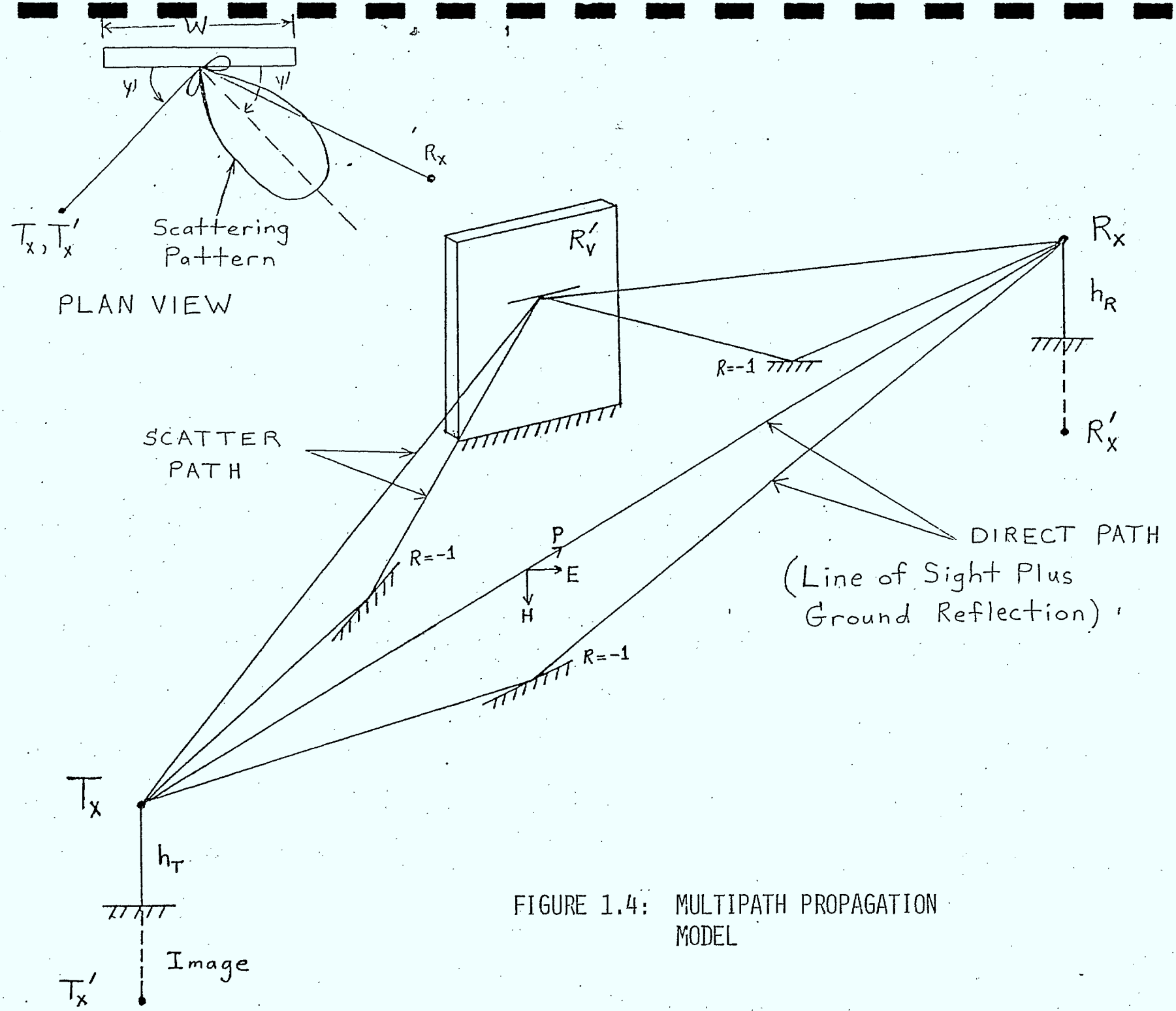

FIGURE 1.4: MULTIPATH PROPAGATION MODEL

prescreening algorithm responsible for eliminating channels not providing acceptable video quality, the propagation program is the most flexible and convenient generator of realistic multipath channels for system evaluation. This simulation model was successfully validated against channel measurements conducted by Communications Research Centre (CRC) personnel. The channel classification algorithm and simulation program results are discussed further in Section 2.2.

In addition to establishing Telidon system performance under typical multipath conditions, the study addressed the teletext pulse shaping issue. The pulse shaping issue has become embroiled in controversy in recent years. The major reason for this is that no one has been able to find the optimum pulse shape which satisfies all the teletext constraints and quantify the performance improvement relative to commonly used pulse shapes like the raised cosine family. This is not at all surprising in light of the extreme complexity of the teletext pulse shaping problem in its most general form. Surrogate performance criteria, which make the problem analytically tractable, have been used by several investigators [14], [18], [45]. These surrogate criteria typically involve properties of the eye diagram. Although these surrogate performance criteria are not equivalent the ideal teletext performance criteria, they have been successfully used to derive pulse shapes that are, in some sence, optimum [14], [15]. In this study, the results of [14] and [15] have been extended. An overall pulse shape, with reduced intersymbol interference and reduced peak overshoots relative to the existing truncated 100% raised cosine pulse shape [19], [45], has been derived. Controlling peak overshoots is

extremely important in teletext applications. The performance improvement obtained with this pulse shape was established with the Telidon channel and performance analysis simulation program.

The Telidon system study also reviewed competing adaptive equalization techniques for alleviating the serious problem of multipath propagation. The Telidon channel simulation program was used to assess the performance improvement which can be achieved by using linear equalization. The relative system performance of attractive error protection codes for Telidon is also compared.

The structure of this report is as follows. Section 2 summarizes the performance of the existing Telidon system in multipath environments. A television video quality classification procedure for multipath channels is presented. Simulation results from the theoretical multipath propagation program, which characterize the nature of the broadcast television channel, are presented and validated against measurement data. The reasons for the sensitivity of the Telidon system to multipath propagation are presented. The degradation that can be attributed to the weak slicing level and clock phase estimation procedures currently employed in Telidon is presented. Recommended improvements to these procedures are made.

Section 3 summarizes the teletext pulse shaping problem and presents an improved overall pulse shape that minimizes peak overshoots and intersymbol interference. The simulated performance with this improved pulse shape is compared with the performance achieved using the truncated 100% raised cosine pulse currently employed in the Telidon system.

Section 4 addresses quasi-synchronous detection. Several of the important design considerations which influence the choice of carrier recovery loop bandwidths in practical television receivers are presented. The simulation approach for investigating the performance with quasi-synchronous detection is described. The second order phase locked loop model, which closely matches loops currently used in television receivers [3], is presented. The simulated performance with quasi-synchronous detection is examined for both averaging and peak detector slicing level decoders with ideal and multipath channels contaminated by additive thermal and mixed impulse-gaussian noise. Performance is indexed according to carrier recovery loop bandwidth.

Section 5 deals with adaptive equalization techniques for broadcast teletext. The relative merits of linear and decision feedback equalization for the broadcast application are discussed. Briefly discussed is the simulation implementation of a practical linear equalizer. The performance improvement obtained by using linear equalization in typical broadcast television multipath conditions is assessed using the Telidon channel simulation program.

Section 6 examines the use of error detecting/correcting codes. A coding analysis program was written which uses the error files generated by the Telidon channel simulation. The analysis routine provides insite into the performance of the codes for real channel errors. The trade-off between coding and equalization is examined and modifications to the existing decoding algorithms are investigated.

2.0 SUMMARY OF THE PERFORMANCE OF THE EXISTING SYSTEM

In this section, the simulated performance of the existing Telidon system in typical multipath and noise environments is summarized. The interested reader is referred to Section 3 of [11] for a more detailed treatment. Performance is characterized in terms of bit error rate, and an example of the packet rejection rate and number of corrupted PDI bytes per record is also provided. A summary of the existing Telidon system and the multipath environment of concern for the broadcast teletext application are reviewed.

2.1 Review of The Existing Telidon System

Before presenting simulation results, it is informative to review some of the more important features of the Telidon system. A simplified system block diagram is provided in Figure 2.1. The data signal is a bipolar pulse amplitude modulated waveform. The baseband transmit pulse shape has a truncated 100% raised cosine specturm. The data signal is inserted into its appropriate place (i.e. timing and dc offset) in the television line (see Figure 2.2). Incorporating the synchronization components of the television line (i.e. the sync pulse and colour burst) is extremely important, especially when investigating performance in multipath environments. The appropriate signal orientation and carrier level are applied to simulate the modulation type and modulation index selected. Attention has been restricted to synchronous detection for the results discussed in this section.

The Telidon system simulation is performed at a complex baseband. That is, all bandpass filtering operations are replaced by equivalent baseband filtering operations. The

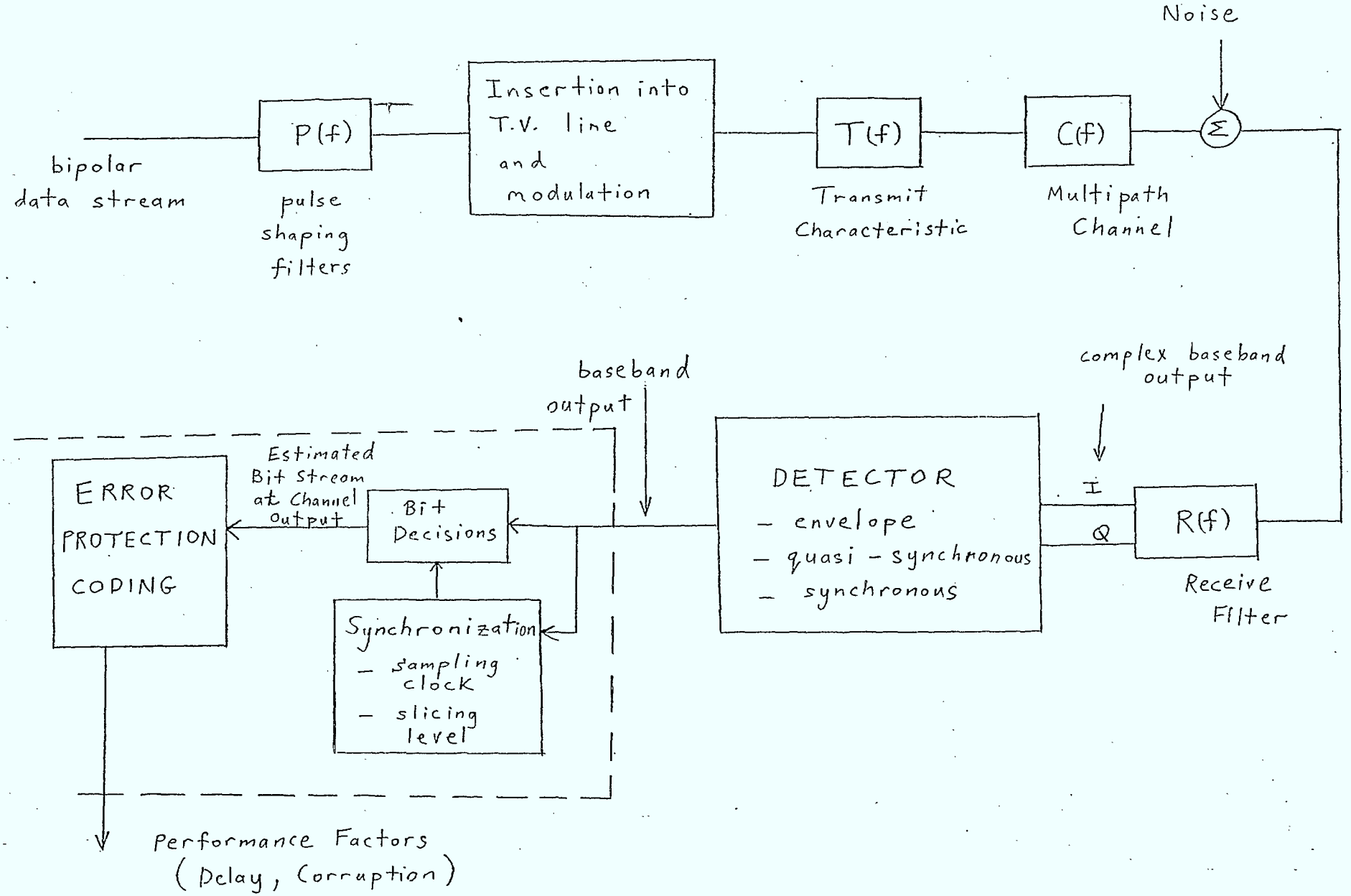

Figure 2.1 : Telidon system block diagram

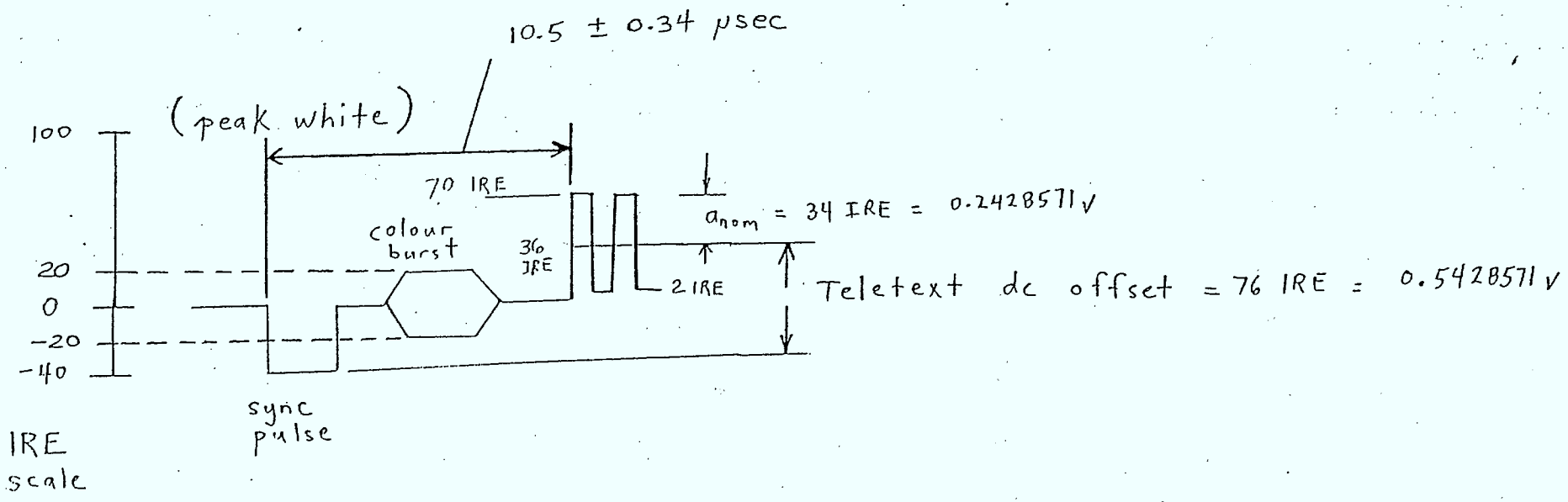

Figure 2.2: Teletext levels from BS-14 [19]

transmit and receive filters presently used in the simulation have ideal characteristics. The amplitude responses are shown in Figures 2.3 and 2.4, and the phase responses are assumed to be zero. The receiver filter response is characteristic of the responses of TV station demodulators. Typical home receivers have IF filters with responses that are down 6 dB at the colour subcarrier, as illustrated in Figure 2.5 [44]. The decreased bandwidth of the home receiver imposes a performance degradation for teletext, as intersymbol interference worsens (eye height is reduced) [15]. There is also the strong possibility that overshoots would increase with such a bandwidth reduction. Although there seems to be considerable data available on the amplitude responses of typical home receivers, there is not much available concerning the phase or group delay responses.

The simulated system presently employs synchronous detection, where carrier recovery is essentially perfect. Carrier recovery systems for synchronous detectors employ phase locked loop circuits with a relatively narrow bandwidth. However, most television receiver carrier recovery systems use phase locked loop circuits with a fairly wide loop bandwidth. This is made necessary by some television applications such as tracking phase variations produced by video game modulators or resulting from incidental phase modulation due to a poor television transmitter. The recovered carrier from the wideband loop is used to demodulate the receiver IF output to obtain a baseband video signal. This process is commonly referred to as "quasi synchronous" detection. It must be noted that phase offsets in the carrier recovery process result in quadrature distortion. This can introduce significant ISI, even though the overall ("inphase") pulse shape satisfies Nyquist's first criterion. Quasi synchronous system performance is discussed in detail in Section 4.

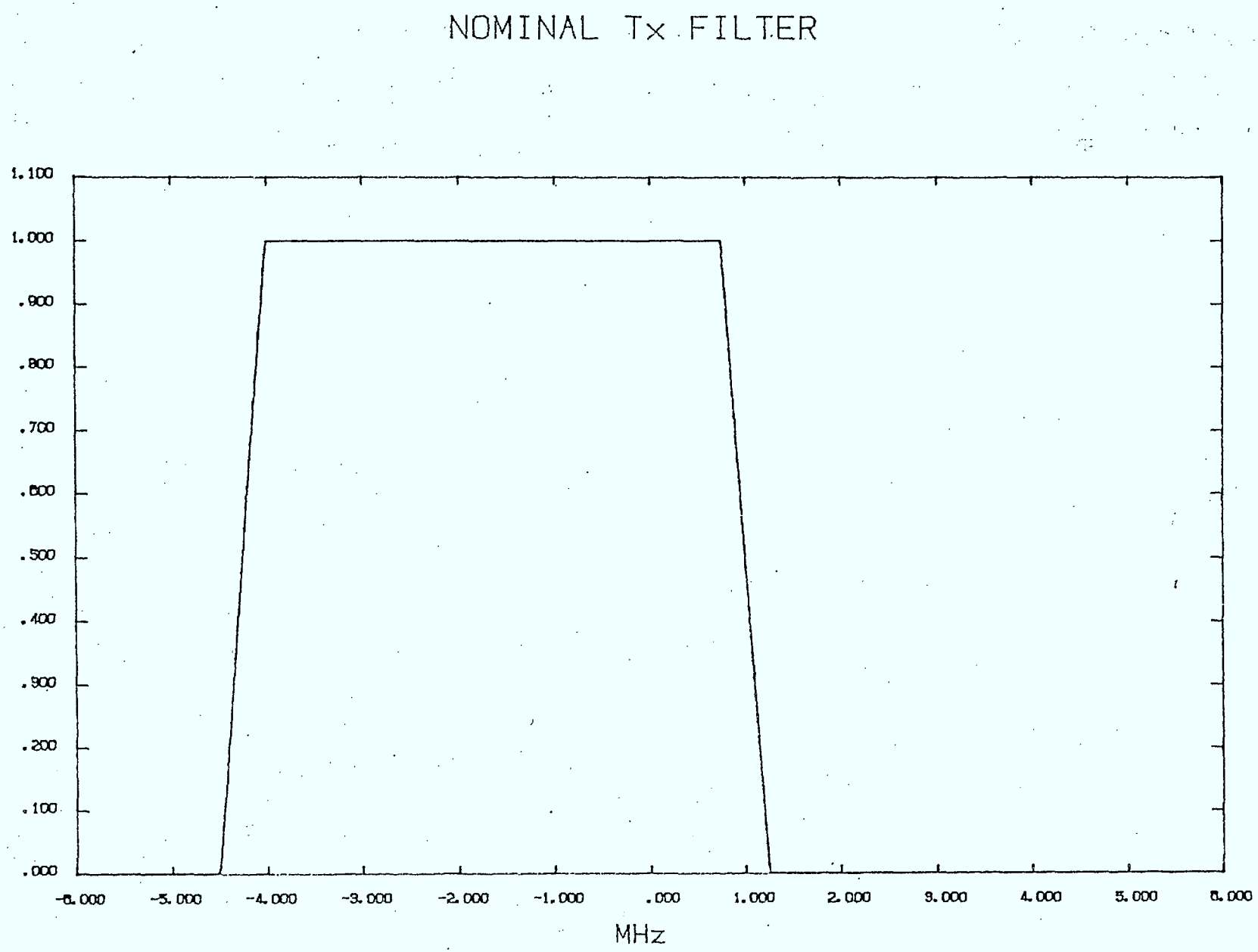

Figure 2.3: Amplitude response of nominal transmit filter

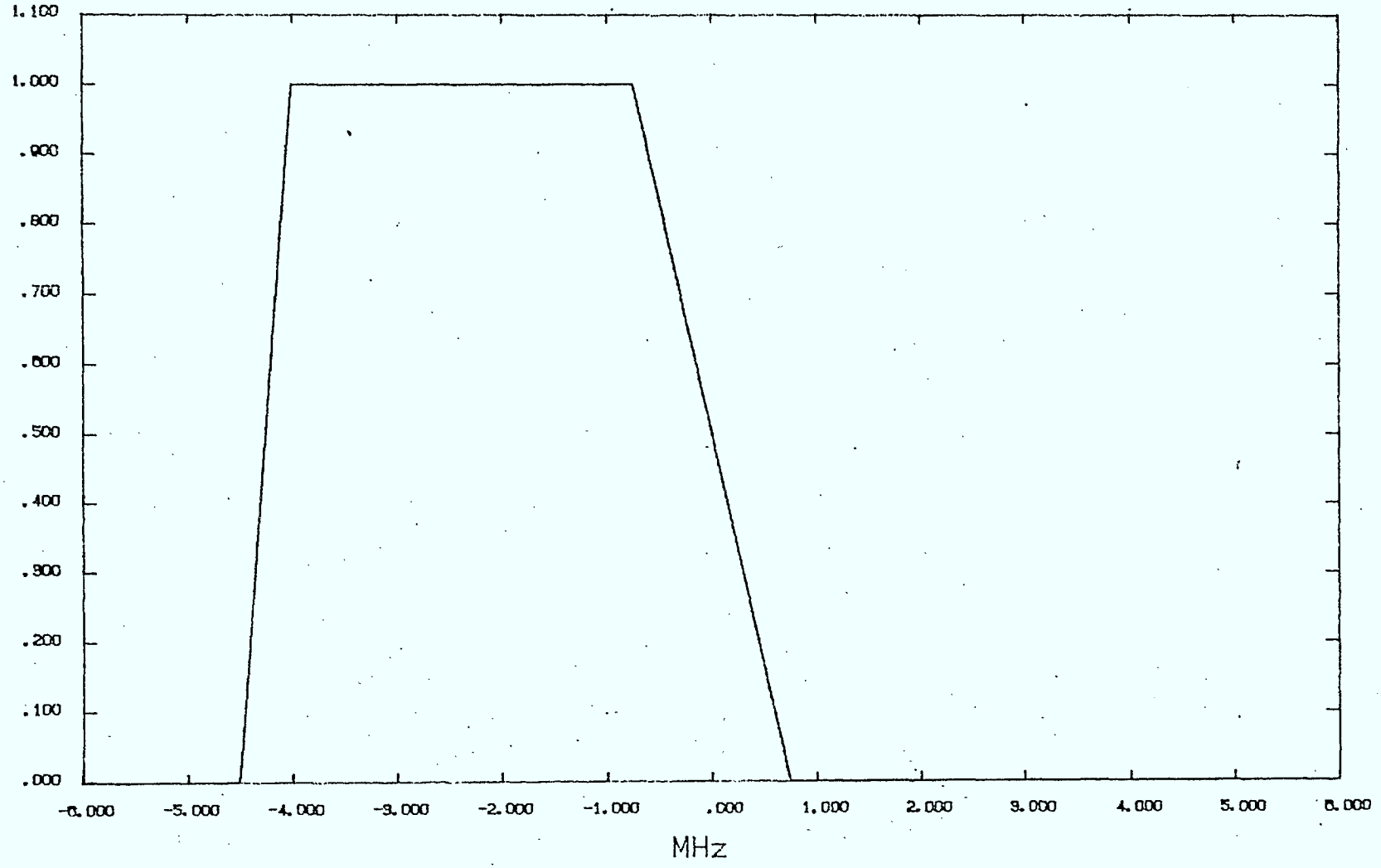

Figure 2.4: Amplitude response of nominal receiver filter

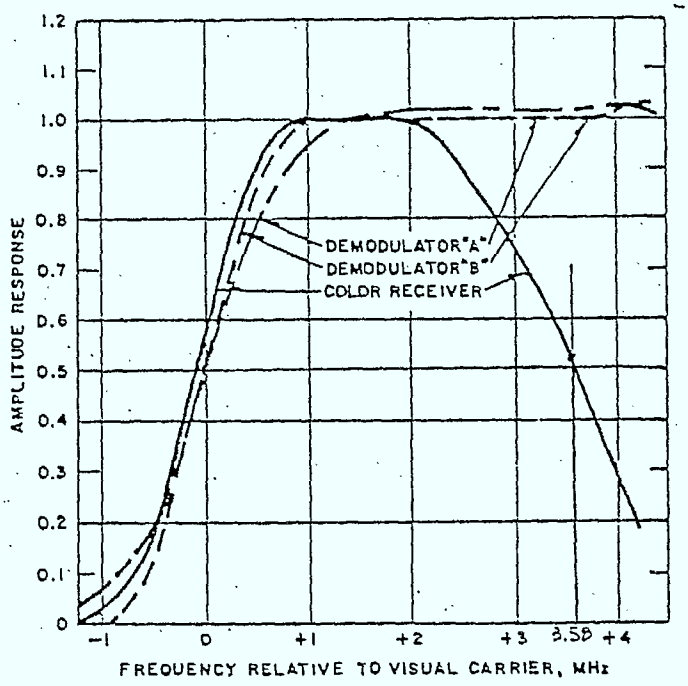

Figure 2.5: Amplitude response of station demodulators and a colour home receiver [44]

The transmit pulse shape specified in [19] is a truncated (low-pass filtered) 100% raised cosine pulse. One of the major deficiencies is that there is no specification given for the critically important low pass filter, which will have a major impact on the attainable overshoot level. It seems that this lowpass filter, responsible for reducing interference with the sound channel, has a nominal 4.0 MHz bandwidth [45]. The characteristics of a commercially available, phase equalized 4 MHz lowpass filter [45] are shown in Figure 2.6, and have been incorporated in the pulse shaping process in the simulation. This "truncated" 100% raised cosine pulse is presently used in the Telidon system.

As has been mentioned earlier [36], the synchronization techniques employed presently in the Telidon system have many deficiencies. It is believed that the performance degradations imposed by non-ideal filter characteristics and quasi-synchronous carrier recovery are small compared to those that can be attributed to these suboptimal synchronization techniques. Because such a significant performance degradation can be attributed to the weak slicing level and clock phase estimation techniques, it is appropriate at this point to discuss some of these deficiencies.

The approach presently employed in the Telidon system will be briefly described. The present system uses the two byte clock sync signal to serially estimate the slicing level and clock phase. It first estimates the slicing level, using two peak detection circuits, one following the most positive signal excursions and the other, the least positive signal excursions. These peak detection circuits have a short charging time and a long decay time. The peak detector outputs are smoothed, and the slicing level taken to be midway between the two peak values. Once the slicing

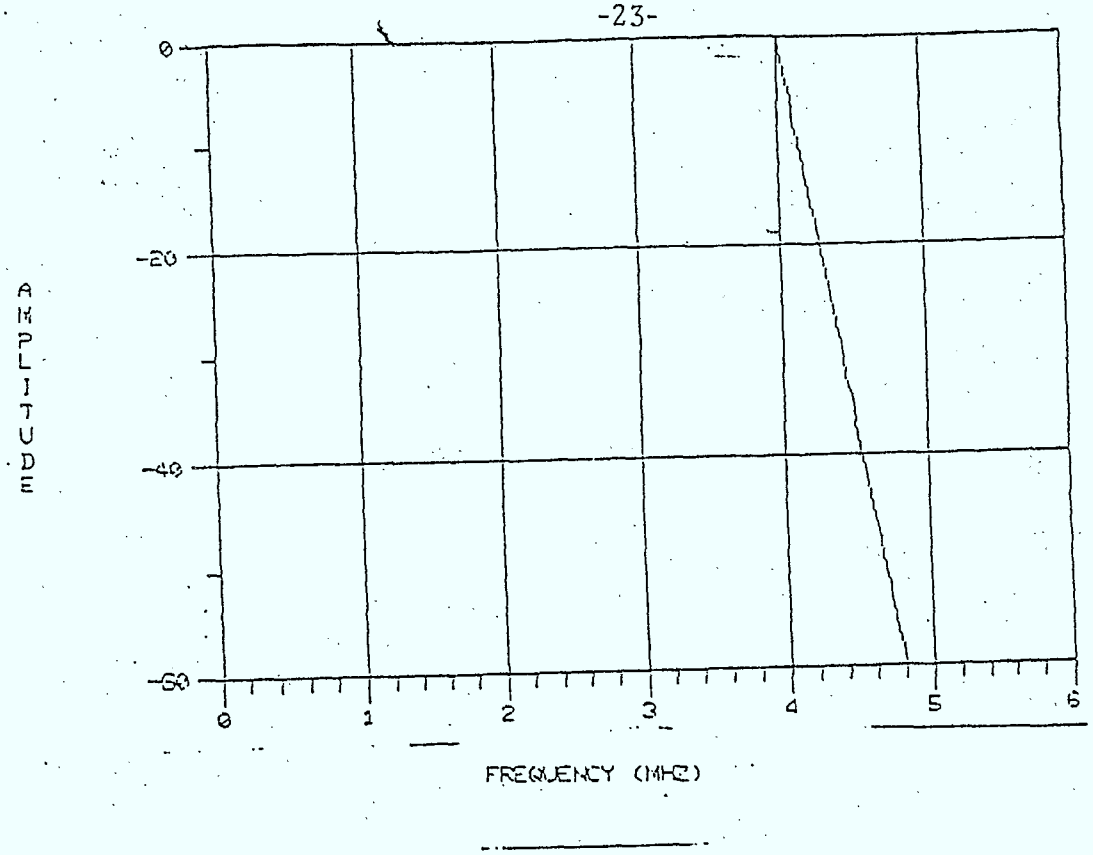

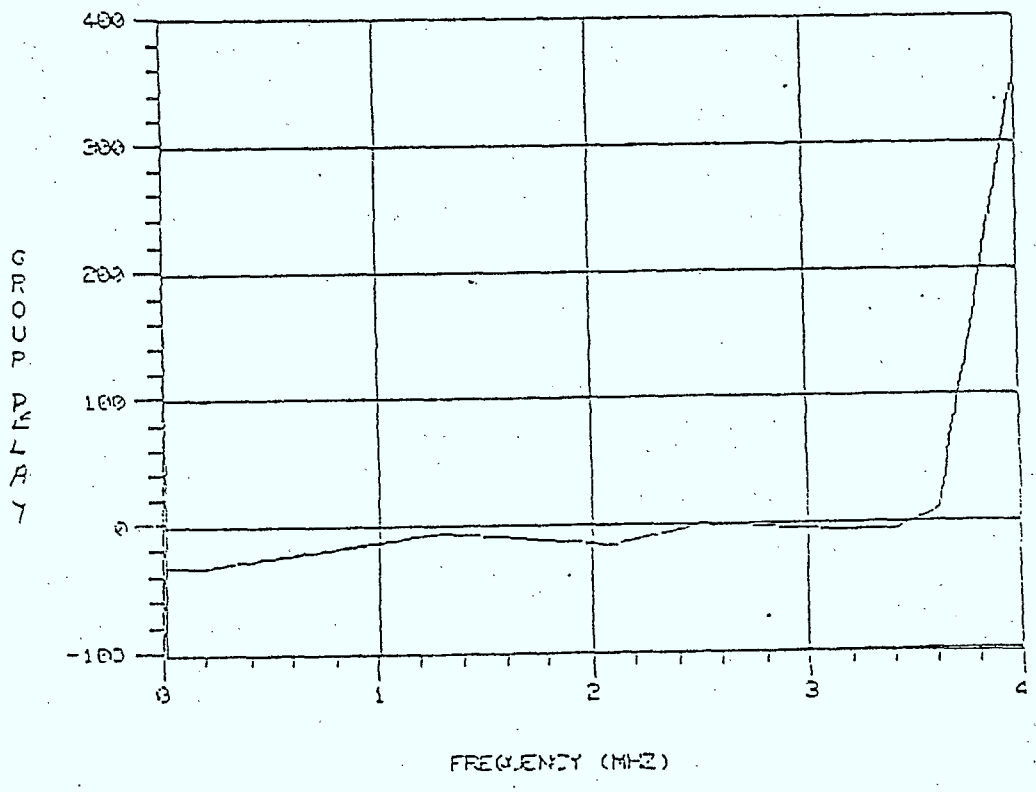

Figure 2.6 : Amplitude and Group Delay Responses of the 4 MHz Low pass Filter Used In The MCS simulation

level is established, the decoder uses a single zero crossing to choose one of five possible clock phases. There are several weaknesses in the procedure that can result in performance falling far short of optimum. Some of these problems are:

(1) The peak detector circuits are sensitive to noise peaks. Consequently, in impulse noise environments, loss of synchronization is likely when an impulse occurs during the portion of the clock sync signal preceding the freezing of the slicing level. An obvious improvement is to average or integrate (approximated by low pass filtering) the received signal to obtain an estimate of the slicing level. Averaging will clearly reduce the sensitivity to impulsive interference. Also, it is not difficult to show that for a data signal with equal numbers of ones and zeros, corrupted by white gaussian noise, that the maximum likelihood estimate of the dc level of the data signal is given by the average of the received signal over the observation period. This averaging principle should be used in future decoders.

(2) Even relatively modest multipath can introduce significant error in the slicing level. This is because the signal level immediately preceding the clock sync signal is at the blanking level (0 IRE) and the average level during the clock sync signal is significantly different (roughly 36 IRE) [19], (see Figure 2.7). Consequently any multipath propagation will result in an apparent shift in level for a duration corresponding to the multipath differential delay. The situation gets even worse when the delay spread is large enough that a delayed

version of the sync pulse or the colour burst gets superimposed on the clock sync signal. The effects are clearly demonstrated in Figures 2.8 and 2.9. In Figure 2.8, a filtered version of a portion of the teletext line received under ideal conditions is presented. In Figure 2.9, the clock sync signal illustrated was received over a multipath channel with a single -6 dB positive echo with a delay spread of 5μsec. The corrupting effect of the sync pulse is evident during the early segment, and the superposition of the colour burst introduces some overshoots and undershoots.

In multipath environments, the slicing level determined by an averaging slicer will also be in error, but is likely to outperform the present technique simply because it is much less peak sensitive. Note that if the slicing level were determined later in the burst (at a time exceeding the largest multipath spread), a better estimate of the dc level would be obtained. As a result, a system that does not freeze the slicing level, but tracks it along the burst, would have superior performance. Because the data burst can itself introduce a dc component (i.e. there is no guarantee or protection against a long string of bits with the same polarity), adaptive slicing level determination ideally must be decision directed. This requirement severely impacts implementation and circuit complexity.

(3) The optimum slicing level may be time varying due to time varying phase errors in the recovered carrier. This is further evidence that adaptive slicing level circuitry may be required.

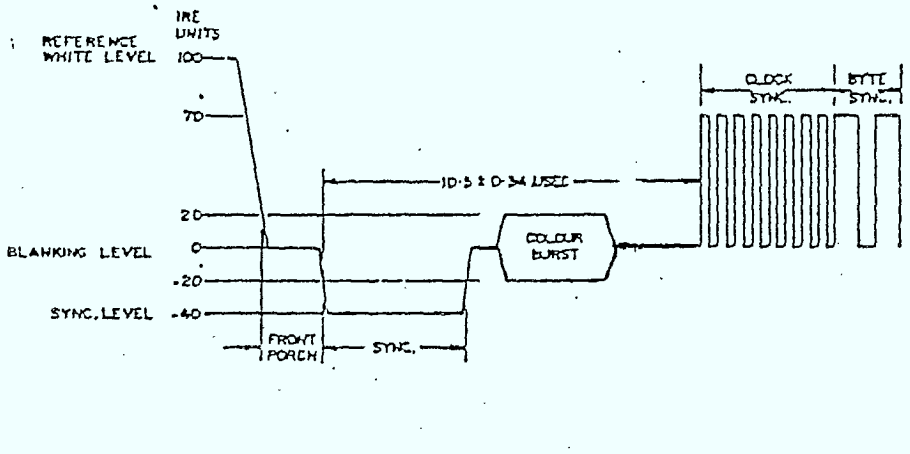

Figure 2.7 : Inserted Teletext Signal [19]

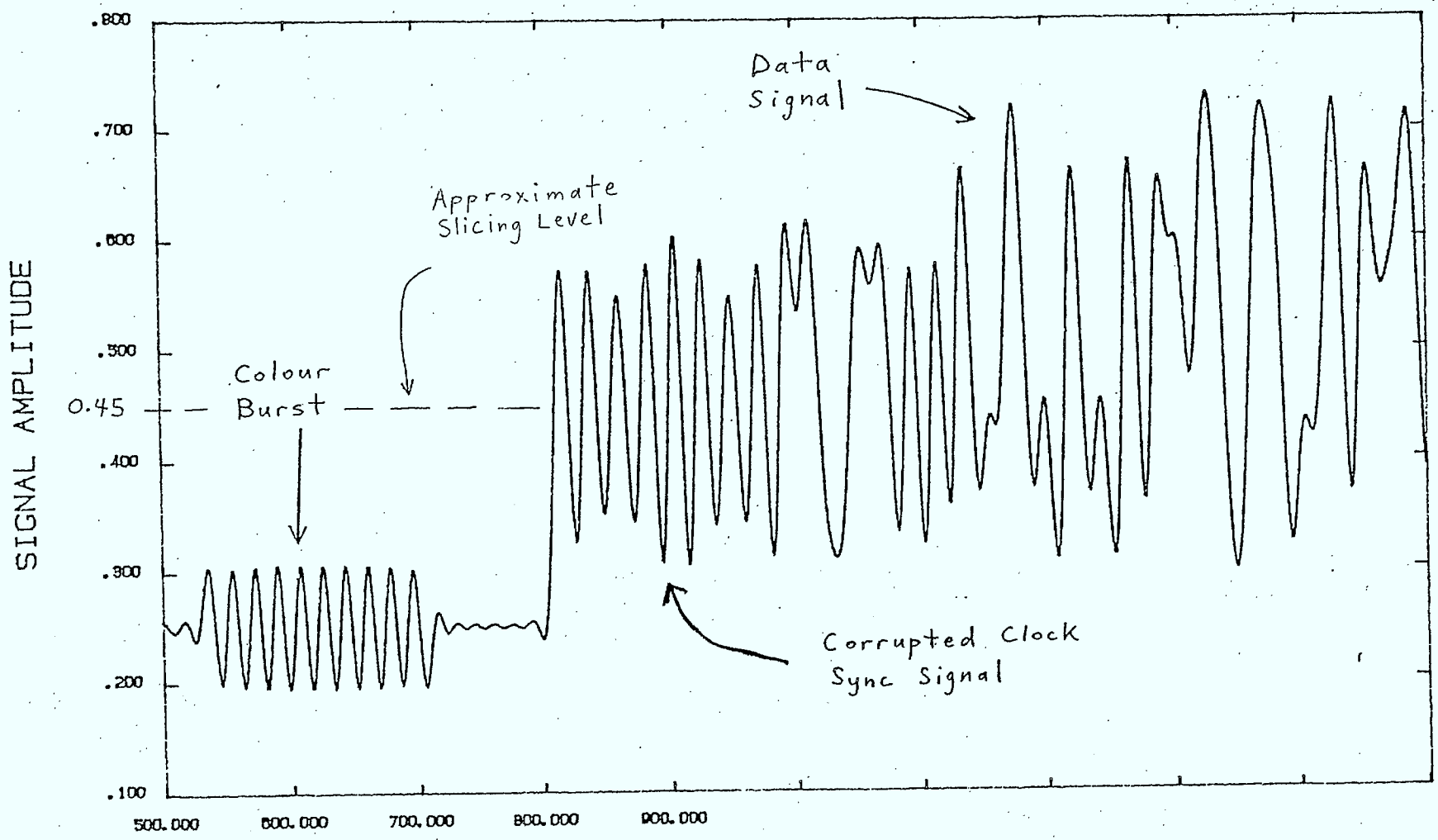

Figure 2.9: Received Clock Sync Signal Over A Multipath Channel With A Single -6 dB Positive Echo With Delay Spread of 5 μsec.

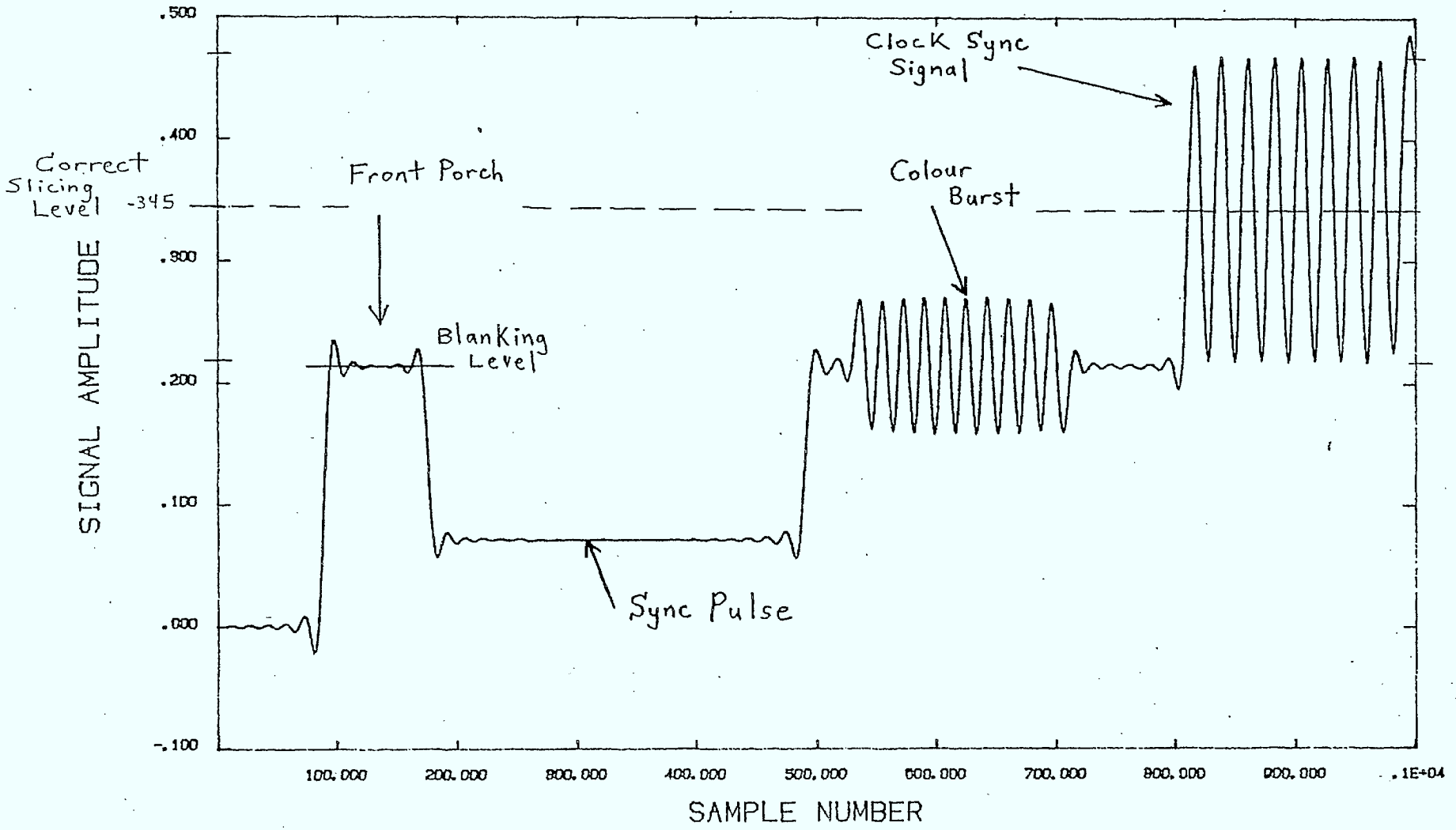

Figure 2.8 : Filtered Received Teletext Line

Some serious problems exist with the technique presently used to estimate clock phase. These are:

(1) An error in slicing level results in an error in clock phase. There is really no reason why bit timing recovery should be so dependent on the slicing level estimation. They are clearly independent problems and should be treated as such. Consequently, in the next decoder phase, a parallel as opposed to serial synchronization technique should be designed.

(2) The sampling clock phase is estimated from only a single zero crossing, and will tend to be very sensitive to noise and other interference.

A recommended improvement for symbol synchronization, which is closely related to the cross-correlation time delay estimation technique (which is optimal in white gaussian noise), is presented in Appendix I of [11]. Time did not permit incorporation of this improved technique in the simulation program. An improved version of the existing decoder that estimates the slicing level by averaging rather than using peak detection circuits, but still uses the inferior timing recovery technique, has been implemented.

Before presenting simulation results, it is informative to discuss the nature of the broadcast television multipath channel.

2.2 Broadcast Television Multipath Channels

One of the most important objectives of the Telidon system study is establishing system performance in typical

multipath environments. In order to do so, one must first gain insight into the nature of the VHF multipath channel. The Telidon RF multipath propagation simulation program [36], [46] and channel measurements conducted by the Communications Research Centre (CRC) personnel were particularly useful. The simulation program, in particular, was instructive in yielding insight into the behaviour of VHF multipath propagation as a function of frequency and environment. The severity of multipath components as a function of delay, for various carrier frequencies and reflector dimensions, is presented in [36] and [47].

An important conclusion that can be drawn from the simulation results is that the statistics of the VHF multipath channel are wildly non-stationary and very sensitive to channel frequency and receiver locality. For example, the severity of multipath increases as the carrier frequency is increased. As indicated in Figure 2.10, when the carrier frequency is 55.25 MHz (channel 2), multipath is not very severe, even for reflectors with an average area of 353.4 m^2. However, when the carrier frequency is 201 MHz, multipath is much more severe. Significant echoes with delays of 10 μsec are common for an average reflector area of 353.4 m^2. As one would expect, the echo strength is a strong function of the reflector dimensions, being worse for large reflectors. The cdf contour for a carrier frequency of 201 MHz and average reflector area of 225 m^2, shown in Figure 2.10, clearly demonstrates this. In [48], the echo strength is shown to be proportional to H^3W, where H represents the reflector height and W the reflector width.

When analyzing multipath channels, it is useful to restrict attention to those channels which provide acceptable video quality signals off-air. It does not make sense to attempt to provide Broadcast Telidon service to customers that

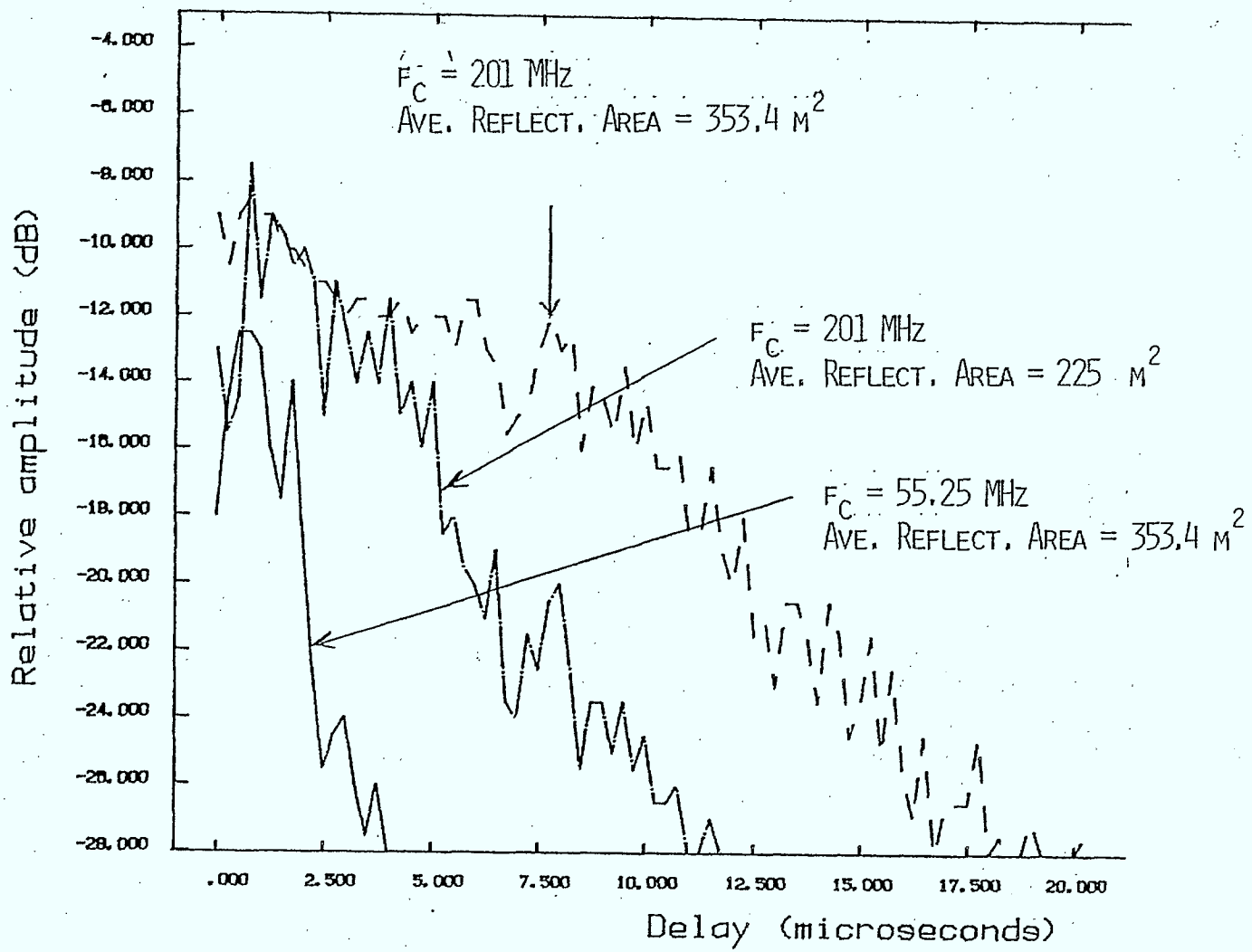

Figure 2.10 : Simulation 99.99% CDF Contours

cannot receive useful television pictures off-air. Consequently, a channel classification (pre-screening) algorithm was developed to identify those channels which would not provide an acceptable video quality signal. This channel classification algorithm is presented in Appendix B. Basically, this algorithm is a precedure for weighting multiple ghosts to obtain an estimate of subjective picture quality. A "perceived DU (desired to undesired) ratio", denoted by PDUR, is used to estimate the subjective quality of a television picture. This ratio is essentially a Signal to Clutter ratio, where each echo has an appropriate weighting applied to account for each echo delay and phase. Stated simply, the video quality acceptability thresholds eliminate extremely bad channels (i.e. those with in band nulls or "near" nulls) from further consideration.

With the incorporation of the channel prescreening algorithm, the Telidon multipath simulation program can be used to generate realistic mutlipath channels for system evaluation. This is also discussed in Appendix B.

As alluded to earlier, channel measurements conducted by CRC personnel were useful for characterizing multipath in the upper VHF band (carrier frequency was 201 MHz) in the Ottawa area. Plots of the measured channel impulse responses can be found in Appendix III of [11]. The tedious information extraction and channel classification process is also presented in Appendix III of [11]. The pertinent details of the channel measurements will be summarized below.

Of the 159 channels classified, 83 chanels were found to provide acceptable video quality (52.2%), while 76 were found to be unacceptable for television viewing (47.8%).

The extremely high percentage of rejected channels (in spite of the fact that a relatively low acceptability threshold was used), tends to suggest that the measurements were biased somewhat towards extreme multipath channels. This was undoubtedly due, in part, to the fact that the investigators were looking for multipath corrupted channels.

Primarily in the downtown area, channels with reflected paths stronger than the main path (which is primarily due to blockage) were observed. Most of these non-minimum phase channels were found to be extremely poor television quality channels. In fact, only six non-minimum phase channels were deemed acceptable.

For the acceptable channels, statistics on the number of significant echo paths were gathered. A significant echo path is defined as one with a DU ratio less than or equal to 24 dB. The mean number of significant echoes was 3.33, with a standard deviation of 1.97.

The magnitudes and delays of the echoes comprising the acceptable video channels have been accumulated in a "scatter table" in Figure 2.11. It is apparent that the majority of echo delays are less than 3 μsec in the Ottawa area. This could be significantly different in other metropolitan areas in North America. By selecting the simulation program parameters to provide an average reflector size of 225 m^2, an occupational domain given by a 3 km x 3 km rectangle about the receiver, and selecting 400 impulse response components (number of reflectors), a reasonable match between the measurement and simulation program results were obtained. This is evident in Figure 2.11, where the vast majority of measurement results fall within the 99.99% cdf contours obtained with the simulation program.

It is evident that for short delays, that one observes measured echo strengths greater than the simulation cdf contour ($\tau < 0.6$ μsec). They are, however, reasonably close to the contour. The reason for this can be attributed to the approximations used in the simulation model for the near field [36], [46], which is one of the known weaknesses of the model. Taking proper account of the near field region is quite difficult, and would increase the complexity of the model considerably. However, given that the vast majority of measurements do fall within the contour bounds, the simulation program is a good working model.

It is also evident from Figure 2.11, that the channel prescreening algorithm eliminates the very bad multipath channels. Acceptable video channels will not have any in band nulls, or even "near" nulls. The video quality classification index, PDUR, is not particularly useful for categorizing data communications channel quality. From the video standpoint, close in echoes are much less annoying than similar strength echoes with longer delays. As a consequence, a channel that is classified as a good video channel may have an appreciable close in echo, and such a channel would not be classified as a good data channel.

The extreme variability of the VHF multipath channel is evident from the measured channel impulse responses and from simulated channel impulse responses. Consequently, in any given locality, the number of potential channels is virtually boundless, and the absolute accuracy of any specific candidate is of relatively little concern. Given the behaviour of the multipath channel, the statistical "average" channel characteristic will tend to have an ideal

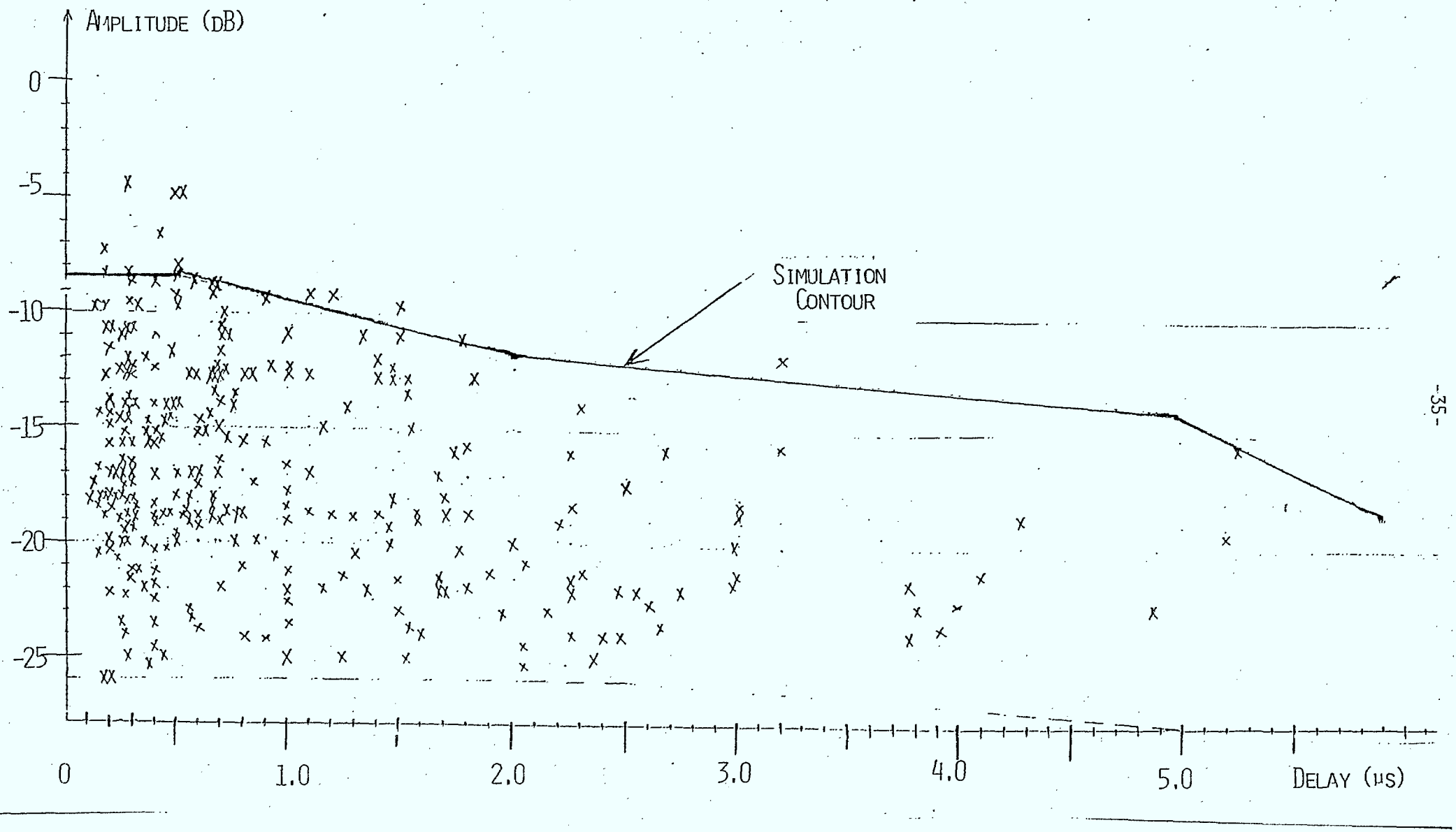

Figure 2.11 : Scatter table for acceptable measured channels in the Ottawa area.

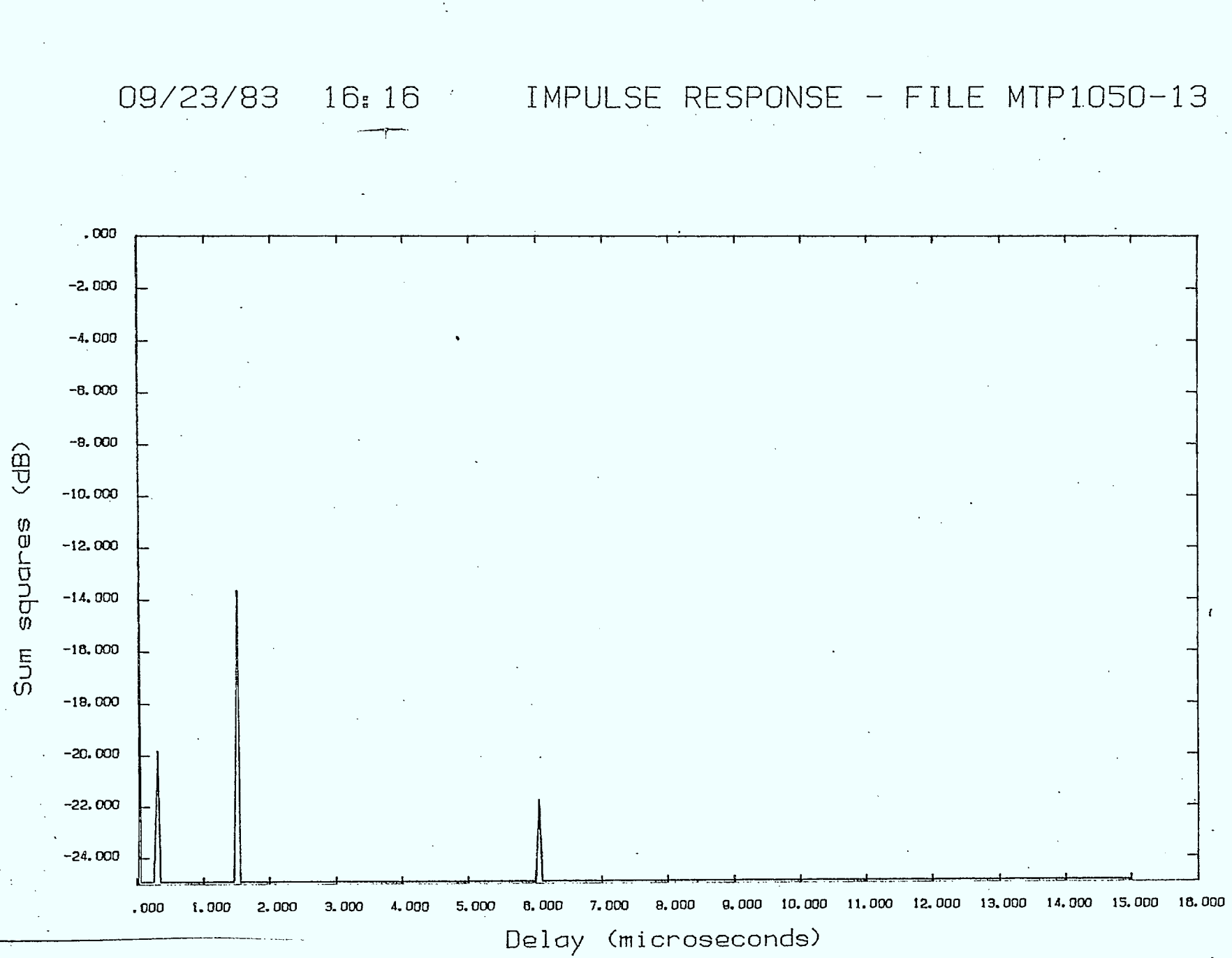

Figure 2.12: Dominant Echoes Of Multipath Channel With PDUR = 13 dB

"white" response. There will clearly be a substantial number of channels with frequency responses considerably different than that of the "average" channel.

The multipath simulation program was used to generate impulse response files, defined by a vector of delays and magnitudes. These impulse responses were generated with simulaton parameters that provided the best match with measured impulse responses obtained in the Ottawa area. The multipath channel subroutine uses this impulse response file, and creates a frequency domain sampled version of the channel frequency response:

$$C(f) = 1 + \sum_{i=1}^{N} m_i \, e^{j\phi_i} \, e^{-j2\pi f d_i} \qquad (2.1)$$

where ϕ_i is the random phase $[-\pi, \pi]$ assigned to each path

m_i is the relative magnitude associated with the i-th echo path

d_i is the relative delay associated with the i-th echo path

N is the number of reflectors (echo paths) comprising the impulse response

A plot of dominant paths of the channel impulse responses that were used to investigate Telidon system performance in multipath environments are provided in Figures 2.12, 2.13, and 2.14. These channels have PDUR's of 13 dB, 14 dB, and

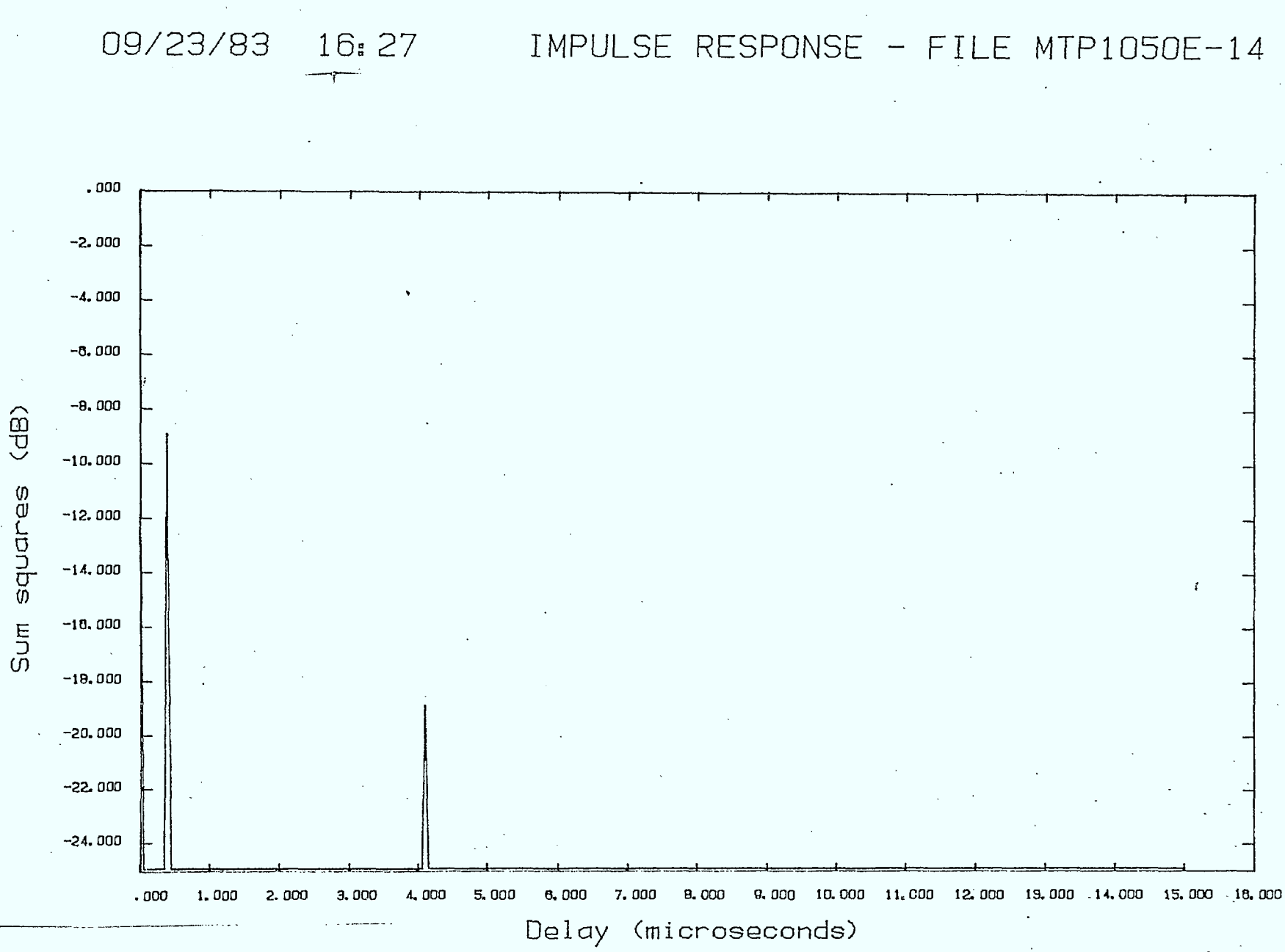

Figure 2.13 : Dominant Echoes of Multipath Channel With PDUR = 14 dB

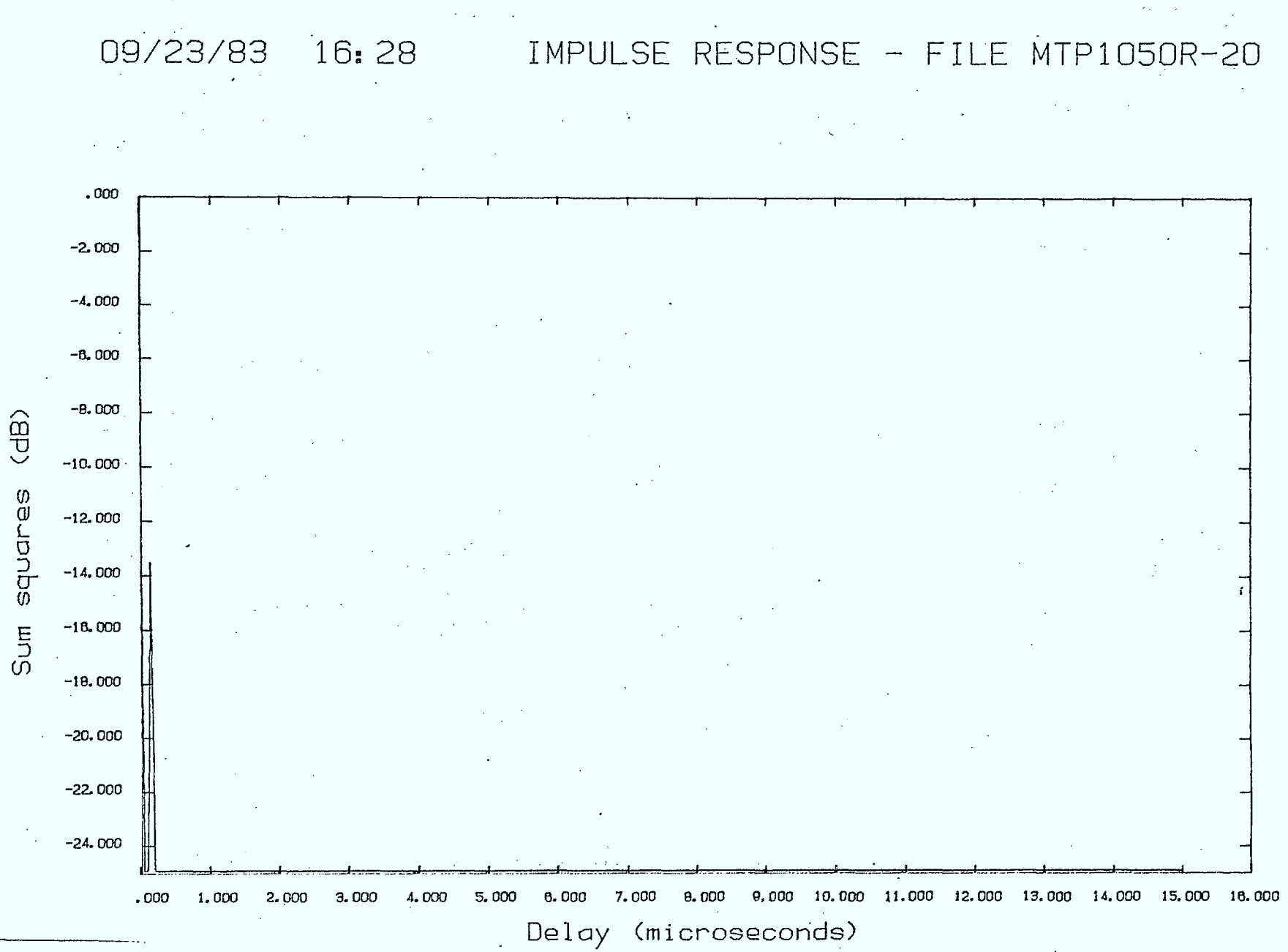

Figure 2.14: Dominant Echoes of Multipath Channel With PDUR = 20 dB

20 dB respectively. As has been mentioned earlier, multipath components can distort the clock sync portion of the teletext signal by superimposing delayed and attenuated versions of the signal preceding the teletext data (i.e. blanking level, colour burst, and sync tips). The degree of slicing level error is a strong function of the phase assigned to the dominant echoes. For example, quadrature echoes (ϕ = 90° or 270°) are much less serious than inphase echoes (ϕ = 0° or 180°).

To ensure a manageable number of simulation runs, attention is restricted to the three multipath channels mentioned above. To characterize performance with each channel, five different random channels (different echo phases are assigned each time) are selected. Runs are then conducted at different signal to noise ratios and for different decoder models.

Due to the impact of channel variation on slicing level error (different phases being assigned to the echoes), significant variation in the output results is observed from run to run. However, on the graphs summarizing performance, only the mean performance over the ensemble of 5 channels is supplied. Error bars are not included because they would spoil the clarity and add little of value.

Performance of the conventional and averaging slicer decoders has been determined with the above mentioned multipath channels in white gaussian noise and "impulse and gaussian noise" mixtures. Determining the appropriate mix of impulse and thermal noise is hampered by the lack of measurement data. The other problem is that, in practice, it would be so variable and dependent on measurement sites

(similar to the multipath channel variability problem) that any choice is likely to valid somewhere, at some time. However, to reduce the degrees of freedom somewhat, the ratio of impulse to thermal noise is fixed at 125.89 (21 dB).

The next section summarizes the existing Telidon system performance in multipath.

2.3 Simulated Performance of the Existing Telidon System

In this section, the performance of two decoder models, the peak detector slicing level decoder presently employed in the Telidon system and an improved averaging slicing level decoder, is investigated. Probability of bit error versus video signal to noise ratio are presented for both multipath and ideal channel conditions. For the simulation runs, the emphasis has been on weighted video signal to noise ratios in the 25 - 30 dB range. From the TASO signal grades presented in Table 2.1, it is apparent the television picture quality is marginal, but still useful, in this video signal to noise ratio range.

The performance of the two decoder models in a thermal noise environment with the 13 dB PDUR multipath channel is provided in Figure 2.15. Also provided on this figure, is system performance with an ideal channel. This figure clearly illustrates the significant performance degradation that the averaging and peak detector decoders suffer relative to ideal slicing and ideal clock recovery. The peak detector decoder suffers roughly a 3 dB performance degradation. The averaging slicing level decoder is somewhat better, suffering only a 1.5 dB performance

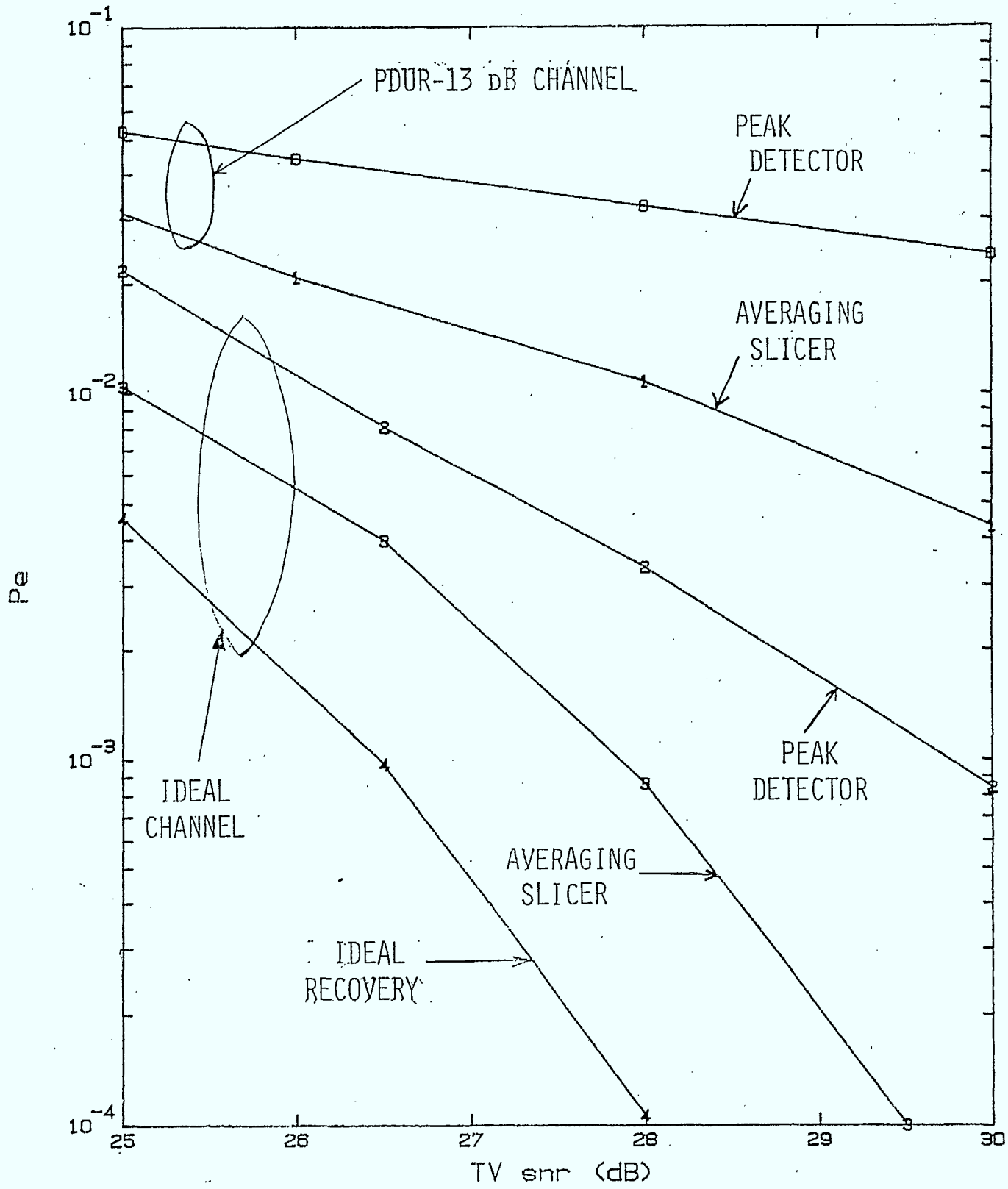

Figure 2.15 : Comparison of system performance in ideal and PDUR-13 dB multipath environments with additive thermal noise

TASO Grade	Unweighted Video SNR (dB)	Weighted Video SNR (dB)
Excellent	42	48.1
Fine	33	39.1
Passable	27	33.1
Marginal	23	29.1
Inferior	16	22.1

Table 2.1: TASO grades versus video S/N

degradation, over the video signal to noise ratio region investigated. Figure 2.15 also illustrates the significant performance degradation imposed by the multipath channel. The superiority of the averaging slicing level decoder is clearly evident in this figure.

In Figure 2.16, performance with ideal slicing (derived from a noise free burst) is compared with ideal recovery (ideal slicing and ideal clock recovery) for an ideal channel corrupted by thermal noise. This allows one to assess the degradation that can be attributed to timing jitter. Over the video signal to noise region investigated, the degradation that can be attributed to the clock recovery procedures used in the current Telidon decoder is approximately 1 dB.

The performance in a thermal noise environment with the 14 dB PDUR multipath channel is presented in Figure 2.17. The significant degradation imposed by multipath is evident in the figure. Note that, for the runs conducted with this channel, the difference between the performance curves for the averaging and peak detector decoders is not as pronounced as it was for the 13 dB PDUR multipath channel (see Figure 2.15). This phenomena is discussed in greater detail in Section 3.3.

The 20 dB PDUR multipath channel, shown in Figure 2.14, has a significant close in echo. The performance of the peak detector and averaging slicing level decoders in a thermal noise environment with this multipath channel is presented in Figure 2.18. In this case, the averaging slicing level decoder is considerably better than the peak detector decoder. The basic performance trends are similar to the results for the 13 dB PDUR multipath channel shown in Figure 2.15.

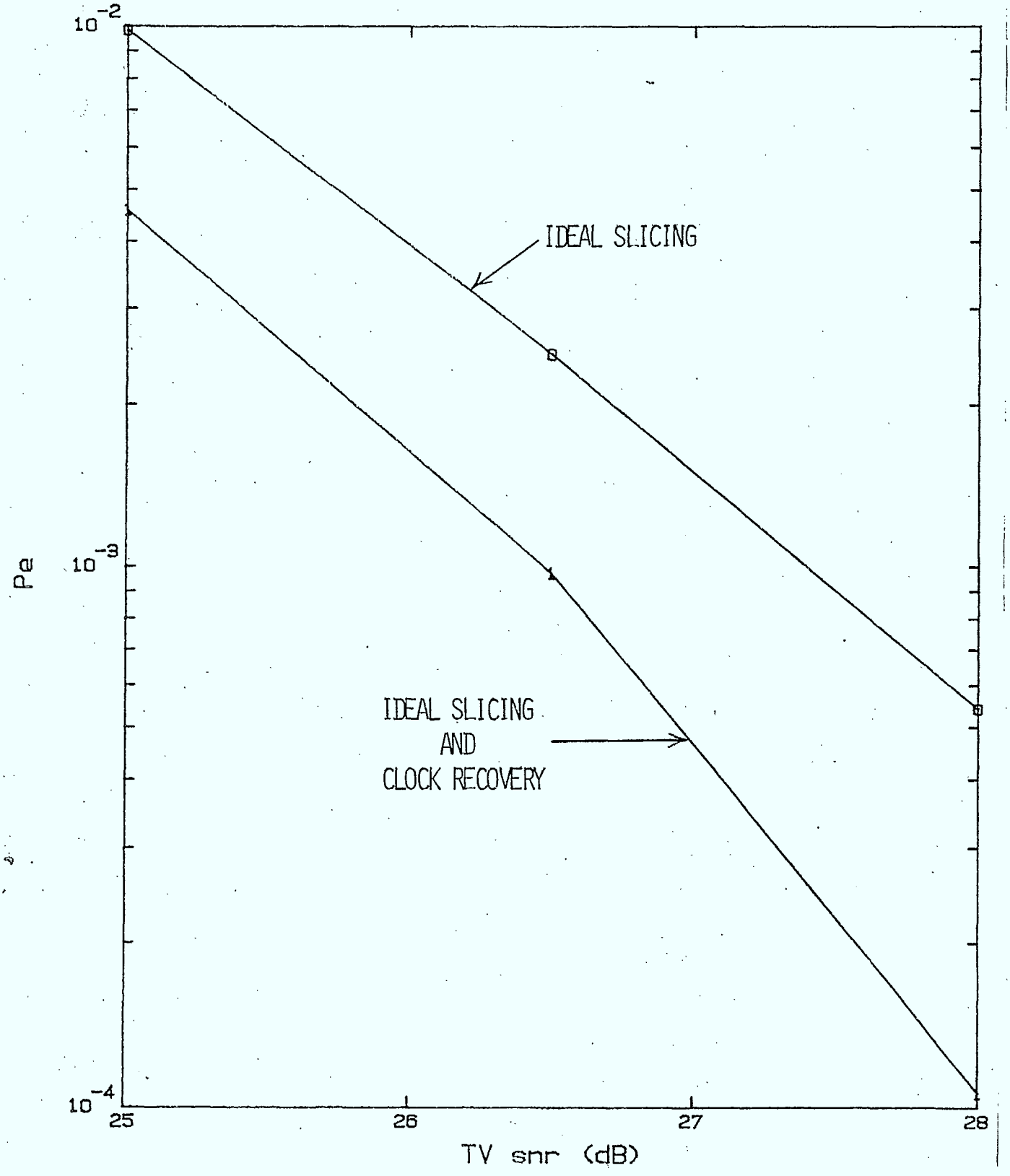

Figure 2.16: Illustration of degradation that can be attributed to the suboptimal clock recovery technique currently used in Telidon decoders in a thermal noise environment with no multipath.

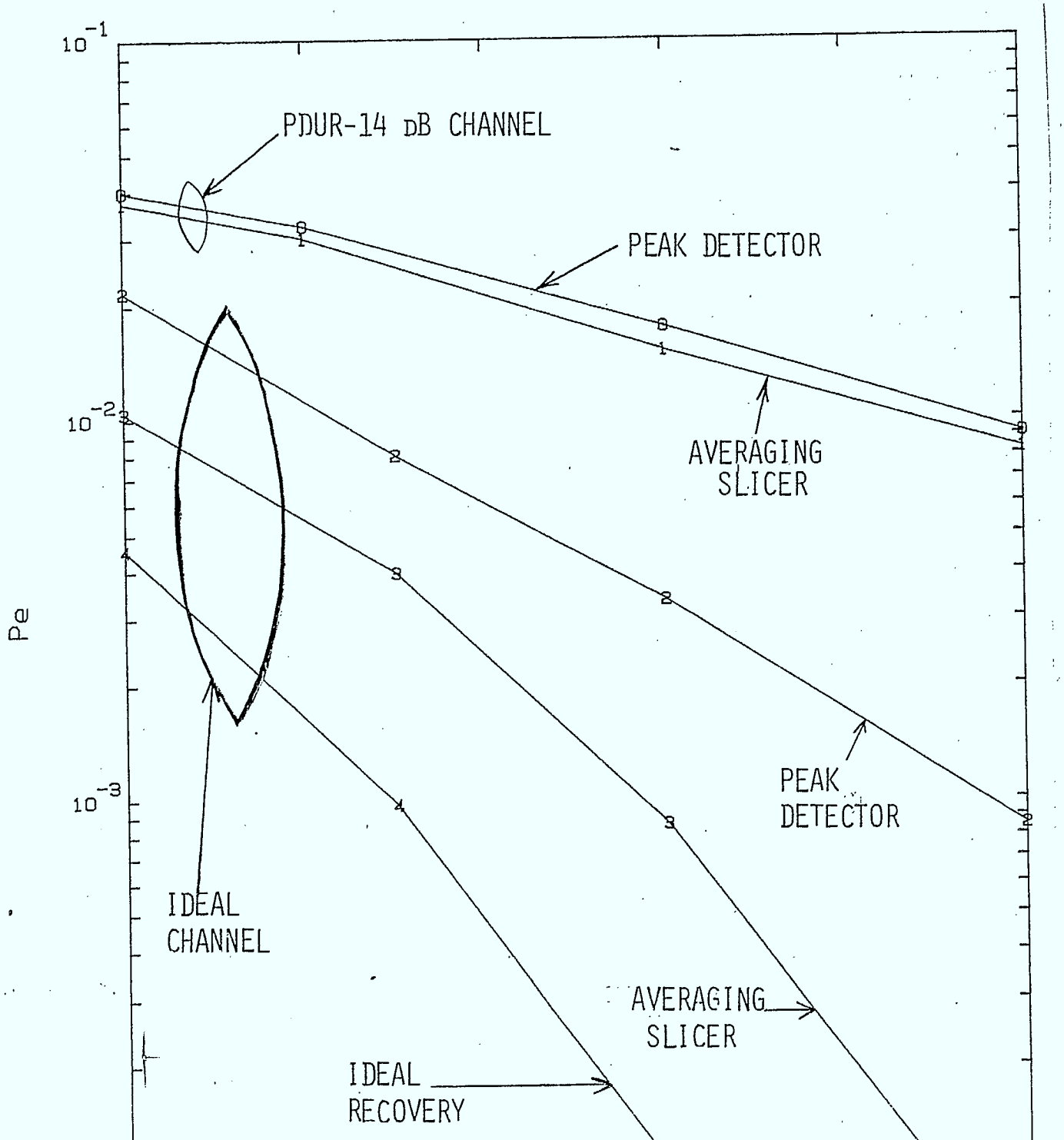

Figure 2.17: Comparison of system performance in ideal and PDUR-14dB multipath environments with additive thermal noise.

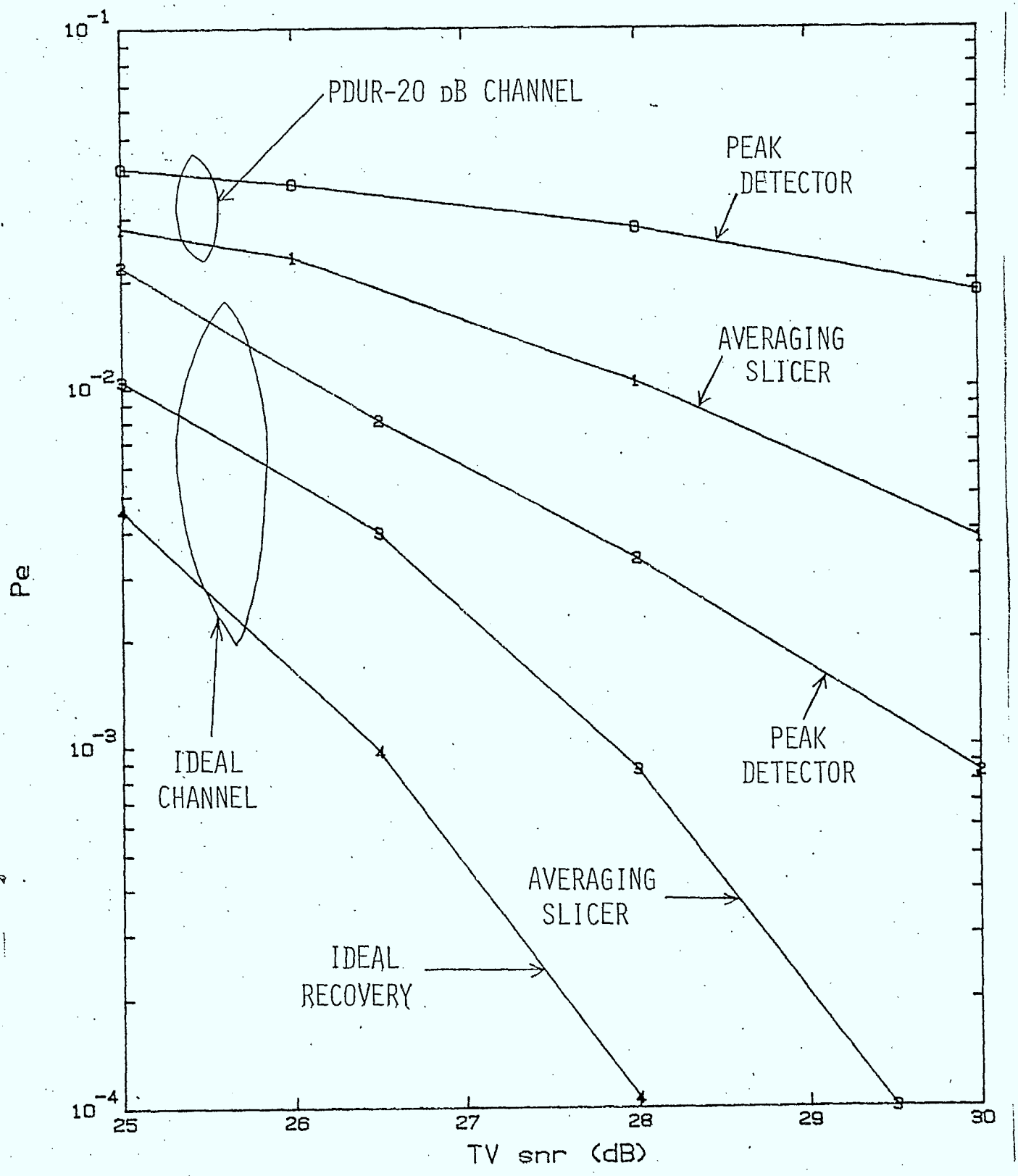

Figure 2.18 : Comparison of system performance in ideal and PDUR - 20 dB multipath environments with additive thermal noise.

The performance in a mixed impulse-gaussian noise environment, with the 20 dB PDUR multipath channel is presented in Figure 2.19. In this noise environment, the averaging slicing level decoder is clearly superior. The bit error rate performance curves exhibit a flatness which is characteristic of impulse noise dominated environments [11]. With the peak detector decoder, the error rate remains in the neighbourhood of 10^{-2}, which is relatively poor performance. With the averaging slicing level decoder, the error rate remains in the neighbourhood of 3×10^{-3}.

Because error correction and detection coding is employed in the Telidon system, the input error rate that can be handled can be relaxed somewhat. However, it is unlikely that the input error rate can exceed 1×10^{-3} without imposing some severe penalty, in terms of either delay or missed errors. The type of noise influences the burstiness of errors (impulse noise is thought to cause bursts of errors) and thereby the choice of error protection coding required to combat errors. Taking 1×10^{-3} as the threshold error rate, it is apparent that the existing system (employing peak detection circuits for slicing level estimation) cannot achieve this performance level with multipath channels near the video acceptability threshold, for video signal to noise ratios corresponding to passible TASA signal grades.

2.3.1 Evaluating the Effectiveness of the Error Protection Coding Presently Employed in Telidon

Since error correction and detection coding is employed in the Telidon system, and also because the system is likely to be subjected to bursts of errors in urban environments, the average bit error rate performance is not the most

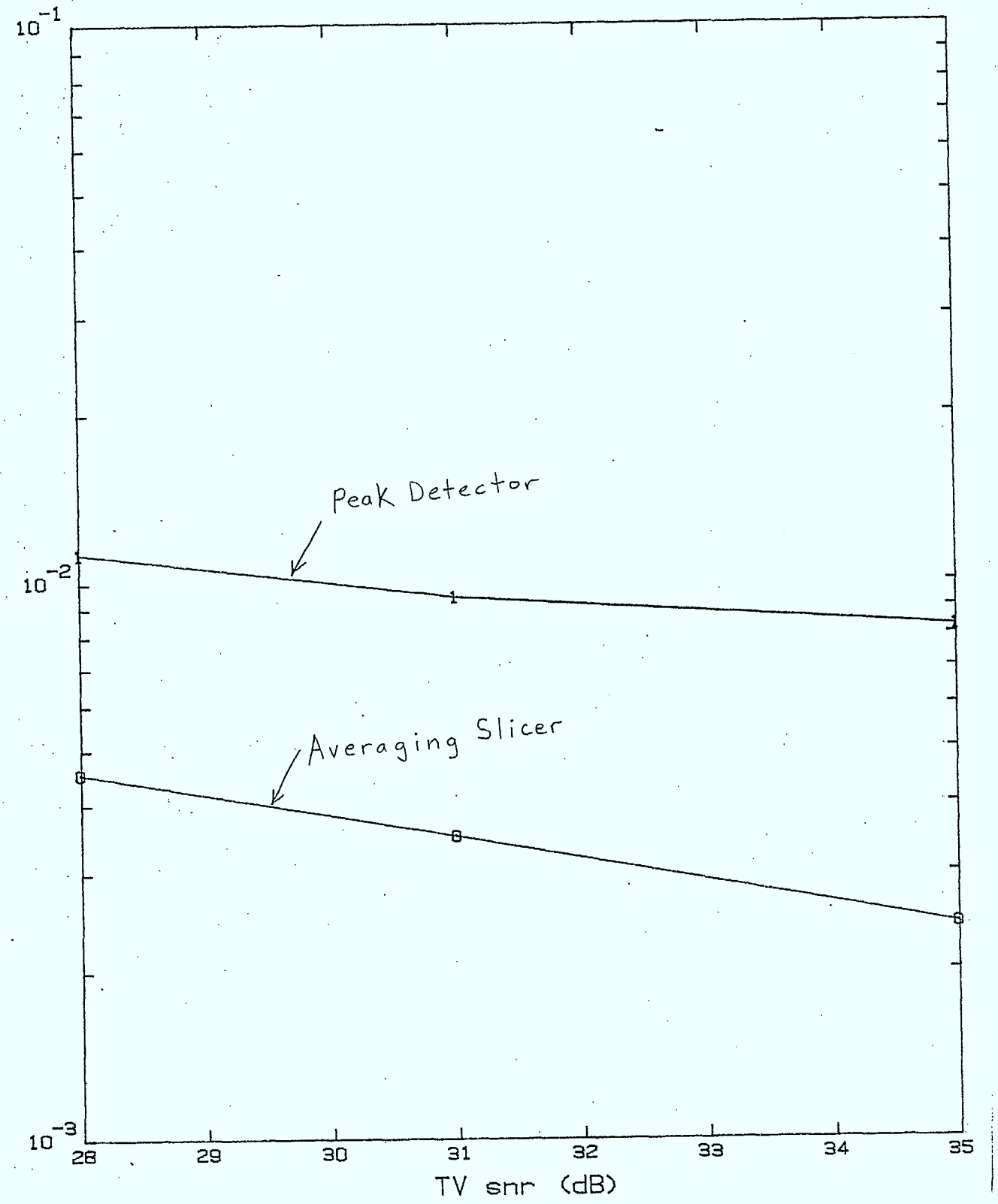

Figure 2-19 : Bit error rate performance in an impulse noise dominated environment with the 20 dB PDUR multipath channel

suitable performance index. More suitable performance indices are the packet rejection rate (delay) and number of corrupting errors per message.

With our simulation program, the errors in the bit stream at the channel output (input to the error correction and detection decoder) are logged. These error sequences can then be analyzed to determine the error autocorrelation function, gap length and burst length distribution functions, and other typical error statistics. These error sequences (after being Exclusive OR'ed with an appropriate [odd parity] zero data sequence) can then be decoded by a series of potential coding techniques to assess their relative performance.

In order to evaluate possible channel and decoder enhancements, a procedure for relating errors to performance degradation (corruption and delay) was developed. To do so, errors had to be categorized as to their severity, which requires knowledge of the Telidon message structure and error protection in use. A proposed categorization of errors is presented in Appendix A, where an attempt to predict the effects of errors within different sections of the Telidon message is discussed. A brief summary will be presented here for completeness. Errors can either be corrected, detected, or missed. Detected errors result in errors can result in either delay or image corruption, depending on their position. By assuming an average record composition (a record was assumed to consist of a 33 byte header block followed by 50 data blocks including prefix segments) expressions were developed for the packet rejection probability, R, and the average number of PDI errors per record, Nc. In order to evaluate these expressions, an error analysis program was developed to measure a number of important intermediate quantities.

The error analysis program was used to determine the packet rejection rate and number of PDI errors per record for the byte parity check and product codes which are presently used in the Telidon system. Analysis performed in Section 3.4 of [11] and Appendix A indicates that a reasonable bound on the average number of PDI errors per record is 6.2 and a bound on the packet rejection rate is 0.025. It has been found that the byte parity check and product codes have no problem achieving the PDI error corruption bound. However, due to their strong detection capabilities, there is difficulty achieving the desired packet rejection rate. Figure 2.20 shows the rejection rate curves for an ideal channel corrupted by additive gaussian noise. The superiority of the product code is clearly evident and expected. The superiority of the averaging slicing level decoder is anticipated because of the lower input error rate. The threshold packet rejection rate is obtained in the neighbourhood of SNR_{TV} = 28 dB with the averaging slicer and in the neighbourhood of SNR_{TV} = 30 dB with the peak detector slicer.

Figure 2.21 presents the rejection rate curves for the 20 dB PDUR multipath channel in a thermal noise environment. It must be emphasized that this channel would provide a relatively good quality television picture. It is not a fringe channel near the video quality acceptability threshold. As is evident from Figure 2.21, this channell imposes a significant performance penalty. It is apparent that reasonable system performance cannot be guaranteed for weighted video signal to noise ratios as low as 30 dB, which is a desired operating point.

Presented in Figure 2.22 are the rejection rate curves for the 20 dB PDUR channel when the noise is a mixture of impulse and gaussian noise (impulse dominated). It is

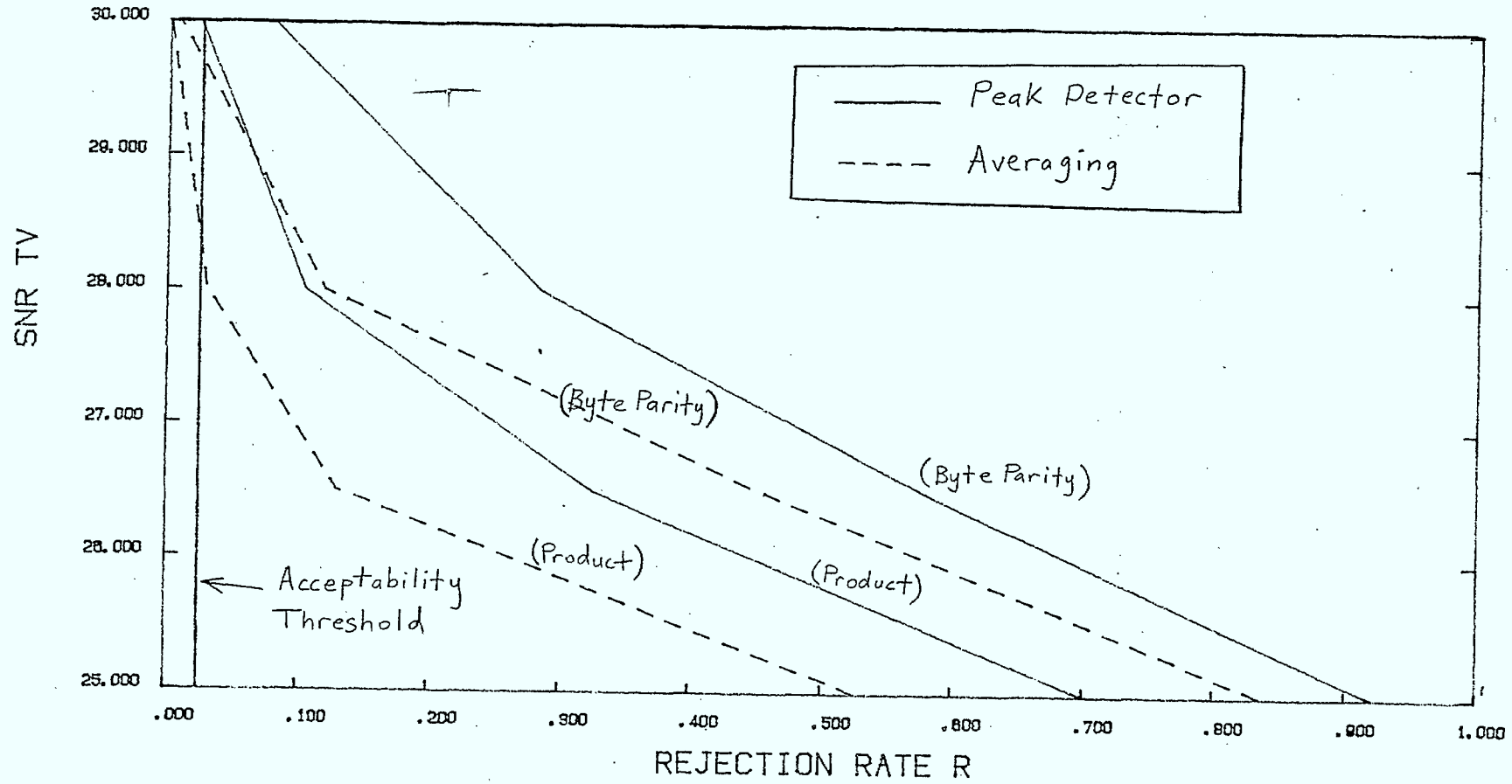

Figure 2.20 : Rejection rate versus video signal to noise ratio for an ideal channel and thermal noise environment

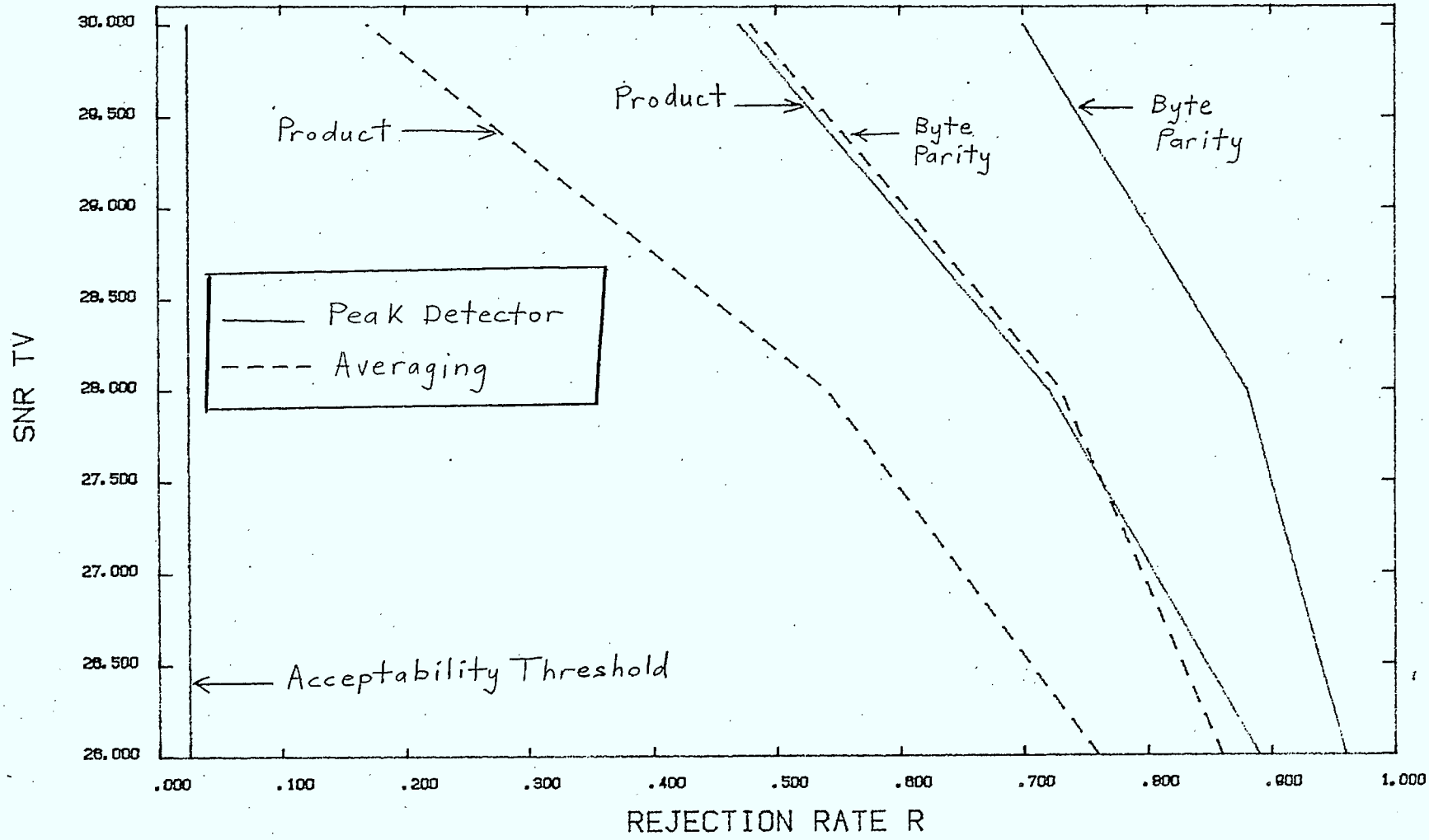

Figure 2.21 : Rejection rate versus video signal to noise ratio for a 20 dB PDUR multipath channel in a thermal noise environment.

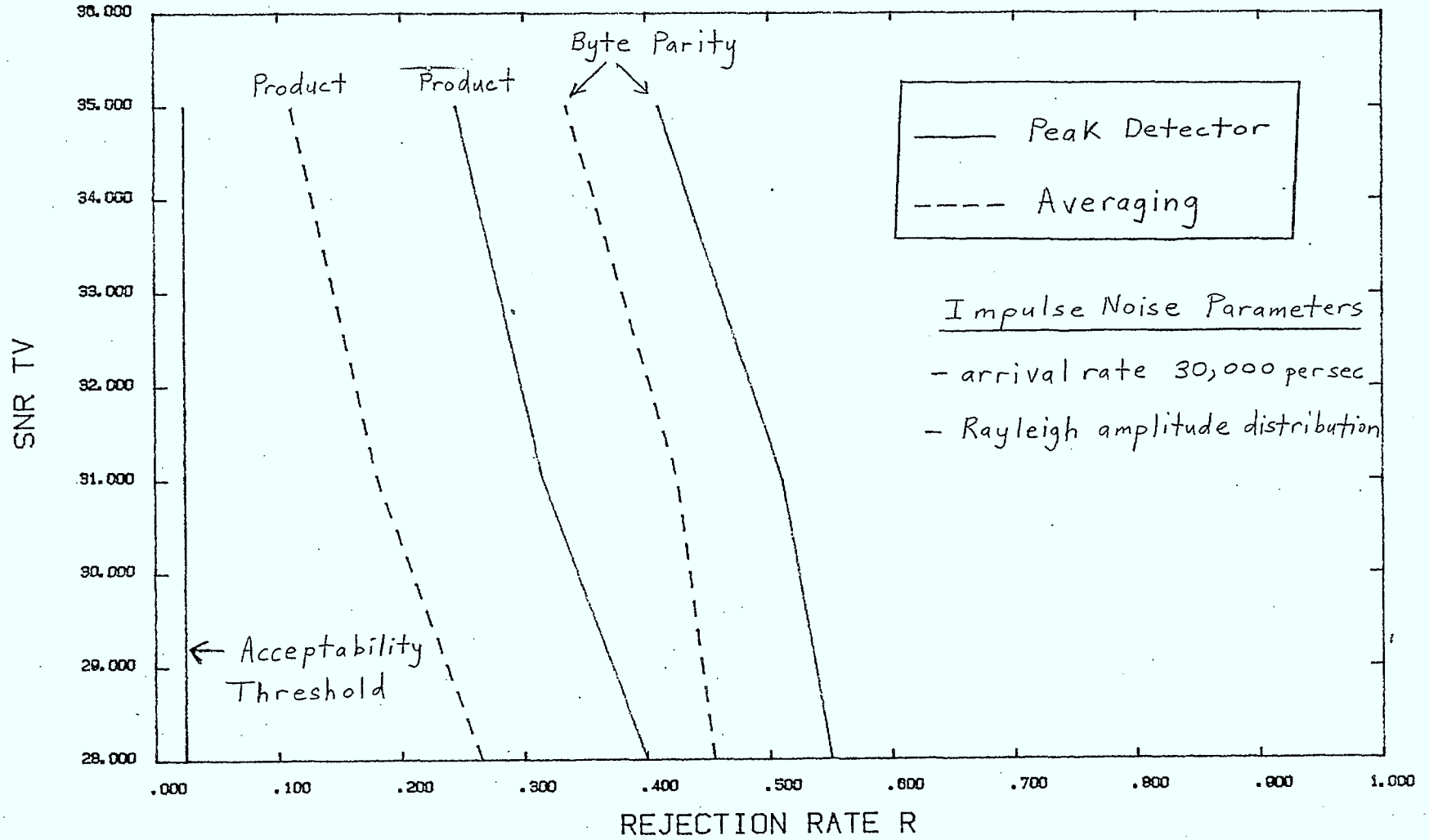

Figure 2.22 : Rejection rate versus video signal to noise ratio for a 20 dB PDUR multipath channel in a mixed impulse - gaussian noise environment (impulse noise dominated)

evident that reasonable performance cannot be achieved in this severe noise environment. Given the behaviour of the error rate curves for this noise environment (see Figure 2.19), it is difficult to foresee any dramatic improvement. Even powerful coding techniques tend not to operate very well at such high input error rates.

The clear superiority of the modified decoder (which determines the slicing level by averaging) has been demonstrated. Future decoders should employ this approach. It must be noted that there still remains a significant degradation relative to ideal recovery. It is anticipated that implementing the recommended clock phase recovery procedure (Appendix I of [11]) should improve performance considerably. Given the potential gain, this should be assigned a high priority. It has also been demonstrated that the existing Telidon system will have difficulty operating successfully in typical multipath environments at reasonable video signal to noise ratios. Adequate performance for multipath channels near the acceptability limit will require either adaptive equalization and/or improved error protection coding schemes.

3.0 COMPARISON OF PULSE SHAPES

3.1 Introduction

The choice of a suitable pulse shape for Canada's television broadcast teletext system has received considerable attention in recent years [13], [14], [15], [16], [17], [18]. Much of the effort has concentrated on raised cosine pulse shapes with various roll-off factors. In fact the current specified pulse shape is a truncated 100 percent raised cosine [19]. It has been pointed out that although the raised cosine family of pulse shapes are fairly good, it may be possible to do better if one searches over a wider class of pulse shapes for the one that is in some sense optimal [16]. The Communications Research Centre let a contract to the University of Toronto to study the pulse shaping problem. The study culminated in a excellent report [14] and several papers [15], [20], [21]. However, certain aspects of pulse shaping were not adequately dealt with. These include:

- minimizing overshoots at the transmitter is not considered.
- the recommended pulse shape is not realizable.
- the zero phase assumption for the frequency response is not justified.

These issues have been considered in the pulse shaping study conducted for this contract. The interested reader can find this study in Appendix I of [11].

The pulse shaping problem is complicated by the number and nature of the objectives that ideally should be simultaneously satisfied. These objectives are such that

the solution to the traditional problem of designing optimal transmit and receive filters for a known additive white gaussian noise channel with the transmit power being constrained, does not yield attractive shaping filters. This will become clearer when the pulse shape objectives are summarized. The other major complication is the fact that the channel and noise characteristics are not known a priori, and are also highly variable from one receiver location to another.

The overall objectives of the pulse shape design are as follows:

- To minimize the probability of bit error subject to the other design objectives being satisfied.

- The overshoots, at both the output of the transmitter and the baseband channel of the receiver, should be constrained at acceptable levels.

- The pulse shape design should lead to specifications that are compatable with current television broadcast specifications.

- The overall pulse shape should be reasonably robust in the presence of multipath.

- The receiver requirements should ideally be kept as simple as possible (i.e. any necessary complexity and stringent specification should be transferred to the transmit side when possible).

- The bandwidth must be constrained to the 4.2 MHz NTSC video bandwidth.

The objective that makes this pulse shape design problem considerably different than the traditional problem mentioned above is the constraint on overshoots. There are several reasons for restricting the overshoots (and undershoots) in the receiver's baseband channel. Reasons given include the avoidance of false synchronization (i.e. overshoots being mistaken for sync pulses by the television receiver) and visibility on retrace (although this is expected to be a relatively weak function of overshoots). Excessive overshoots have also been blamed for causing audio buzz although the sources of audio buzz do not appear to be very well understood. It is also desirable that the peak amplitude of the transmit signal be constrained to the region in which the power amplifier is fairly linear, in order to avoid signal distortion, which in turn can result in interference to the sound carrier [7] and degrade the performance of the data transmission. Clearly the transmit pulse shape will affect the peak amplitude of the transmitted signal. A major conclusion from the pulse shaping study (Appendix I of [11]) is that the peak transmit signal level cannot be properly included in the overall pulse shape design until a representative collection of transmit IF filter frequency responses (both magnitude and group delay) and until a nominal receiver characteristic has been chosen.

Another equally important reason why the teletext pulse shaping problem deviates from the traditional formulation is that in many cases the dominant type of noise is likely to be impulse noise, as opposed to thermal noise. Restricting attention to the gaussian noise situation, optimum performance is obtained by performing the appropriate shaping at both the transmit and the receive sides of the transmission link. Unfortunately, this increases the complexity (and thus cost) of the teletext

receiver, and is in direct conflict with the objective of keeping the receiver requirements as simple as possible.

From the nature and number of overall objectives of pulse shape design, the task of selecting a pulse shape that satisfies all the objectives is indeed a difficult one. One possible approach, for meeting the objectives is to define a massive non-linear optimization that attempts to simultaneously achieve the above goals. However, before such a chore could be undertaken, the pulse shaping problem requires further refinement and formulation. For example, the acceptable overshoot levels at both the output of the transmitter and the baseband output of the receiver must be determined. An analytical approach for specifying these quantities would invariably involve investigating the audio buzz phenomena. Experimental approaches could be used to subjectively evaluate acceptable constraints on overshoots at the receiver output.

If the pulse shape optimization attempts to include multipath propagation by optimizing performance over an ensemble of possible channels, great care must be taken to avoid certain pitfalls. First of all, the collection of multipath data must be performed in a complete and unbiased fashion, to avoid obtaining a biased result. Secondly, the selection of an overall performance index requires careful thought. The reason for this is that most performance criteria, that would seem reasonable to apply, tend to implicitly weight the poorer members of the ensemble of channels (i.e. those with a relatively high bit error rate) more than good members. Consequently, if one is not careful, the likely result of the optimization might be to sacrifice the performance of the good channels in order to achieve a marginal improvement for the poor channels.

A simpler approach is to try to decompose the problem into several smaller and more manageable problems (that are hopefully approximately orthogonal) and handle each one separately. This was the approach to the pulse shape problem taken in this contract, as there was insufficient time to formulate the nonlinear optimization and to gather the necessary data to adequately model system parameters, let alone solve the nonlinear optimization.

The ultimate gauge of the performance of a specified pulse shape is the probability of bit error achieved. Due to intersymbol interference, the evaluation of error probability becomes rather involved. Although a number of techniques for estimating the bounds on the error probability are available [13], [24], the more accurate bounds are non trivial and often do not have general applicability due to simplifying assumptions implicit in their derivation. Consequently, in most work that has been done to date on pulse shaping for teletext [14], [15], [18], certain properties of the eye diagram (i.e. eye height, eye width, and overshoots) have been used as figures of merit for various pulse shapes. The profile of the eye diagram was used as a basis of comparison for various pulse shapes in Appendix I of [11]. The next section is devoted to summarizing the pulse shape design work presented in Appendix I of [11].

3.2 Recommended Pulse Shape for Teletext

For the purpose of overall pulse shape design it is assumed that the peak constraint at the receiver baseband output is active. Given this peak constraint, a reasonable figure of merit is the ratio of the eye opening to the peak-to-peak signal level, denoted by a/c. The transfer function,

impulse response, and eye diagram that correspond to a pulse shape that is almost the same as the one outlined in BS-14 [19], can be seen in Figure 3.1. For this pulse shape, a/c ≈ 0.65 (-3.7 dB), and the eye width is about 0.9.

Several overall pulse shapes were derived in references [14] and [15] that are in some sense optimal. For their recommended pulse shape, Sousa and Pasupathy [14], [15] have selected the one that minimized the squared error in the Nyquist II criterion subject to the Nyquist I criterion. The transfer function corresponding to that pulse shape is illustrated in Figure 3.2. For this pulse shape a/c ≈ 0.75 (-2.5 dB) and the eye width is approximately 0.83. The discontinuities in the transfer function of Figure 3.2 are troublesome because they given rise to a long tail and precursor in the impulse response. Besides making the pulse shape difficult to approximate, the long tails and precursor aggravate the peak overshoots.

The pulse shape can be made realizable by windowing the impulse response with a Hamming window [22], which will tend to smooth the frequency response. Ideally, one would like a relatively short window to keep the impulse response as short as possible. Windowing, however, introduces spectral spreading. This spectral spreading increases as the window duration is reduced. One must seek a reasonable tradeoff between window duration and keeping the majority of signal energy within the NTSC 4.2 MHz bandwidth.

This approach was applied to the pulse shape of Figure 3.2. Quadratic tapering was introduced above 4.0 MHz to make the transfer function strictly bandlimited to avoid the interference with the sound carrier. The resulting transfer function is given by:

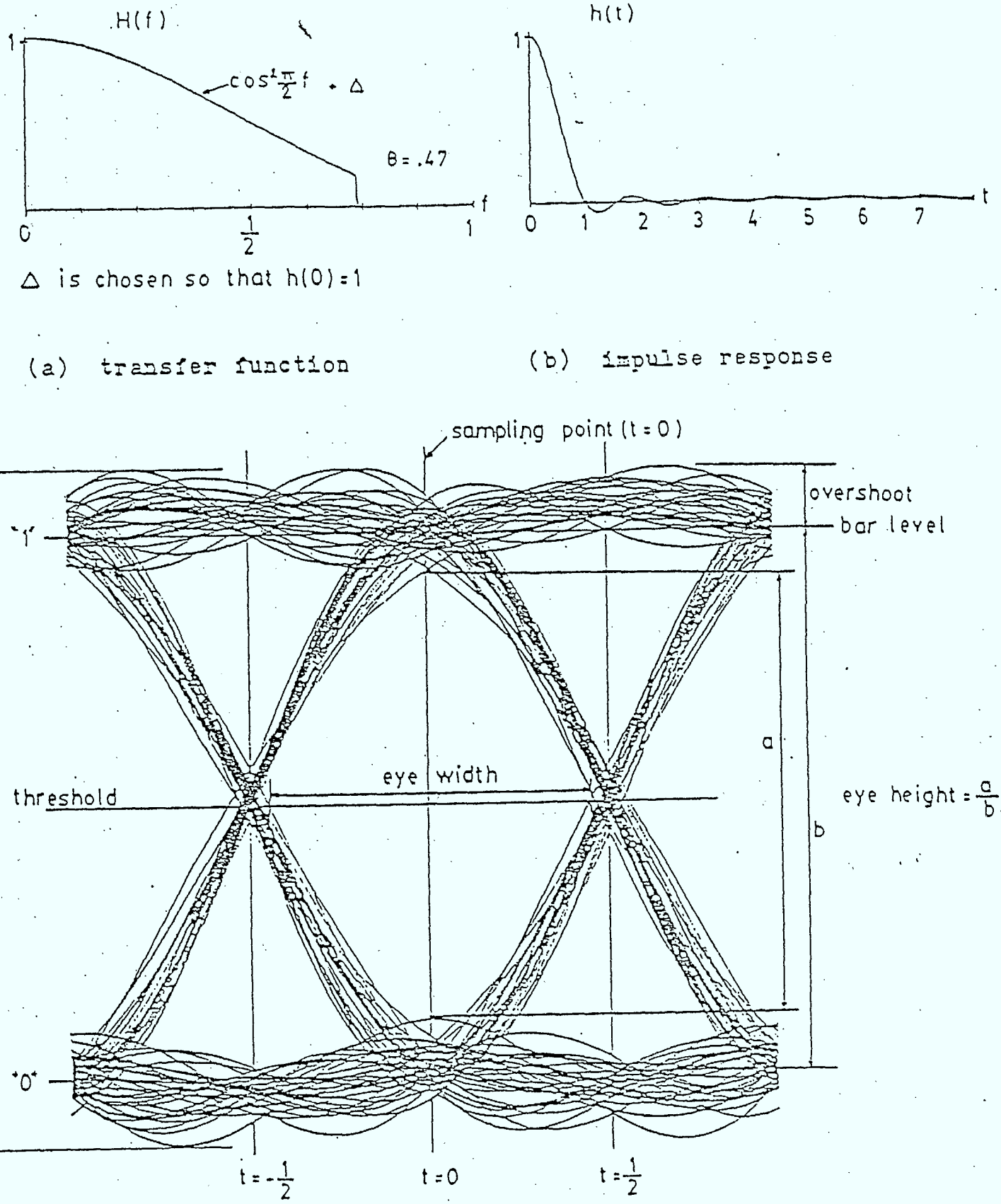

Figure 3.1 : The transfer function, impulse response, and eye diagram corresponding to a pulse shape that is almost the same as the one specified in BS-14 (from [14])

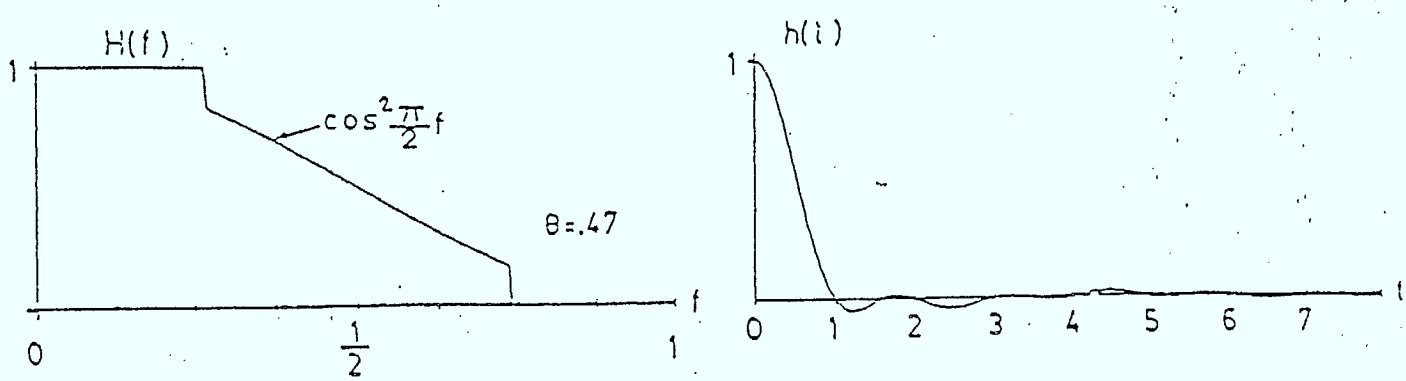

(a) transfer function

(b) impulse response

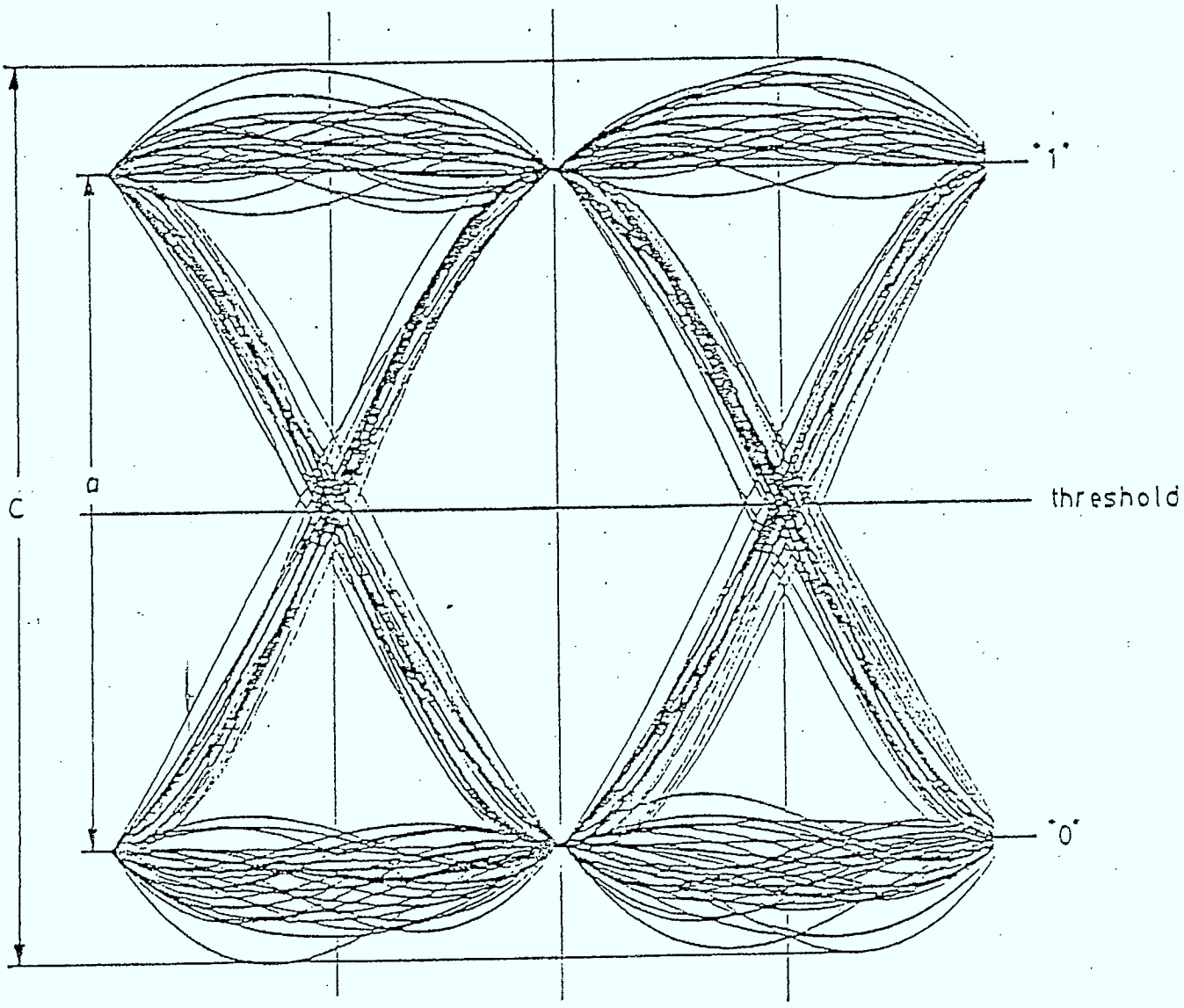

(c) eye diagram

Figure 3.2 : The transfer function, impulse response, and eye diagram that correspond to the pulse shape recommended in [14] and [15]

$$H(f) = 0.501 + 0.543 \cos [0.54856f]$$
$$- 0.015 \cos[(3)(0.54856)f]$$
$$- 0.035 \cos[(5)(0.54856)f]$$
$$- 0.002 \cos[(7)(0.54856)f] \qquad |f| \leq 4.0$$
$$+ 0.012 \cos[(9)(0.54856)f]$$
$$- 0.003 \cos[(13)(0.54856)f]$$

$$H(f) = -0.1883|f|^2 + 1.125|f| - 1.3045 \qquad 4.0 \leq |f| \leq 4.4$$

$$H(f) = 0 \qquad |f| \geq 4.4 \qquad (3.1)$$

where f is in MHz. This transfer function is illustrated in Figure 3.3.

The eye profile is shown in Figure 3.4. For this eye, $a/c \simeq 0.77$ (-2.3 dB), which is better than the pulse shape of Figure 3.2 by 0.2 dB. The shorter precursor and tail region of the impulse response, because there are no discontinuities in the transfer function, is the major reason for this. The 'a/c' for this pulse shape is 1.4 dB better than the truncated 100% raised cosine transfer function. The eye height and eye width for the eye profile of Figure 3.4 are 0.96 and 0.89 respectively. Both of these values are quite acceptable given the bandwidth limitation. Because of the generally good properties of the

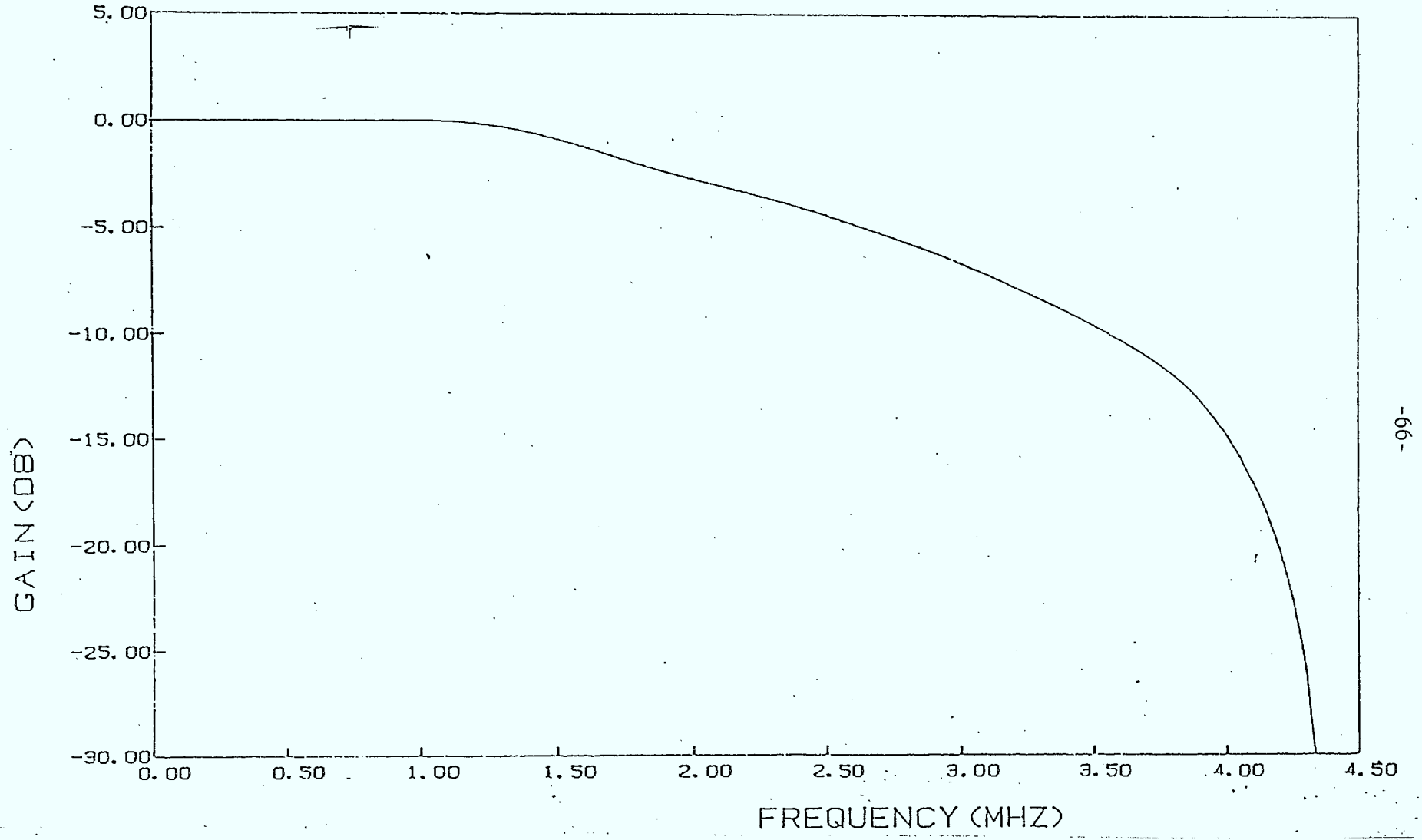

Figure 3.3 : The transfer function that is given by equation (3.1).

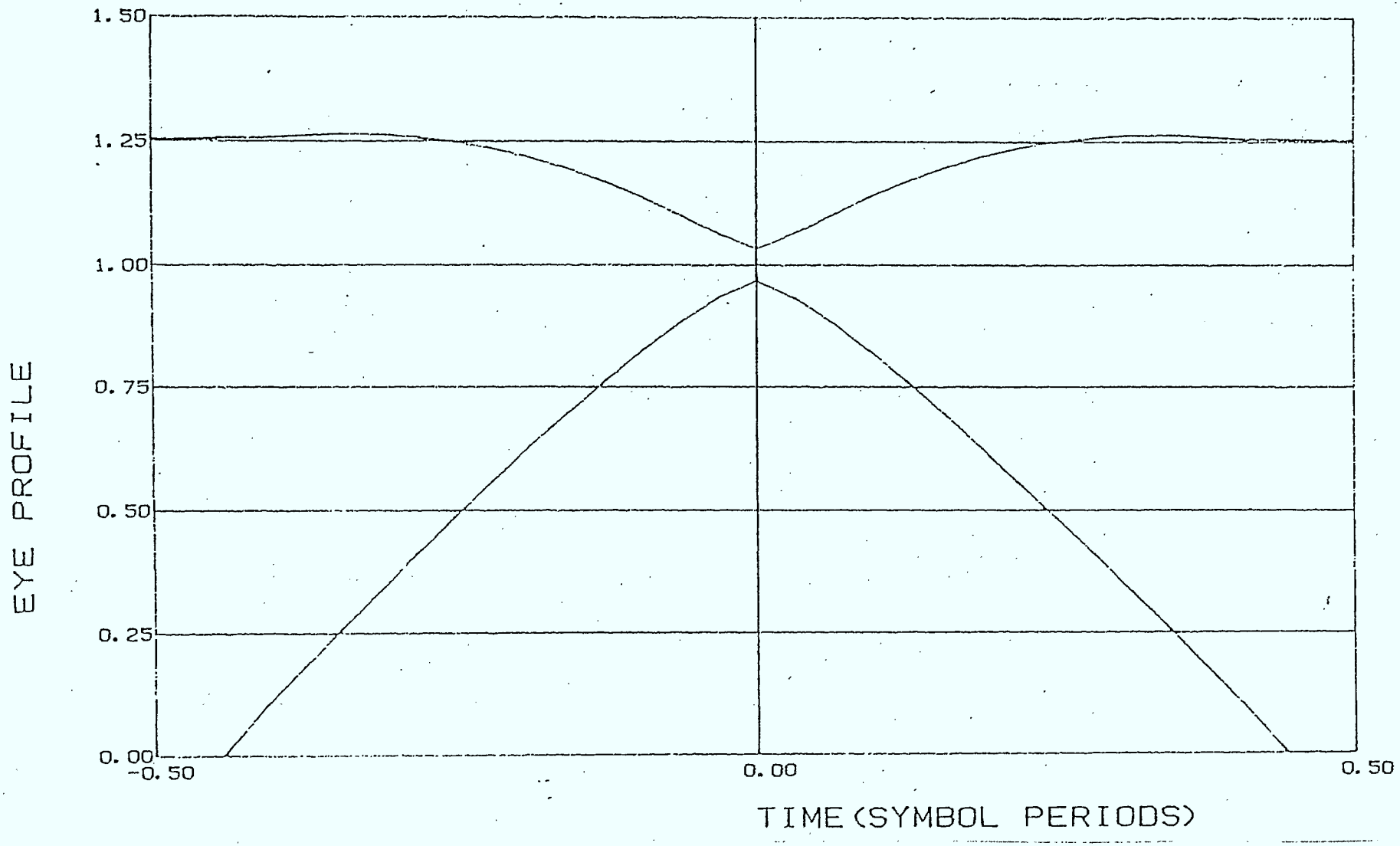

Figure 3.4 : The eye profile that corresponds to the transfer function given in equation (3.1).

transfer function given in equation (3.1), it is recommended as the nominal overall pulse shape transfer function.

In Figure 3.5, the transfer functions of some of the pulse shapes specified in [15], after a Hamming window has been applied to the impulse responses, are illustrated. The curve labels (i.e. 2C, 2D, 2E, 2F, 2G) refer to Figure 2 of reference [15]. Note that over the frequency range of interest, all the curves are within 2 dB of the curve 2E (the resulting transfer function after Hamming windowing of Sousa and Pasupathy's [14], [15], recommended pulse shape). Given that an optimal pulse shape transfer function will likely be within 2 dB of the recommended nominal transfer function and given that the uncertainty in the combined channel (i.e. transmit equipment, the propagation path, and receive equipment) will often exceed 2 dB, it may be that we are at the point of diminishing returns in the optimization of the overall pulse shape. To demonstrate this, consider a multipath channel with a single reflected path:

$$C(f) = 1 + c\, e^{-j2\pi fD}. \qquad (3.2)$$

This transfer function has a "rippled" magnitude and group delay characteristic. The size of the amplitude response ripple is a function of the strength of the reflected path. This is illustrated in Figure 3.6. Even for relatively modest multipath consisting of a single reflected path that is 10 dB weaker than the direct path, the resulting overall transfer function would be 2.4 dB higher than nominal at some frequencies and 3.3 dB lower than nominal at other frequencies. This level of ripple is on the order of the differences between transfer functions illustrated in Figure 3.5. What this suggests is that optimal pulse shaping is

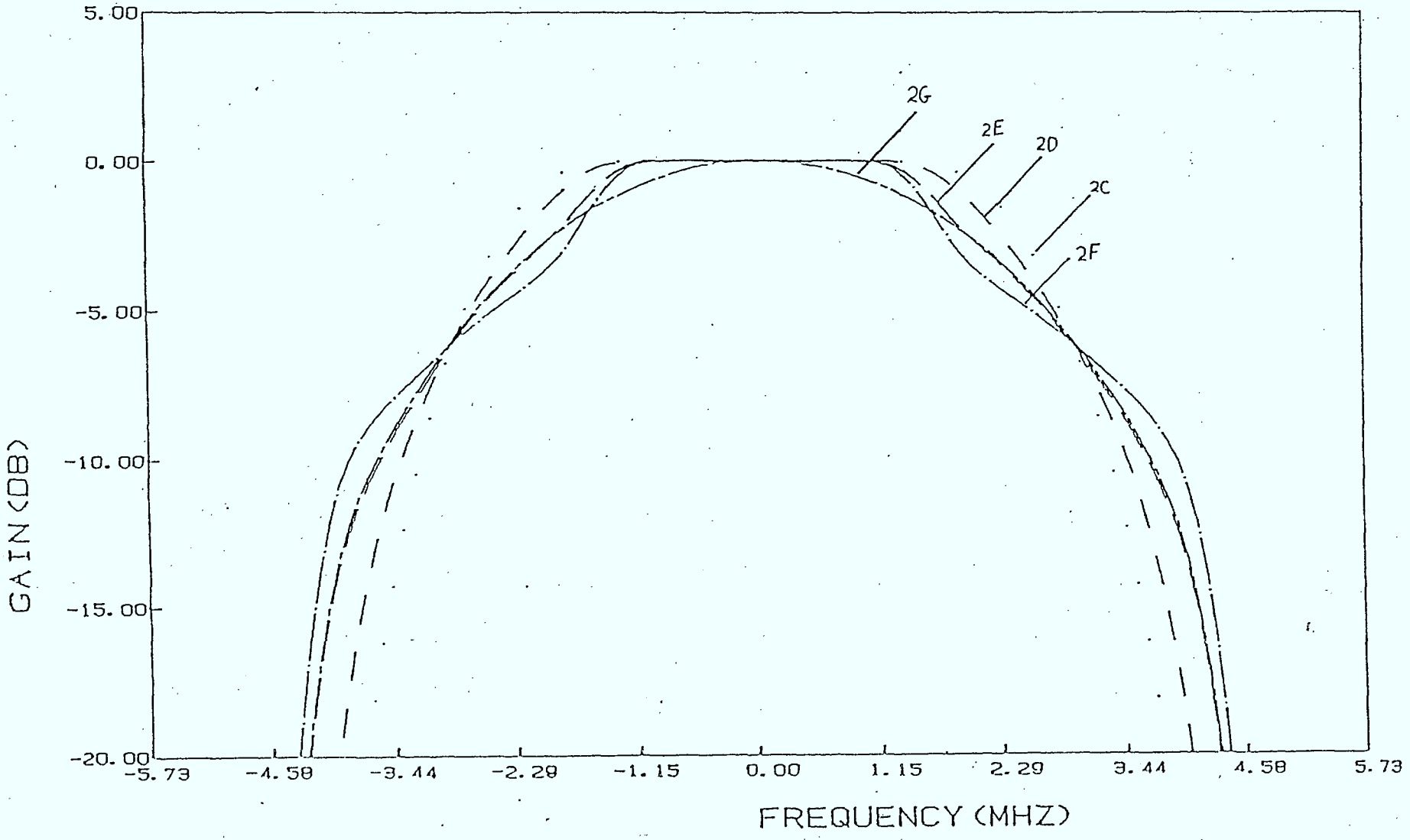

Figure 3.5 : The transfer functions of some of the pulse shapes derived in [15], after a Hamming window has been applied to the impulse responses.

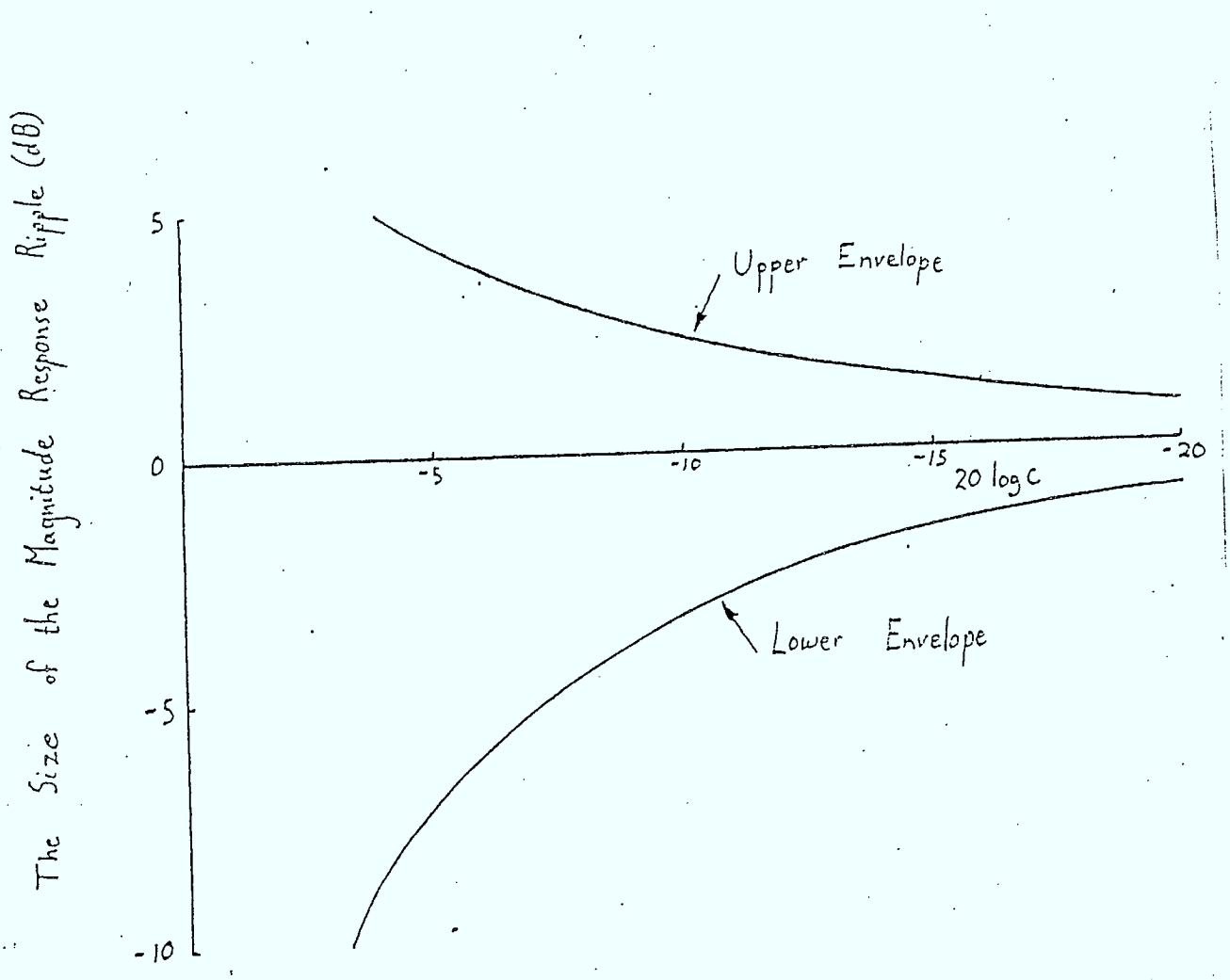

Figure 3.6 : The size of the magnitude response ripple as a function of the strength of the reflected path.

unlikely to be an effective weapon against multipath propagation, as relatively weak multipath can introduce significant distortion. If the overall channel response incorporates a "nominal multipath" channel, the overall response for a good channel could exhibit significant frequency response ripple, thereby compromising performance on good channels. In fact, performance would be compromised on any channel differing from the "nominal" multipath channel.

This would imply that the pulse shape should be designed for good channels (i.e. no multipath) and that any channel that is severely corrupted by multipath should be equalized at the receiver.

3.3 Pulse Shape Simulation Results

The purpose of this section is to assess the performance improvement which can be achieved by using the pulse shape that was recommended in the previous section (i.e. equation 3.1). The transmit and receive filter characteristics used were nominal (zero phase) transfer functions. The amplitude control constraint employed maintained the same peak overshoots at the baseband output of the receiver as those obtained with the existing BS-14 system. With this constraint active, the amplitude of the data impulses for the recommended pulse shape are a factor of 1.027 (0.2 dB) higher than those for the truncated 100% raised cosine (BS-14) pulse shape. The video or TV signal to noise ratio is independent of the data impulse amplitude. It controls only the input noise variance. Consequently the increase in data impulse amplitude results in an increase in the effective data signal to noise ratio. In addition to this 0.2 dB increase in effective signal to noise ratio, intersymbol

interference is also reduced with the recommended pulse shape. This is clearly illustrated in Figure 3.7, which shows the envelope of the eye diagrams for the truncated 100% raised cosine pulse shape and the recommended pulse shape.

The simulation results for an ideal channel in thermal noise environments are presented in Figure 3.8. For ideal recovery, the recommended pulse shape improvement is roughly 0.6 dB. For the averaging slicing level decoder, the recommended pulse shape improvement is in the same neighbourhood (approximately 0.4 dB). For the peak detector slicing level decoder, the recommended pulse shape improvement is approximately 0.75 dB. It is apparent that the reduced peak sensitivity and the reduction in intersymbol interference achieved by using the recommended pulse shape provides some performance improvement over the existing system for ideal channels corrupted by thermal noise.

The simulation results for the 13 dB PDUR multipath channel (echo magnitude versus delay plot shown in Figure 2.12) in a thermal noise environment are presented in Figure 3.9. Note that at each video signal to noise ratio, the error rate presented is averaged over five different random channels. Each random channel has the same echo magnitude versus delay characteristic, but different phases assigned to each echo (echo phases were randomly assigned). For both the averaging and peak detector slicing level decoders, there is a noticeable improvement obtained with the recommended pulse shape. For video signal to noise ratios above 30 dB, the improvement is roughly 0.7 dB with the averaging slicing level decoder and roughly 0.9 dB with the peak detector slicing level decoder. Note that the improvement gained by using an averaging slicing level decoder with the existing

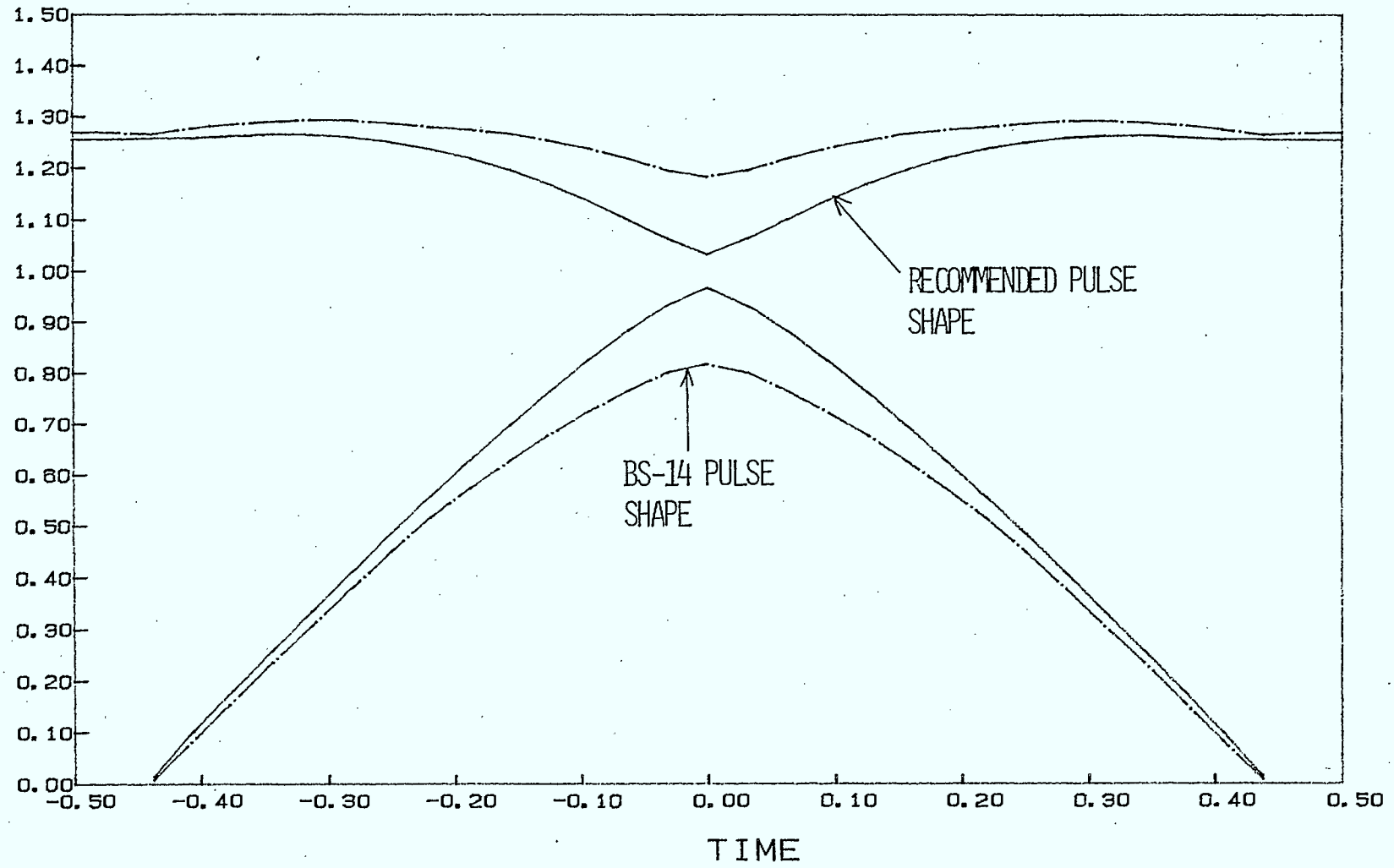

Figure 3.7: Upper and lower envelopes of the eye diagrams for the recommended and truncated 100% raised cosine pulse shapes.

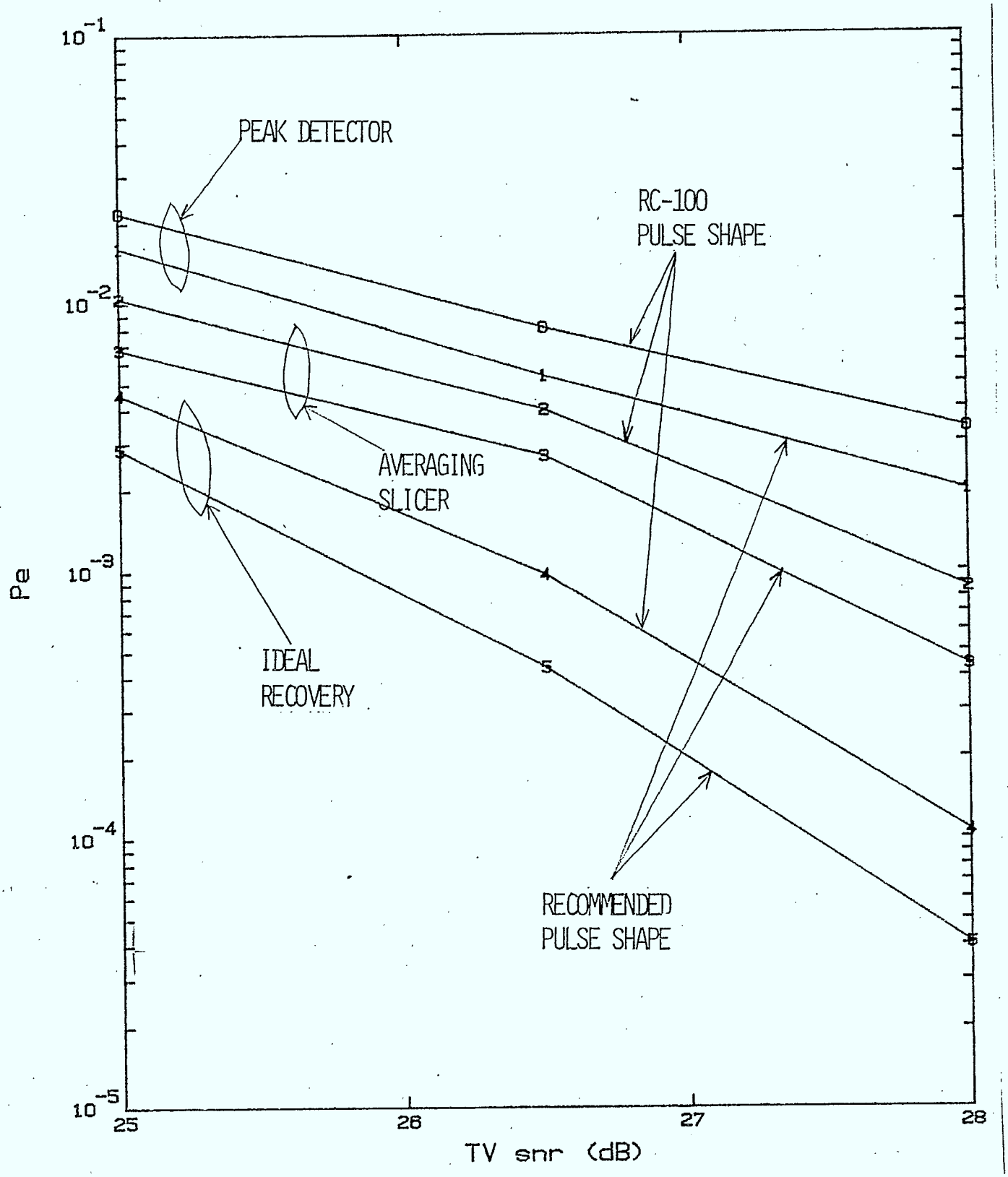

Figure 3.8: Pulse shape simulation results for an ideal channel in thermal noise environments.

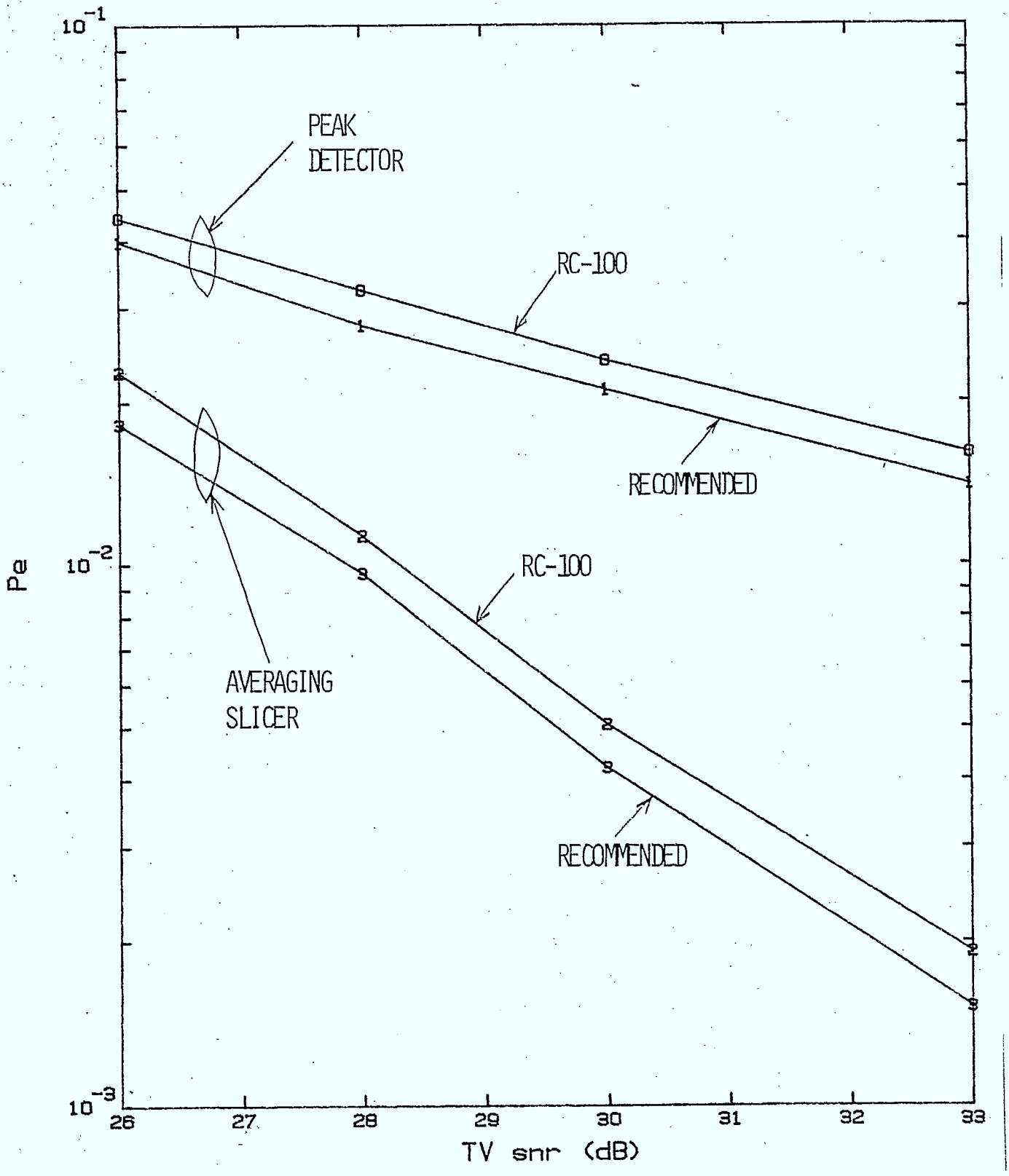

Figure 3.9: Pulse shape simulation results for the 13 dB PDUR multipath channel in a thermal noise environment.

truncated 100% raised cosine pulse shape far outweighs the improvement gained by using the recommended pulse shape with the presently used peak detector decoder.

The simulation results for a 20 dB PDUR multipath channel (whose echo magnitude versus delay plot is shown in Figure 2.14) in thermal noise environment are presented in Figure 3.10. A noticeable improvement (roughly 0.6 - 0.9 dB) is obtained with the recommended pulse shape for both the averaging and peak detector slicing level decoders. Note that this is in part due to the increase in the amplitude of the data signal that can be transmitted when the recommended pulse shape is used (because of reduced overshoots). The superiority of the averaging slicing level decoder is clearly evident in Figure 3.10.

The simulation results for a 14 dB PDUR multipath channel (echo magnitude versus delay plot shown in Figure 2.13) in a thermal noise environment are presented in Figure 3.11. A noticeable improvement, roughly 0.5 dB, is achieved with the recommended pulse shape. The most surprising thing about these results is the apparent converging of the performance curves for the averaging and peak detector slicing level decoders for this multipath channel. For the 13 dB and 20 dB PDUR multipath chanels, significant improvements were obtained with the averaging slicing level decoder. The performance of the peak detector slicing level decoder is better with the 14 dB PDUR channel than it is with the 20 dB PDUR channel. This is surprising because the 20 dB PDUR multipath channel is a better video quality channel. Justification of the results obtained in Figure 3.11 is provided below.

It has been discovered that the slicing level error distribution is noticeably biased in the negative direction for the peak detector slicing level decoder. That is the

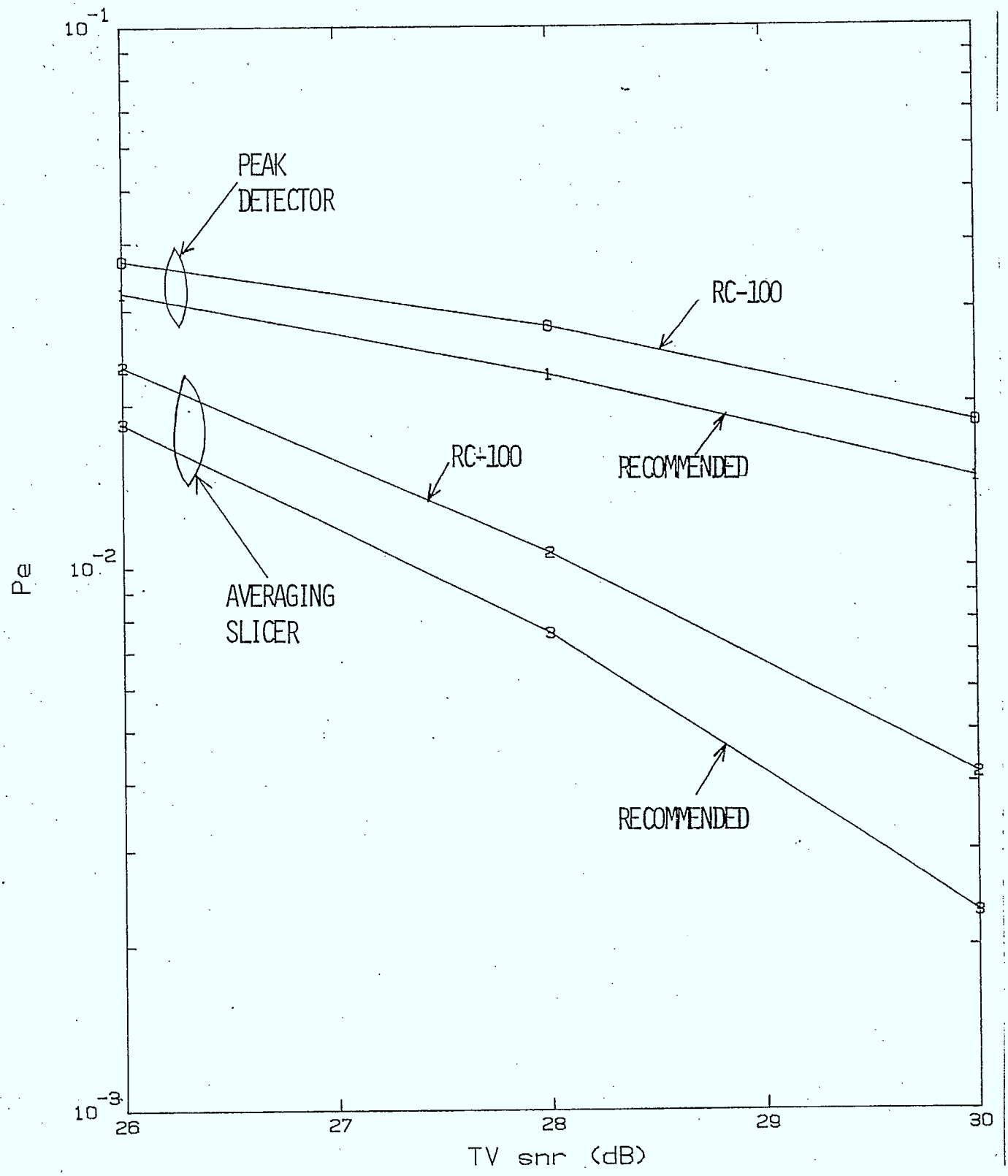

Figure 3.10: Pulse shape simulation results for the 20 dB PDUR multipath channel in a thermal noise environment.

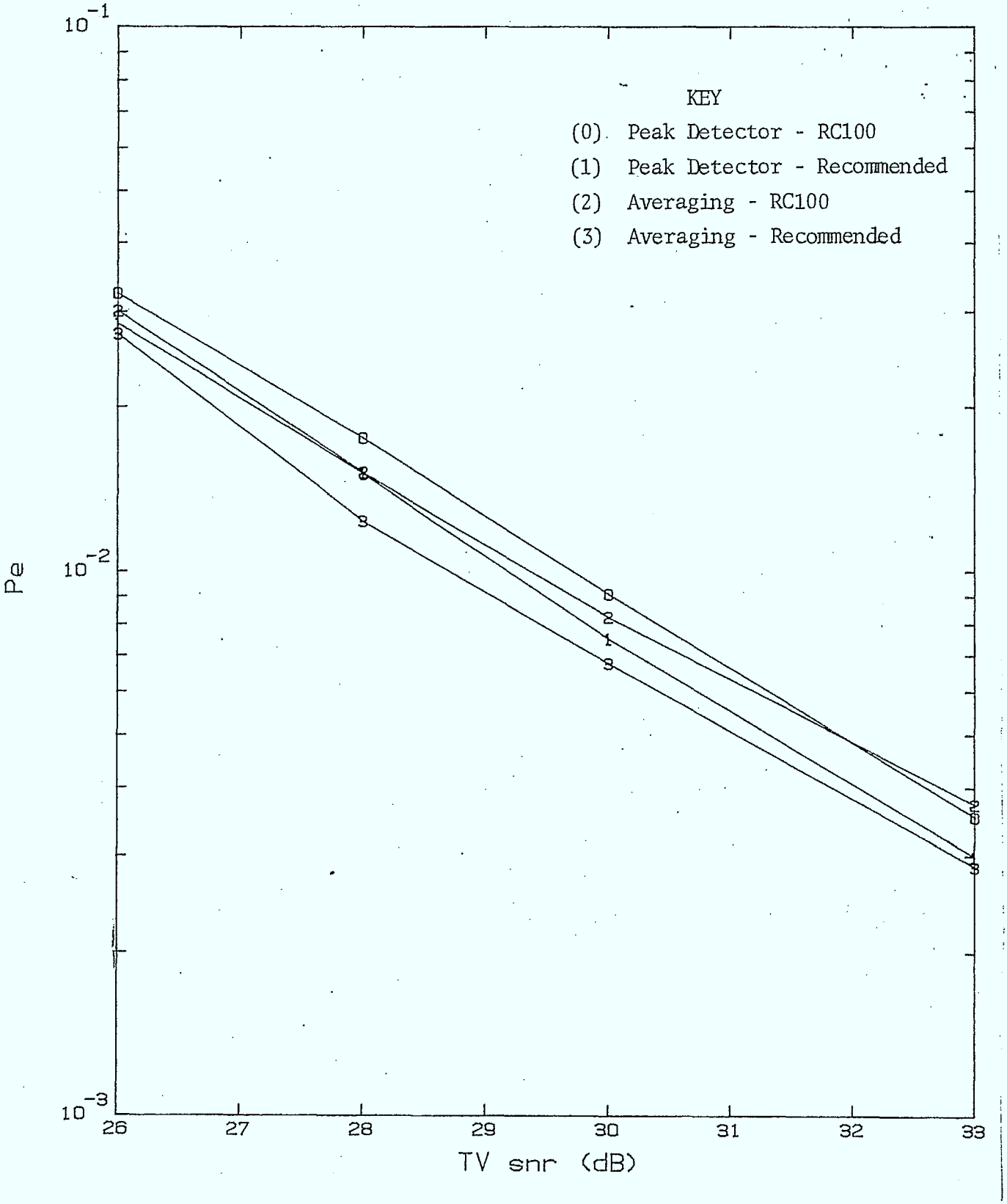

Figure 3.11: Pulse shape simulation results for the 14 dB PDUR multipath channel in a thermal noise environment.

estimated slicing level tends to be below the theoretical dc-offset of the signal. A slicing level error distribution, for a peak detector decoder with an ideal channel in a thermal noise environment (video SNR = 28 dB), provided in Figure 3.12 demonstrates this. The mean offset is roughly -0.018 V and the theoretical slicing level for a modulation index of 87.5% is 0.343 V. The received data impulse amplitude, in the absence of intersymbol interference is a = 0.12 V. For a slicing level error equal to the mean offset given above, the degradation factor relative to ideal recovery would be:

$$\text{Degrad} = 20 \log_{10} \left(\frac{a}{a - 0.018}\right) = 1.4 \text{ dB}.$$

Note that this calculation assumes ideal clock recovery. However it is well known that slicing level errors introduce clock recovery offsets, which would result in further degradation. Figure 3.13 presents the slicing level error histogram for the averaging decoder for the same scenario as used in deriving Figure 3.12 for the peak detector decoder. With the averaging decoder the mean offset in the slicing level is reduced considerably. The standard deviation of the distribution is also smaller than obtained with the peak detector. This is not surprising in light of the non-linear behaviour of the peak detection circuits.

The slicing level error distribution for the peak detector decoder was obtained using peak detector reference voltages and charging time constants extracted from observed upper and lower peak detector responses [36]. As can be seen from Figure 3.14, the reference voltages for the upper and lower peak detectors are not symmetrically located about the

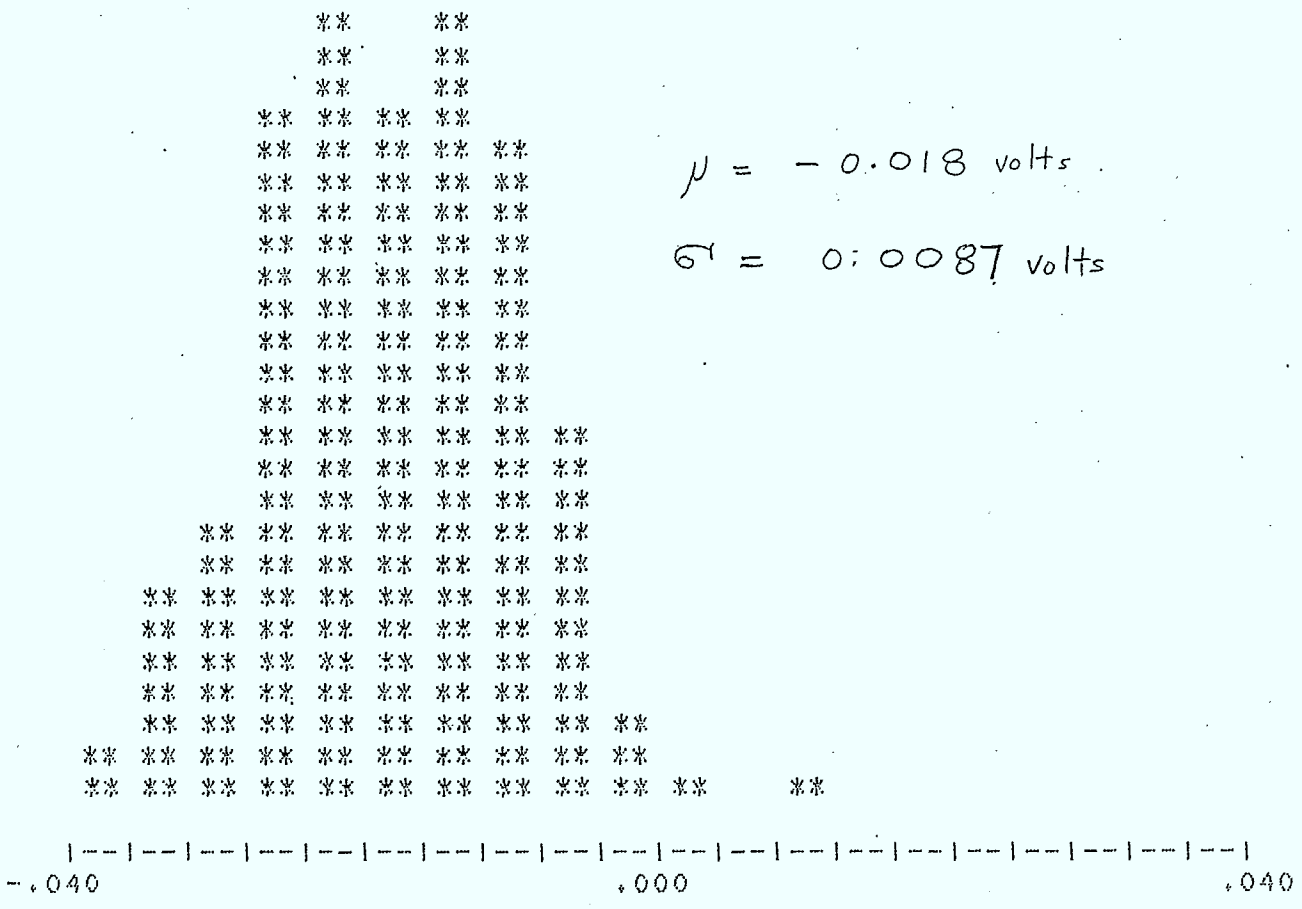

Figure 3.12 : Slicing level error histogram for the peak detector slicing level estimation technique (ideal channel and video SNR = 28 dB)

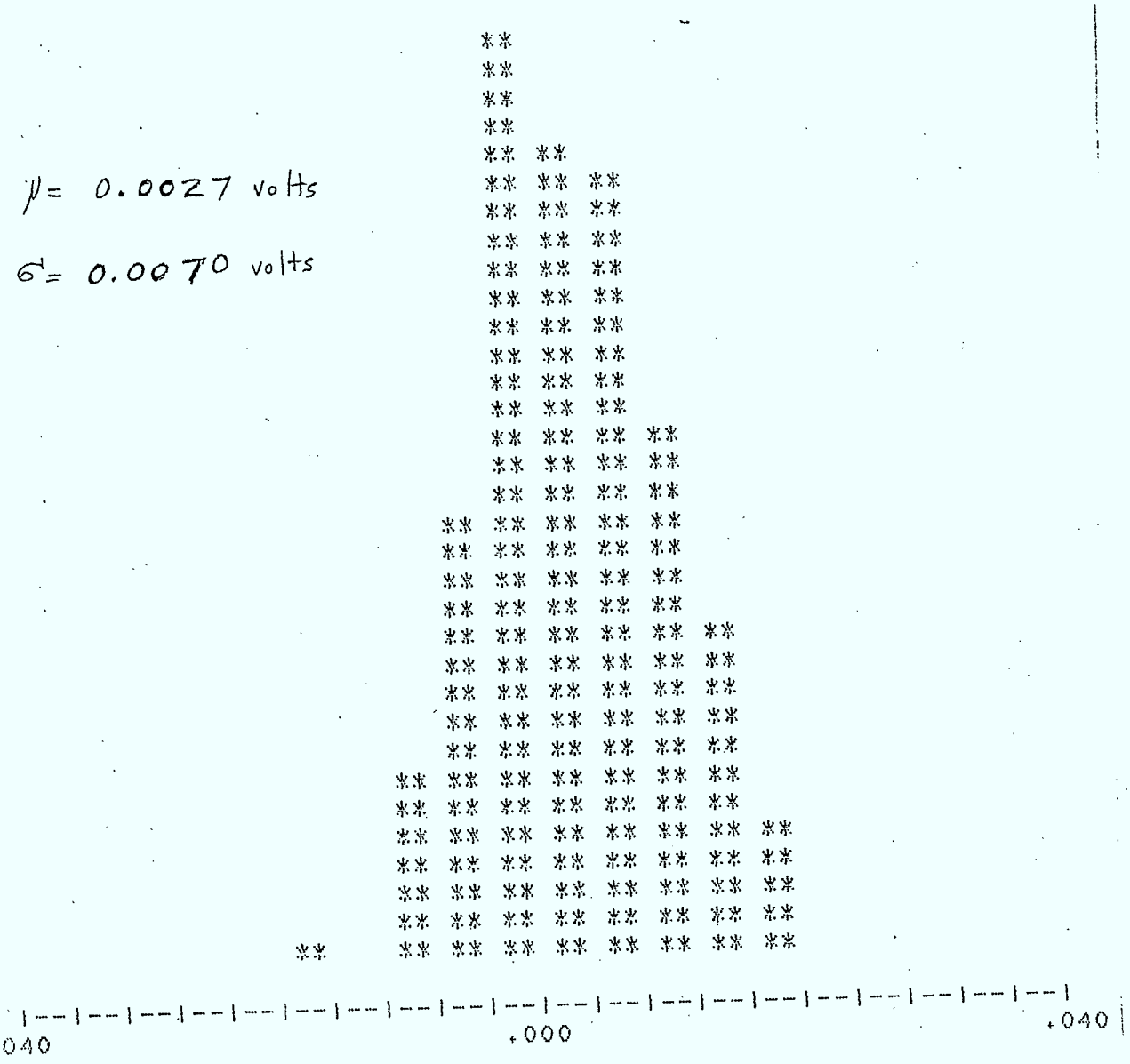

Figure 3.13 : Slicing level error histogram for the averaging slicing level estimation technique (ideal channel and video SNR = 28 dB)

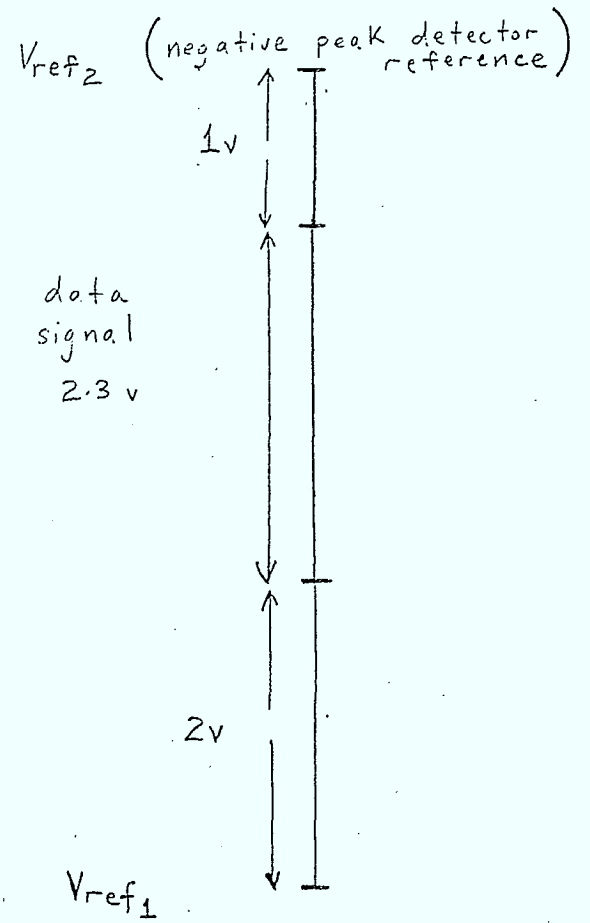

a) Signal Voltages For Decoder

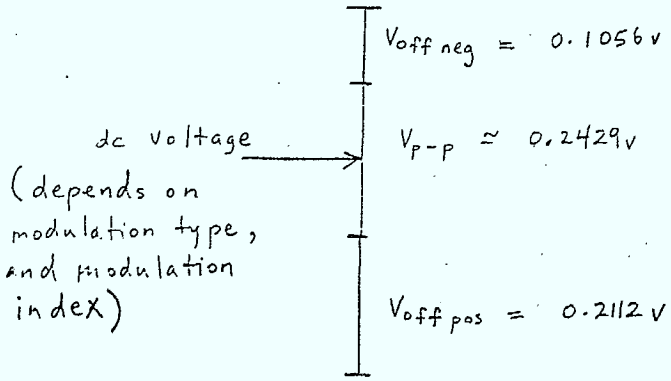

b) Signal Voltages In The Simulation

Figure 3.14 : Asymmetric peak detector reference voltages (from [46])

nominal dc-offset of the teletext signal. The activation period for the peak detection circuits is restricted because the slicing level must be established before the end of the twelfth bit period for clock recovery. Ignoring the first four to five bits of the clock sync signal, as the present decoder does, makes the situation even worse. The slicing level bias in the negative direction tends to suggst that the upper peak detector is not attaining the upper signal envelope soon enough. This is not surprising in light of the asymmetrical reference voltage settings and the short observation window.

For multipath channels with relatively strong close in echoes, like the 14 dB and 20 dB PDUR channels used in this simulation, the dc-offset of the signal is strongly dependent on the phase of the dominant echo (constructive, destructive, or quadrature). This effect is illustrated in Figure 3.15 for constructive (ϕ=0°) and destructive (ϕ=180°) inphase echoes for a simple single echo channel. It is apparent that constructive inphase echoes tend to worsen the asymmetric reference voltage settings of the peak detector circuits. This suggests that more severe slicing level bias errors would occur for constructive inphase echoes. Figure 3.16 shows the slicing level error distribution for the peak detector slicer for a 20 dB PDUR channel when the phase of the predominate close in echo is -12.9° (essentially a constructive echo). In this case, the error performance is still relatively poor (2.77×10^{-2}) at a reasonably good video signal to noise ratio of 30 dB. In fact, there was even a packet rejected because it had greater than 30% errors, signifying a loss of synchronization. In this case, the slicing level bias error is considerably worse than it was for the ideal channel, and is a major contributing factor to the poor error performance. However, when the echo phase is predominately quadrature (ϕ=101.7°), the bit

$$c(t) = \delta(t) + 0.316\, e^{+j\phi}\, \delta(t - 2.5\mu s)$$

(a) Single '-10dB' echo channel

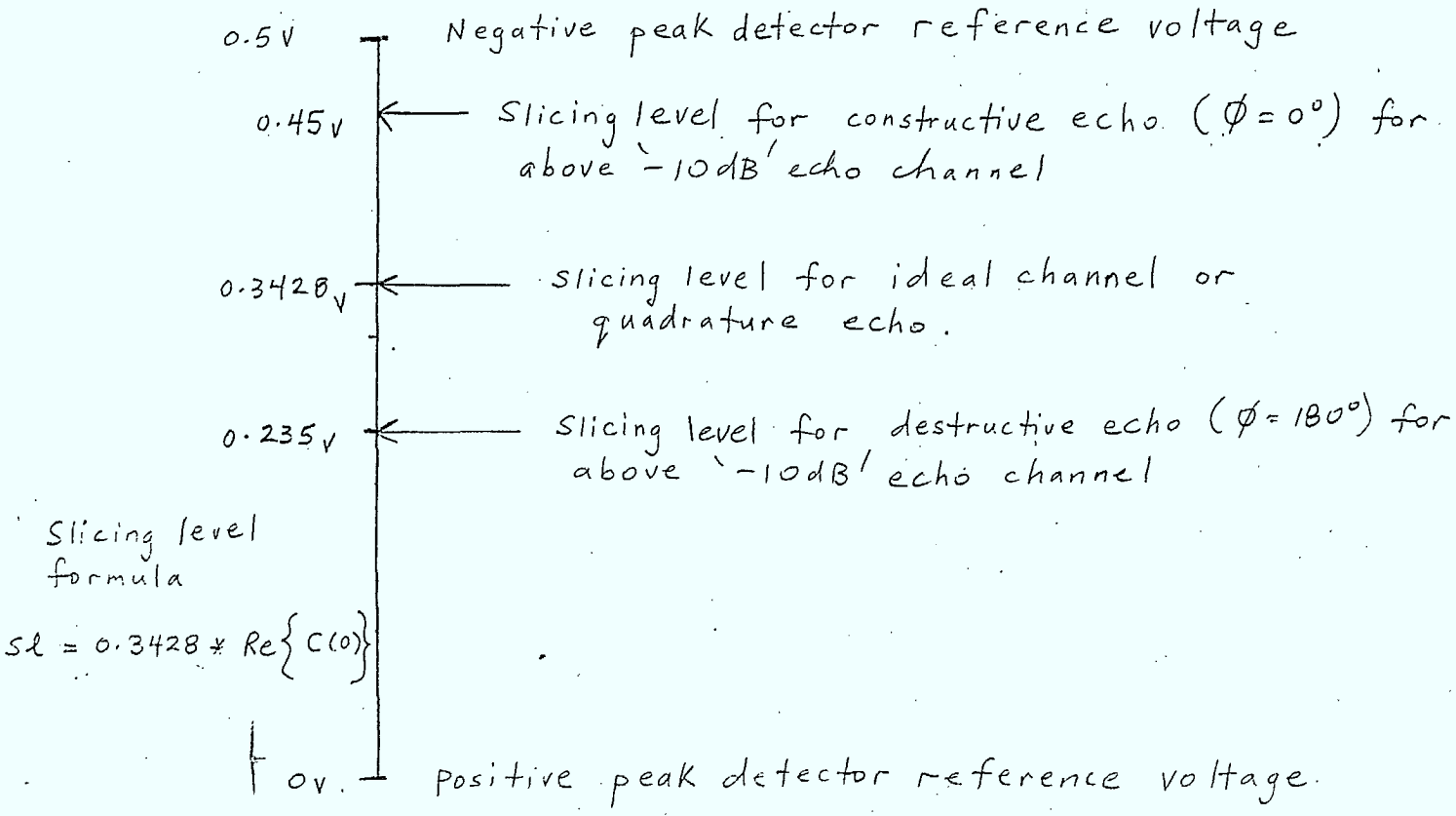

b) Slicing levels compared to reference settings for constructive and destruction echoes with the single '-10dB' echo channel.

Figure 3.15 : Variations in slicing level due to echo phasing with a single echo channel.

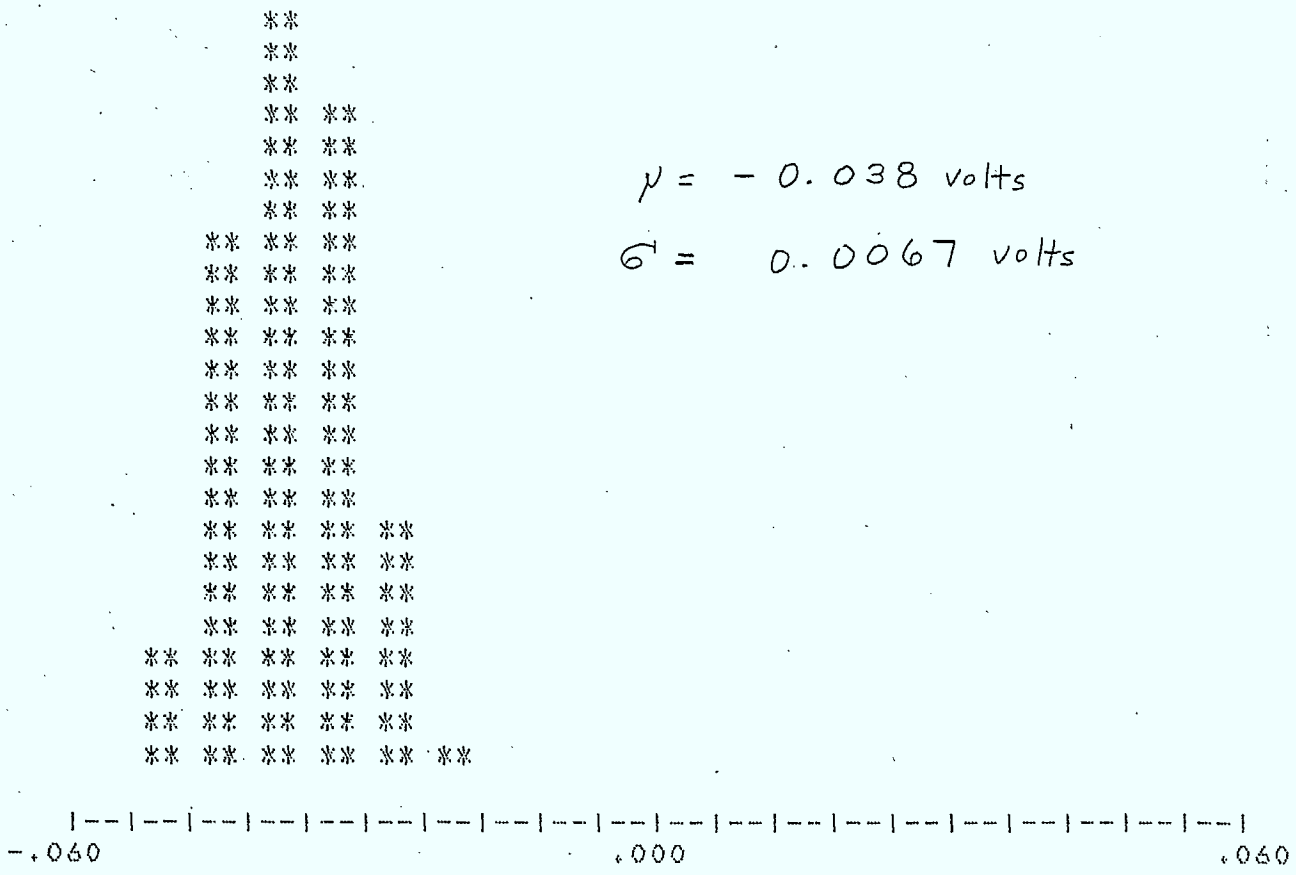

Figure 3.16 : Slicing level error histogram for the peak detector slicing level estimation technique (20 dB PDUR multipath channel and video SNR = 30dB)

error rate at a video signal to noise ratio of 30 dB is 2.22×10^{-3}. This performance improvement can be attributed to a smaller slicing level bias error and decreased intersymbol interference introduced by quadrature echoes.

The performance of the averaging slicing level decoder is not so drastically affected by predominately constructive inphase echoes. The error rate for the situation where the predominate echo has a phase of -12.9° is considerably better with the averaging slicing level decoder ($p_e=2.02\times10^{-3}$). The slicing level error distribution for this case is shown in Figure 3.17. A comparison of Figure 3.17 with its counterpart for the peak detector slicer, Figure 3.16, reveals the major reason for the superiority of the averaging slicer decoder; namely, reduced slicing level bias errors.

Similar results are obtained with the 13 dB PDUR multipath channel. The peak detector slicing level error distribution for the situation where the two dominate echoes are predominately constructive inphase echoes (video SNR=33 dB) is presented in Figure 3.18. A very pronounced negative slicing level bias error is observed. The error rate in this case is approximately 4×10^{-2}, which is quite poor. With more favourable (less constructive) echo phasing, the error rate is reduced to approximately 6×10^{-3}. The peak detector slicing level error distribution in this case (see Figure 3.19) has a less severe bias, thereby resulting in improved performance. With the averaging slicer, the error rate for the situation where the dominate echoes are essentially inphase is 4.5×10^{-4}. Relative to the peak detector decoder, this represents an improvement of two orders of magnitude. This improvement is not surprising

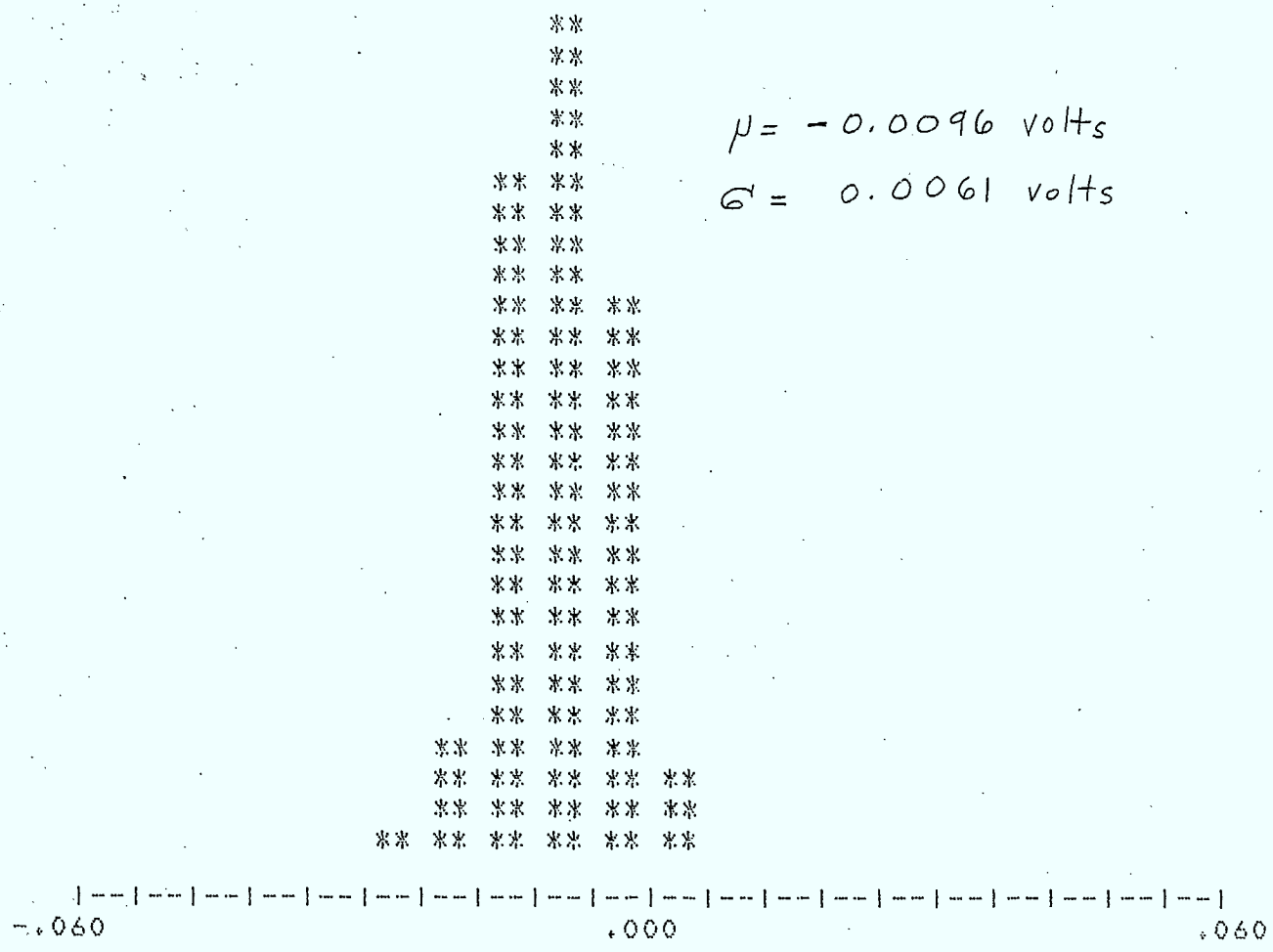

Figure 3.17 : Slicing level error histogram for the averaging slicing level estimation technique (20 dB PDUR multipath channel and video SNR = 30 dB)

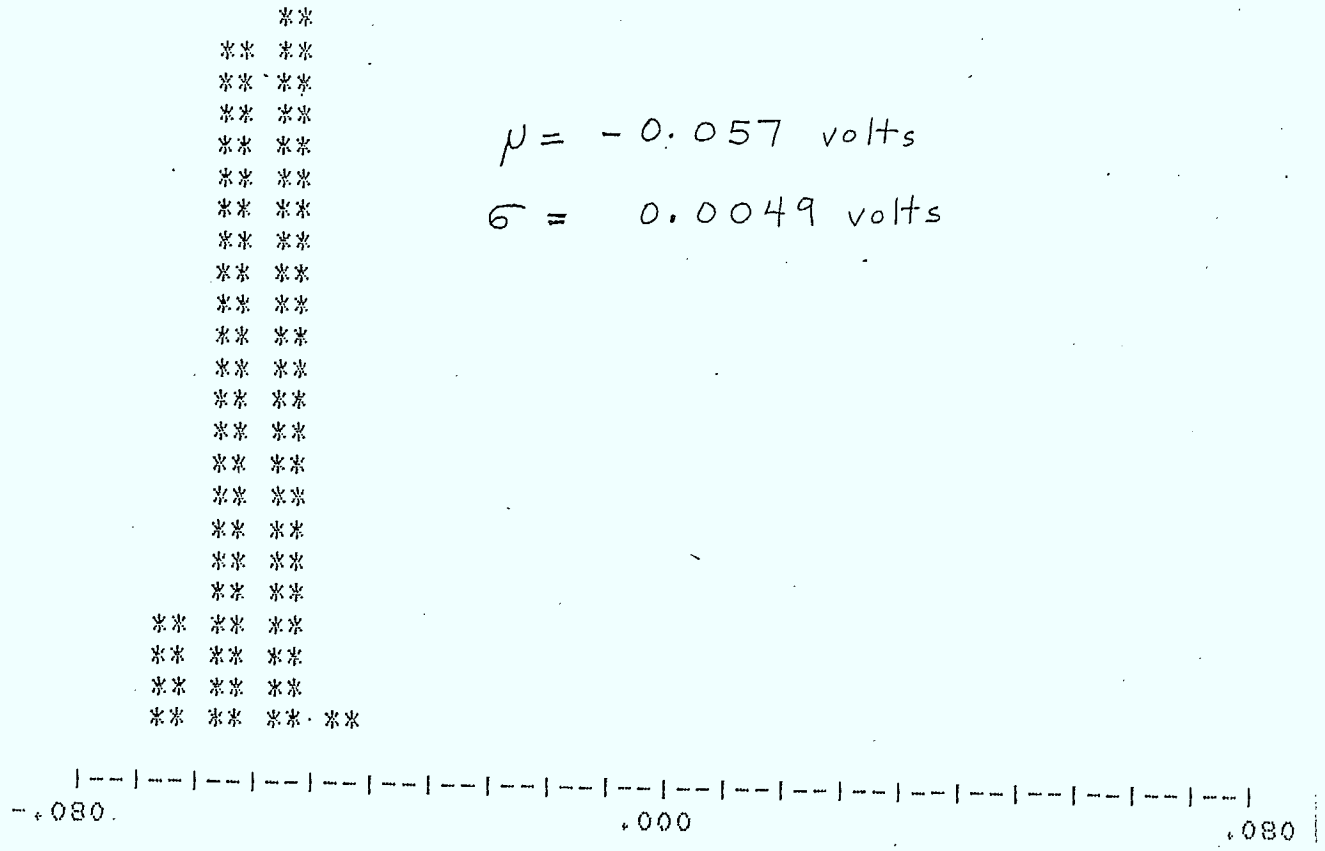

Figure 3.18 : Peak detector slicing level error histogram for the 13 dB PDUR multipath channel (dominant echoes predominately constructive) for a video SNR of 33 dB.

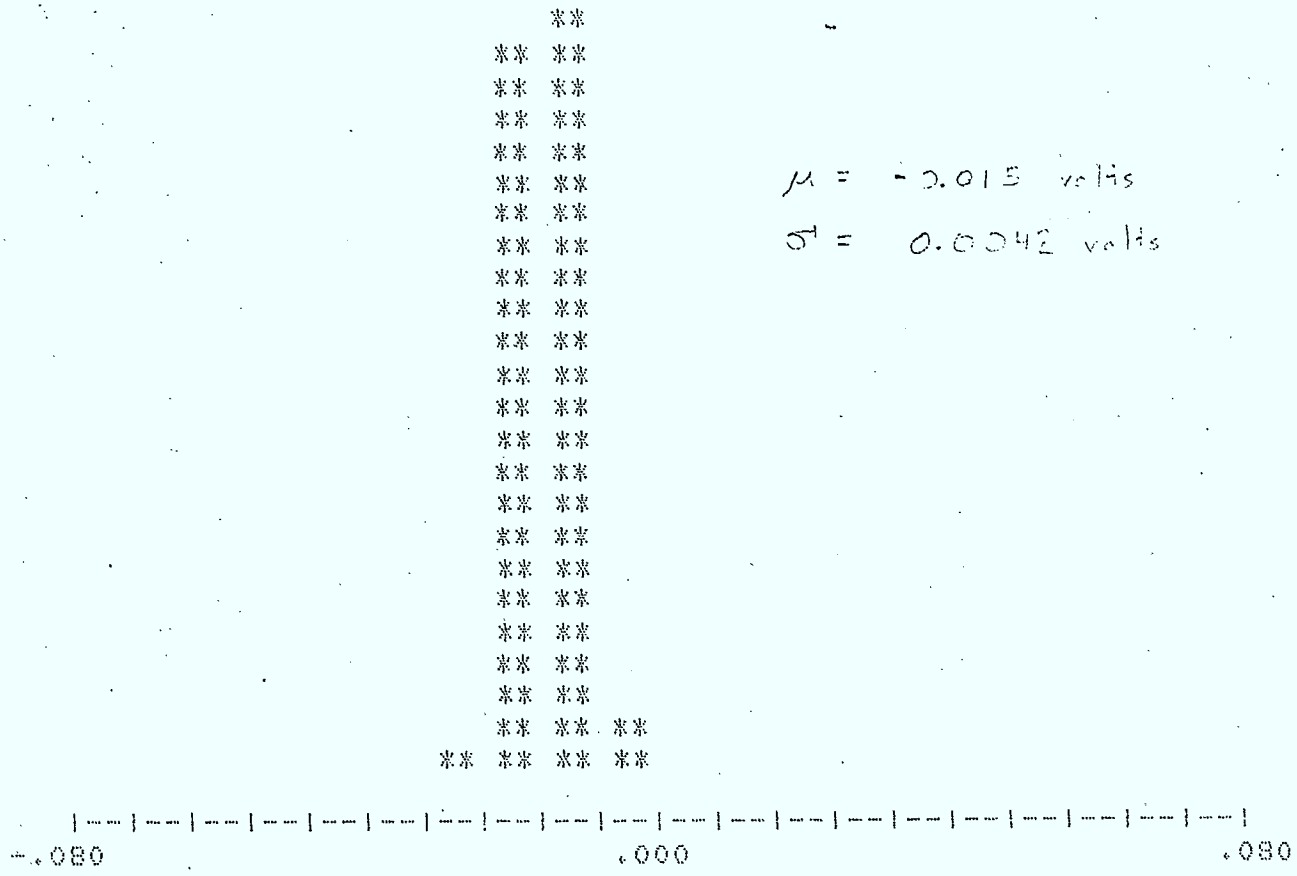

Figure 3.19 : Peak detector slicing level error histogram for the 13 dB PDUR multipath channel (dominant echoes predominately quadrature) for a video SNR of 33 dB.

when one compares the averaging slicing level error distribution for this case (see Figure 3.20) with the peak detector slicing level error distribution of Figure 3.18.

When examining performance with a specific multipath channel, five distinct channels are constructed by randomizing the echo phase. This was done to obtain some indication for the variation of performance with changing echo phase, which is in practice a highly variable and volatile parameter. The intention was not to statistically characterize system performance over all possible channels with a specific echo magnitude versus delay characteristic. Such a task would be formidable, simply because the number of channel perturbations that would have to be investigated becomes prohibitive. On the detailed output listings for each simulation run, the phases assigned to the dominant echoes are provided. This information can be useful for rationalizing simulation results. An examination of these output listings for the 13 dB and 20 dB PDUR multipath channels revealed that the worst case situations for the peak detector decoder (constructive, inphase echoes) occurred. Figures 3.16 and 3.18 clearly demonstrate the effect of such echoes on the peak detector slicing level error. An error analysis program has been developed to determine the average error rate, standard deviation, and confidence interval estimates. The output of this program for the 13 dB and 20 dB PDUR multipath channel runs is provided in Table 3.1. The standard deviation for these runs indicates considerable variability in bit error rate performance.

An investigation of the detailed output listings for the 14 dB PDUR multipath channel runs revealed that the worst case situation (constructive echoes) did not occur. As a result, one would expect the peak detector slicing level errors to

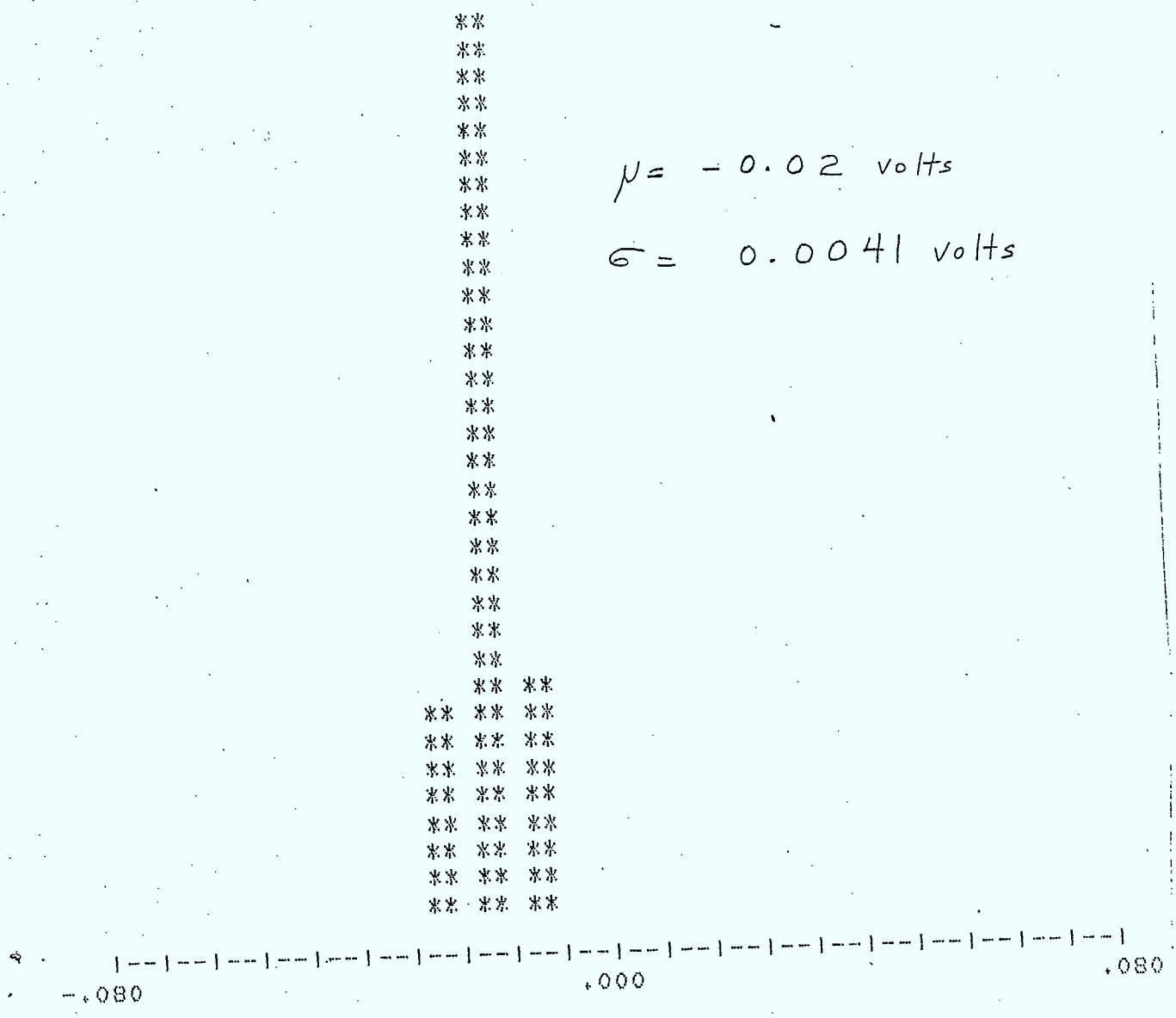

Figure 3.20 : Averaging slicing level error histogram for the 13 dB PDUR multipath channel (dominate echoes predominately constructive) for a video SNR of 33 dB

be much less severe than obtained with the other multipath channels. This is immediately apparent from the peak detector slicing level error distribution shown in Figure 3.21, for the 14 dB PDUR multipath channel. It is not surprising that error performance with the peak detector decoder would be better with the runs conducted with the 14 dB PDUR channel than for those conducted with the 13 dB and 20 dB PDUR channels. Consequently, the surprising result of improved peak detector decoder performance on a lower quality video grade channel, presented in Figure 3.11, can be justified on the basis of reduced slicing level bias errors. As indicated in Table 3.2, there is less variance in error performance for the simulation runs conducted with the 14 dB PDUR channel.

Given the asymmetric reference voltage settings for the peak detector circuits and the short estimation window, it is not surprising that the peak detector decoder is sensitive to multipath. Decreasing the charging time constant is one way to ensure that the peak detector attain their desired levels. This is not recommended because it would make the system even more sensitive to noise peaks. Ensuring symmetric reference voltage settings under ideal channel conditions and increasing the length of the activation period would be sensible improvements. Activating the peak detection circuits earlier (after the first bit of the clock sync signal) is advisable. Decoupling the slicing level estimation and clock phase extraction would allow for an expansion of the slicing level estimation window.

Given the clear superiority of the averaging slicing level technique demonstrated in Figures 3.9 and 3.10, attempts to improve the peak detection slicer should be regarded as interim or temporary solutions. Future decoders should employ the averaging technique for slicing level estimation. It must be remarked that any slicing level estimation

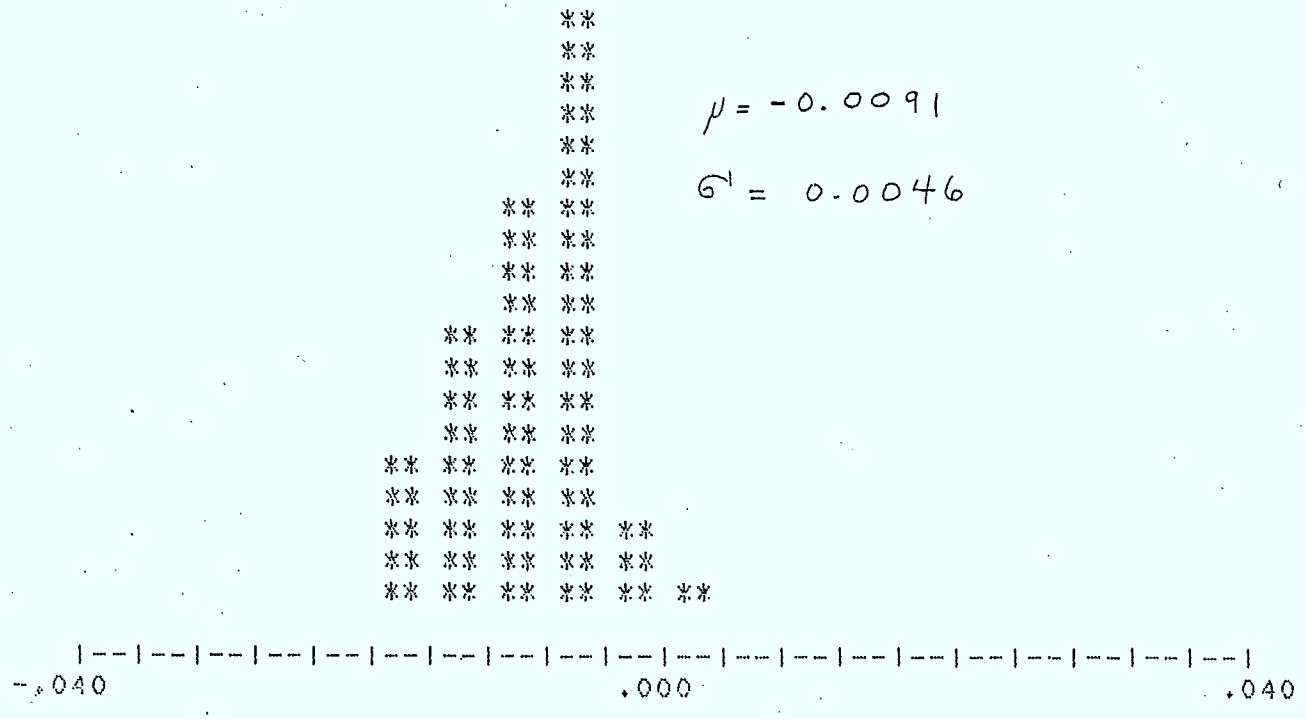

Figure 3.21 : Peak detector slicing level error histogram for the 14 dB PDUR multipath channel for a video SNR of 33 dB.

	SNR	ERROR	STANDARD DEV	% PACKET LOSS
PDUR-13	26	2.3E-02	6.6E-03	0.4
	38	1.1E-02	4.7E-03	0.4
	30	5.1E-03	1.7E-03	0.0
	33	1.9E-03	1.2E-03	0.0
PDUR-20	26	2.4E-02	1.4E-02	2.4
	28	1.1E-02	7.3E-03	0.8
	30	4.2E-03	3.4E-03	0.5

Table 3.1

	SNR	ERROR	STANDRAD DEV	% PACKET LOSS
PDUR-14	26	3.0E-02	6.6E-03	2.8
	28	1.5E-02	3.2E-03	2.8
	30	8.2E-03	2.6E-03	0.8
	33	3.7E-03	1.7E-03	0.0

Table 3.2

technique that is restricted to using the clock sync signal will be adversely effected by multipath, which can superimpose portions of the colour burst and line sync pulse onto the clock sync signal. Note that if the slicing level were determined later in the burst (at a time exceeding the largest multipath spread), a better estimate of the teletext dc offset would be obtained. Consequently, adaptive slicing level estimation would yield better performance. The difficulty with adaptive slicing level estimation is complexity. Because the data burst can itself introduce a dc component (there is no guarantee or protection against a long string of bits with the same polarity), the process must be decision directed. If it were possible to change the format of the teletext line, significant performance improvements in multipath environments could be obtained without adaptive slicing level estimation. This involves moving the clock sync and word sync bytes to the middle of the teletext line, and using a half line CCD delay line to delay the signal for extracting the data signal after the slicing level and clock phase have been determined. In this case, severe multipath induced slicing level bias errors would be removed. This proposal should be given serious consideration, because it might alleviate the need for an expensive adaptive teletext equalizer.

Simulation results for a 20 dB PDUR multipath channel in a mixture of impulse and gaussian noise (impulse noise 125.89 times stronger than gaussian component) are presented in Figure 3.22. For the averaging decoder, performance with the recommended pulse shape is slightly better than with the truncated 100% raised cosine pulse shape. With the peak detector decoder, the improvement with the recommended pulse shape is considerable. The clear superiority of the

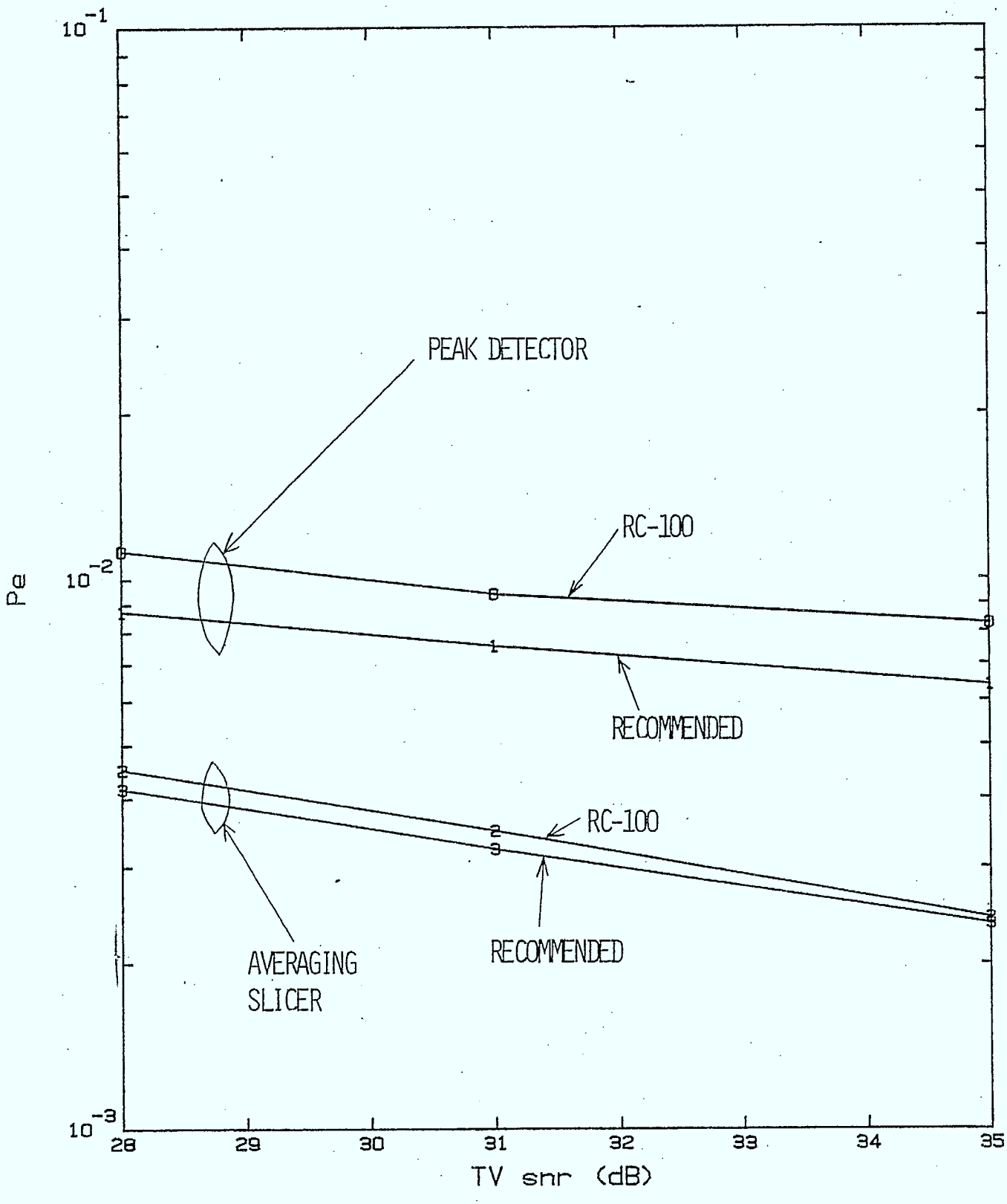

Figure 3.22: Pulse shape simulation results for the 20 dB PDUR multipath channel in an impulse noise dominated environment.

averaging slicing level decoder is evident in Figure 3.22. The probability of error curves exhibit a flatness which is characteristic of impulse noise dominanted environments. It is clear that improving the slicing level estimation technique provides a greater performance gain than simply changing the pulse shape.

4.0 TELIDON SYSTEM PERFORMANCE WITH QUASI-SYNCHRONOUS DETECTION

This section begins with a brief introduction of the television broadcast teletext system model and quasi-synchronous detection. The complex baseband representation of a television broadcast teletext system is provided in Figure 4.1. Due to the asymmetric nature of the transmitter and receiver filtering operations, a quadrature component signal is generated. The baseband signal generated by the receiver depends on the type of video detector. The simplest detector is the envelope or diode detector. The quadrature component gives rise to non-linear distortion.

Bluestein [1], has modelled the vestigial sideband filter mathematically (at complex baseband), and computed the ideal envelope detector response for various test signals (2T pulse and, modulated 12.5T pulse). Non-linear distortion causes a 2T pulse transition from zero carrier to peak carrier pulse to be broadened. However, when the 2T pulse transition is from peak to zero carrier, the envelope detected pulse is narrowed. For teletext signals, the pulses with polarity closest to the black video level will be broadened considerably, and the pulses with polarity closest to the white video level will be narrowed considerably.

The quadrature distortion introduced by envelope detectors will clearly have a significant performance penalty on broadcast teletext systems. The movement in the television industry for the last several years has been towards synchronous demodulation. If the carrier frequency and phase are properly determined, quadrature distortion can ideally be completely eliminated from the video output. The premise on which the vestigial sideband television system is based is that the receiver filter is constructed in such a fashion that coherent demodulation results in an undistorted

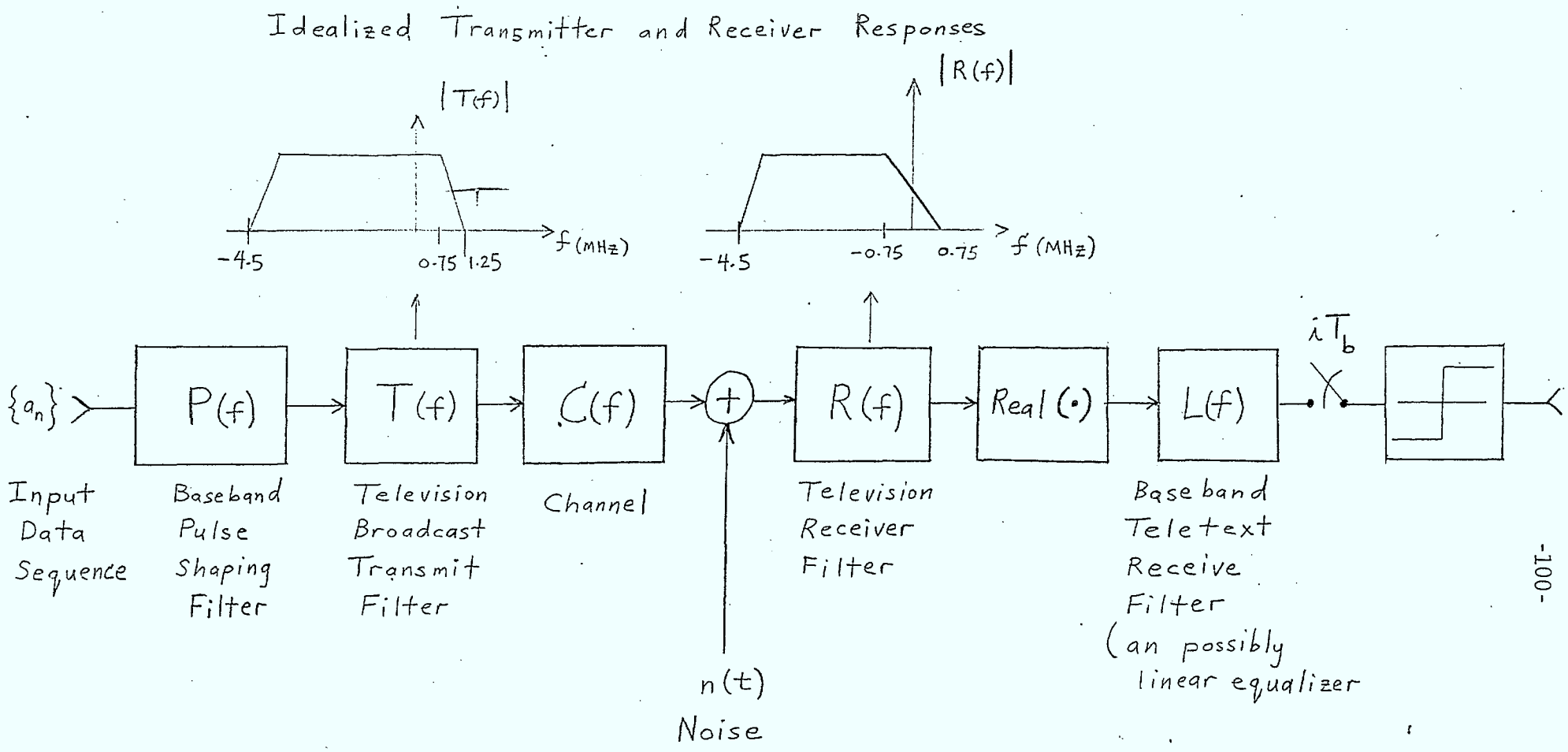

Figure 4.1 : Baseband model for broadcast television based teletext transmission

version of the input video signal. The constraint that this places on the receiver characteristic is that the sum $R(f) + R(-f)^*$ must be constant. An idealized receiver characteristic is shown in the block diagram of Figure 4.1. The most critical region of the response is the linear skirt (Nyquist region) of the receiver response. Precise amplitude and group delay control is required to prevent distortion. This is difficult to accurately control because of the sharp attenuation curves of the transmitter and receiver responses, which give rise to group delay distortion. In practice, most systems are non-ideal due to economonic constraints in production which prohibit precise control in this skirt region of the response. Even so, synchronous detection does reduce the level of quadrature distortion considerably.

Carrier regeneration at the receiver is made more difficult by the vestigial sideband nature of the receiver IF filter which introduces phase modulation of the transmitted carrier. Ideal carrier recovery techniques with narrowband reference channels (whose purpose it is to strip away this Nyquist slope incidental phase modulation) have until recently not been very practical. Some of the reasons for this include:

(1) Incidental phase modulation from poorly maintained transmitters can result in long phase error transients with narrowband recovery loops. In extreme cases the loop may unlock, and cycle skip until lock is re-established, resulting in an unuseable picture.

(2) The tuning systems of television receivers in the early 1970's produced an IF signal whose picture carrier frequency was dependent on picture content [2]. Consequently, there can be rapid frequency

excursions as a function of picture content. These tuning changes can be catastrophic when the loop bandwidth is on the order of one or several times the horizontal scan rate (15.75 kHz). A narrowband phase locked loop cannot follow fast changes resulting in sluggish behaviour and may even periodically unlock producing an unuseable picture.

As a result systems employing phase locked loop recovery techniques had to employ loop bandwidths of several hundred kHz. Systems employing such wideband reference channels are referred to as quasi-synchronous demodulators. Historically, quasi-synchronous recovery refers to the technique by which the carrier is estimated by passing the output of a conventional IF filter into a tuned circuit pre-filter and bandpass limiter combination. This technique is commonly referred to as the "carrier stripping" approach. In many cases the bandpass limiter pre-filter is a simple L-C tank circuit. An indepth analysis of this carrier recovery techique is presented in [1] and summarized in Appendix C.

The major design variable in the traditional quasi-synchronous carrier recovery technique is the selection of the pre-filter bandwidth. The peak phase error is reduced by selecting a narrow bndwidth. Unfortunately, this is accompanied by long transients which can result in significant phase errors persisting for long time periods, degrading the subjective picture quality. The other major factor discouraging the selection of a narrowband pre-filter is the increased sensitivity to mistuning. Practical bandwidths are on the order of the extent of the linear skirt of the receiver IF filter [1]. Unfortunately, this allows in more of the quadrature distortion that is produced by the Nyquist slope of the receiver IF when the television set is properly tuned. A serious implementation problem is

preserving the phase shift of the signal from the output of the limiter to the input of the product detector [3]. Since realistic high frequency circuits contain undesired phase shifts, and there are wide IC to IC variations, compensation for these phase shifts can be difficult. Due to the improved tracking capabilities of phase locked loop recovery procedures, most current television receivers employ this recovery technique.

4.1 Quasi-Synchronous Design Considerations

There are several advantages to be gained with phase locked loop synchronous detection. A few of these are listed below:

(1) elimination of intermodulation effects such as the 920 kHz beat that results because of intermodulation between the colour subcarrier and the sound carrier with envelope detectors.

(2) no chroma-to-chroma crosstalk as a result of distortion associated with sound trapping [2].

(3) improved signal-to-noise ratios under weak signal conditions (no rectification of the noise as is the case with an envelope detector).

(4) highly modulated high frequency video information is properly reproduced because of the lower quadrature distortion.

(5) a potential improvement in the sound quality because unwanted phase perturbations are not transferred to the sound carrier.

There are several factors which influence the design of the carrier recovery loop. A block diagram of a typical carrier recovery loop discussed in a paper authored by Zenith employees [3] is presented in Figure 4.2. A detailed discussion of PLL recovery circuits is presented in Appendix C. It is evident that most conventional carrier recovery loops follow the receiver IF filter and consequently must contend with Nyquist slope generated incidental phase modulation. The major reason for this is economic in nature. The Nyquist slope generated incidental phase modulation could be avoided by placing the carrier recovery loop before the receiver IF. In this case, the signal in the reference channel centered about the picture carrier is double sideband in nature, and no incidental phase modulation is produced in the reference channel. However, this requires extra gain in the reference channel and accurately maintaining the phase balance between the two signal paths, thereby increasing the cost of the television receiver.

The asymmetrical nature of the receiver IF filter about the picture carrier frequency (45.75 MHz) introduces phase modulation in the resultant output signal (due to the generation of a quadrature component). The phase modulation introduced is strongly dependent on the characteristics of the video signal. A detailed discussion of the incidental phase modulation introduced by the Nyquist slope region of the receiver IF filter in response to synchronization signals is presented in Appendix C. The phase modulation introduced by a typical teletext line is illustrated in Figure 4.3. Note that peak phase errors in the neighbourhood of 25° are prevalent over the teletext portion of the line. Ideally one would like to remove this Nyquist slope incidental phase modulation. In the absence of other signal impairments, this can be achieved with a narrowband loop. Undoubtedly some residual video dependent incidental phase modulation will persist.

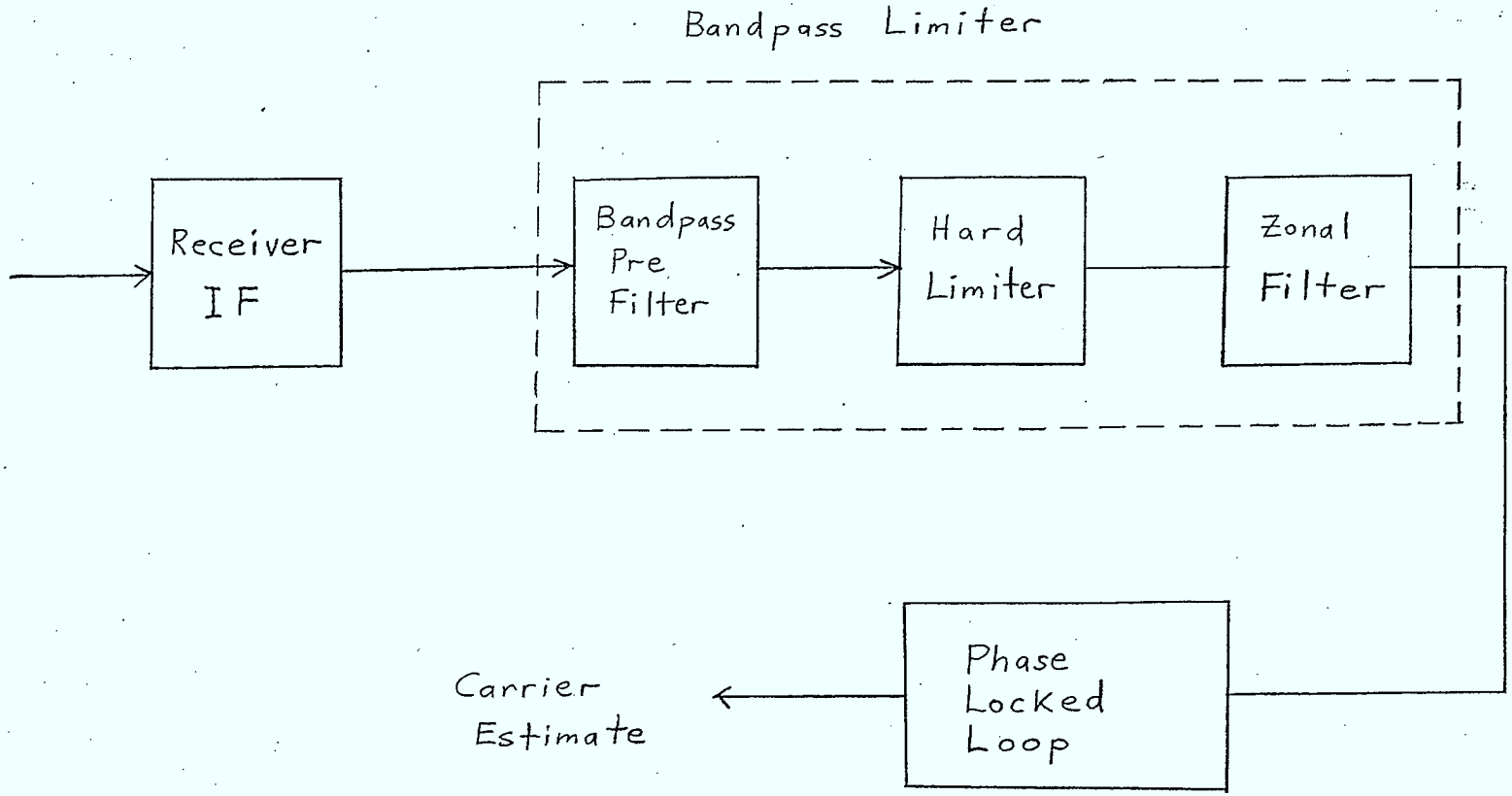

Figure 4.2: Block diagram of a typical carrier recovery loop [3].

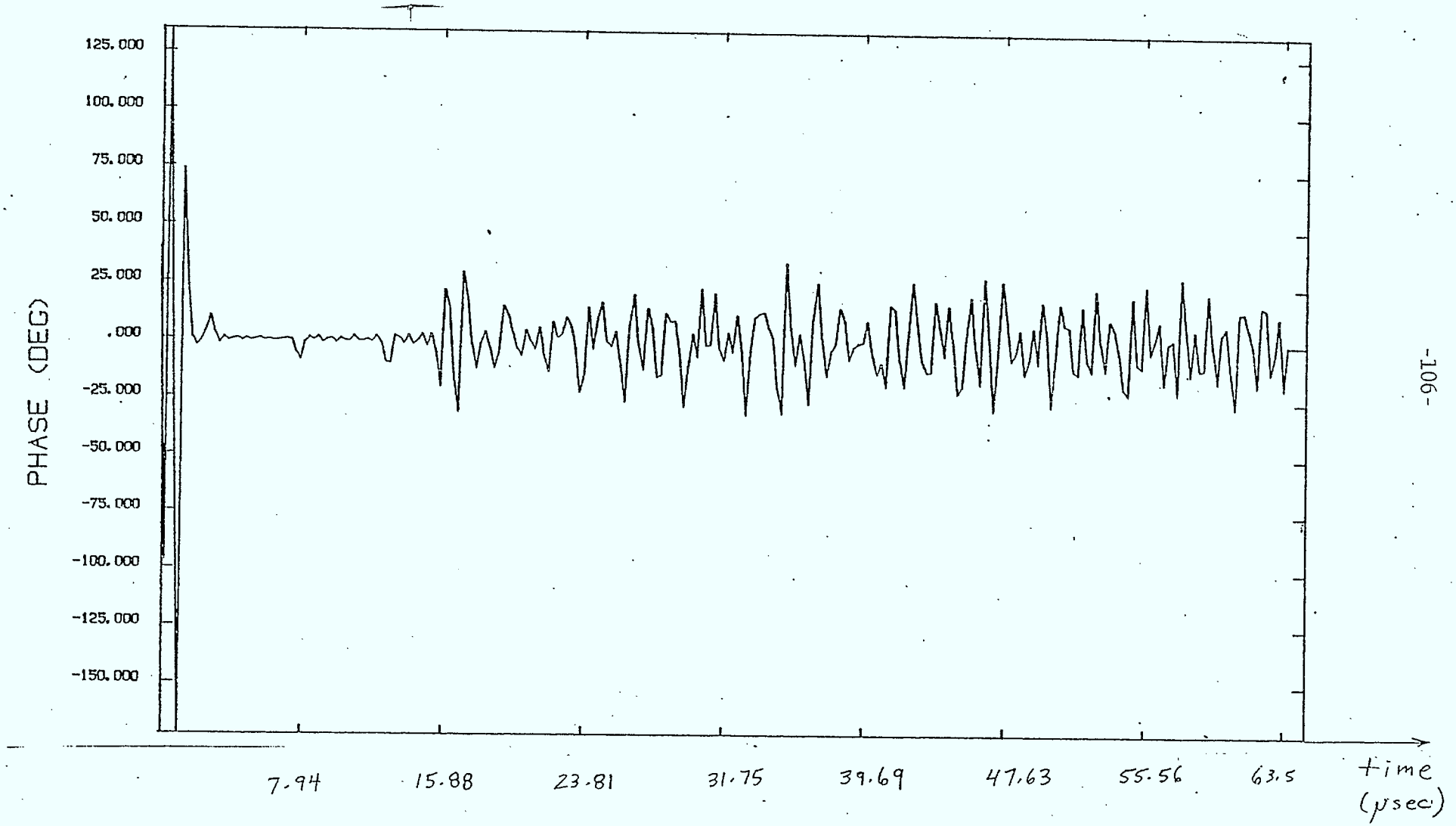

Figure 4.3: Nyquist slope introduced incidental phase modulation for a typical teletext burst.

A major difficulty in design of television receiver carrier recovery loops is the presence of other signal distortions. These signal impairments fall under the general category of incidental phase modulation. Linear AM to PM incidental phase modulation caused by the linear skirt of the receiver filter has already been discussed. Other major sources of incidental phase modulation are non-linear parametric and transit time effects. This is the major source of transmitter incidental phase modulation, but it can also occur at the receiver tuner. The choice of tuning system greatly influences the type of carrier acquisition system. For example, if the tuner allows rapid frequency excursions (phase modulation) that depend on picture content, one would not select a narrowband recovery loop. With AFC feedback control [4] and advances in digital PLL synthesizers [5, 6], which provide more accurate and stable TV tuning, the incidental phase modulation introduced by current TV receivers is much improved (with respect to the tuning systems mentioned in [2] which introduce rapid frequency excursions).

Transmitter induced incidental phase modulation is a signal impairment which must be tracked by the carrier recovery system. In [7], it is claimed that current (well-maintained) transmitters can hold the incidental phase modulation to within 1° over 120 IRE units not including the sync pulse. In [8], which discusses the effects of incidental phase modulation induced by TV Transmitters on TV signals, the phase shift versus power output characteristic of a Klystron amplifier is provided in Figure 8 of reference [8]. The phase shift induced on a blanking level signal is approximately 15° and on a white signal a phase shift in the neighbourhood of 5° is induced. It is apparent that old (or poorly maintained) transmitters can introduce significant incidental phase modulation. This is especially true of inexpensive local RF sources incorporated in video games.

In order to track this incidental phase modulation, the bandwidth of the recovery loop must be increased.

Another important consideration is audio buzz. For Canadian and U.S. Television broadcasting, the sound and visual carriers are processed separately until the passive diplexer [7]. Consequently, no direct transfer of incidental phase modulation takes place in the transmitter. As demonstrated in [7], an envelope detector will fully transfer any phase modulation on the visual carrier to the sound (aural) carrier. The FM sound detector detects these video signal related angle modulations and the sync and blank components cause the characteristic buzz sound. If a quasi-synchronous receiver with a wide reference channel is used, the incidental phase modulation will similarly be transferred to the aural carrier. With a synchronous detector with a narrow reference channel, only low frequency incidental phase modulation will be transferred. A narrowband loop seems superior from the audio buzz standpoint.

An interesting tradeoff in the design of the phase recovery loop arises. While the narrowband loop reduces audio buzz, it may not adequately track transmitter induced visual incidental phase modulation. This would result in a degradation in the quality of the video signal. A wider band reference channel would provide better video quality at the expense of increased audio buzz. Another thing that can discourage the design of very narrowband reference channels is that in some tuning systems, the visual carrier and aural carriers can acquire equal amounts of incidental phase modulation. In this case envelope and quasi-synchronous detectors eliminate incidental phase modulation from the sound carrier. However, a synchronous detector does result in a sound carrier with incidental phase modulation, and consequently the audio buzz problem does exist.

It is important to identify the most serious cause of incidental phase modulation. Given the improvements in television tuners, the most serious incidental phase modulation would appear to be either transmitter induced or caused by the Nyquist slope of the receiver IF fitler. In [7], signal to buzz ratios (SBR), for a constant blank level test signal with a 1° transmitter incidental phase modulation characteristic (typical of current transmission equipment) and incidental phase modulation generated by the receiver IF, are computed. The SBR's for Nyquist slope generated incidental phase modulation are considerably worse (by approximately 22.8 dB) than for transmitter incidental phase modulation. It is now apparent that reducing Nyquist slope incidental phase modulation is crucial for improving the audio buzz problem. Therefore, for broadcast television applications, the carrier recovery loop bandwidth should be chosen to be only as wide as necessry to track transmitter incidental phase modulation (so as not to compromise video quality), allowing the loop to filter out a considerable amount of Nyquist slope induced video incidental phase modulation.

It is appropriate at this point to discuss some improvements to conventional carrier recovery. Routing the reference channel around the receiver IF is one way to eliminate the Nyquist slope incidental phase modulation, although it is expensive. A technique for re-establishing the double sideband symmetry when the reference channel is located after the receiver IF is presented in [2]. It basically involves inverting the frequency sense of the signal about the picture carrier and adding this signal back to the original to re-establish double sideband symmetry before amplitude limiting. The drawback of this technique is complexity, as two phase locked loops, two product detectors, and a frequency doubler are required. Another possible improvement was proposed in [7] to reduce the audio

buzz problem. This was a split intercarrier sound receiver where the Nyquist incidental phase modulation is eliminated by a specially designed IF filter in the carrier recovery loop that creates a symmetric response about the visual carrier. This would be an expensive addition, but with increased interest in good quality monophonic sound and multichannel sound, such improvements may be commercially available in the near future.

As discussed in [3], the PLL parameters have to be optimized while considering operation with non-standard signals (i.e. video game RF modulators). In [3], it is claimed that a PLL 3 dB bandwidth of approximately 100 kHz is the minimum limit after an evaluation of existing potential signal sources. The claim in [3] that a loop with narrow bandwidth can cause audio buzz is only valid for video game modulators which introduce phase modulation on both the video and aural carriers. From above discussion, this is clearly not valid for well maintained transmitters. It is appropriate at this point to mention a relatively simple improvement to television carrier recovery loops. The loop bandwidth could easily be made switch selectable by switching an additional resistor or capacitor in or out of the loop filter circuit. A narrowband loop could be used for receiving broadcast television signals and a wider band loop for video game and home computer modulators.

Other important issues in loop design are frequency and phase acquisition. A detailed investigation of these issues is beyond the scope of this study. They are briefly addressed in Appendix C. The details of phase locked loop design will not be pursued here. Some discussion is presented in Appendix C. A second order loop is particularly attractive from an implementation and performance standpoint. A common second order loop with an active loop filter has a closed loop transfer function (see Appendix C):

$$H(s) = \frac{2\zeta w_n + w_n^2}{s^2 + 2\zeta w_n + w_n^2} \quad . \tag{4.1}$$

The amplitude response of this transfer function for various damping factors (ζ) are provided in Figure 4.4 [9]. The one sided noise equivalent loop bandwidth, B_L, is given by [9, 10]:

$$B_L = \frac{w_n}{2}\left(\zeta + \frac{1}{4\zeta}\right) \quad . \tag{4.2}$$

It can be easily shown that the 3 dB bandwidth of this loop is given by:

$$f_{3dB} = \frac{w_n}{2\pi}\left[1 + 2\zeta^2 + \sqrt{2(2\zeta^4 + 2\zeta^2 + 1)}\right]^{\frac{1}{2}} \quad . \tag{4.3}$$

The zero dB crossing point is given by:

$$f_{0dB} = \sqrt{2}\ \frac{w_n}{2\pi} \quad . \tag{4.4}$$

If a second order loop is employed for phase locked detection, experiment suggests that a damping factor between 1.0 and 1.5 is best [9].

The phase locked loop transfer function of a commercially available carrier recovery loop [3] is provided in Figure 4.5. For this loop $w_n = \frac{2\pi(50)}{\sqrt{2}}$ rad/sec and $f_{3dB} \approx 110$ kHz. A second order loop with damping factor $\zeta = \sqrt{2}$ gives a reasonable match to this transfer function. The corresponding one sided noise equivalent bandwidth is approximately 177 kHz.

In our investigation of quasi-synchronous carrier recovery, attention will be restricted to the above second order loop.

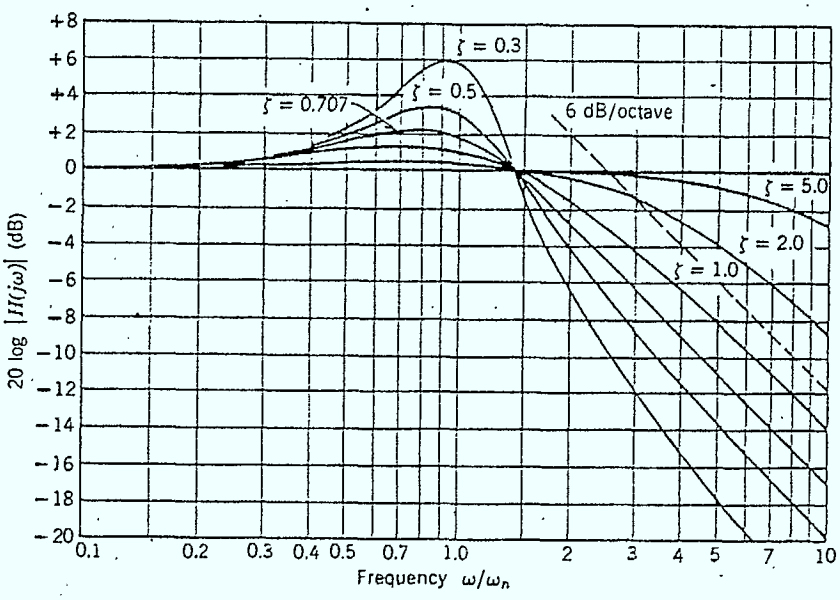

Figure 4.4: Frequency response of high gain lag-lead filter second order loop (after [9])

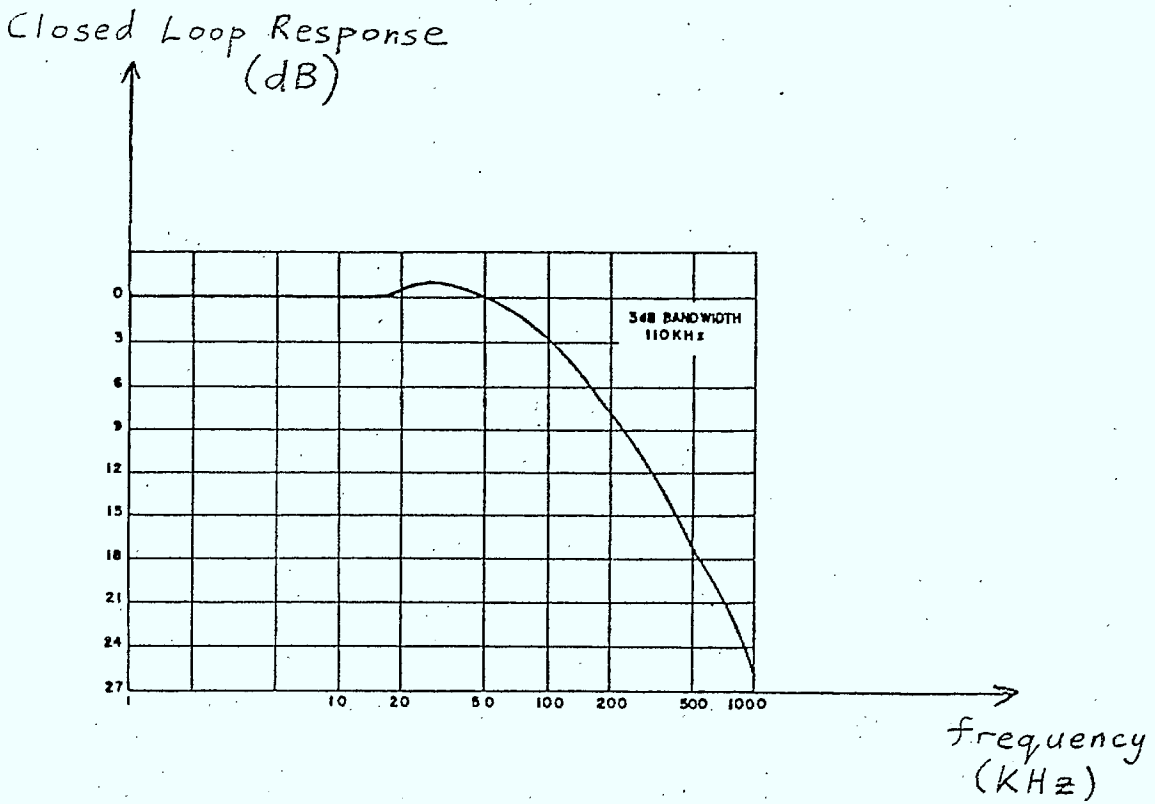

Figure 4.5 : Closed loop response of PLL carrier recovery system presented in [3].

The loop bandwidth and damping factor will be programmable, and realistic values will be used in teletext performance evaluation simulations.

4.2 Simulation Approach For Quasi-Synchronous Detection

A simplified block diagram of quasi-synchronous detection is provided in Figure 4.6. The time domain complex demodulation of the receive filter output by $\exp\{-j\ \phi_e\ (nT_s)\}$ imposes a significant computational penalty relative to synchronous demodulation. In addition to the sample by sample time domain multiplication, an additional inverse and forward FFT are required. The existance of a reasonable phase error model for quasi-synchronous detection would save the computational effort of extracting the exact phase error sequence for each teletext burst. Unfortunately, no such random process models are in existance. Even if one did exist, one would have to carefully examine the assumptions on which it was based to ensure that there is a reasonable match with one's application. A phase error model would likely be for a specific carrier recovery configuration, and despite the fact that it may be indexed according to loop bandwidth, it would not be of general applicability.

An attempt was made to characterize the phase error process of a quasi-synchronous PLL carrier recovery loop which follows the receiver IF and its troublesome Nyquist slope region. The source of the phase error was the video signal low frequency spectral components, which are unbalanced by the receiver IF, giving rise to incidental phase modulation. The video signal was modelled as a gaussian signal with a dc offset and gaussian autocovariance function. The details of the model development and analysis are provided in Appendix C. It suffices to say that the Nyquist slope region complicates the analysis, making only the evaluation of phase error bounds possible. From Appendix C, a gaussian

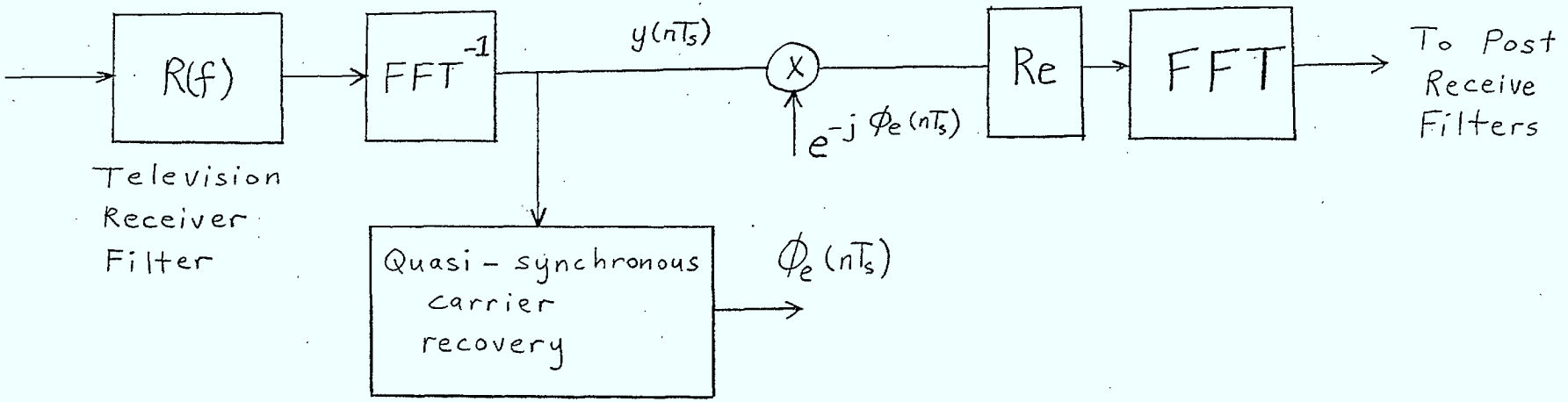

Figure 4.6 : Quasi - synchronous detection

video process that occupies the same voltage region of the television line with a correlation time of 2.675 μsec (approximately $\frac{1}{20}$ of the video portion of a TV line), gives rise to a gaussian phase error process with standard deviation σ_o, where

$$15.6° \leq \sigma_o \leq 22°,$$

for a second order loop with one sided noise equivalent bandwidth of 100 kHz. It is quite apparent that a typical video process can cause appreciable phase error in a quasi-synchronous recovery loop. This is mainly due to the fairly long correlation times, which result in relatively narrowband spectra. Consequently, a relatively wideband loop is not very effective at filtering out this sort of distortion.

The above model is valid for estimating phase error bounds for normal television viewing. The phase error characteristics are a strong function of the correlation time of the video process, becoming worse as the correlation time is increased. For typical quasi-synchronous detectors, the recovery loop bandwidth is usually greater than 100 kHz. As a result, the memory of the recovery loop is typically less than 10 μsec. For quasi-synchronous teletext systems using the vertical blanking interval, past picture content will have a negligible impact on the carrier recovery phase error. Only for systems with very narrow reference channels (synchronous detectors) will past picture content have any effect. Even in this case, the impact will likely be small compared to the influence of the data stream on the teletext line.

For quasi-synchronous VBI teletext systems, the phase error process for the television picture portion of the broadcast is definitely not valid. What one must establish is the

influence of the data signal on the carrier recovery loop. The data signal is definitely not gaussian and is a much faster varying process (the bit period is only 0.175 μsec, which is more than an order of magnitude smaller than the correlation time of the video process used for estimating the phase error standard deviation). The disturbing low frequency spectral content will not be as great as it is for a typical video process, and consequently, the quasi-synchronous phase errors should be considerably better.

To accurately characterize the phase error process, the phase error will be extracted on a burst by burst basis. Since we are not interested in simulating transient behaviour, the output phase error can be obtained by filtering the input phase error by the closed loop response of the phase locked loop. The basic phase recovery model is illustrated in Figure 4.7. A second order loop with programmable one sided noise equivalent bandwidth, B_L, and damping factor, ζ, is used in the simulation model.

There are a number of advantages of simulating the phase extraction process as opposed to a mathematical performance analysis. The complexity of the analysis of the phase corruption due to video effects conducted in Appendix C is evidence of this. Furthermore, the effect of noise was not considered in the analysis presented in Appendix C. The analysis with noise is complicated by the presence of the non-linear bandpass limiter. The limiter introduces signal suppression (which is a function of input signal to noise ratio) and the non-linear behaviour introduces spectral spreading of the noise. Rigorous mathematical analysis of these effects is extremely complex and strongly dependent on the characteristics of the limiter pre-filter and post limiter zonal filter. The simulation approach allows one to accurately characterize the behaviour of the recovered phase

error in various noise environments and under various multipath conditions, without the need for complicated analysis.

The major limitation of the simulation approach is that potential non-ideal signal impairments (such as transmitter incidental phase modulation) are not incorporated. The incorporation of such effects would be a major undertaking, involving modelling the characteristics of the nonlinearity of transmitter amplifiers (which may not be adequately modelled by simple static input-output characteristic curves [11]). These effects can have a major impact on the selected carrier recovery loop bandwidth. The approach taken here is to select typical bandwidth parameters used in existing recovery loops designed to operate with non-standard signals.

4.2.1 Simulation Model

The simulation block diagram is shown in Figure 4.7. The phase extraction technique implemented employs a second order phase locked loop with transfer function:

$$H(f) = \frac{1 + j\ 2\zeta\ (\frac{2\pi f}{w_n})}{[1 - (\frac{2\pi f}{w_n})^2] + j\ 2\zeta\ (\frac{2\pi f}{w_n})} \quad . \tag{4.5}$$

where $w_n = \frac{2\ B_L}{(\zeta + \frac{1}{4\zeta})}$

B_L is the one-sided noise equivalent bandwidth of the loop which is an input parameter.

ζ is the damping factor which is an input parameter (typically $\frac{1}{\sqrt{2}} \leq \zeta \leq 1.5$).

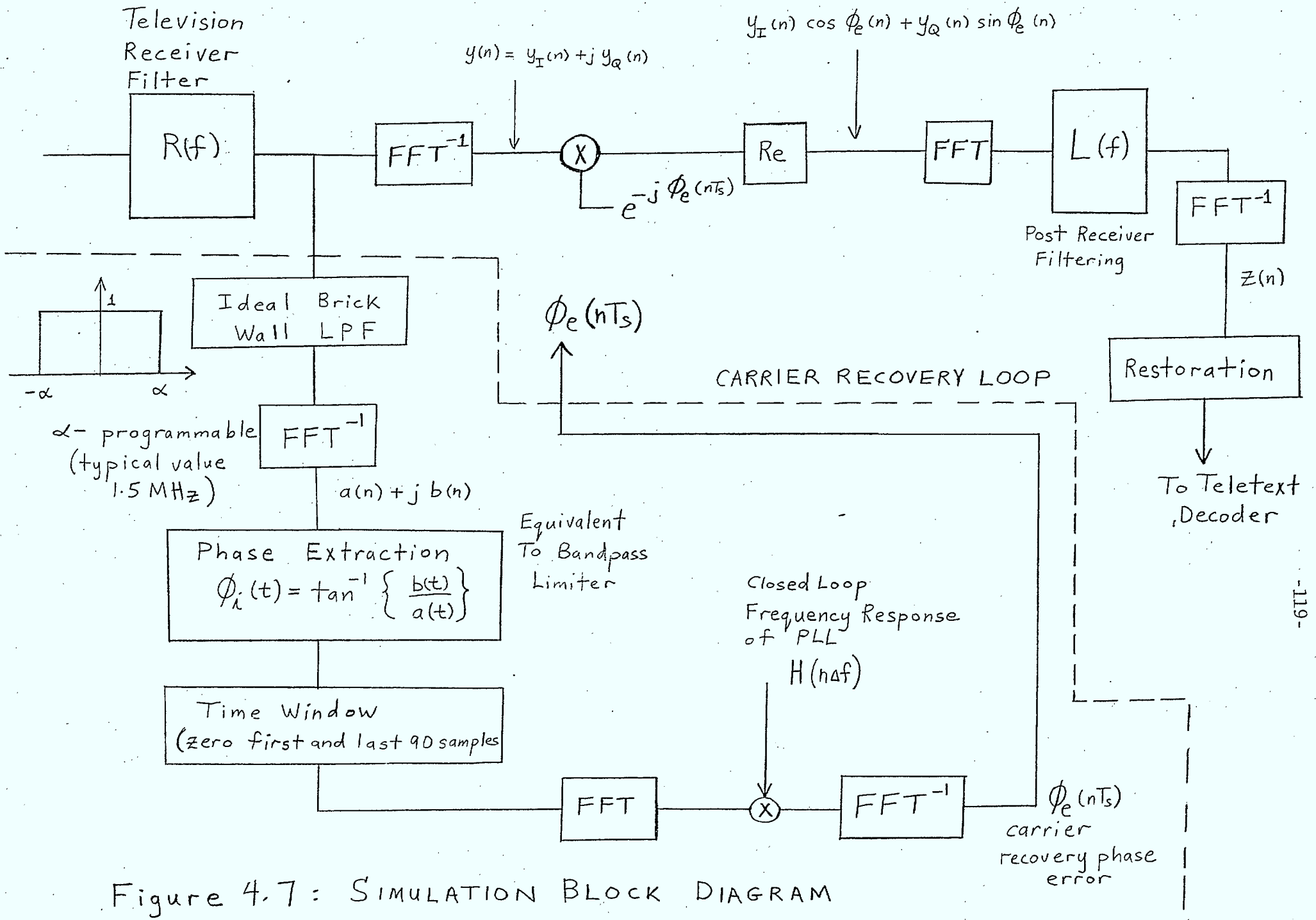

Figure 4.7: Simulation Block Diagram

The 3 dB bandwidth of the loop is computed and supplied as an output parameter.

From [3], 3 dB loop bandwidths as low as 100-300 kHz are now practical. These recovery loops represent the forefront in quasi-synchronous performance. Historically, quasi-synchronous loop bandwidths have been quite wide, being on the order of the linear skirt bandwidth of the receiver IF (750 kHz). To represent these systems, a noise equivalent bandwidth of 1 MHz (3 dB bandwidth of 632 kHz) has been selected.

The pre-filter of the bandpass limiter has been, for simplicity, chosen to be a 1.5 MHz ideal brick wall complex baseband filter (which represents a 3 MHz bandpass filter). The frequency domain signal at the output of this filter is transferred to the time domain, and the phase of the signal extracted. Due to the format of a teletext line, the inphase component at the input to the phase extractor is usually positive, implying that the phase at the output of the bandpass limiter is usually between $\pm \frac{\pi}{2}$. This phase function is then transformed to the frequency domain, filtered by the loop transfer function, and transformed back to the time domain. This output signal represents the quasi-synchronous phase recovery error which is used to complex demodulate the receiver filter output.

There are clearly some limits on the loop bandwidth which can be realistically simulated. The memory (most significant region) of the phase locked loop impulse response has a time duration of $(\frac{1}{B_L})$ seconds. If B_L becomes too small, one requires the phase information from the previous burst. To avoid circular convolution effects from having an influence on the clock run-in sequence portion of

the line, the impulse response memory must be less than 13.3 μsec, which implies that B_L (min) = 75 kHz. For $\zeta = 1$, and B_L = 75 kHz, the impulse response is four orders of magnitude below its initial value at the end of a TV line (63.5 μsec). Therefore the maximum frequency domain sample width is approximately 15.75 kHz. The frequency interval used in the simulation program is 15.38 kHz (the number of samples per bit (11) times the data rate (5.727272 MHz) divided by the number of frequency domain samples (4096)). The simulation program issues a warning whenever $B_L \leq 75$ kHz.

When investigating quasi-synchronous detection in multipath environments, the issue of circular convolution effects must be addressed. In the Telidon simulation all filtering operations are performed in the frequency domain, and consequently circular convolution effects occur. However, with the present choice of parameters (sampling rate and number of samples), the clock run-in sequence and data burst are uneffected by circular convolution if the echo length is less than 13.3 μsec. From the investigation of multipath conducted in [11], significant echoes beyond 10 μsec are unlikely. However, circular wraparound of the end of the data burst into the synchronization portion of the line does occur. This is not particularly troublesome because it can be thought of as representative of the multipath corruption from the previous line. In fact, this is an excellent representation of the actual situation when the preceeding line is in fact a teletext line.

After complex demodulation and taking the real component, the detected signal must be converted back to the frequency domain for processing by post receive filters and possibly an equalizer.

Since television signals are transmitted using negative modulation, this must be used for accurately characterizing the phase recovery process. Furthermore, the output signal must be restored (orientation reversal) before being submitted to the slicing level and symbol synchronization procedures of the teletext decoder. In the next section some basic results are presented.

4.2.2 Carrier Recovery Phase Error at Various Points in the Phase Extraction Process

To assess the phase error that can be attributed to the synchronization signals, the data in the teletext burst was zeroed. The phase error at the input to the phase locked recovery loop, which is representative of the phase error that can be attributed to a traditional carrier stripping quasi-synchronous recovery procedure (with a pre-filter bandwidth of 3.0 MHz), is illustrated in Figure 4.8. The peak phase error at the beginning of the burst is appreciable, but dies out very quickly (short transient). Over the portion of the burst where the clock run-in sequence is located, peak errors in the neighbourhood of 10° are evident. The phase error over the teletext portion of the burst is relatively small.

The carrier recovery phase error introduced by the synchronization signals for a second order phase locked loop ($\zeta = 1$) with one sided noise equivalent bandwidths (B_L) of 100 kHz, 200 kHz, and 1.0 MHz are illustrated in Figures 4.9, 4.10, and 4.11 respectively. As anticipated the narrowband loop yields superior performance. Over the major portion of the teletext line, the phase error is negligible.

The phase error at the input to the phase locked loop recovery system for a typical teletext burst is illustrated

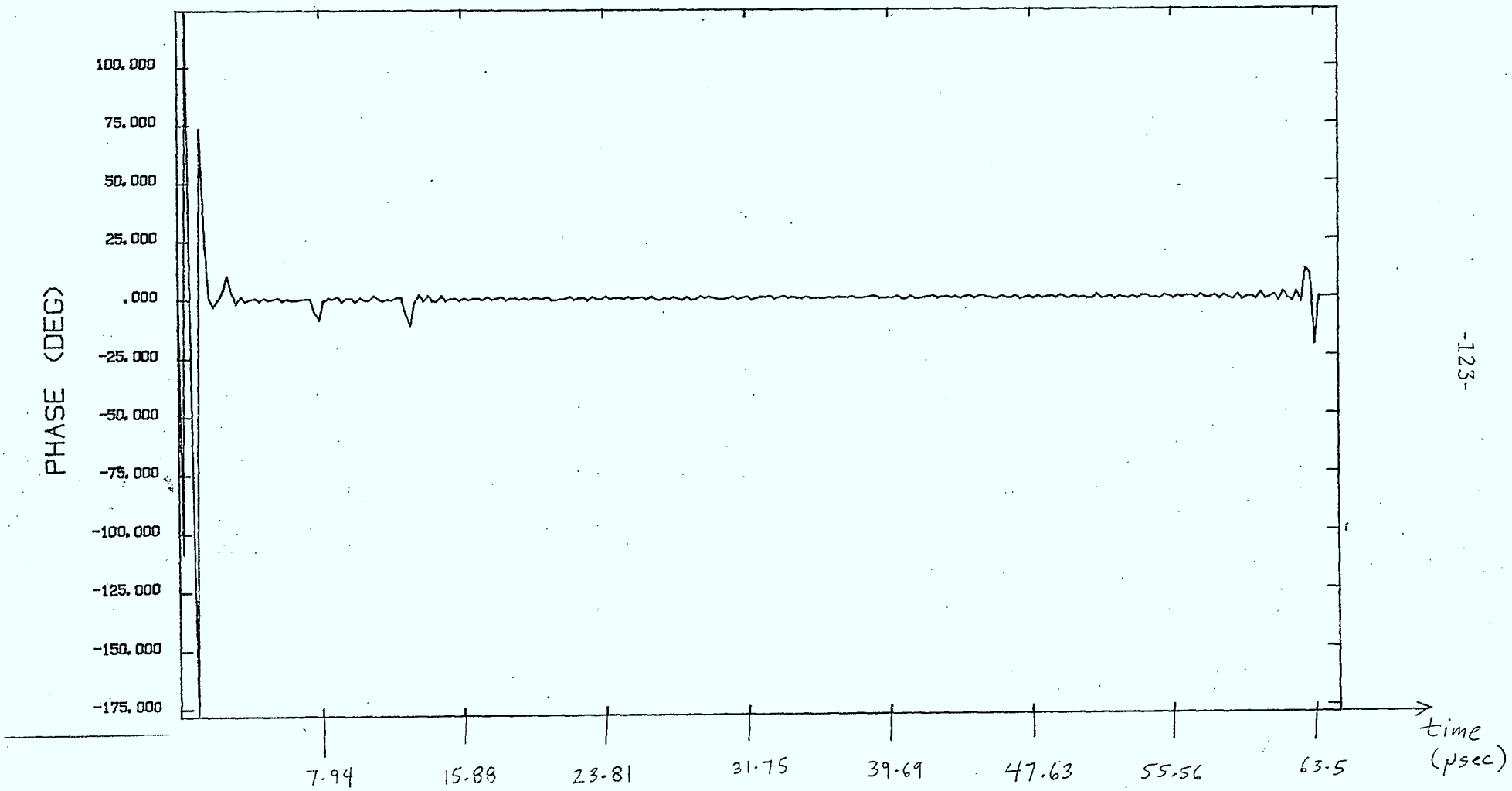

Figure 4.8 : Phase error at input to the phase locked loop due to the synchronization signal.

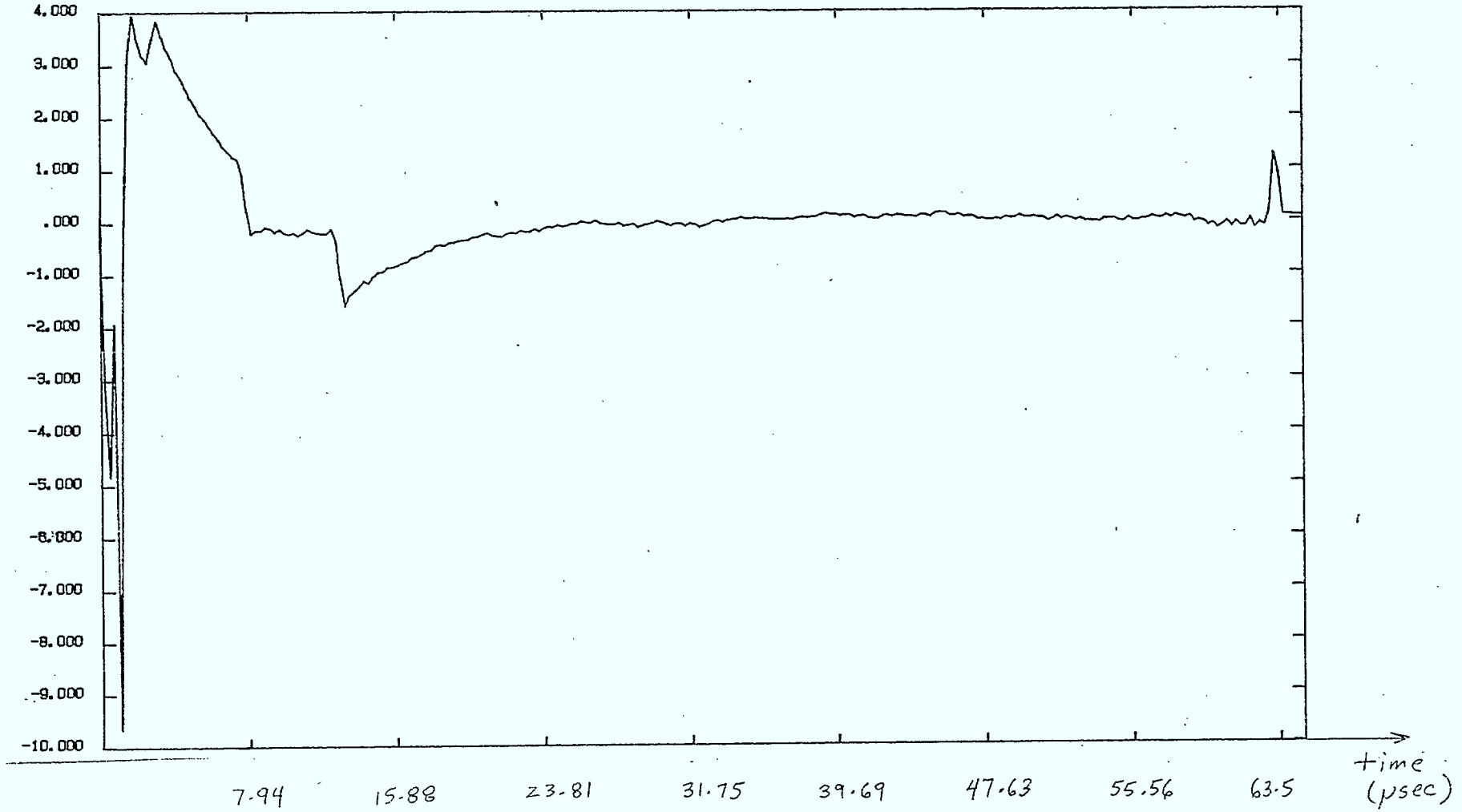

Figure 4.9 : Carrier recovery error induced by the synchronization signals for B_L = 100 KHz.

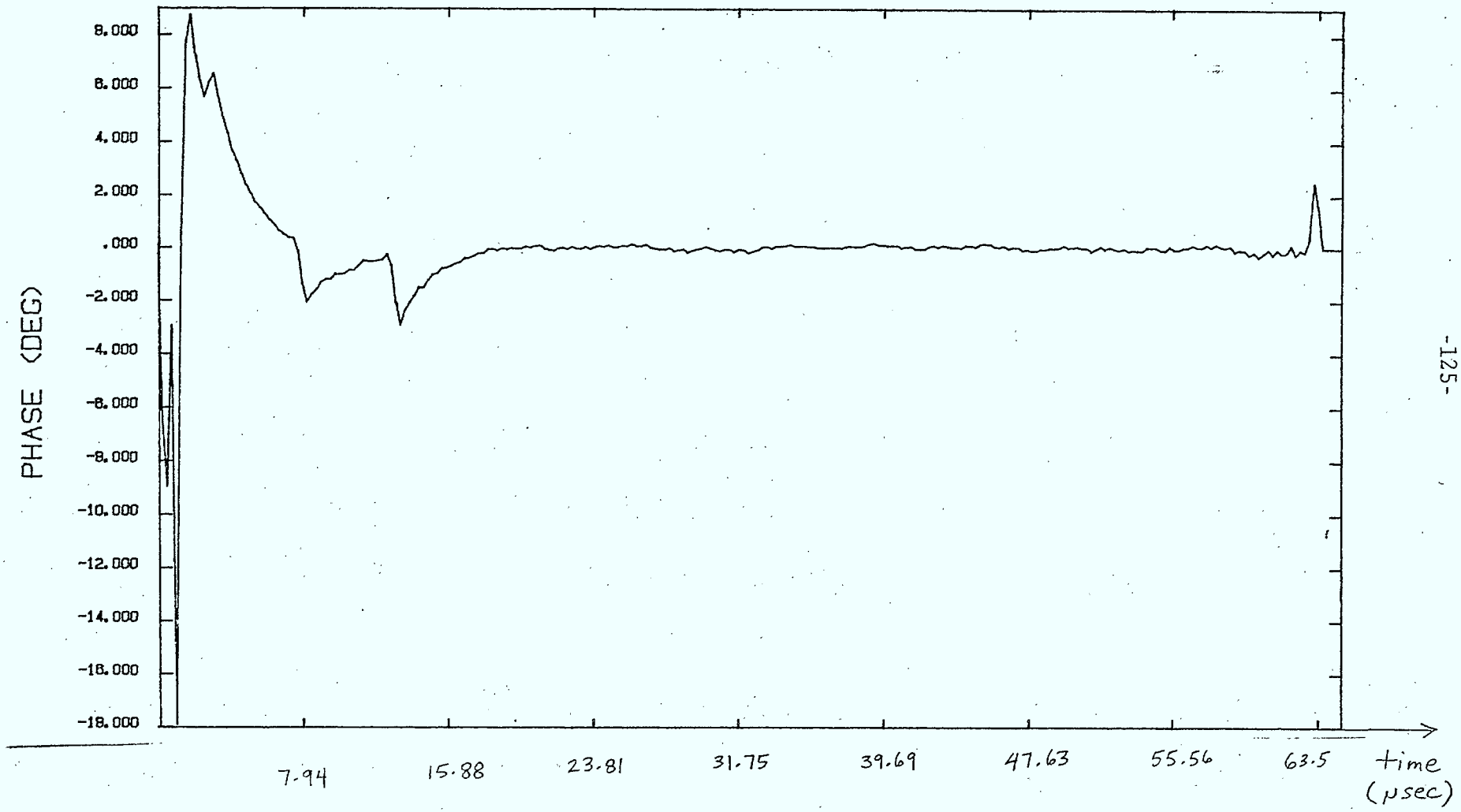

Figure 4.10 : Carrier recovery phase error induced by the synchronization signals for B_L = 200 KHz.

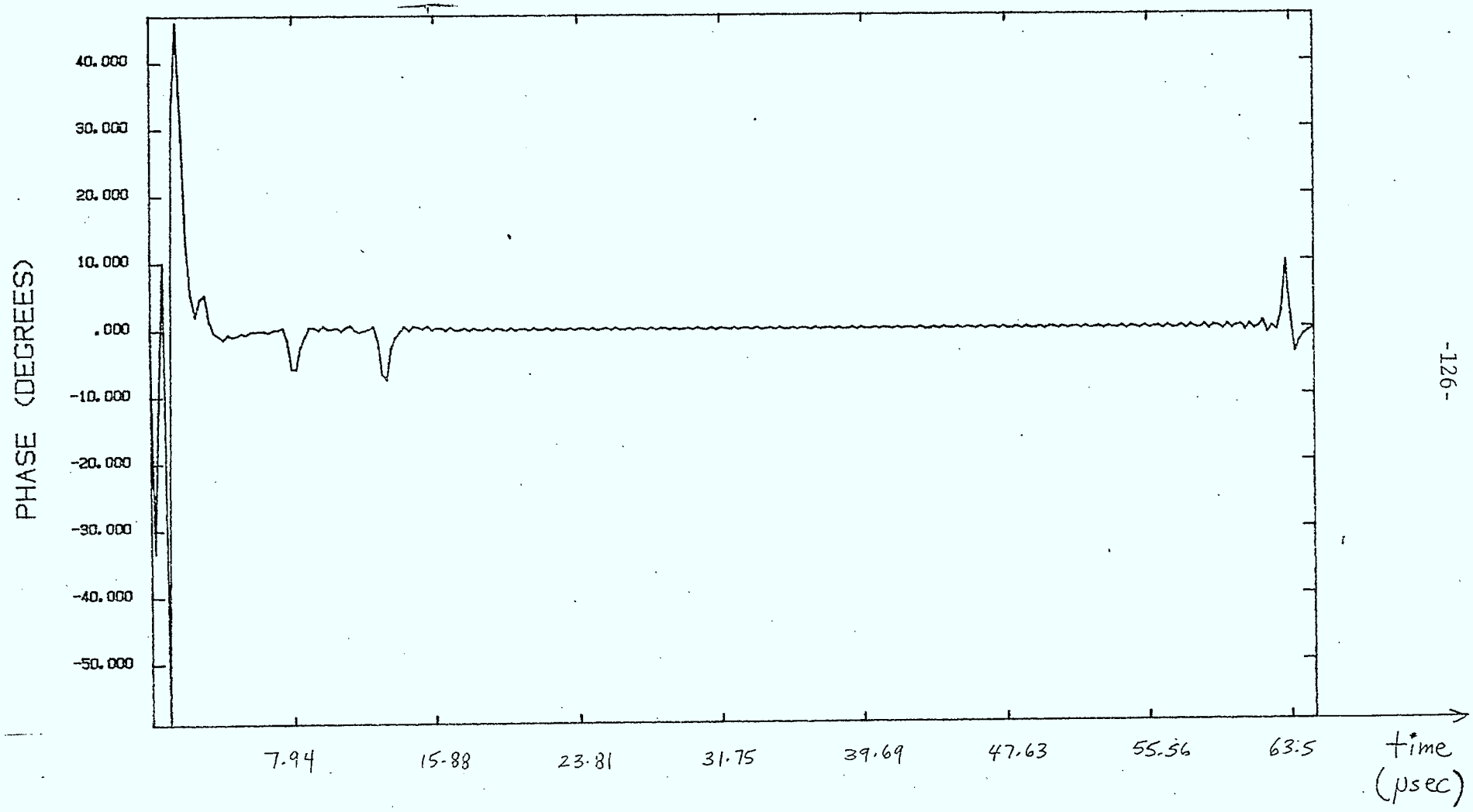

Figure 4.11: Carrier recovery phase error introduced by the synchronization signals for $B_L = 1$ MHz.

in Figure 4.12. Over the crucial portion of the teletext burst, the peak phase error is on the order of 25°. It is apparent that a traditional carrier stripping quasi-synchronous detector would introduce appreciable intersymbol interference.

The carrier recovery phase errors for B_L = 100 kHz, 200 kHz, and 1.0 MHz are illustrated in Figures 4.13, 4.14, and 4.15 respectively. The superiority of the narrowband loop is clearly evident (peak phase error only 1°). The peak phase error for the 200 kHz loop bandwidth loop is in the neighbourhood of 2° over the teletext portion of the burst. This is not much worse than the narrowband loop. Consequently, the teletext system performance of systems employing narrowband carrier recovery loops (100 kHz - 300 kHz) will not be much worse than that obtained with true synchronous detection. The carrier recovery phase error for a wideband loop (B_L = 1 MHz) is considerably worse than that obtained with a narrowband loop. The peak phase error is in the neighbourhood of 15°, which is not excessive. A small degradation relative to synchronous detection should occur because of increased intersymbol interference and increased peak sensitivity due to quadrature distortion.

4.3 Telidon System Performance With Quasi-Synchronous Carrier Recovery

Before presenting simulation results with quasi-synchronous detection, it is informative to examine some of the consequences of carrier recovery phase offsets. In pulse shape design, the transfer function of the inphase channel, $H_I(f)$, is chosen to meet or nearly meet Nyquist's first criterion [11]. The transfer function of the quadrature channel has a global asymmetry about f=0 due to the vestigial nature of the broadcast television system. In

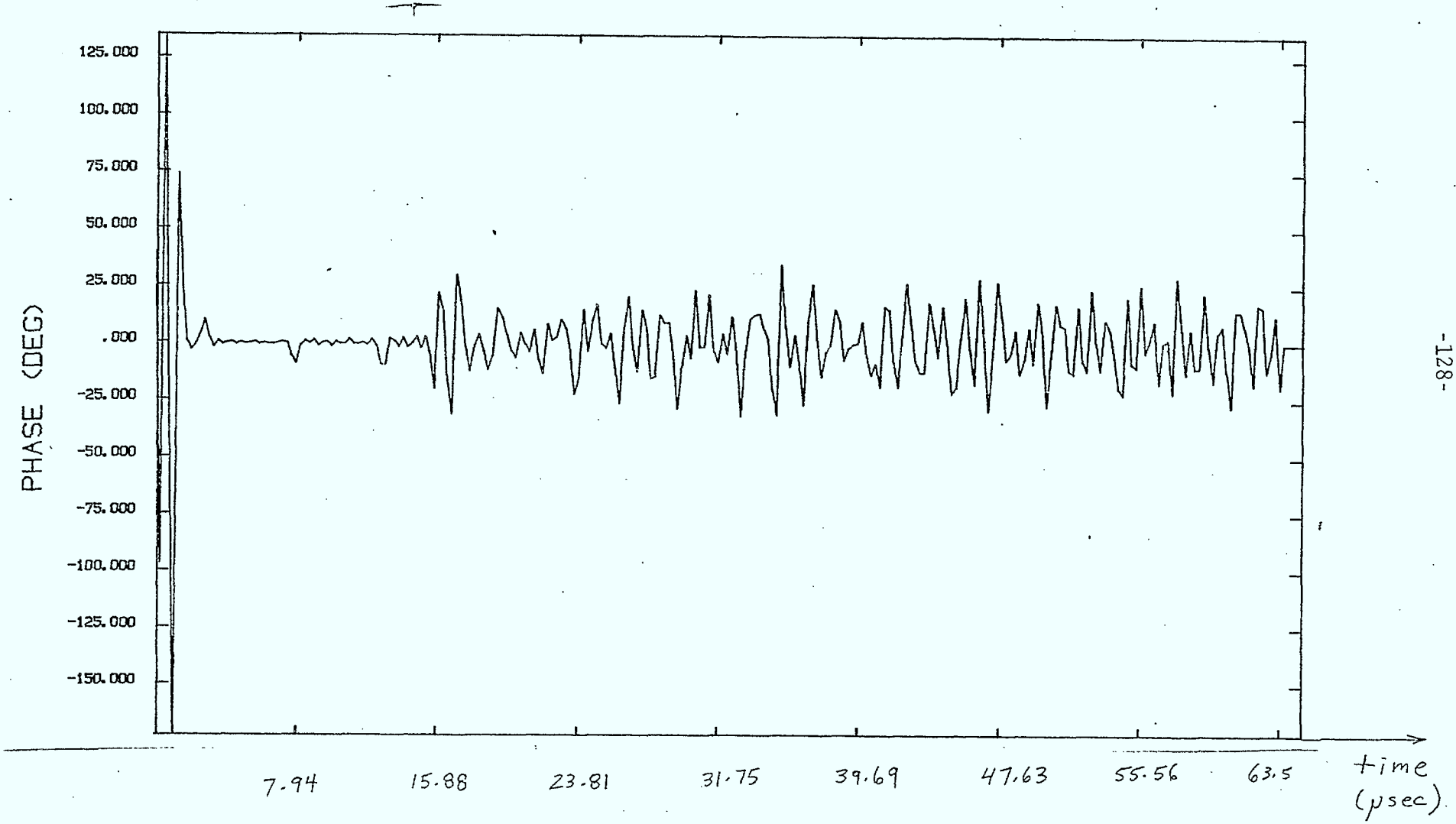

Figure 4.12 : Phase error at input to the phase locked loop for a typical teletext burst.

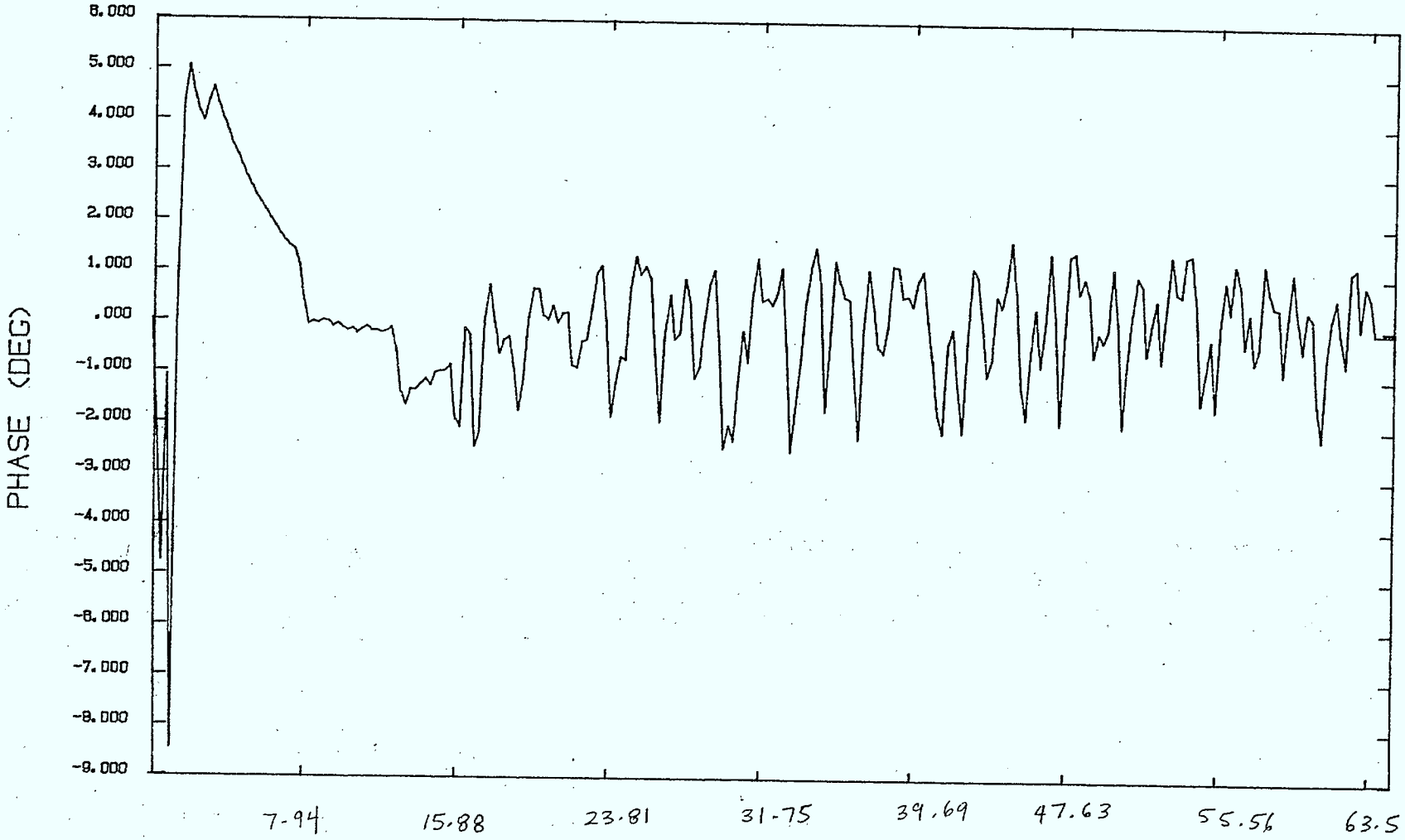

Figure 4.13 : Carrier recovery phase error for a typical teletext burst for $B_L = 100\,KHz$

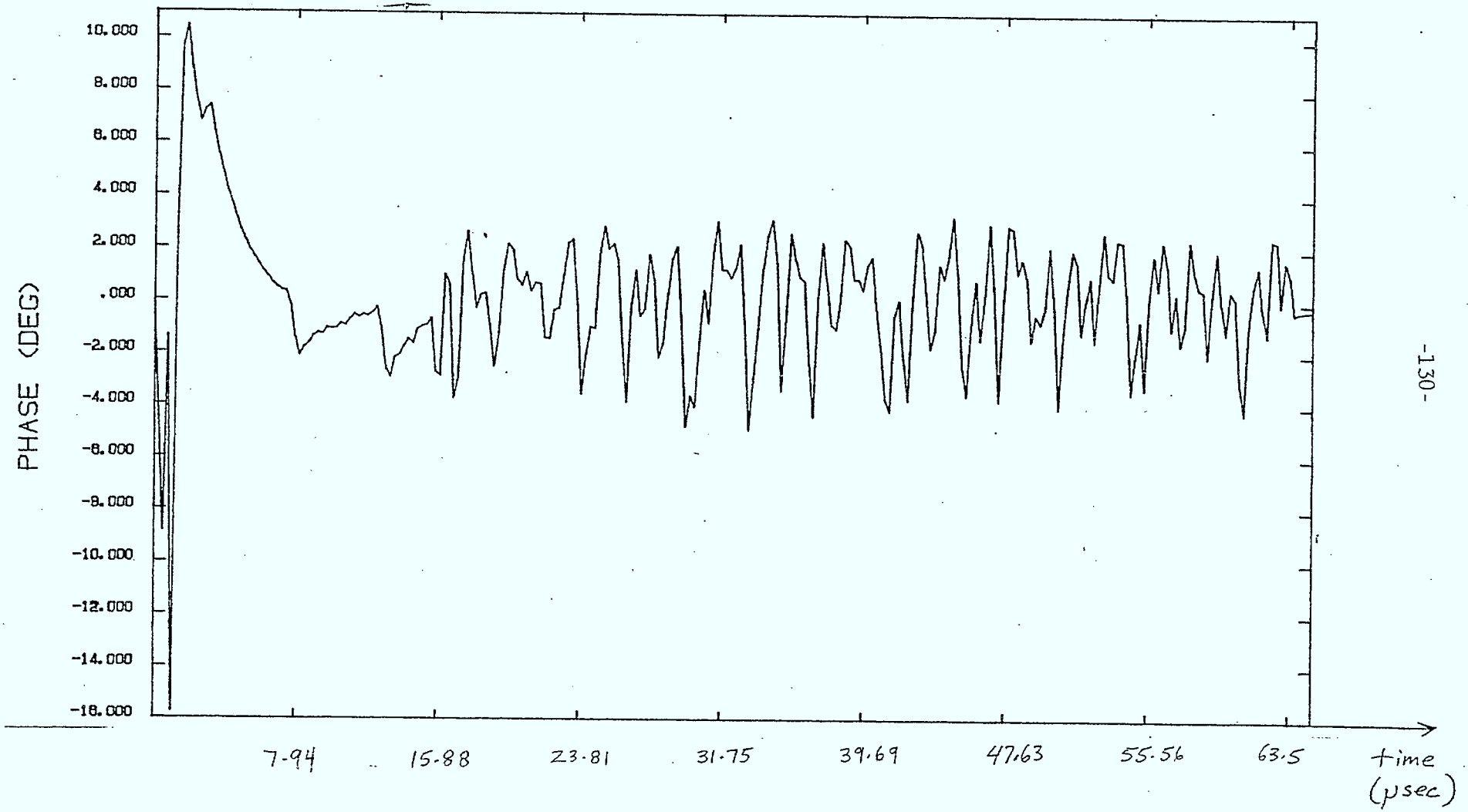

Figure 4.14: Carrier recovery phase error for a typical teletext burst for $B_L = 200$ KHz.

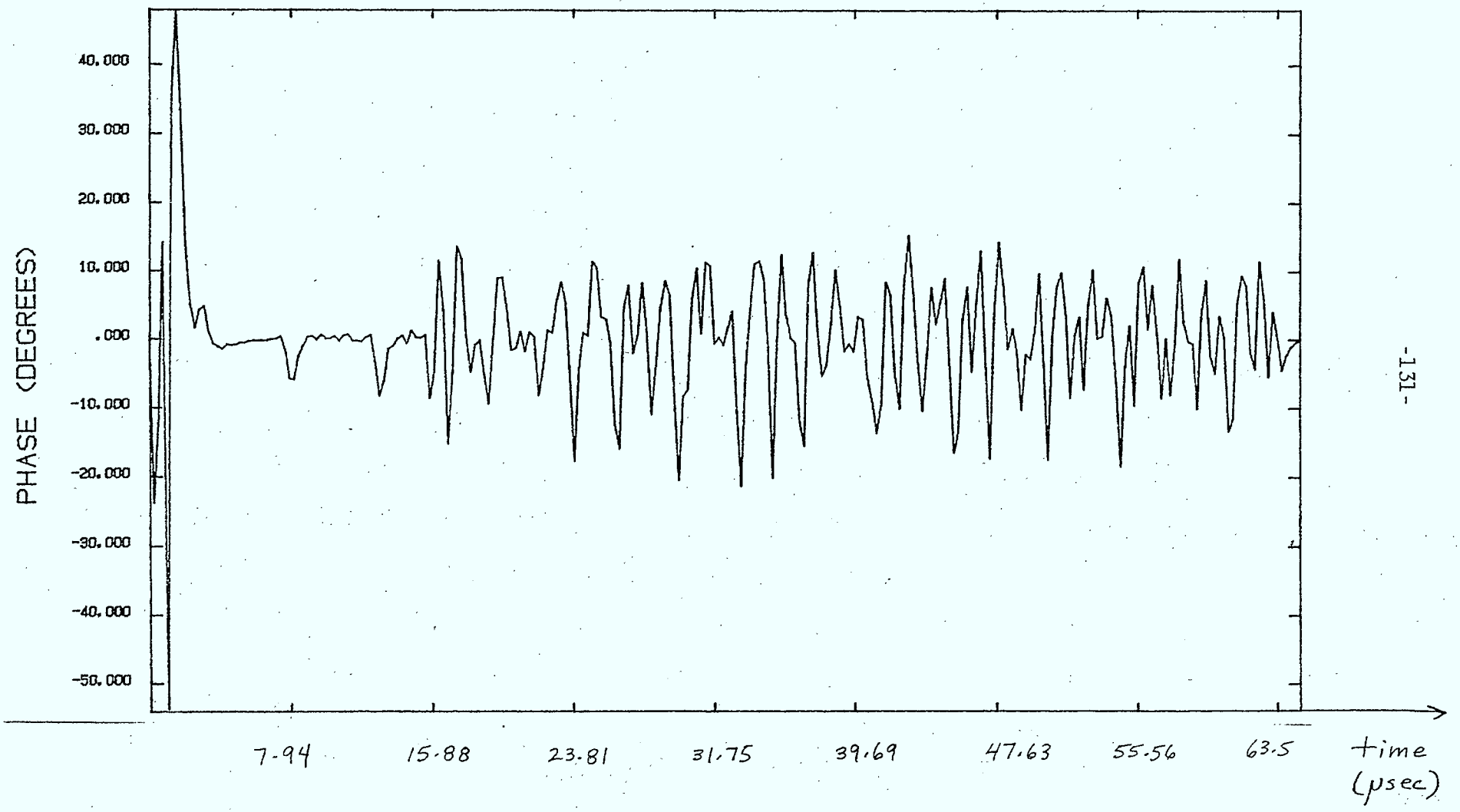

Figure 4.15 : Carrier recovery phase error for a typical teletext burst for $B_L = 1.0$ MHz.

general, $H_Q(f)$ will not satisfy Nyquist's first criterion [11]. For ideal carrier recovery, there is no reason why it should. However, when there is a phase offset, θ, due to non-ideal carrier recovery, the impulse response is:

$$h_\theta(t) = (\cos\theta)\, h_I(t) + (\sin\theta)\, h_Q(t),$$

where $h_I(t)$ and $h_Q(t)$ are the impulse responses corresponding to $H_I(f)$ and $H_Q(f)$, respectively. Note that even though the overall pulse shape may satisfy Nyquist's first criterion, significant intersymbol interference can result due to non-ideal carrier recovery because $h_Q(t)$ will not have the desired zero crossings. The implication of this is that quasi-synchronous detection will impose a performance degradation due to increased intersymbol interference. The results of the previous section (see Figures 4.13 and 4.14) indicate that the degradation for narrowband recovery loops should be small (peak phase errors are only in the neighbourhood of 1° to 2°).

Telidon system performance with quasi-synchronous detection for an ideal channel and gaussian noise environment is summarized in Figures 4.16 and 4.17. The weighted signal to noise ratios at which runs were conducted are 25 dB, 27 dB and 29 dB. The pulse shape used in the quasi-synchronous simulation runs was the truncated 100% raised cosine pulse presently used in the Telidon system. The one sided noise equivalent bandwidths, B_L, considered were 300 kHz and 1 MHz. The wideband (1 MHz) loop is characteristic of the traditional wideband quasi-synchronous detectors, while the narrowband (300 kHz) loop is representative of state of the art quasi-synchronous detectors. In fact, such narrowband loops are often referred to as synchronous detectors. Performance with the averaging slicing level decoder is

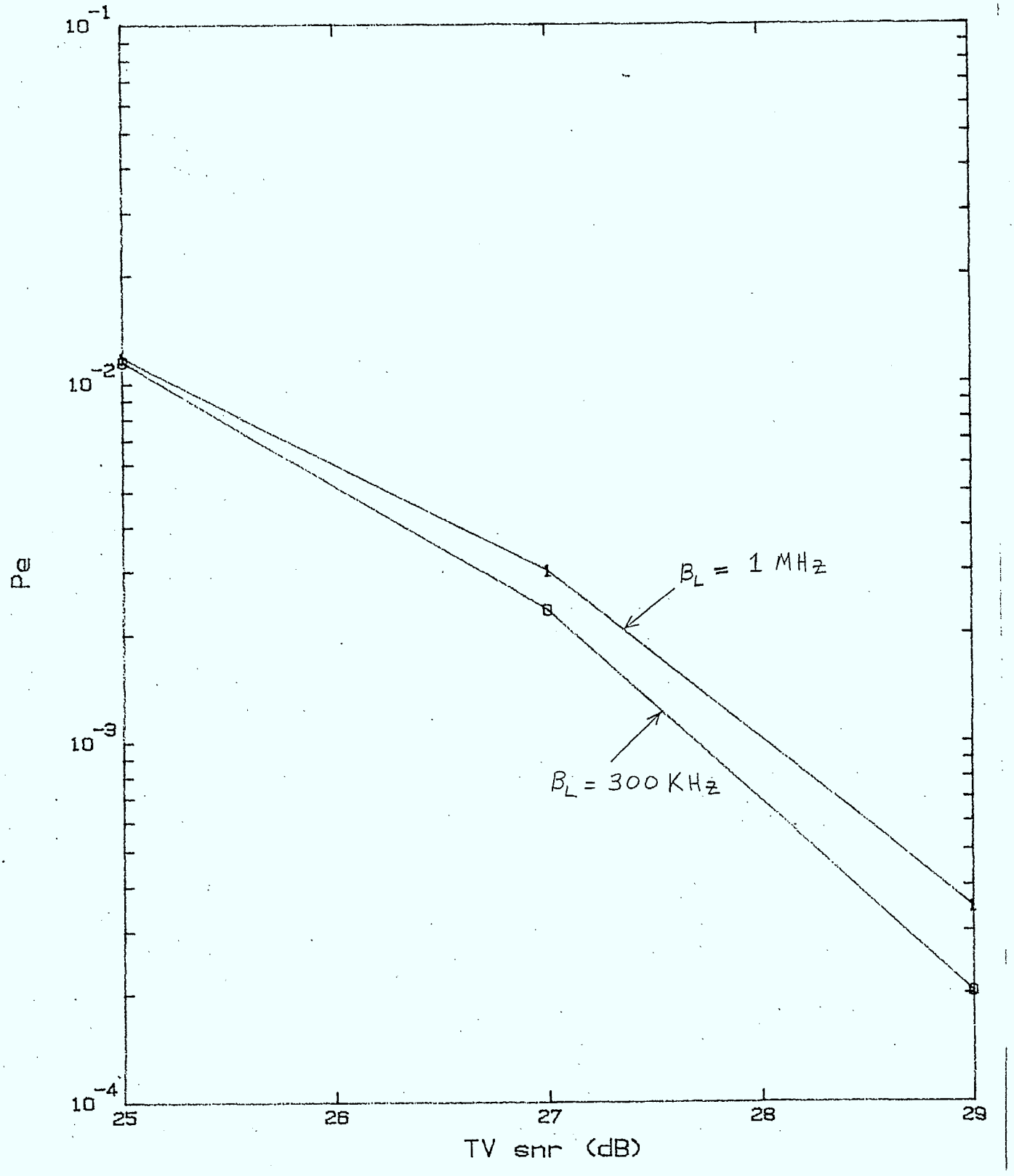

Figure 4.16: Simulated quasi-synchronous performance with an averaging slicing level decoder for an ideal channel and thermal noise environment.

presented in Figure 4.16. As expected, system performance is degraded by using the wideband carrier recovery loop. However, the amount of degradation is relatively small; being only 0.3 - 0.4 dB.

Performance with the peak detector decoder is presented in Figure 4.17. At the lower video signal to noise ratios, there is virtually no difference between the performance obtained with the narrow and wideband recovery loops. At higher video signal to noise ratios, there is a very minor degradation with the wideband carrier recovery loop. At this point, one must be cautioned that the simulation program does not incorporate non-ideal signal impairments such as transmitter and receiver generated incidental phase modulation. In practice, the tuner systems used in quasi-synchronous demodulators are inferior to those used in synchronous demodulators. The increased incidental phase modulation introduced by inferior tuners (i.e. those where there can be signal dependent carrier frequency shifts), would introduce additional quadrature distortion and would thereby degrade system performance. Incorporating these signal distortions in the simulation program would be a difficult chore, that is clearly beyond the scope of this study.

Quasi-synchronous system performance in a mixed impulse-gaussian noise environment is presented in Figure 4.18. When determining the bit error rate, packets that were rejected ($\geq$30% errors) are not considered in the calculation. The reason for this is that the major cause for packet rejection is loss of word sync, in which case the extracted and transmitted data sequence are not properly compared. The number of word sync losses is provided in Figure 4.18 at a video SNR of 25 dB. Without these numbers,

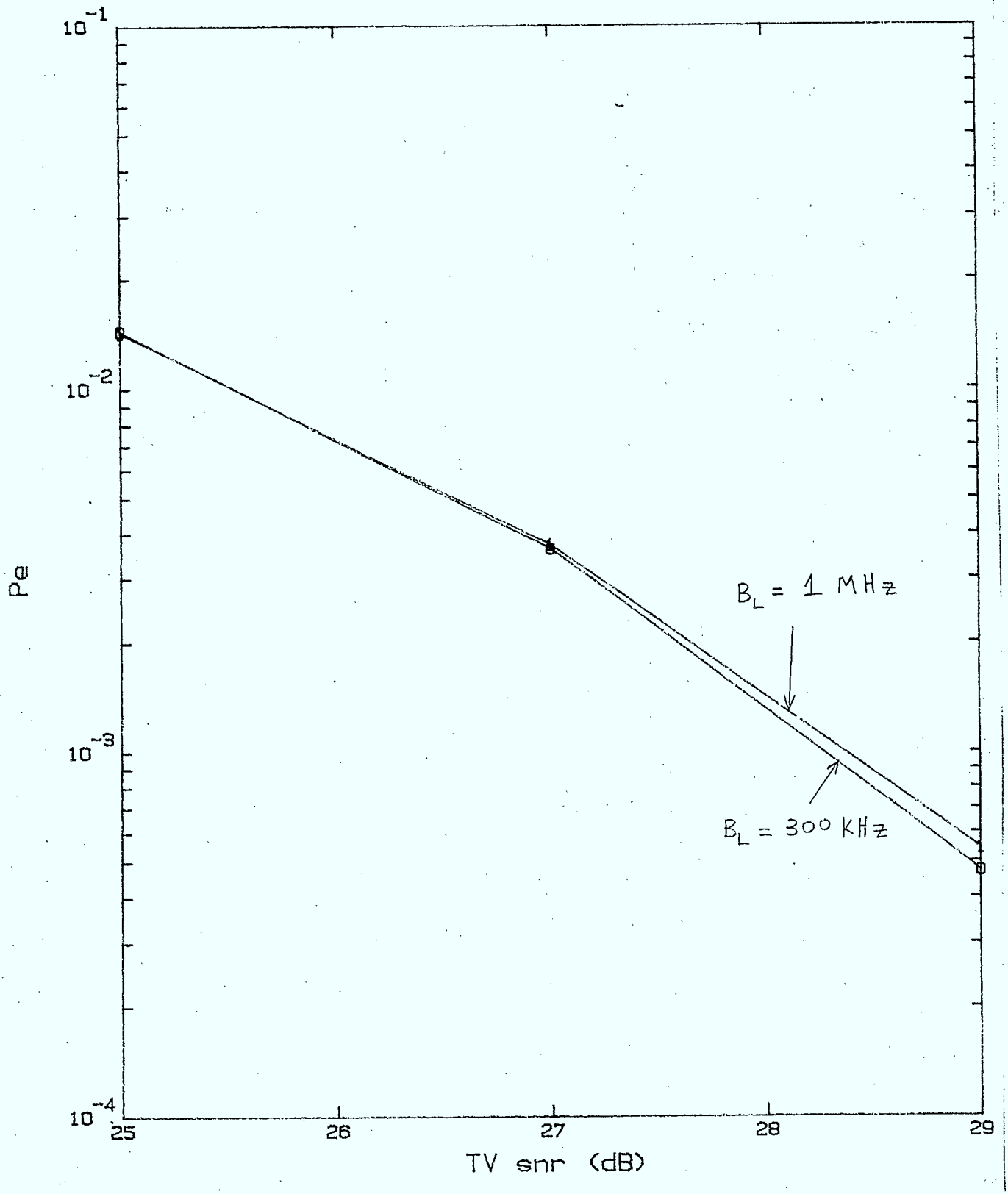

Figure 4.17: Simulated quasi-synchronous performance with a peak detector decoder for an ideal channel and thermal noise environment.

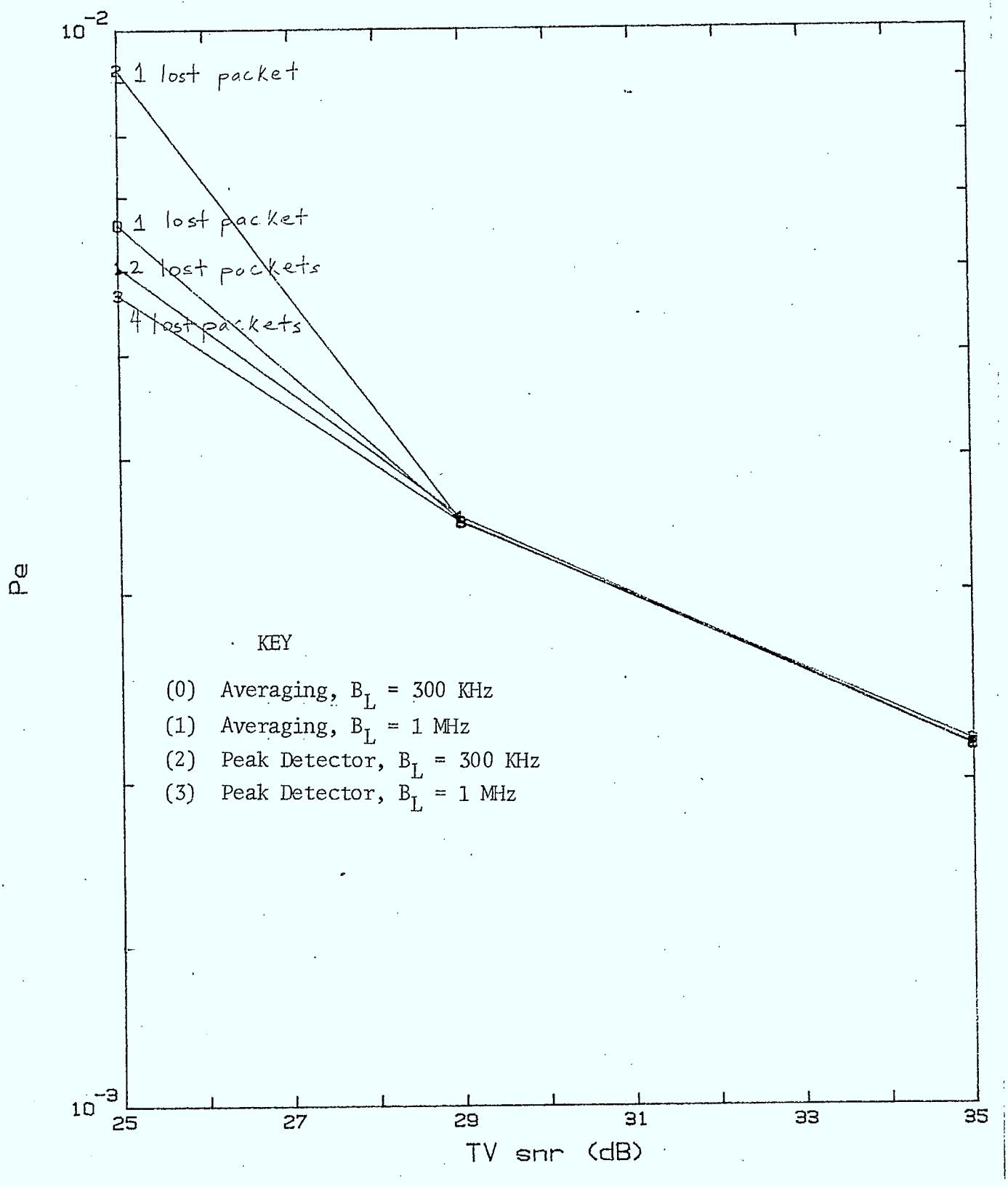

Figure 4.18: Simulated quasi-synchronous system performance with an ideal channel in an impulse noise dominated environment.

the curves are somewhat misleading. The averaging slicing level decoder and the narrowband carrier recovery loop are superior at this video signal to noise ratio. However, at higher video signal to noise ratios, there is virtually no difference between decoders and carrier recovery loop bandwidths for the impulse noise dominated environment.

The performance of quasi-synchronous detectors in a thermal noise environment with a 20 dB PDUR multipath channel is presented in Figure 4.19. The superiority of the averaging slicing level decoder is clearly evident. In this multipath environment, the difference between the performance achieved with the narrowband and wideband carrier recovery loops is quite small for both the averaging and peak detector decoders. The difference is noticeably greater ($\approx$0.5 dB) for the peak detector decoder, which is exactly opposite from the results obtained with the ideal channel.

The major conclusion of this section is that <u>well designed</u> quasi-synchronous carrier recovery loops suffer relatively minor degradations (approximately 0.5 dB) compared to narrowband (synchronous) carrier recovery, in the multipath and noise environments of interest to the broadcast Telidon application. By well designed, we are referring to loops with tuners that do not introduce excessive incidental phase modulation.

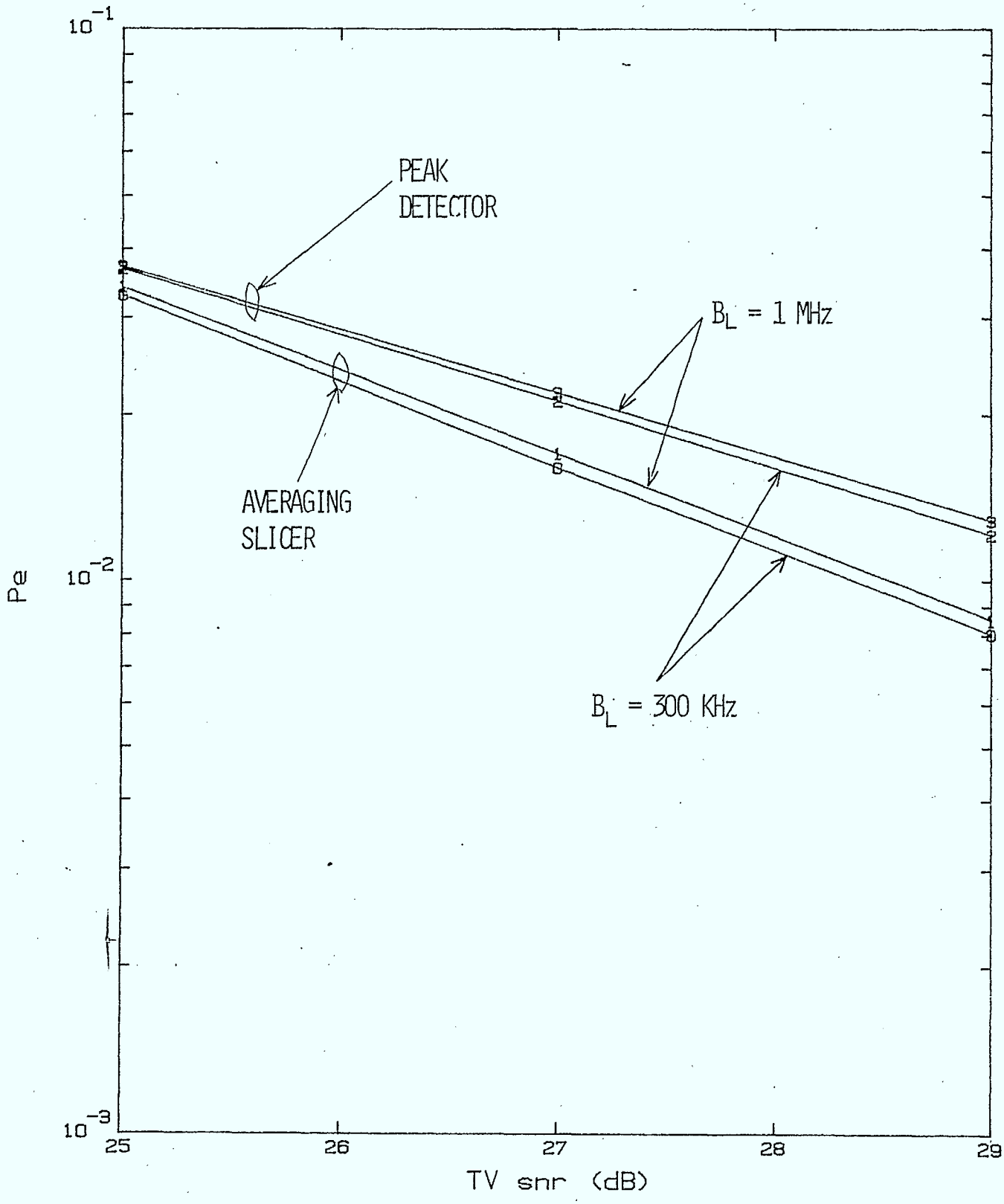

Figure 4.19: Simulated quasi-synchronous system performance with the 20 dB PDUR multipath channel in an impulse noise dominated environment.

5.0 EQUALIZATION FOR TELETEXT SYSTEMS

The purpose of this section is to establish the potential performance gain that can be obtained with equalization. We begin by reviewing some of the pertinent facts from Appendix I of [25] which deals with adaptive equalization for broadcast teletext.

5.1 Overview

For the equalization study, it is assumed that some form of coherent demodulation is used at the receiver. In this case, the complex baseband model, shown in Figure 5.1, can be applied. Here, P(f) is the teletext pulse shaping filter, and since this filter is implemented at baseband, it will have a purely real impulse response. T(f) is the effective television transmit filter, which includes the effects of the transmitter's IF filter, zonal filters, harmonic filter, and any fixed equalizer. Since this frequency response must be asymmetrical about the carrier frequency, its baseband representation will have a complex impulse response. C(f) is the frequency response of the channel, including multipath and transmit and receive antennas.

In the simulation, C(f) is represented as

$$C(f) = \hat{C}(f)\left(\sum_{p=1}^{P} c_p(t)\, e^{-j2\pi f T_p(f)} \right) \qquad (5.1)$$

where $\hat{C}(f)$ is the channel response in the absence of multipath, P is the number of propagation paths, and $c_p(t)$ are the complex path gains, and $T_p(t)$ are the path delays,

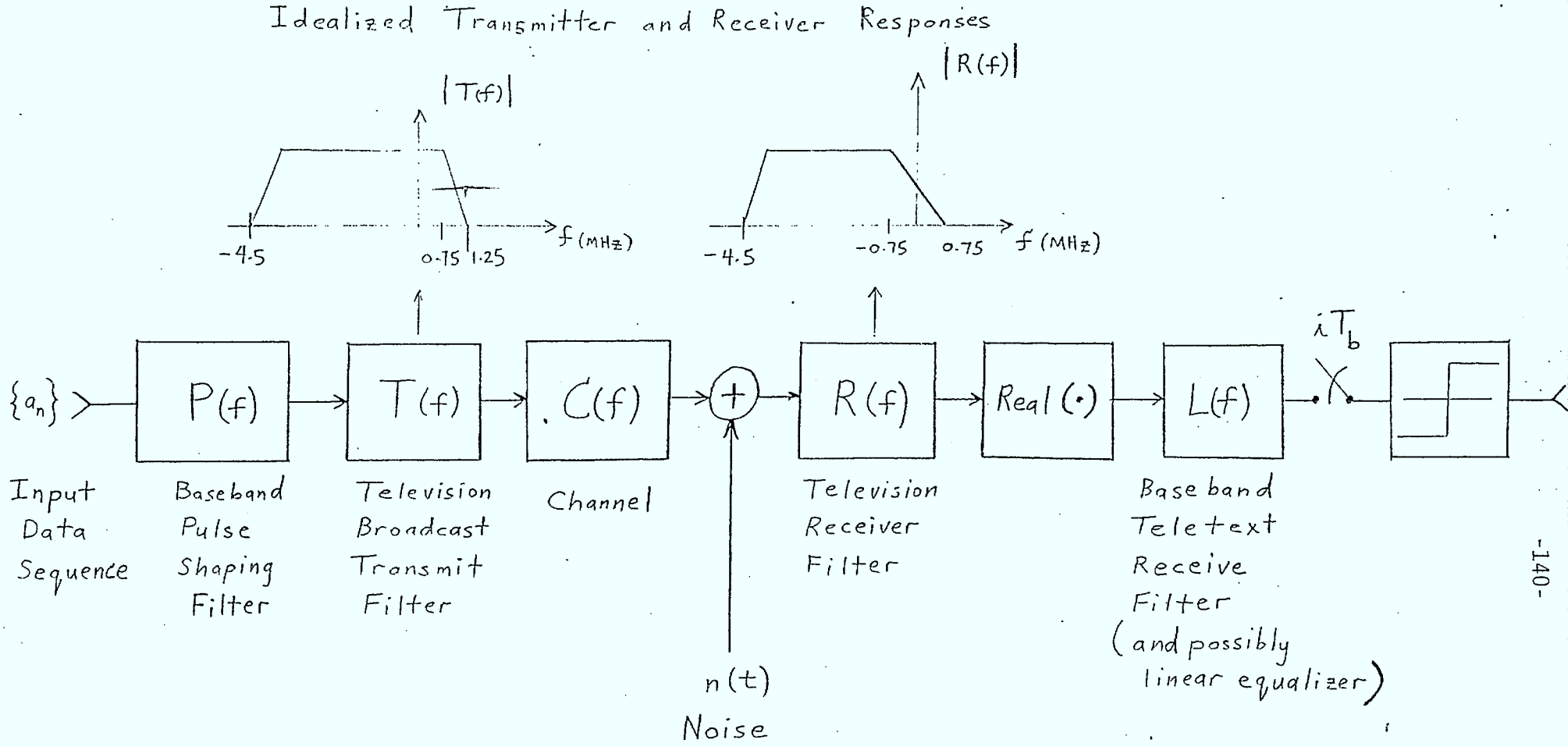

Figure 5.1 : Baseband model for broadcast television based teletext transmission

which can be time varying (due to the effects of non-ideal carrier recovery jitter and movement of the antennas in the wind). R(f) is the effective television receiver filter. For vestigial sideband demodulation, R(f) must be asymmetrical about the carrier frequency, and its baseband representation will have a complex impulse response. L(f) is the teletext receive filter. For the purposes of this study, idealized zero-phase nominal responses are assumed for the transmit and receive filters.

In general adaptive equalization can be used to compensate for a wide range of signal transmission impairments, which include:

(i) multipath propagation,

(ii) quadrature distortion,

(iii) deviations from nominal channel and nominal filters,

(iv) coloured noise and interference, and

(v) nonlinear distortion.

When multipath propagation is present with vestigial sideband transmission, the inphase channel does not experience pure multipath but rather a superposition of the multipath channel operating on both the inphase and quadrature channels. The distortion due to multipath propagation can consist of two components, one from the inphase channel and one from the quadrature channel.

While on the topic of multipath propagation it is worth while reviewing the nature of the multipath progation that is encountered with the broadcast Telidon application. The characterization of off-air measurements in the Ottawa area

performed by CRC and the results of simulation and analysis performed at MCS were summarized in Section 2. A few aspects relevant to teletext equalization will be discussed here.

The imposition of an acceptability threshold (from a television viewing standpoint) greatly restricts the possible range of channels. The amplitude responses of the channels cannot exhibit "inband nulls" in their frequency responses, as such channels would undoubtedly be unacceptable from a video quality stanspoint. Typical amplitude responses are illustrated in Figures 5.2 and 5.3, the first being for a channel with a PDUR of 13 dB (near the acceptability threshold), and the second for a PDUR of 20 dB (fairly reasonable video quality). Although these amplitude responses exhibit rippling, the channels are quite far from exhibiting in band nulls.

A question of interest of equalization is, are the vast majority of multipath channels encountered minimum phase? Of the 160 impulse responses measured, 83 were deemed to represent acceptable video channels. Of the 83 acceptable channels, only 6 were found to be non-minimum phase [11].

Multipath, quadrature distortion, and departure from nominal characteristics are linear in nature. It has been shown [26] that linear equalization can also be used to improve performance when nonlinear impairments are present, such as AM to AM and AM to PM conversion that is typical of power amplifiers.

An adaptive equalizer is capable of improving performance when coloured noise or interference is present. In essence, the adaptive equalizer improves performance by emphasizing the portions of the spectrum where the signal to noise ratio is good and deemphasizing portions of the spectrum where the signal to noise ratio is poor.

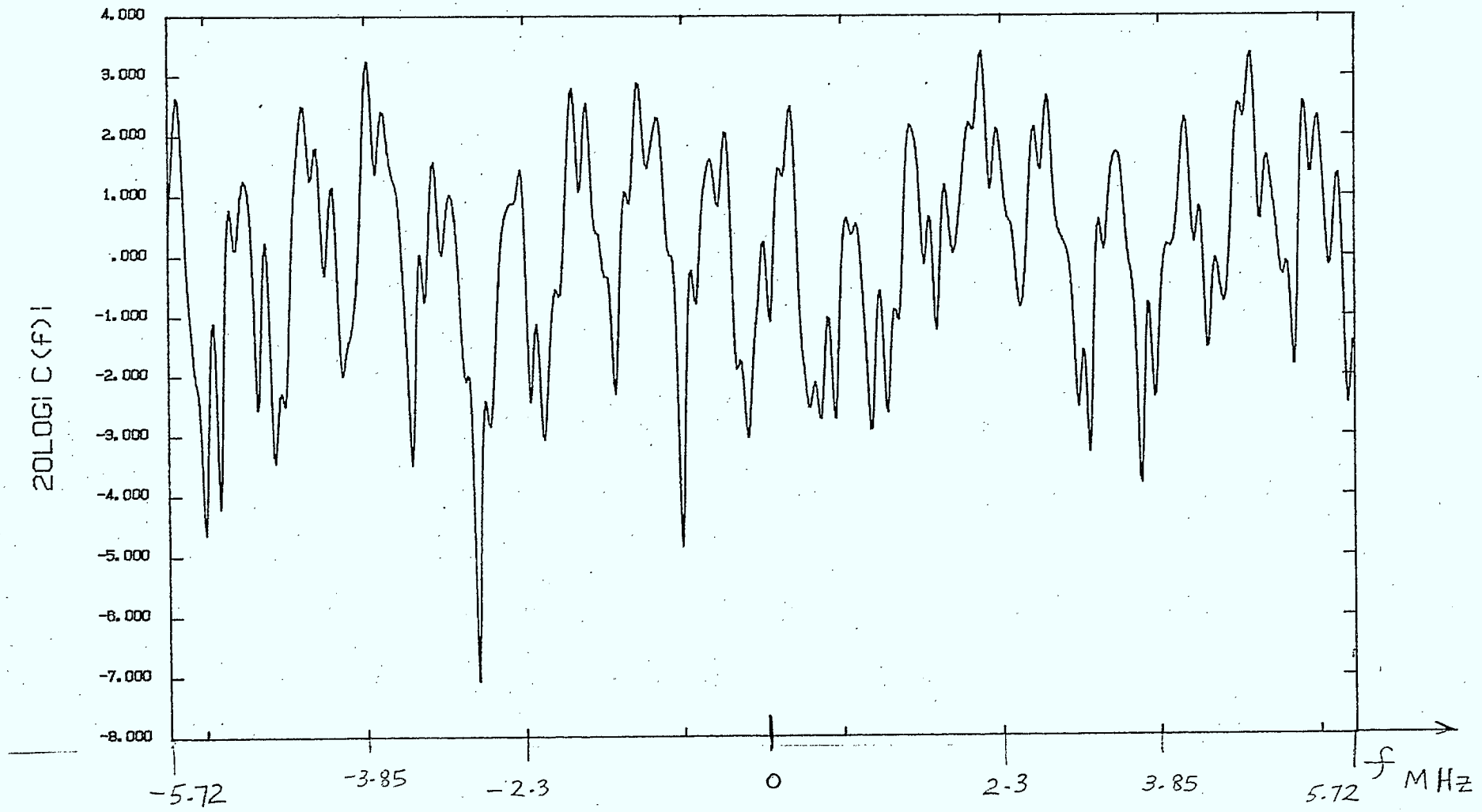

Figure 5.2 : Amplitude response of 13 dB PDUR multipath channel

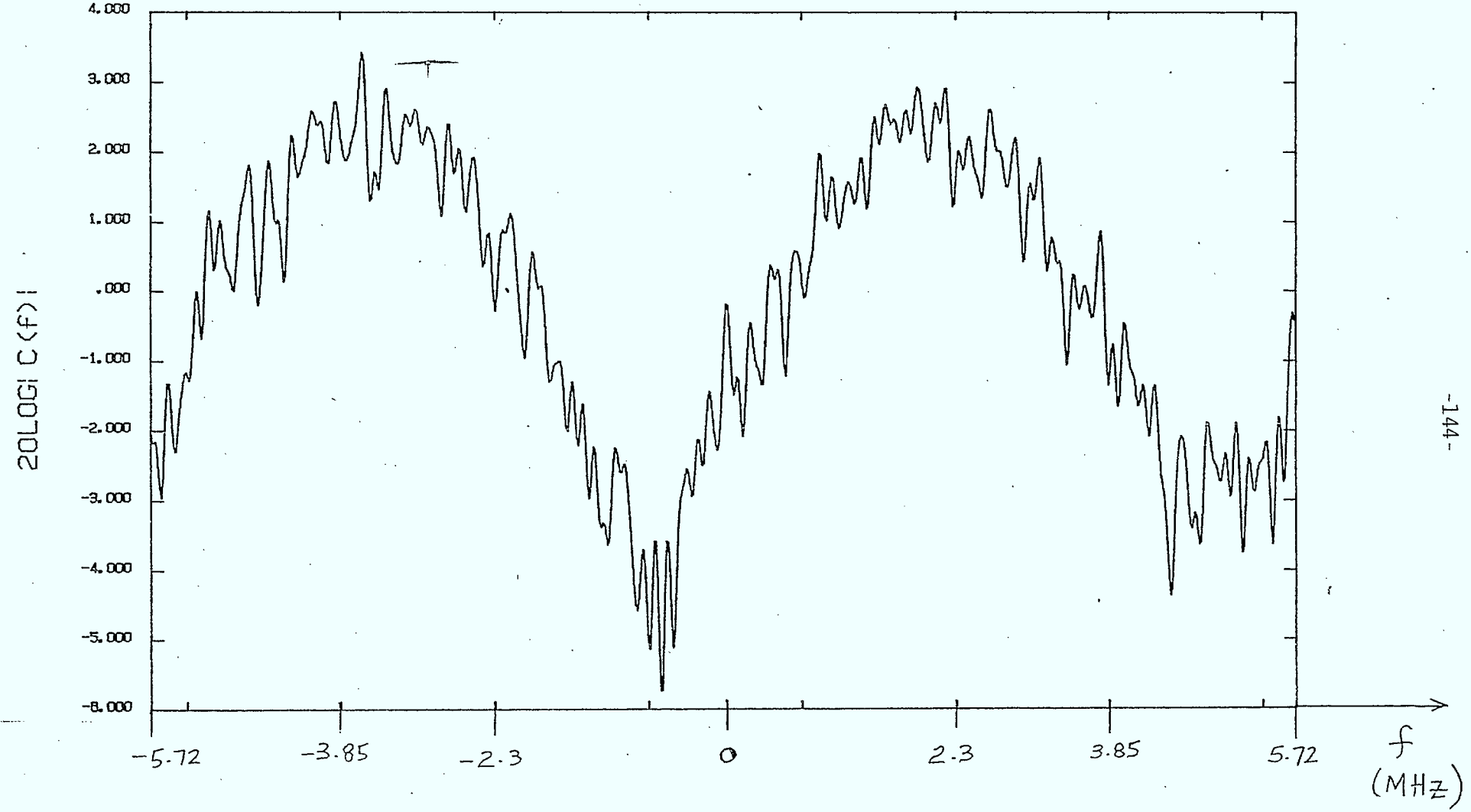

Figure 5.3 : Amplitude response of 20 dB PDUR multipath channel

There are two different locations in the complex baseband model where linear equalization can be applied (see Figure 5.4). It is well known that in general the optimum linear equalizer is complex (see Figure 5.4(b)). In order to perform complex equalization, the equalization must either be performed at IF or quadrature demodulation must be performed and the convolution of the complex demodulated signal and complex equalizer response performed. A less complex alternative is to perform real linear equalization following video detection (see Figure 5.4(a)). Since it is expected that much of the future broadcast Telidon receive equipment will only have access to the real video signal, one will therefore be constrained to use real equalization. For typical multipath channels it is expected that the loss incurred, due to ignoring the signal energy in the quadrature channel will be less than a couple of dB. Since the goal is to propose an economically practical adaptive equalizer, attention has been restricted to real equalization.

The fundamentals of equalization techniques will only be briefly reviewed here. The inherent weakness of any linear equalization scheme is noise enhancement, which is especially severe for channels with nulls or near nulls. This is due to the tendency of the equalizer, even for minimum mean square linear equalization, to invert the channel characteristic. To achieve good BER performance on channels with nulls or near nulls, nonlinear techniques such as decision feedback equalization or maximum likelihood sequence estimation must be employed. The major advantage of decision feedback equalization is that lower mean squared error (less noise enhancement) arises because of the increased degrees of freedom afforded by subtraction of ISI due to past decisions. However, decision errors are more disastrous and tend to propagate.

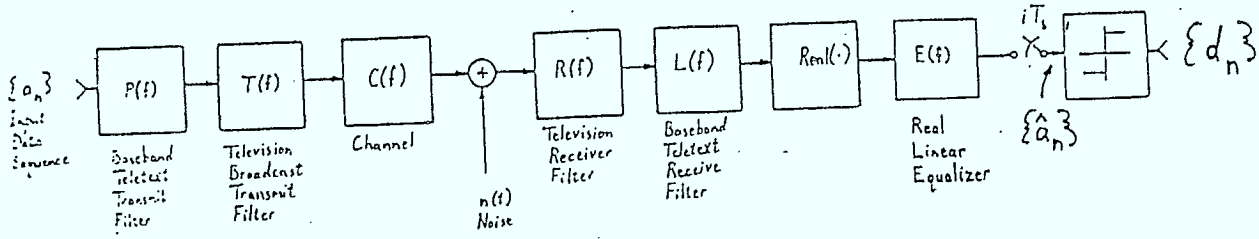

(a)

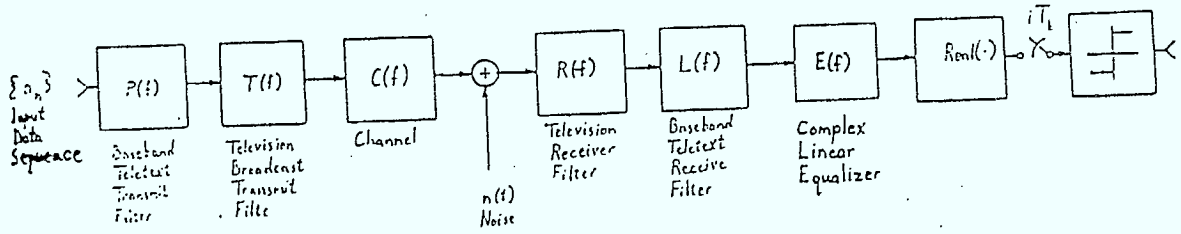

(b)

Figure 5.4 : Two possible locations for linear equalization in the complex baseband model.

Both linear and decision feedback equalizers are usually implemented as tap delay line structures (transversal filters) which are easy to adapt. For implementation reasons, it is often desirable to choose the sampling rate to be the lowest multiple of the baud rate which exceeds the minimum sampling rate given by Nyquist's sampling theorem. For the Telidon application an appropriate tap spacing for the transversal filter is $T_b/2$, where T_b denotes the bit period. Note that from Nyquist's sampling theorem, absolutely nothing is gained from going to smaller tap spacings except added complexity. The number and density of echoes is completely irrelevant for the bandlimited teletext channel. In general, the most desirable arrangement for a decision feedback equalizer is to have a T/2 spacing for the transversal filter and a T tap spacing for the pure decision feedback section.

For coefficient adaptation with linear equalization, the most common criteria is the minimization of the mean square error between the equalizer output and the data decisions (if a known training sequence is available, this can replace the potentially inaccurate data decisions). An iterative gradient-based adaptive algorithm, similar in nature to classical adaptive equalizer introduced by Widrow and Hoff (see Figure 5.5), is a reasonable choice because the channel characteristics change slowly with time. It avoids the computationally intensive tasks of estimating the covariance matrix, A, and correlation vector, b, in the direct solution procedure:

$$\underline{c}_{opt} = A^{-1} \underline{b} \qquad (5.2)$$

where

$\underline{c}_{opt}$ is a vector denoting the optimal equalizer coefficients,

$$\underline{b} = E\{\underline{y}(n)\, a_n\}$$

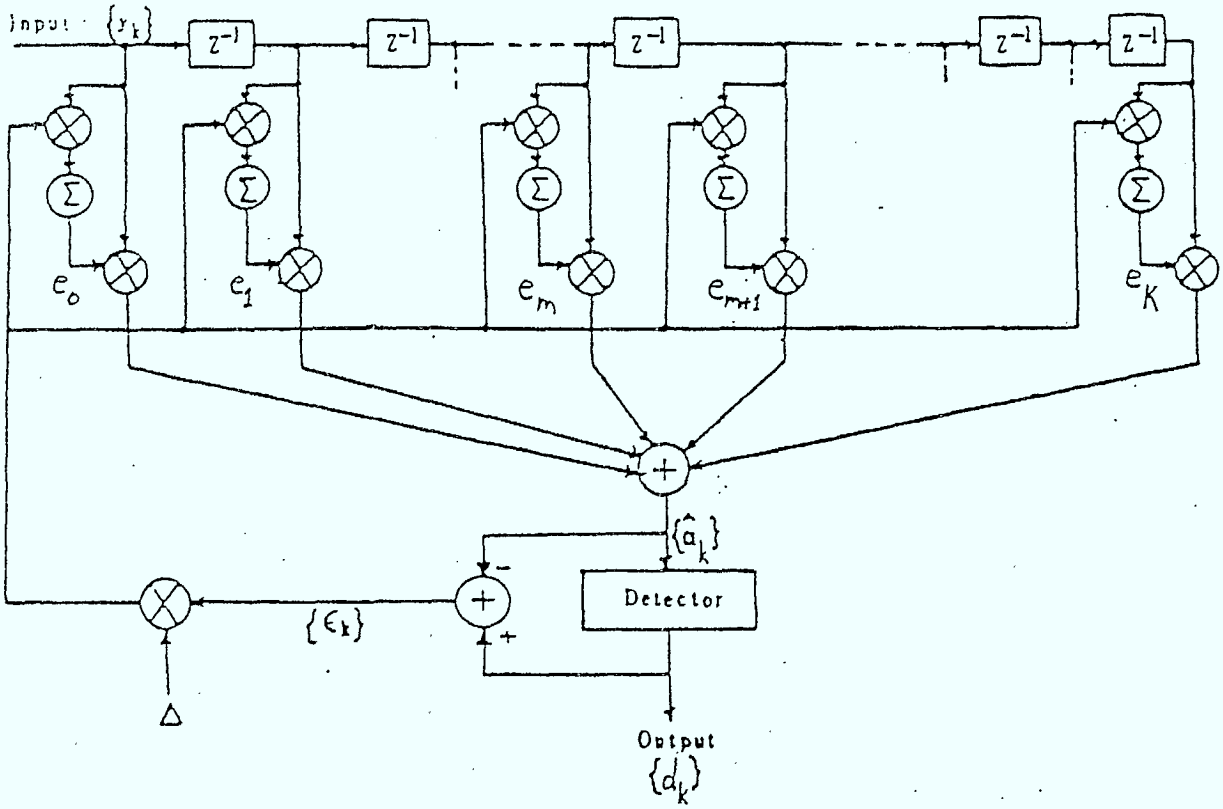

Figure 5.5 : A block diagram illustrating the structure of a typical gradient-base adaptive equalizer [31].

$$\underline{y}(n) = \begin{bmatrix} y(n) \\ y(n-1) \\ \\ y(n-N) \end{bmatrix}$$

$y(n)$ is the sampled channel output,

$A = E[\underline{y}(n)\ \underline{y}(n)^T]$ (channel covariance matrix),

E denotes the expectation operator, and

T denotes matrix (vector) transposition.

An analogous procedure can be derived for updating the coefficients of a decision feedback equalizer [27].

It must be emphasized that real time coefficient adaptation is probably not practical at teletext data rates. It is doubtful that it could be achieved at reasonable cost. A non-real time coefficient adaptation algorithm would have to be developed. It is important to note that the iterative closed-loop nature of the adaptive algorithm must be maintained if inherently nonlinear techniques are used to realize the equalizer's programmable filter [11] (e.g. CCD [28] or analog electronics [29]). When nonlinear techniques are used an open-loop approach such as the direct solution of optimum equalizer coefficients is unlikely to perform well because of the nonlinear relationship between the tap control signal and the effective tap weight. This is illustrated for a CCD transversal filter [28] in Figure 5.6. An iterative closed-loop type of adaptation technique can compensate for this kind of monotonic nonlinearity without unduly complicating the algorithm.

The choice of a training sequence for the adaption of the equalizer is worthy of some discussion. A training signal that looks like an uncorrelated data signal is the best

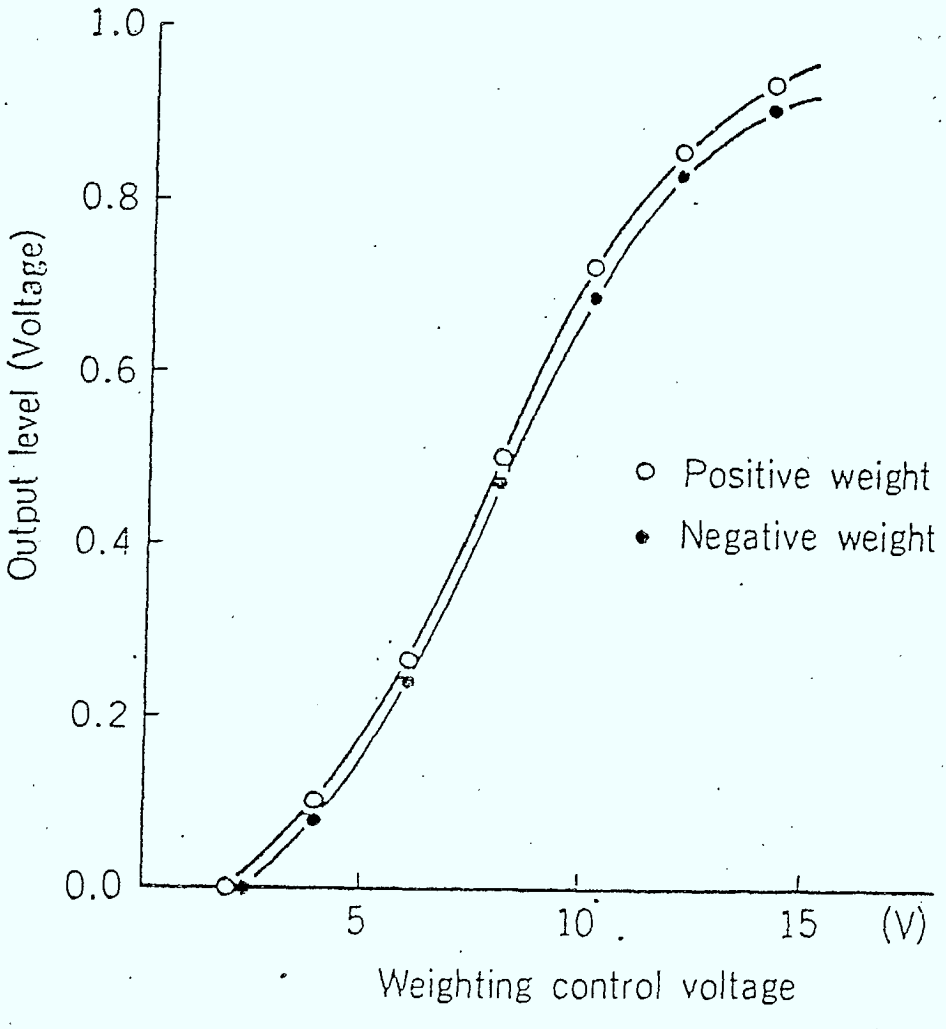

Figure 5.6 : An illustration of the nonlinear control characteristic of a CCD transversal filter tap weight [28].

choice from a couple of theoretical points of view. Note that the A matrix and $\underline{b}$ vector in equation (5.2) are dependent on the transmitted signal. The clear conclusion is that if the optimal tap weights for the reception of "random" data are desired, then the equalizer should be trained using a transmitted signal closely resembling random data. The desirability to use a data-like training signal is even more evident when one considers the use of the equalizer for compensating for nonlinearities in the channel (i.e. transmitter's power amplifier). By using a linear equalizer, one is implicitly fitting a linear model to a non-linear channel. It is well known that the linear model that is the best fit (according to some specified criterion) to a nonlinear system, is highly dependent upon the stimulus (input) that the system is given [30]. Therefore, the teletext data signals may be the most appropriate channel stimulus, as well as being one of the most convenient.

As pointed out earlier the major advantage of decision-feedback equalization over linear equalization is the ability of the former to provide reasonably good performance for channels with in band nulls or near nulls. Examples which demonstrate the vastly superior performance of decision feedback over linear equalization for such channels are provided in [25], [31]. One should be cautioned against placing too much emphasis on such channels, as the requirement that a useable television picture is provided prescreens such channels.

Another interesting feature of the measured channel impulse responses in Volume 2 of [11] is that there is usually no precursor. For such channels all that is needed is a pure decision feedback section, which is well suited for VLSI implementation [25]. The determination of the coefficients is in fact an impulse response estimation problem.

Techniques for estimating the impulse response of a pulse amplitude modulated data communications system in an optimal (least squares) fashion are available [32], [33], [34]. Unfortunately, the direct computation of the equalizer coefficients using the above approach is probably too computationally intensive to be realized on a fixed word length microprocessor. A gradient based iterative technique for estimating the channel impulse response is illustrated in Figure 5.7 [31]. If the slicing level is removed prior to equalization, the data decisions are ±1, implying that no multiplications are required.

Pure decision feedback equalization has some advantages over linear equalization. One of these is that it will not "smear" strong impulses in the way that a linear equalizer will. It must however cope with the problem of decision errors in the feedback portion of the equalizer. This often gives rise to the propagation of errors [35]. Another advantage of pure decision feedback equalization is that channels with in band nulls can be successfully equalized. However, this is only an advantage in the unlikely event that one expects to receive teletext over a channel that is not capable of receiving an acceptable quality video signal (from a television viewing standpoint). The other advantage is that it is more suited to a VLSI digital implementation.

A major advantage of linear equalization is the equalizer is also capable of equalizing the video signal as well as the data signal. The extreme sensitivity of the Telidon system to multipath has been demonstrated in Section 2.3. This is due mainly to the structure of the teletext line, where relatively modest amounts of multipath can superimpose portions of the colour burst or line sync pulse on the two byte clock synchronization signal. The most serious consequence of multipath propagation is

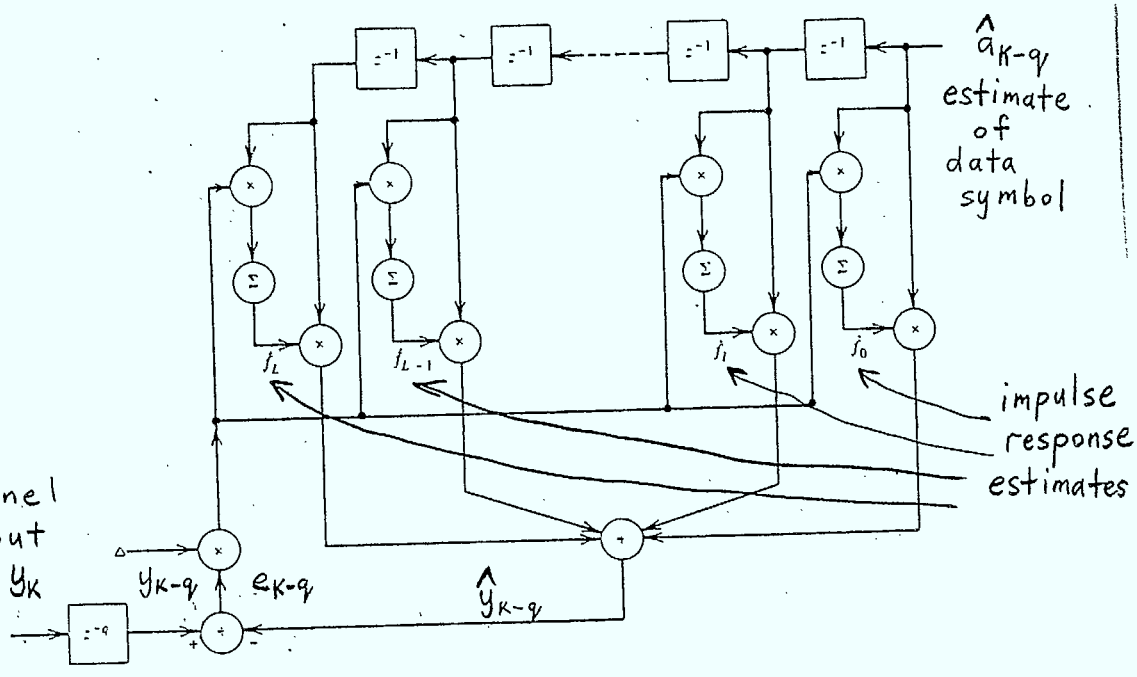

Figure 5.7 : Adaptive transversal filter for estimating the channel impulse response. [31]

synchronization failure. If the linear equalizer is placed in front of the synchronization (slicing level estimation and symbol timing recovery), this extremely serious problem can be alleviated. A decision feedback equalizer could not cope with this situation because the synchronization signals are not data like signals. Given the potential for decreasing the sensitivity of the Telidon system to multipath propagation and loss of synchronization, linear equalization represents the most promising approach.

Before discussing the implementation of the equalizer used in the simulation program, the required number of taps for a linear equalizer will be discussed. The choice of the number of taps combined with the tap spacing (i.e. $T_b/2$) defines the support* of the equalizer. For the equalizer to be effective, the support of the equalizer must be at least as great as the spread of the channel. Preferrably it should be several times greater. This will be clearly illustrated in the next section. From the measurements conducted in the Ottawa area [11], most of the significant echoes have delays less than 3 μsec, and the longest delay was 8 μsec. Thus for mutipath equalization near downtown Ottawa an equalizer with a support of at least 3 μsec (i.e. at least 35 T/2-spaced taps) should be used. Even longer equalizers are likely to be required for larger cities or at higher frequencies (e.g. UHF band).

The support of an equalizer is extremely important. The dismal performance of the Philips teletext equalizer during off-air tests conducted by RCA in New York city is evidence of this [25]. The Philips equalizer was designed with a support on the order of 1 μsec, and its intended purpose

*By "support" we are referring to the shortest segment of time, beyond which the unit sample response is effectively zero.

was reducing short echoes (0.5 - 1 μsec) in Teletext signals [29]. Thus it should not be surprising that it was not capable of equalizing many of the metropolitan New York channels, where many echoes are likely to have delays several times greater than what the equalizer was designed for. The Philip's equalizer would probably perform quite well for most CATV channels where the dominant echoes are expected to have delays less than 400 nsec [25]. It must be emphasized that the reason for the failure of the Philip's equalizer in the RCA off-air tests is that the support is simply not long enough. It is not due to the density of echo paths or the possible non-specular nature of the reflections, as some people have suggested.

The next section discusses the implementation of the equalizer used in the simulation program. Implementation considerations for teletext equalization are presented in Appendix D.

5.2 Implementation of a Linear Equalizer for the Simulation Program

An optimal linear receiver, where the overall channel is constrained to satisfy the Nyquist I criterion, is used in the simulation program. For the situation depicted in Figure 5.8(a), with a white gaussian noise channel, the optimum linear receiver is given by:

$$E_{opt}(f) = \frac{K\, H_I(f)^*}{\sum_n \left|H_I(f + \frac{n}{T_b})\right|^2} . \qquad (5.3)$$

where K is an arbitrary constant.

Note that the form of this optimum receiver is a matched filter followed by a transversal filter. The optimal receiver for non-white gaussian noise is easily determined by inserting a noise-whitening filter (which by the theorem of reversibility [54] does not effect error performance) and applying the optimal receiver for white noise channels. The situation is depicted in Figure 5.8(b), and the optimal receiver filter is given by:

$$E_{opt}(f) = \frac{K\, H_I(f)^*/W(f)}{\sum_n \frac{\left|H_I(f + \frac{n}{T_b}\right|^2}{W(f + \frac{n}{T_b})}} . \qquad (5.4)$$

From the complex baseband model provided in Figure 5.1, one can identify the overall complex channel response, H(f), as

$$H(f) = P(f)\ T(f)\ C(f)\ R(f)\ L(f),$$

and the noise shaping filter, N(f), as:

$$N(f) = R(f)\ L(f).$$

The noise spectrum at the input to the real equalizer is proportional to W(f), where

$$W(f) = \frac{1}{2}\{\,|N(f)|^2 + |N(-f)|^2\} .$$

The overall impulse response of the inphase (real) channel is given by:

$$H_I(f) = \frac{1}{2}[H(f) + H(-f)^*] .$$

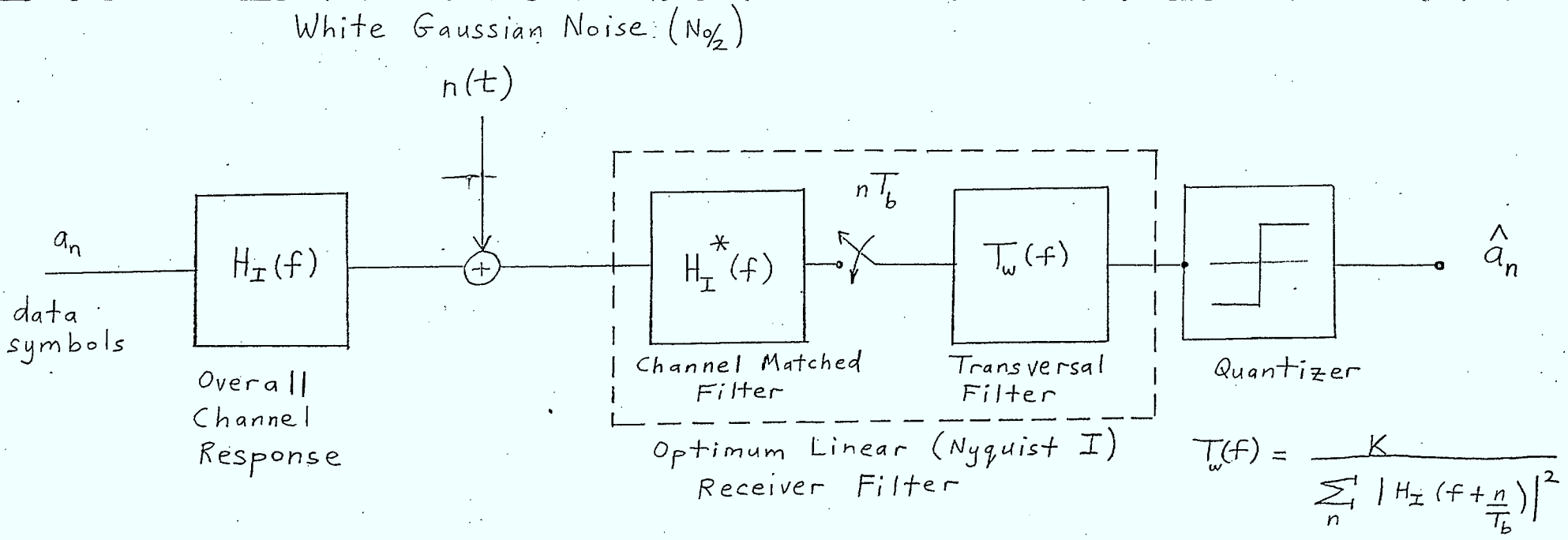

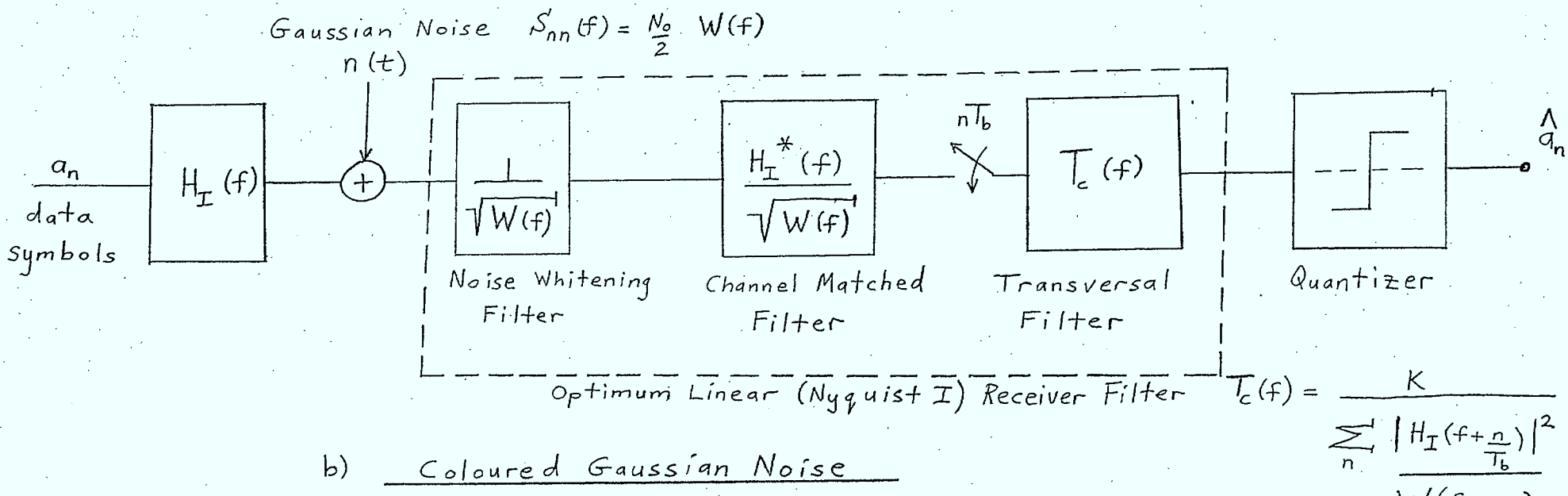

Figure 5.8: Optimum linear equalization subject to Nyquist's criterion for no intersymbol interference.

The transfer function of the optimum linear equalizer (under the constraint that the overall channel satisfies Nyquist's criterion for no intersymbol interference) can be expressed as:

$$E_{opt}(f) = \frac{K\, H_I^*(f)/W(f)}{\frac{|H_I(f)|^2}{W(f)} + \frac{|H_I(f-1/T_b)|^2}{W(f-\frac{1}{T_b})}} \quad 0 \leq f \leq \frac{1}{T_b} . \tag{5.5}$$

as $H_I(f)$ and $W(f)$ are bandlimited at a frequency lower than the data rate, $1/T_b$. The equalizer response for frequencies in the range $\frac{-1}{T_b} \leq f \leq 0$ is easily obtained using the complex conjugate symmetry property of the transfer function of a real signal (i.e. $E_{opt}(-f) = E_{opt}(f)^*$). It is trivial to show that (5.5) is identical to the expression presented in equation (2.14) of [25]. The appropriate value of K for our simulation program is $T_b/2$. In this case, the gain factor for the spectrum of the sampled signal is M/2. However, since the digital sampling gain, M, is applied on the input data signal in our simulation, the appropriate value of K for FFT processing is 0.5.

An equalizer with 128 taps at T/2 spacing has been chosen for the simulation. This number of taps was chosen because some of the more promising hardware approaches to realizing a programmable teletext equalizer are capable of realizing 128-tap equalizers. Furthermore, it is sufficiently greater than the minimum number of 35 taps required for the Ottawa area. This was realized by inverse transforming the optimal equalizer transfer function, applying an appropriate time domain window (704 samples at the high

sampling rate used in the simulation program corresponds to 128 T/2 spaced samples). The resulting impulse response was retransformed to the frequency domain for filtering the data signal. Further details are provided in Appendix E.

The form of the optimum linear receiver filter (under the Nyquist I constraint) and the optimum MMSE linear equalizer are quite similar. The transfer function of the optimum MMSE equalizer is given by [55]:

$$E(f) = \frac{K\, H_I^*(f)/W(f)}{\sum_n \frac{|H_I(f+/T_b)|^2}{W(f+\frac{n}{T_b})} + \frac{K\, N_o/2}{\dot{\dot{S}}_{aa}(f)}} \qquad (5.6)$$

where $\dot{\dot{S}}_{aa}(f)$ denotes the spectrum of the data signal, and

K is an arbitrary constant (commonly equal to T_b).

The only difference between the two expressions is the term in the denominator that depends on the noise power and data spectrum. An adaptive T/2 spaced transversal MMSE equalizer with a very large number of taps would converge to this transfer function. From a simulation viewpoint, the problem with the MMSE equalizer is its dependence on the signal to noise ratio and the data spectrum. Furthermore, it may not be valid to assume a white data spectrum for the Telidon system, as no scrambling of the data is performed. From the simulation standpoint, it is much easier to characterize the performance with the linear equalizer constrained to satisfying Nyquist I. The achievable error performance with a MMSE equalizer should be at least as good, and potentially better (due to the ability to tradeoff ISI for less noise enhancement).

5.3 Evaluating the Improvement Provided By Linear Equalization

The extreme sensitivity of the Telidon system to multipath has been demonstrated in Sections 2.3 and 3.3. This is due mainly to the structure of the Telidon teletext line, where relatively modest amounts of multipath can superimpose portions of the colour burst or line sync pulse on the two byte clock synchronization signal. Preceding the slicing level and clock phase extraction by a linear equalizer can alleviate the multipath problem to some degree. The purpose of this section is to determine the performance improvement that can be achieved by linear equalization.

The simulated performance of the linear equalizer using an averaging slicing level decoder with the 13 dB PDUR multipath channel in a thermal noise environment (for the truncated 100% raised cosine pulse shape) is presented in Figure 5.9. The linear equalizer provides a considerable performance improvement. One cannot achieve the performance level attained with an ideal channel. Given the noise enhancement property of linear equalizers, this is not at all surprising. At a weighted video signal to noise ratio of 30 dB, the error rate before equalization is in the 1×10^{-2} neighbourhood. Error protection coding will be relatively ineffective with input bit error rates this high. Ideally, one would like to have a functional teletext system with video signal to noise ratios in the 30 dB region. With the linear equalizer, the error rate is reduced to the 1×10^{-3} neighbourhood, which is relatively close to the threshold where error protection coding becomes effective.

The simulated performance of the linear equalizer using an averaging slicing level decoder with the 14 dB PDUR multipath channel in a thermal noise environment (for the

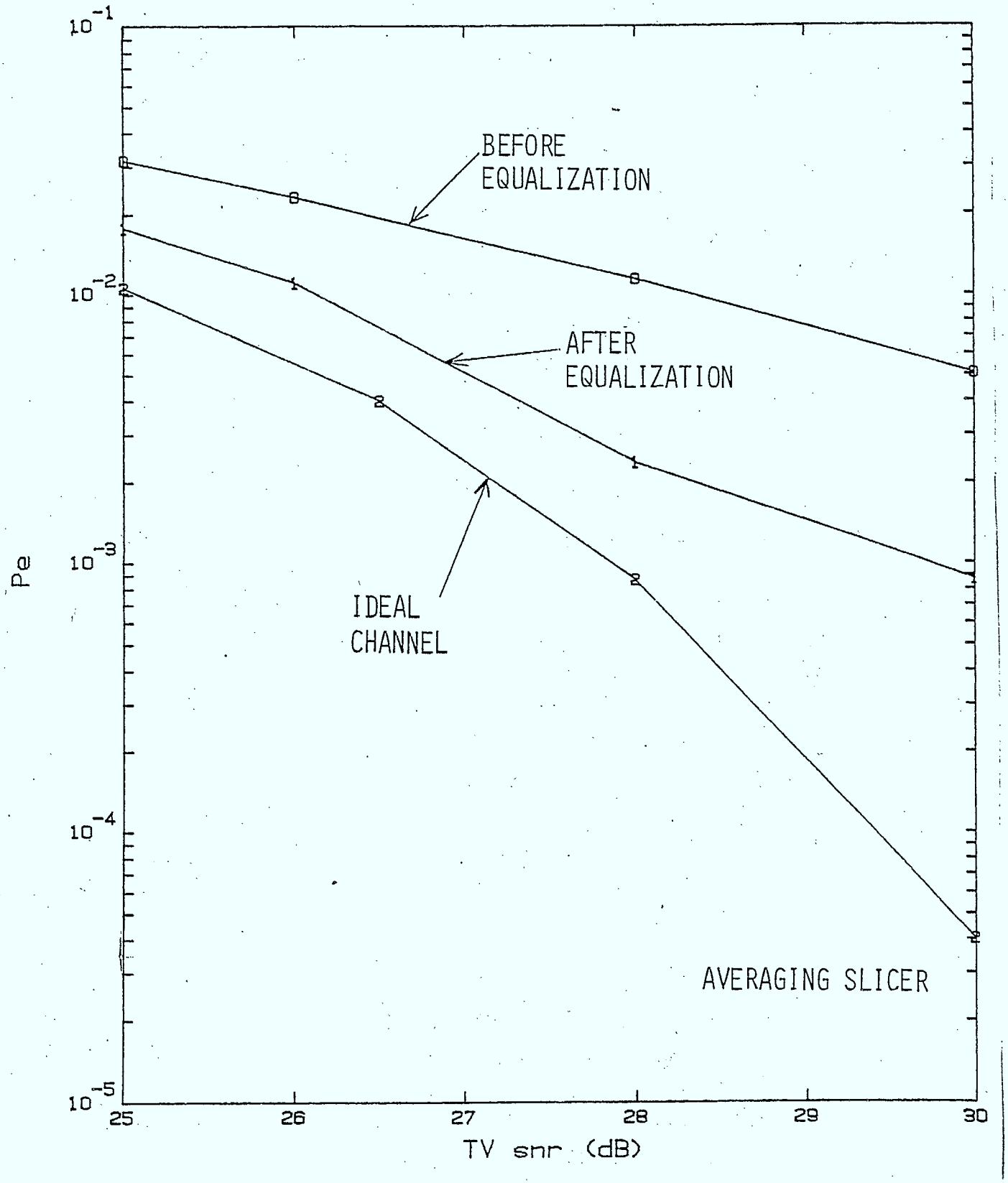

Figure 5.9: Linear equalizer performance with the 13 dB PDUR multipath channel in thermal noise.

truncated 100% raised cosine pulse shape) is presented in Figure 5.10. The trends are basically the same as in Figure 5.9. The linear equalizer provides a considerable improvement in bit error rate performance, and is, as expected, worse than results for an ideal channel. The linear equalizer performance improvement ($p_e \simeq 6.5 \times 10^{-3}$ at a video signal to noise ratio of 30 dB) makes the operation of the broadcast Telidon system feasible at video signal to noise ratios as low as 30 dB for multipath channels near the video quality acceptability threshold.

Figure 5.11 shows the linear equalizer improvement with an averaging slicing level decoder in a thermal noise environment with a 20 dB PDUR multipath channel. This multipath channel has a reasonable television quality index, despite a significant close in echo. The linear equalizer improvement is considerable ($\simeq$3-4 dB) with this multipath channel. With this channel, the performance of the linear equalizer comes closer to the ideal channel performance than it did with the 13 dB and 14 dB PDUR multipath channels. At a weighted video signal to noise ratio of 30 dB, the error rate with a linear equalizer is approximately 4×10^{-3}. With this input error rate to the decoder, error protection coding will be effective, implying that reasonable system performance can be achieved at video signal to noise ratios as low as 30 dB in reasonable multipath environments.

Figure 5.12 summarizes linear equalizer performance in a thermal noise environment with all three multipath channels and both decoder types. The clear superiority of the averaging decoder is evident. With the averaging slicer, the linear equalizer performance is best for the multipath channel with the highest television video quality rating, and is worst for the multipath channel which has the

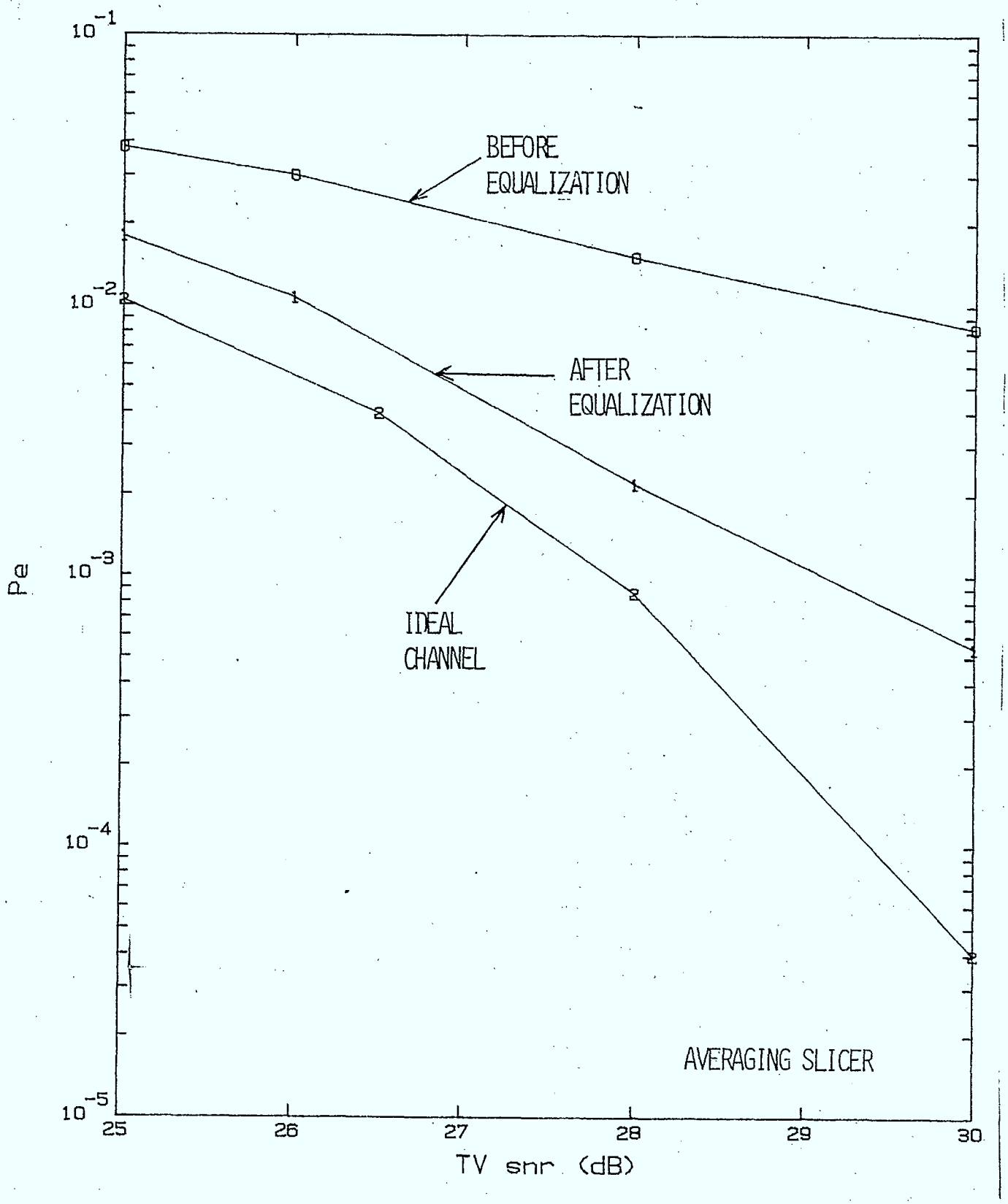

Figure 5.10: Linear equalizer performance with the 14 dB PDUR multipath channel in thermal noise.

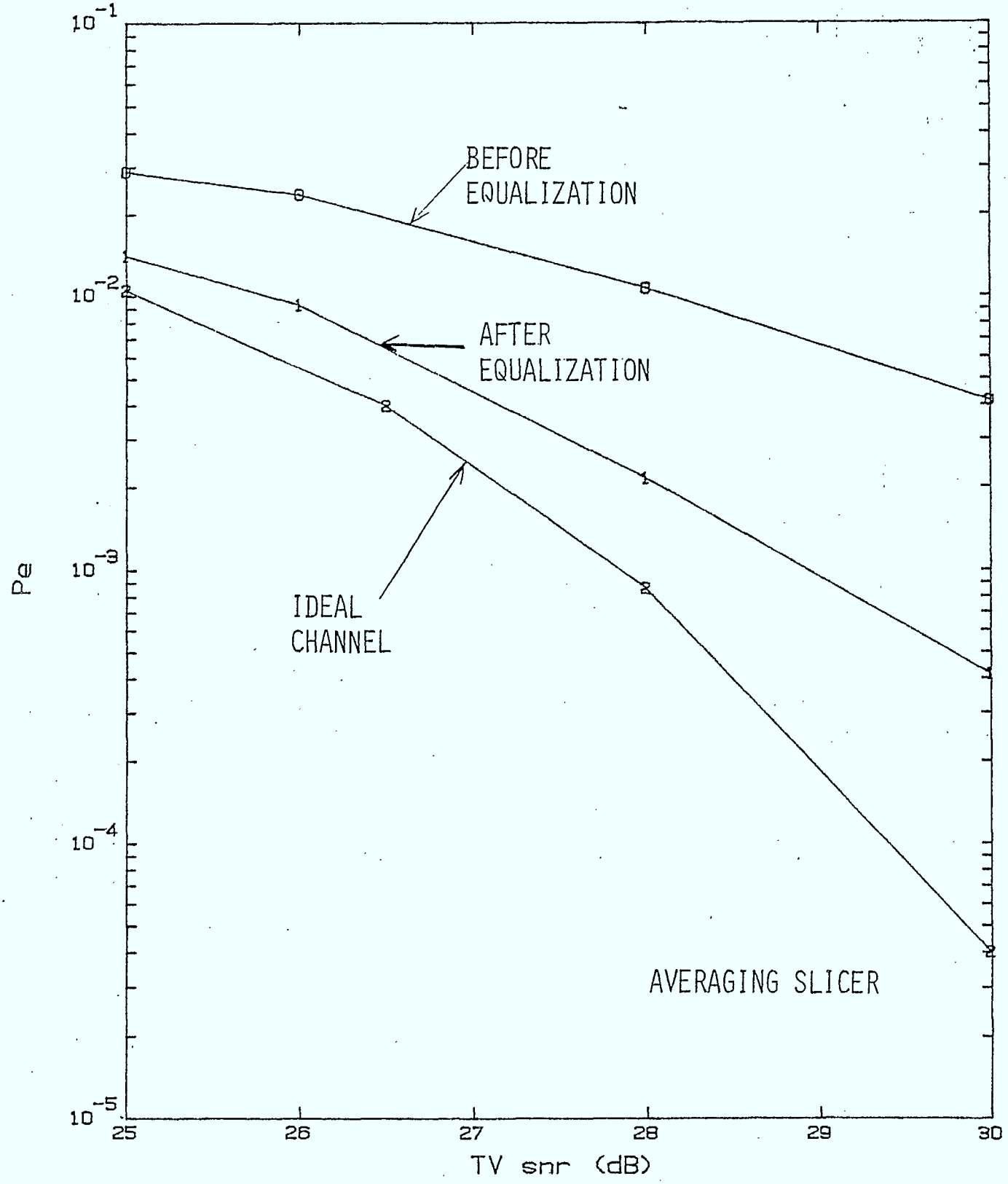

Figure 5.11: Linear equalizer performance with the 20 dB PDUR multipath channel in thermal noise.

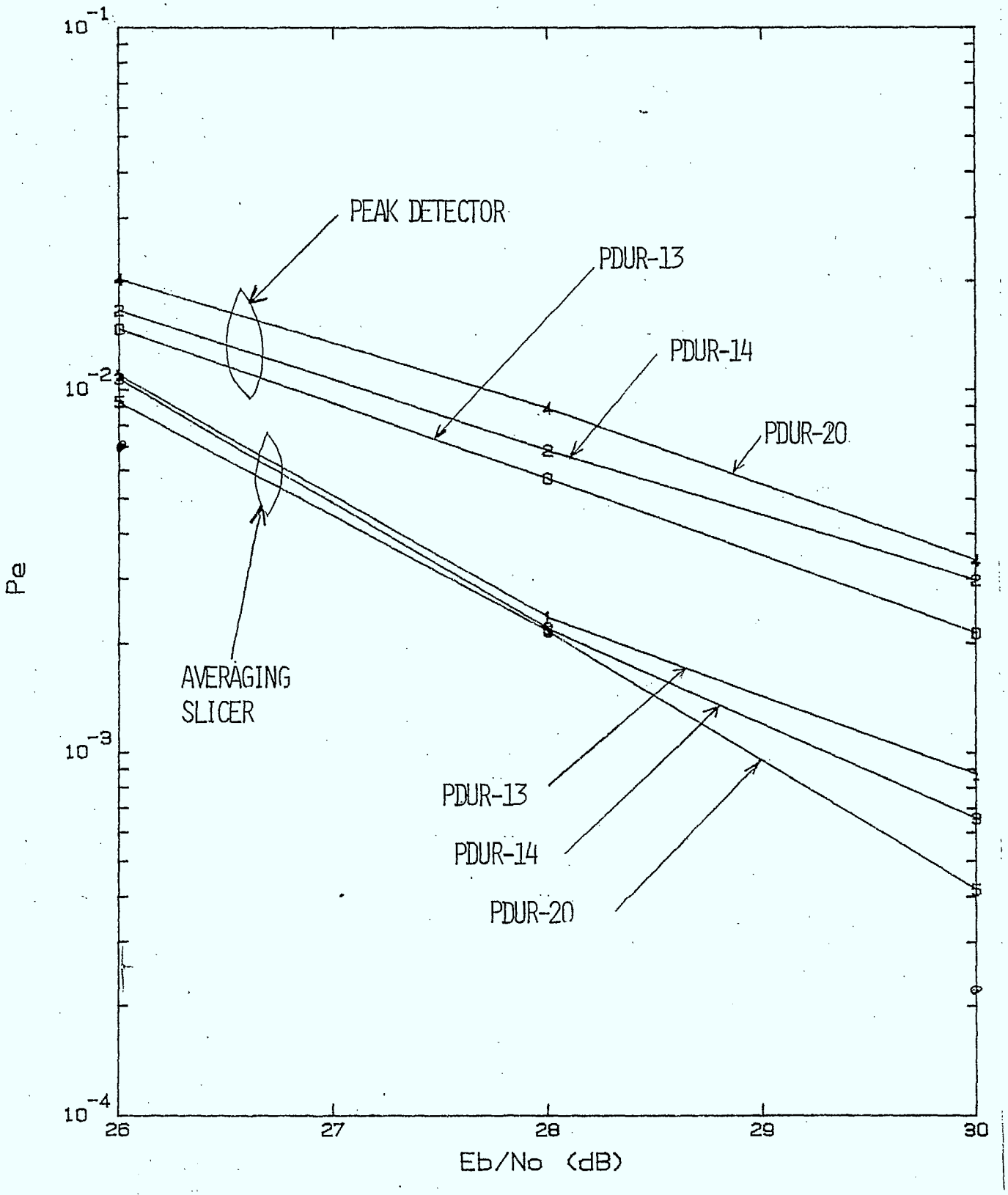

Figure 5.12: Summary of linear equalizer performance in white gaussian noise.

lowest, but still acceptable, video quality index. This is not surprising in light of the noise enhancement property of linear equalization. This trend is not repeated for the peak detector decoder. The best television video quality channel actually has the worst system performance with the peak detector decoder. Note also, that in multipath environments, the peak detector decoder error performance is at least a factor of two above the $1x10^{-3}$ threshold error rate for a SNR_{TV} = 30 dB. Even with the most powerful codes advocated for the Telidon system, adequate system performance cannot be guaranteed with an input bit error rate this high.

Figure 5.13 illustrates the performance of the linear equalizer with an averaging slicing level decoder in a mixed impulse - gaussian noise environment with a 20 dB PDUR multipath channel. This noise environment is impulse dominated (impulse noise 125.89 times stronger than thermal noise component). There is virtually no improvement in bit error rate with the linear equalizer. In fact, at the lower video signal to noise ratio (SNR_{TV} = 28 dB), performance seems to be degraded. The likely explanation is the tendancy of a linear equalizer to smear noise impulses, thereby prolonging their duration. A comparison of the peak detector and averaging slicing level decoder performance in this impulse dominated noise environment is presented in Figure 5.14. At the lower video signal to noise ratio (SNR_{TV} = 28 dB), performance is virtually the same. However, at higher video signal to noise ratios (SNR_{TV} > 31 dB), the averaging slicing level decoder performance is roughly 2 dB better than that attained with the peak detector decoder. Comparing Figure 5.14 with Figure 3.22, one observes that the linear equalizer provides a considerable performance improvement in this

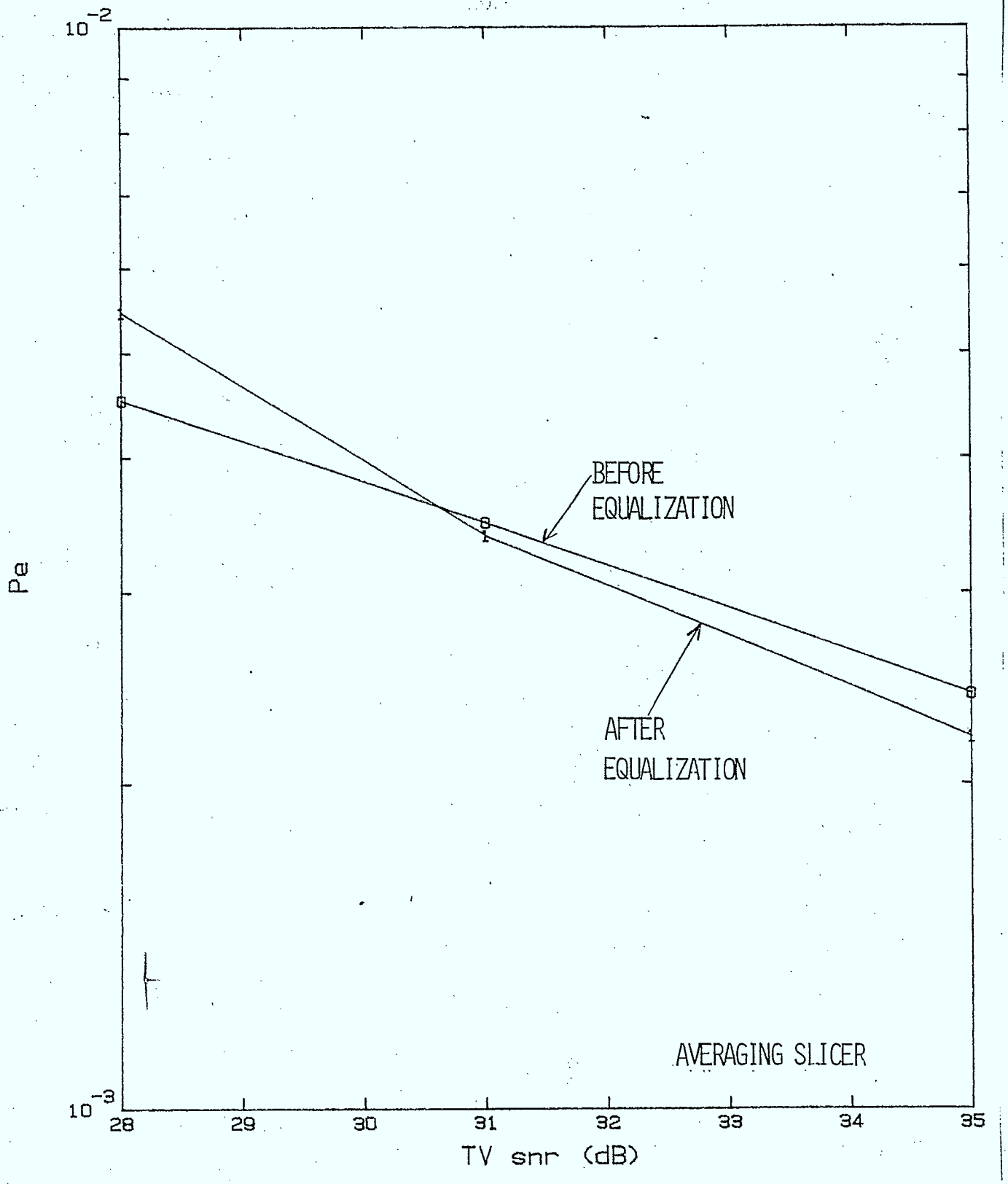

Figure 5.13: Linear equalizer performance with the 20 dB PDUR multipath channel in an impulse noise dominated environment.

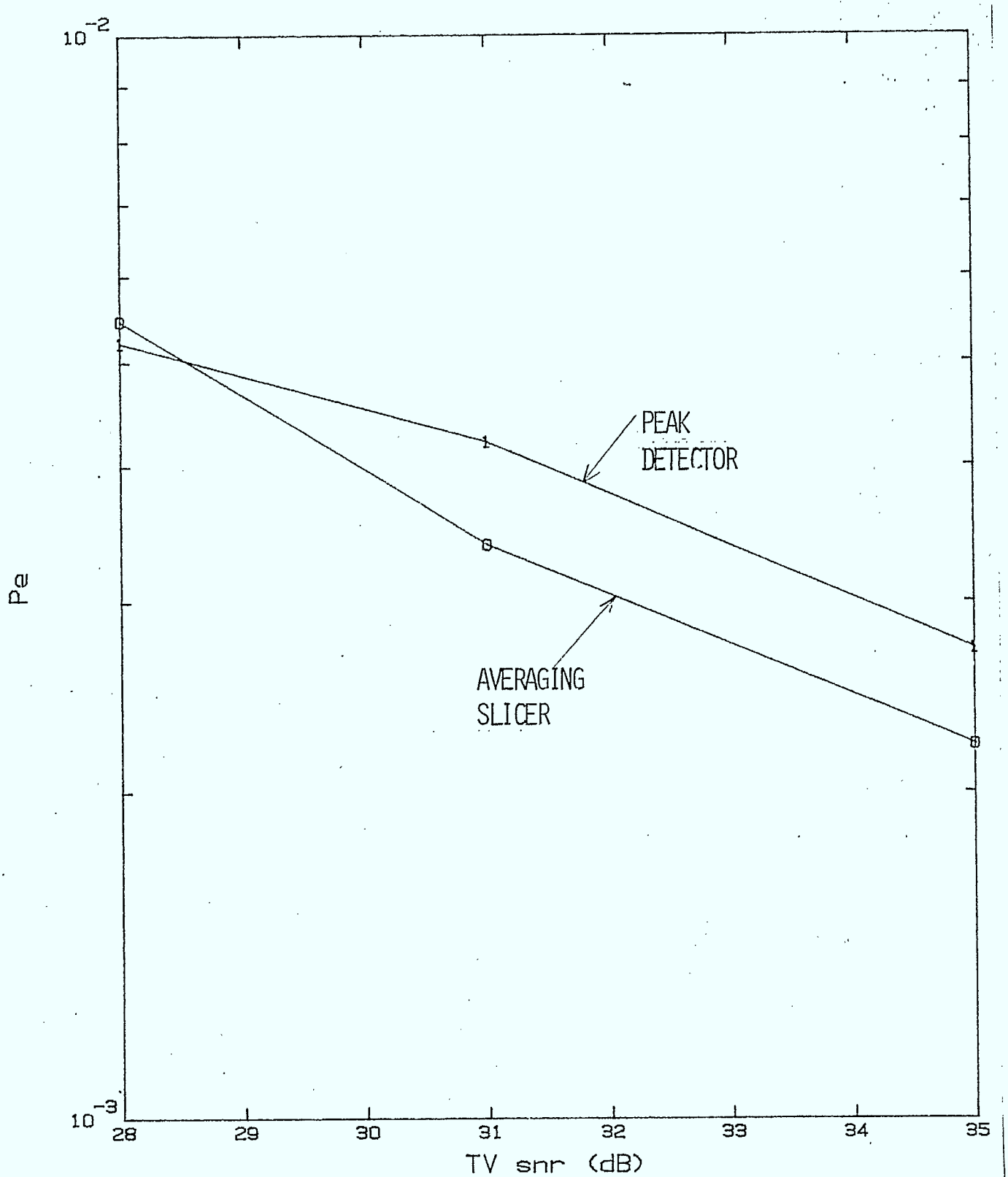

Figure 5.14: Comparison of peak detector and averaging slicing level decoder performance with a linear equalizer in an impulse noise dominated environment (PDUR-20dB channel)

noise environment with the peak detector decoder. The major reason for this is a reduction of the multipath induced peak detector slicing level bias errors when a linear equalizer precedes the estimation of the slicing level. It must be remarked that this noise environment is quite severe, being strongly dominated by impulse noise. This probably represents the worst case, as opposed to typical, operating noise environment for the broadcast Telidon system. One should, therefore, be cautioned against placing too much emphasis on this noise environment, when assessing the linear equalizer improvement.

Figure 5.15 compares the performance of the linear equalizer with the recommended and truncated 100% raised cosine pulse shapes in thermal noise environments. The superiority of the averaging slicing level decoder is clearly evident in this figure. The improvement with the recommended pulse shape indicated in this figure is anticipated because of the increased data signal amplitude that can be transmitted, because of reduced overshoots.

In thermal noise environments, linear equalization provides a considerable performance improvement. Successful system operation with video signal to noise ratios as low as 30 dB should be possible for multipath channels near the video quality acceptability boundary. Performance in severe impulse noise environments is not improved very much with linear equalization. The tendency of the linear equalizer to smear impulses, thereby prolonging their duration, negates the performance improvement provided by a reduction in intersymbol interference and reduced slicing level bias errors.

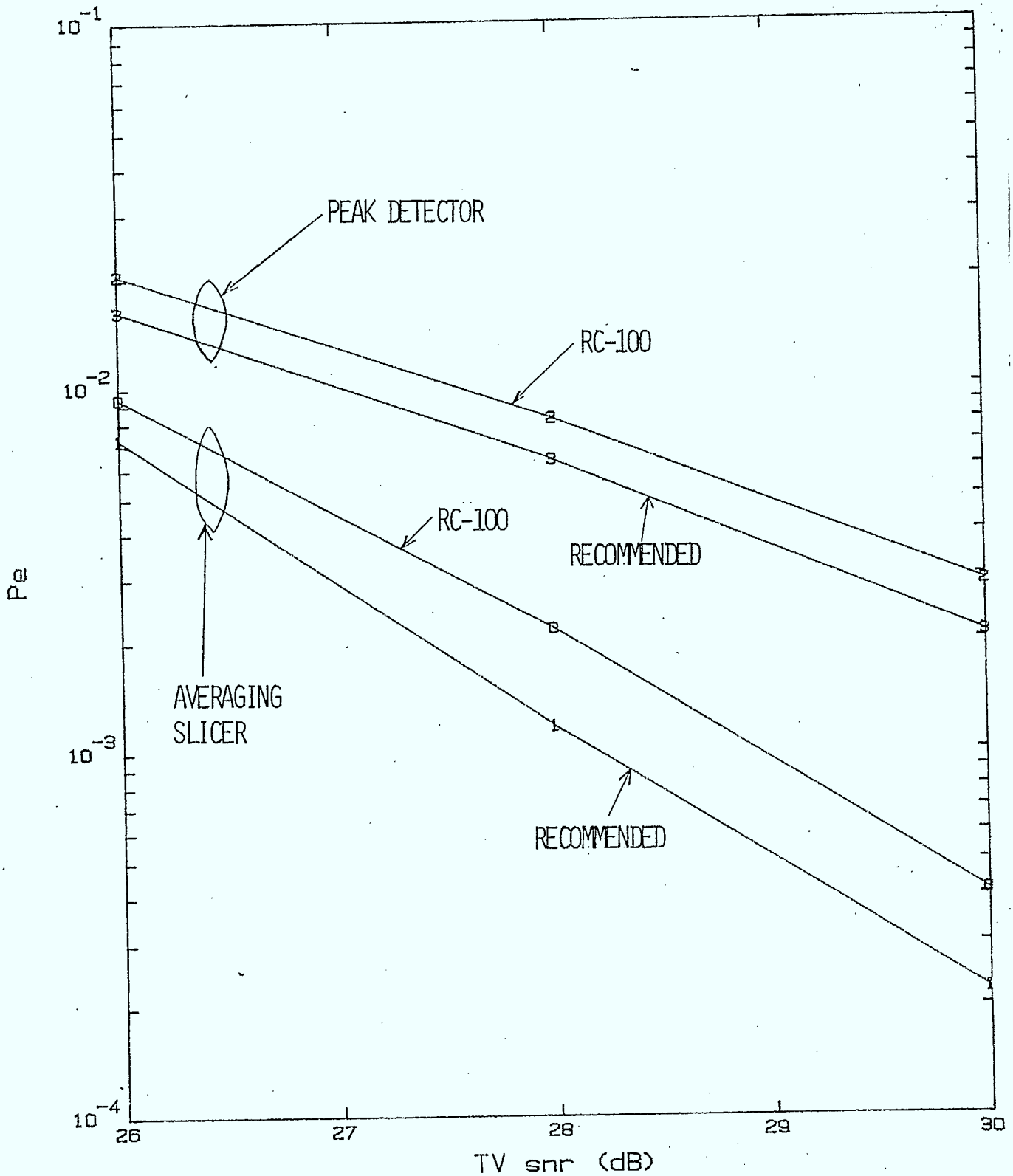

Figure 5.15: Simulated pulse shape performance with a linear equalizer in a thermal noise environment (PDUR-20dB channel)

6.0 ERROR PROTECTION CODING EVALUATION

A good deal of research has been carried out to specify suitable codes for the Telidon system. This research has resulted in the specification of a variety of codes, all with different detection/correction capabilities [56]-[60]. The present task is to select the most suitable code from amongst those proposed. In order to fulfil this task, some criterion for "suitability" must be established. In the past, the codes have been assessed with two parameters:

1) Decoding failure
2) Decoding error

where a failure is defined as a detectable but not correctable error, and a decoding error is an error condition in which the decoder either incorrectly decoded the packet or perceived an erroneous packet as error free. Common performance indices have been: the probability of a decoding error/failure and the mean number of pages until a decoding error/failure (where the definition of a page has varied). While these parameters allow the codes to be ranked amongst one another, the question of suitability to the Telidon system is unanswered. In order to decide upon a suitable code, the decoding error/failure must be related to the Telidon users perception of the system performance. For example, if the probability that a packet contains a decoding error is 10^{-8} for one code and 10^{-10} for another, the user will probably not detect any difference in the performance of the two systems. In the first case approximately 2,000,000 pages* would have to be

---

* where the average page is assumed to be 50 packets.

examined before an error could be found, and in the second case approximately 200,000,000 pages would be required. On top of this, the impact of the error may be very small if not undetectable. (In the worst case, a user would have to use the system to the tune of 100 pages/day for about 55 years before an error might occur).

The above example illustrates the need to specify the performance indices which relate to the users perception of acceptable system performance. The most precise way to establish the performance indices is through subjective evaluation by a sample of users. At the present time, during system design, this approach is not feasible. To circumvent this problem, an attempt has been made to relate the performance of a code to the users perception of the system performance. Appendix A outlines the approach and assumptions made. In Appendix A two figures of merit have been specified, viz:

R - the overall packet rejection rate

N_c - the number of picture description errors (PDI) per record (50 packets/record).

and an effort has been made to establish realistic bounds for these parameters. The initial estimates place the acceptable packet rejection rate, $R_{(max)}$, at 2.5×10^{-2} and $Nc_{(max)}$ at 6.2. In comparing these bounds with those established for the Japanese system, we find that the Japanese system has a much more stringent requirement for rejection rate (6.2×10^{-3}), while close agreement is obtained for the number of PDI errors/record. It must be

emphasized that the figures of merit established for Telidon are only preliminary estimates and that subjective testing should follow to produce estimates with a greater degree of confidence.

In the past, the performance of the codes has been evaluated for a binary symmetric channel, as well as a number of burst noise models. The binary symmetric channel and burst noise models provide a good starting point for the evaluation of the codes. However, before a conclusive decision can be reached as to which code is most suitable for the Telidon system, the performance of the codes must be determined for "real" channel/system characteristics.

The Telidon data transmission simulation, TELSIM, provides the needed "real" channel/system characteristics. However, the computational demands of the simulation prohibit the direct inclusion of a coding analysis component into the simulation. Too many packets would have to be sent (very long simulation runs) to provide meaningful results. To get around this problem, a separate coding analysis program, CODING, was written. This program was designed to analyse the output of many simulation runs with the hope that a sufficient data base could be obtained by concantinating the results of many short simulation runs. The analysis program is also compatible with the error files obtained from CRC field measurements. This compatibility makes the coding analysis program a very useful tool for further study.

The error files generated by the simulation, TELSIM, form the data base used in our coding recommendation. This data base is unfortunately too small to isolate one code and hence make a definite coding recommendation. However, many valuable insights into the gains and expected performance of the different codes have been obtained. Issues such as

the tradeoff between coding and equalization have been resolved and the places where further work is required have been highlighted.

The remainder of this chapter is structured as follows: Section 6.1 contains a brief description of the codes examined; Section 6.2 outlines the general conclusions and trends observed for the codes, under various channel conditions. Section 6.3 discusses the coding vs equalization tradeoff. The overall conclusions and recommendations for further work are contained in the final section, Section 6.4.

6.1 The Codes

A variety of codes with greatly differing error correction/detection capabilities hae been proposed for the Telidon system. The codes proposed range from a simple byte parity check, capable of detecting any odd number of errors confined to a byte, but with no error correction possible, to complex bundle structures which can reconstruct entire packets. To assess the coding requirements of the Telidon system, a sample set, representative of the different degrees of coding strength, have been selected. The codes considered are:

1) Byte Parity
2) Product Code
3) Carleton 1-byte Code
4) Carleton 2-byte Code
5) Bundle Code (encoded with the Carleton 2-byte code).

As well as being representative of the varying degrees of coding possible, these codes may be combined into a single coding/decoding strategy, as they are compatible with one

another. The use of these codes in combination was proposed and is detailed by Mortimer and Moore in [56].

Other codes such as the SAB codes [53], [57], [58] might have been considered here. However, a good sample set is perceived in those codes specified above. Before describing the individual codes, a brief review of the packet structure will be given.

(i) Packet Structure

A line of Telidon information is shown in Figure 6.1. The first three bytes are for synchronization purposes, therefore, this portion of the line is pertinent only to the 'Telidon channel', not the 'Telidon decoder'. At the beginning of each line, there are line prefix bytes and a variable number of header bytes. All of these prefix and header bytes have been specified to be Hamming (8,4) encoded [19], thus enabling single bit/byte error correction and detection of an even number of bit errors in a byte. The prefix identifies the packet by way of a three byte address. It also indicates the structure of the remaining packet; for instance, the number of suffix bytes to be used is indicated in the prefix.

All bytes following the prefix, including the optional suffix bytes and encoded header bytes, form the data block. This block consists of 25 to 28 bytes. The last one, two or three bytes are optimally taken up as suffix bytes, used for error detection and correction.

Data Line

The Data Line consists of a string of 288 bits (impulses) having the following format:

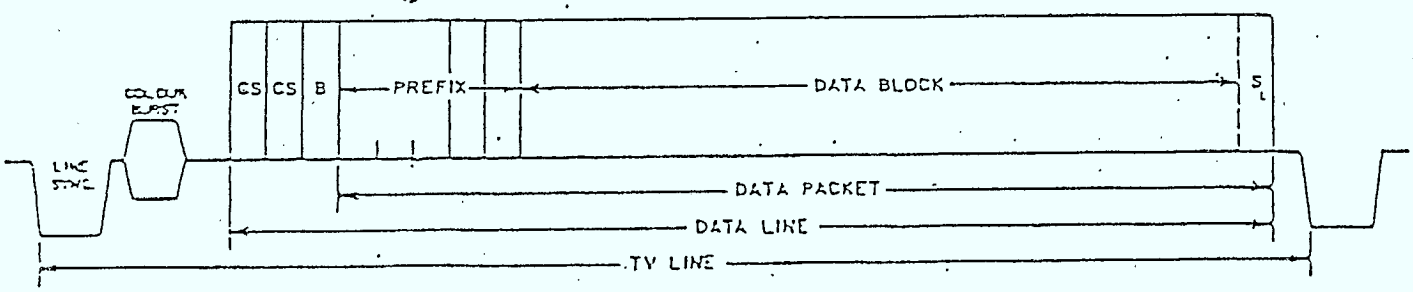

Figure 6.1: Packet Structure

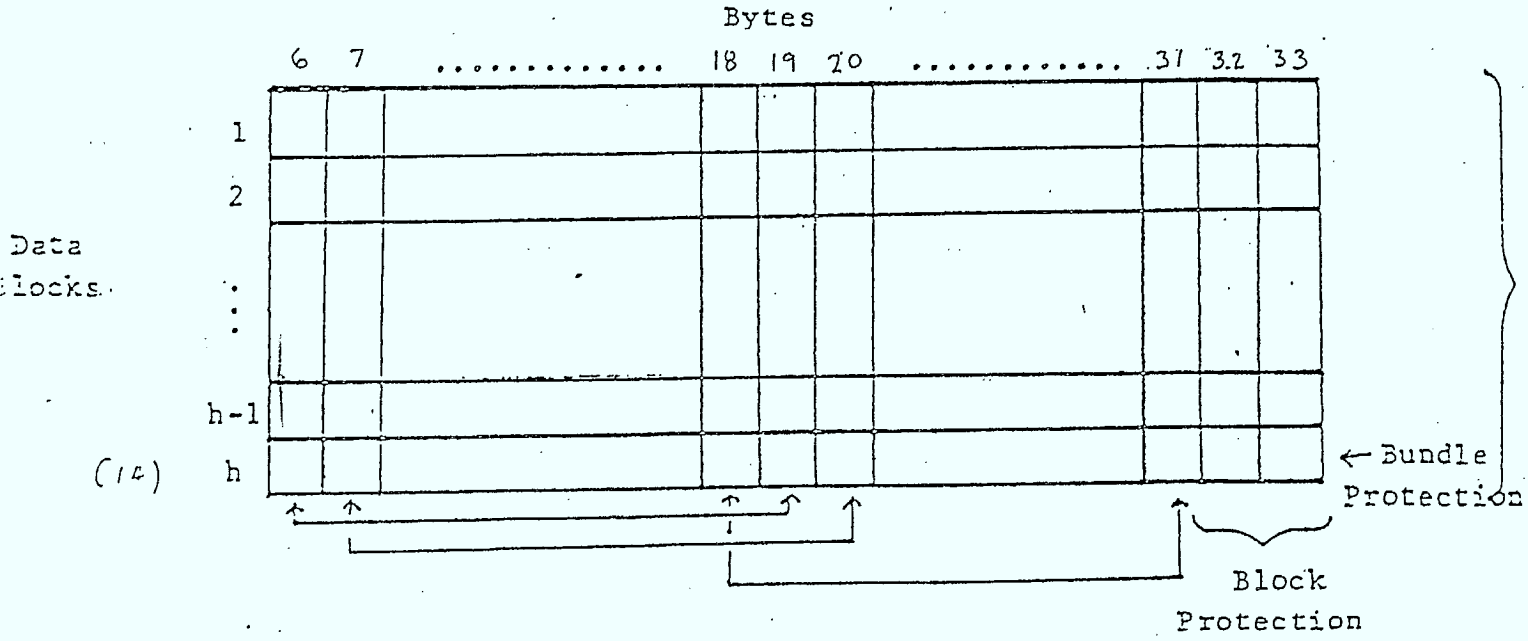

Figure 6.2: Bundle Structure

The codes under investigation operate on the data block. The effect of the double encoding on the header bytes is not considered. For notational purposes we shall denote the prefix bytes, B_1 through B_5 and the data bytes, B_6 through B_{33}. The suffix bytes will be treated as data bytes, in that an error in the suffix bytes will count as an error in the data.

The codes proposed for the data block will now be described.

a) Byte Parity

A requirement under BS-14 [19] is that all of the bytes in the data block must have odd parity. The parity check bits allow for the detection of any error pattern that introduces an odd number of errors into a data byte. Byte parity alone has no error correction capabilities and it represents the minimum amount of coding allowed.

b) Product Code

The Product code is simply a row column parity check. It is capable of correcting one bit error in the 28 byte data block, and detecting any odd number of errors/byte or any error pattern confined to one byte.

The suffix byte, B_{33}, for the product code is defined as:

$$B_{33} = \sum_{i=6}^{32} B_i \qquad (6.1)$$

The suffix byte is used to check column parity, while the row parity check is handled by the odd byte parity. The Product code was proposed for the Telidon system by Sablatash & Storey and is clearly described in [59].

(c) Carleton 1-byte code

The Carleton 1-byte code has the same correction capabilities as the Product code, however, it has greater error detection capabilities. The suffix byte, B_{33}, is given by

$$B_{33} = \alpha^{117} \sum_{i=6}^{32} B_i \alpha^{B_i} \qquad (6.2)$$

where α^j is an element in a Galois field specified by the generator polynomial

$$x^8 + x^7 + x^4 + x^3 + x + 1 = 0 \qquad (6.3)$$

and the elements

α^0	00000001
α^1	00000010
α^2	00000100
α^3	00001000
α^4	00010000
α^5	00100000
α^6	01000000
α^7	10000000

(6.4)

A detailed description of the code is given in [60].

(d) Carleton 2-byte code

The Carleton 2-byte code is a combination of the Carleton one byte code and the Product code. It is capable of correcting any single byte error and any 2 byte erasures (parity errors). The packet is encoded such that B_{33} meets the Product code requirements (1), and B_{32} is choosen such that B_{33} also meets the Carleton 1-byte codes requirements (2). This is accomplished as follows:

Let $$P_p = \sum_{i=6}^{32} B_i,$$

$$P_c = \alpha^{117} \sum_{i=6}^{31} B_i \alpha^{B_i},$$

then we wish B_{32} and B_{33} such that:

$$P_c = \alpha^{117} B_{32} \alpha^{8(32)} \Big|_{\text{mod } 127} = B_{33}$$

$$P_p + B_{32} = B_{33}$$

Solving for B_{32} gives

$$B_{32} = \alpha^{14}(P_c + P_p)$$

A detailed description of the code is provided in [56].

(e) Bundle Code

A number of possible bundle strategies have been suggested for Telidon [56]. The approach considered here is that recommended by Mortimer and Moore [56]. A bundle of the Bundle code consists of 14 data blocks (packets). Thirteen of these are identical to packets encoded with the Carleton 2-byte code. The 14th packet contains 2 byte suffixes for packets formed by interleaving the bytes of the previous 13 data blocks. (See Figure 6.2). Suffix bytes in the 14th block are calculated on the basis of the 14th block alone. The choise of 14 lines (13 data lines and one line of vertical suffixes) allows the vertical codewords to be Carleton 2-byte codewords. The details of the Bundle code structure are given in [56].

6.2 General Performance Characteristics

It is difficult to propose one coding scheme over another when many of the key issues* are still unresolved. (Also, at the present time, only a limited data base is available to test the performance of the codes). However, it is possible to give an indication of general performance 'trends', of the different coding schemes, which shed a good deal of light on the problem. When more firm system parameters become available, the appropriate coding decisions should become obvious.

6.2.1 Performance of the Codes

The first observation deals with the performance of the codes on error files generated for an ideal channel and a

*Performance indices have not been firmly established. Also, the operating video SNR of the system is not firmly defined.

white noise environment. Figures 6.3 and 6.4 show the actual rejection rate (obtain from simulation error files) in comparison to the rejection rate predicted by the binary symmetric channel for the Carleton 2-byte code and the Product code. In the case of the Carleton 2-byte code, the rejection rate tends to diverge from the predicted value as the input bit error rate decreases. At a probability of error of about 10^{-3}, the rejection rate is about a factor of 10 higher than expected. The Product code also diverges from the predicted value as the input bit error rate decreases, however, the divergence is much more gradual.

The performance of the Bundle code is closely linked to that of the Carleton 2-byte code. The increased rejection rate of the Carleton 2-byte code drastically effects the performance of the Bundle code. If the input bit error rate to the Bundle decoder is too great, the decoder can actually cause an increase in rejections relative to byte parity. A graph comparing the rejection rate of the Bundle code for the error files from the simulation to files which simulate a binary symmetric channel is provided in Figure 6.5. It is important to note that the points on this graph are taken from a very small data base and may not be indicative of the mean performance.

The increased rejection rate for the codes over the value predicted by the binary symmetric channel is not surprising. Clearly some degradation may be expected as the noise after the receive filter is not completely uncorrelated. Also, the self noise (intersymbol interference) causes the noise process characterizing the error files to differ from the gaussian model. However, these factors do not appear to be the main reason for the discrepancy. Preliminary observation indicate that the

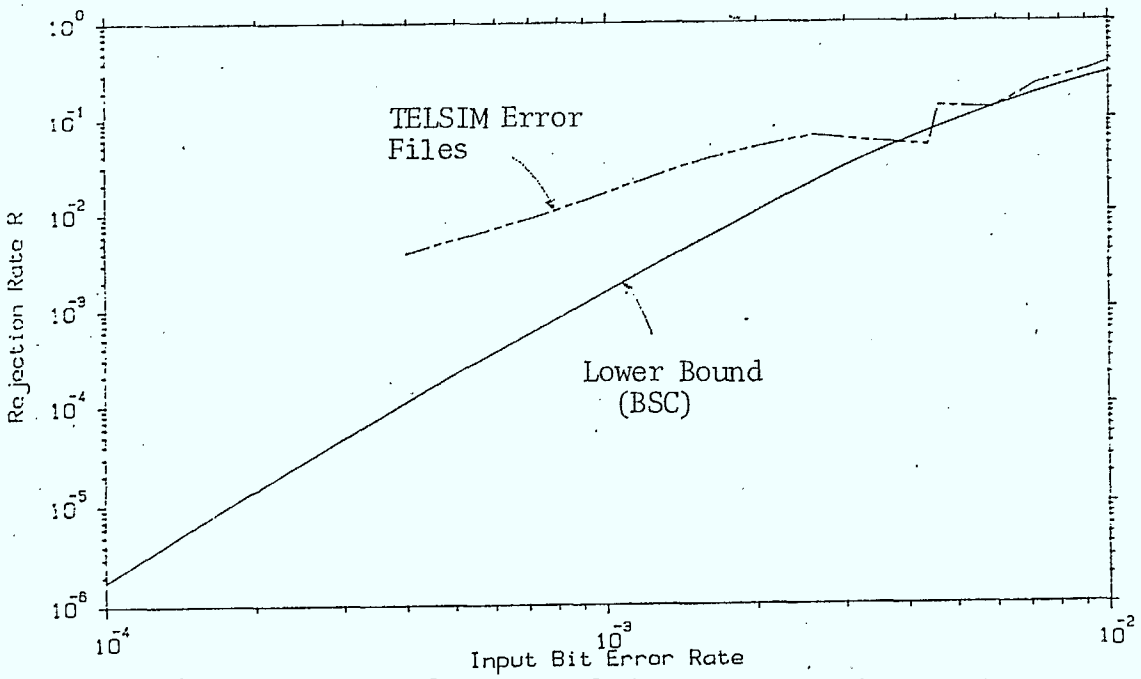

Figure 6.3: Performance of the Carleton 2-byte code on an ideal channel with white gaussian noise.

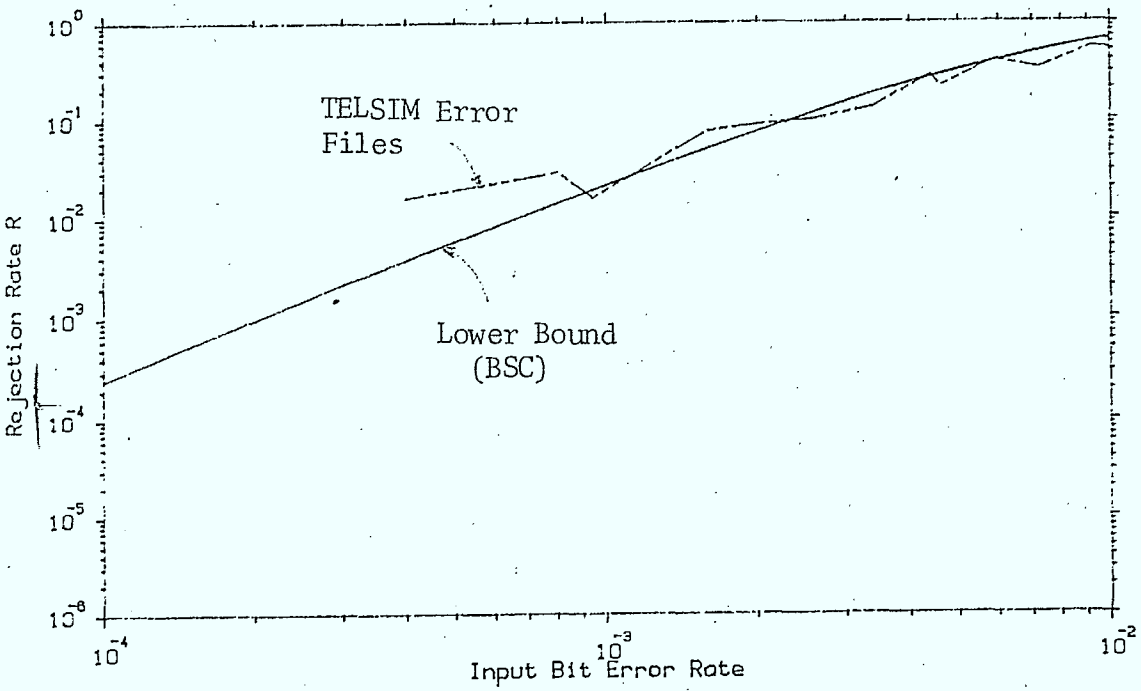

Figure 6.4: Performance of the Product code on an ideal channel with white gaussian noise.

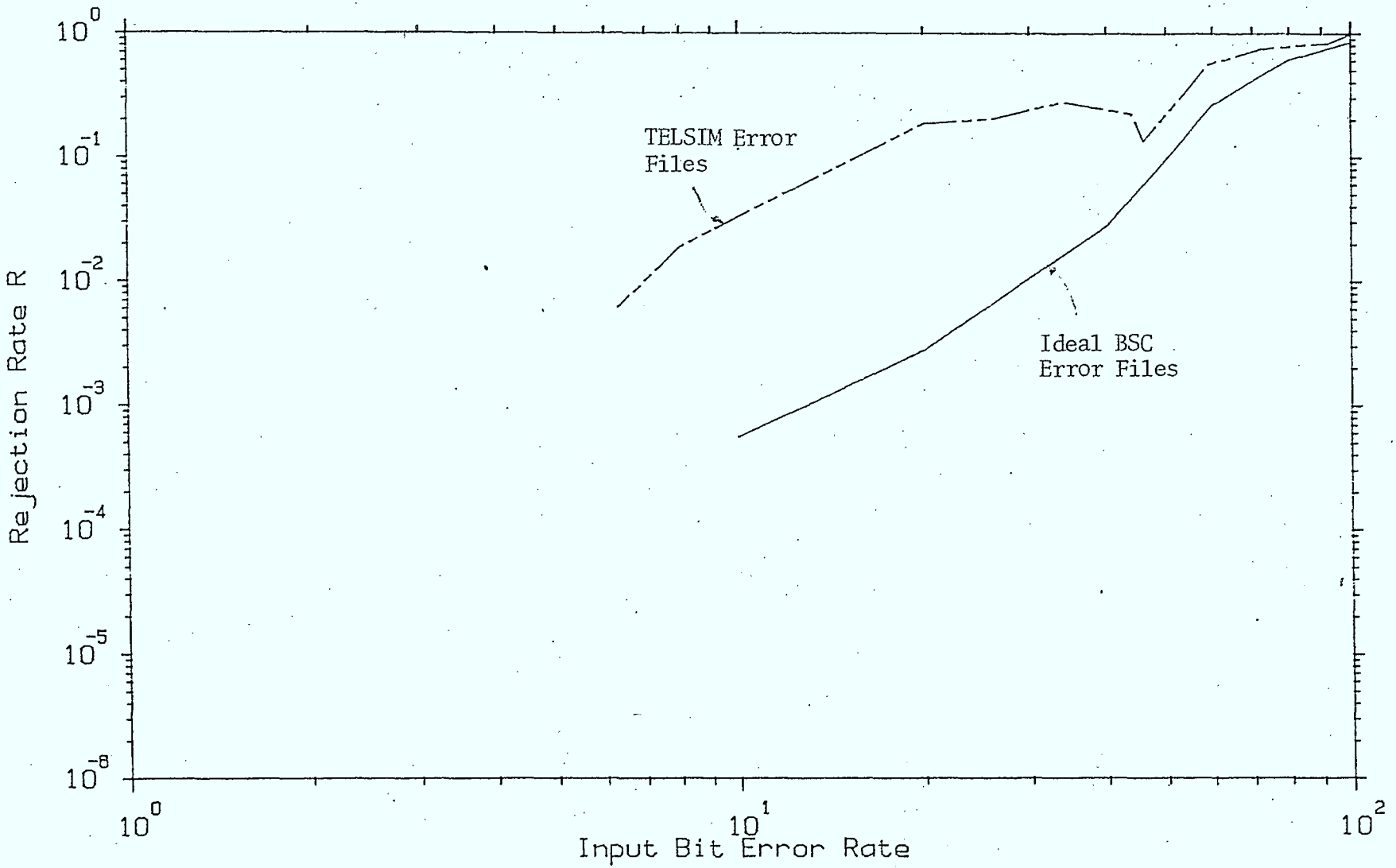

Figure 6.5: Performance of the Bundle code on an ideal channel with white gaussian noise.

errors in the individual packets are essentially evenly distributed, however, the number of errors/packet may vary substantially from packet to packet. Table 6.1 shows a histogram of the number of bytes in error in a packet for a typical white noise error file.

The last column in Table 6.1 gives the equivalent (binary symmetric) input bit error rate that would lead to the normalized histogram value (column 3). Column 4 indicates that if the underlying error rate is due to white Gaussian noise, the probability of error varies substantially from packet to packet. Again it should be noted that the file for Table 6.1 is relatively small, however, this file is indicative of the distribution of errors observed for other files with larger data bases. This phenomenon of a fluctuating error rate from packet to packet can be explained by recalling the sensitivity of the system to slicing level and bit timing recovery errors. A small offset in either or both parameters results in a much greater probability of error for a packet. The slicing level offsets and bit timing recovery offsets are governed by random processes. The samples at any given time result in an underlying error rate for the packet.

If we hypothesize that the errors in a packet are still independent, but that the error rate for a particular packet is a functon of the slicing level and bit timing error (determined at the start of the packet), the divergence of the rejection rate from the predicted values appears to make sence. For the Product code, the rejection rate (for independent errors) is a function of the square of the input probability of error. If the input probability of error is fluctuating, the rejection rate at the higher bit error rate will tend to increase the overall

# of Bytes in Error in a Packet	Frequency of Occurance (F)	F/(total # of Packets)	Equivalent White Noise P_e
0	646	.861	5.7×10^{-4}
1	79	.104	4.5×10^{-4}
2	16	.021	$1. \times 10^{-3}$
3	2	2.7×10^{-3}	$1. \times 10^{-3}$
4	3	4×10^{-3}	3×10^{-3}
5	2	2.7×10^{-3}	4×10^{-3}
6	2	2.7×10^{-3}	6×10^{-3}
7	1	1.3×10^{-3}	7×10^{-3}
11	1	1.3×10^{-3}	1.7×10^{-2}

Overall Probability of Error 8×10^{-4}

Total Number of Packets 750

TABLE 6.1

rate. For the Carleton 2-byte code, the rejection rate is a function of the cube of the input probability of error. The higher degree with respect to the input probability of error causes the rejection rate to be dominated to a greater extent (relative to the Product code) by the higher input bit error rates, resulting in a greater increase in the overall rejection rate.

The implications of this hypothesis are two fold. First, the degradation (relative to independent errors of a particular code's performance is a function of the error correction capabilities of the code. For an 'n' error correcting code, the rejection rate (assuming the corruption rate is small) is a function of p^{n+1}*, where p is the input bit erro rate. The higher the value of 'n+1' the greater the influence of the fluctuations in p. Thus, 'more powerful' codes tend to pay a penalty in the Telidon operating environment.

The second implication is that, as the errors are bursty in a packet wise sense, the most suitable coding technique is one which attempts to correct errors in a packet by packet fashion. This observation tends to support a bundle format. It does suggest, however, that the underlying code in the bundle could be quite simple** and still achieve good performance relative to more complex codes, which are likely to experience severe degradations.

The apparent dependence of the 'packet error rate' on the bit timng and slicing level errors suggests a possible error model for the Telidon channel. Using the simulation

*All errors of degree n or less are corrected.
**The Product code is a good candidate.

program TELSIM, the bit error rate could be functionally related to these two parameters. Then, by taking measured distributions of the slicing level and bit timing offsets, an output process could be defined that represents the probability of error for any given packet. Using this process, independent errors could be generated on a packet by packet basis. To illustrate this, consider the case where the only system impairment (other than a white gaussian noise process) is a noisy slicing level error. Assuming that there is no intersymbol interference at the sampling instants, the probability of error for a given packet would be

$$P_{e(packet)} = \frac{1}{2} Q(\frac{a+\gamma}{\sigma}) + \frac{1}{2} Q(\frac{a-\gamma}{\sigma})$$

where

a is the amplitude of the signal at the sampling instant,

σ is the standard deviation of the noise,

and

γ is a random variable representing the distribution of the slicing level error.

Thus, by characterizing the process γ, a series of error probabilities could be generated and used as input to a binary symmetric channel which generates one packet of errors for every error probability. The task of relating the errors to the slicing and bit timing errors is beyond the bounds of the current study. However, it would provide a good starting point for future work in coding evaluation. This would avoid the need for conducting long simulation runs with TELSIM, thereby dramatically reducing the computation complexity and evaluation time.

6.2.2 Rejection/Corruption Tradeoff

The second important performance characteristic observed deals with the relationship between the rejection and corruption rates of codes. In [60], Mortimer points out that a trade-off exists between decoding failure (rejection) and decoding errors (corruption). Reinterating his observations we have

$$P_{CD} + P_{DF} + P_{DE} = 1 \qquad (6.5)$$

where

P_{CD} = probability of correct decoding

P_{DF} = probability of a decoding failure

P_{DE} = probability of a decoding error.

Given a fixed correction capability (P_{CD} = constant) the error and failure rates may be traded off. Mortimer uses this observation to point out that no code has simultaneously good performance with regard to both decoding failures and errors. What is not pointed out is the relative impact of errors and failures on the system performance. Using the bounds established in Appendix A for the rejection/corruption rates, we find that, for all of the codes, the limiting parameter is the rejection rate. Figures 6.6 and 6.7 illustrate this for a binary symmetric channel. In Figure 6.7 we see that both the Product code and the Carleton 2-byte codes are below the corruption threshold at an input bit error rate of 10^{-2}. However, the required input bit error rates to meet the Telidon threshold rejection rate (see Figure 6.6) are 10^{-3} and 3×10^{-3} for the Product and Carleton 2-byte codes respectively. The margin is further widened if it is found

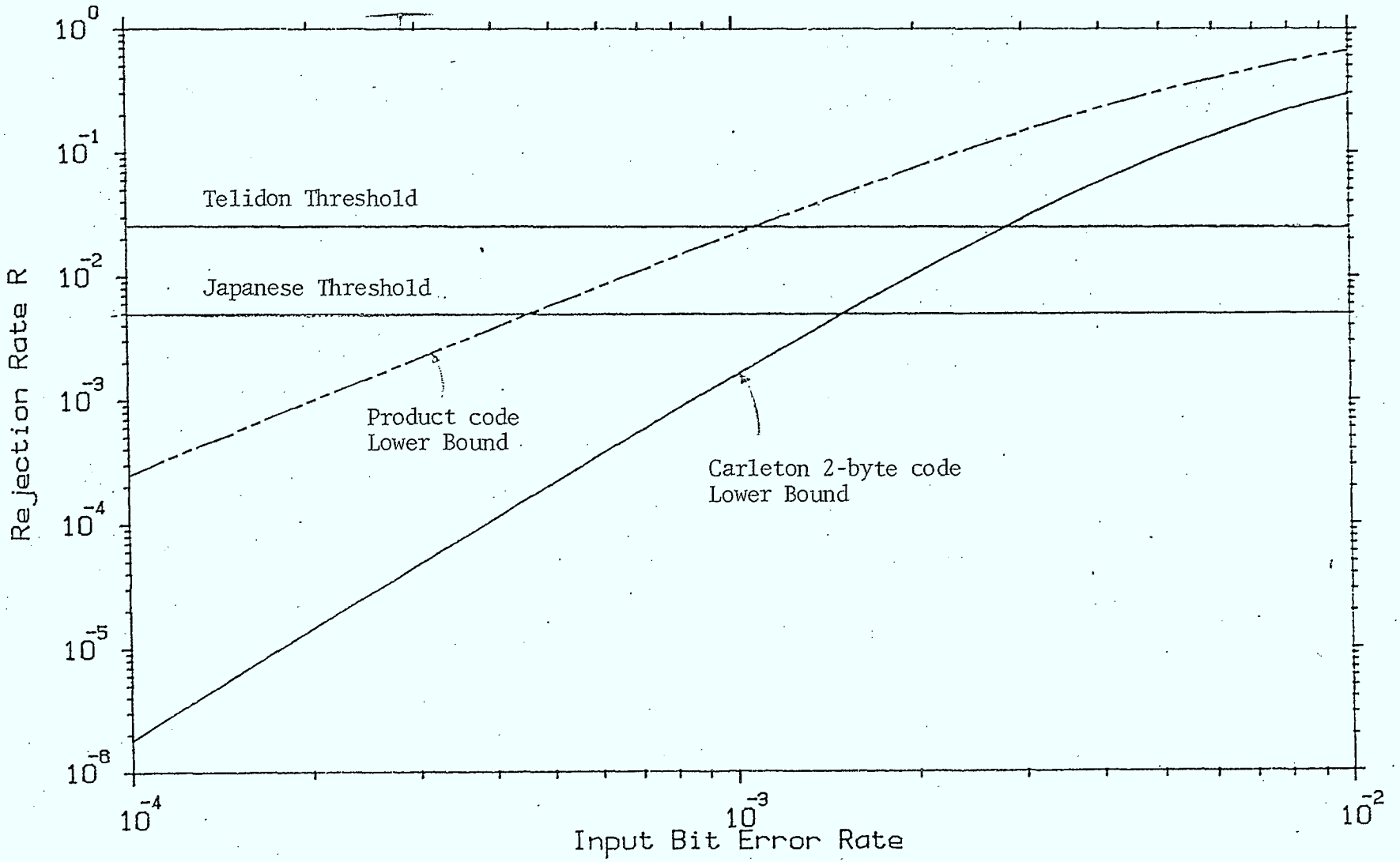

Figure 6.6: Lower bounds on the rejection rate for the Product and Carleton 2-byte codes assuming a binary symmetric channel.

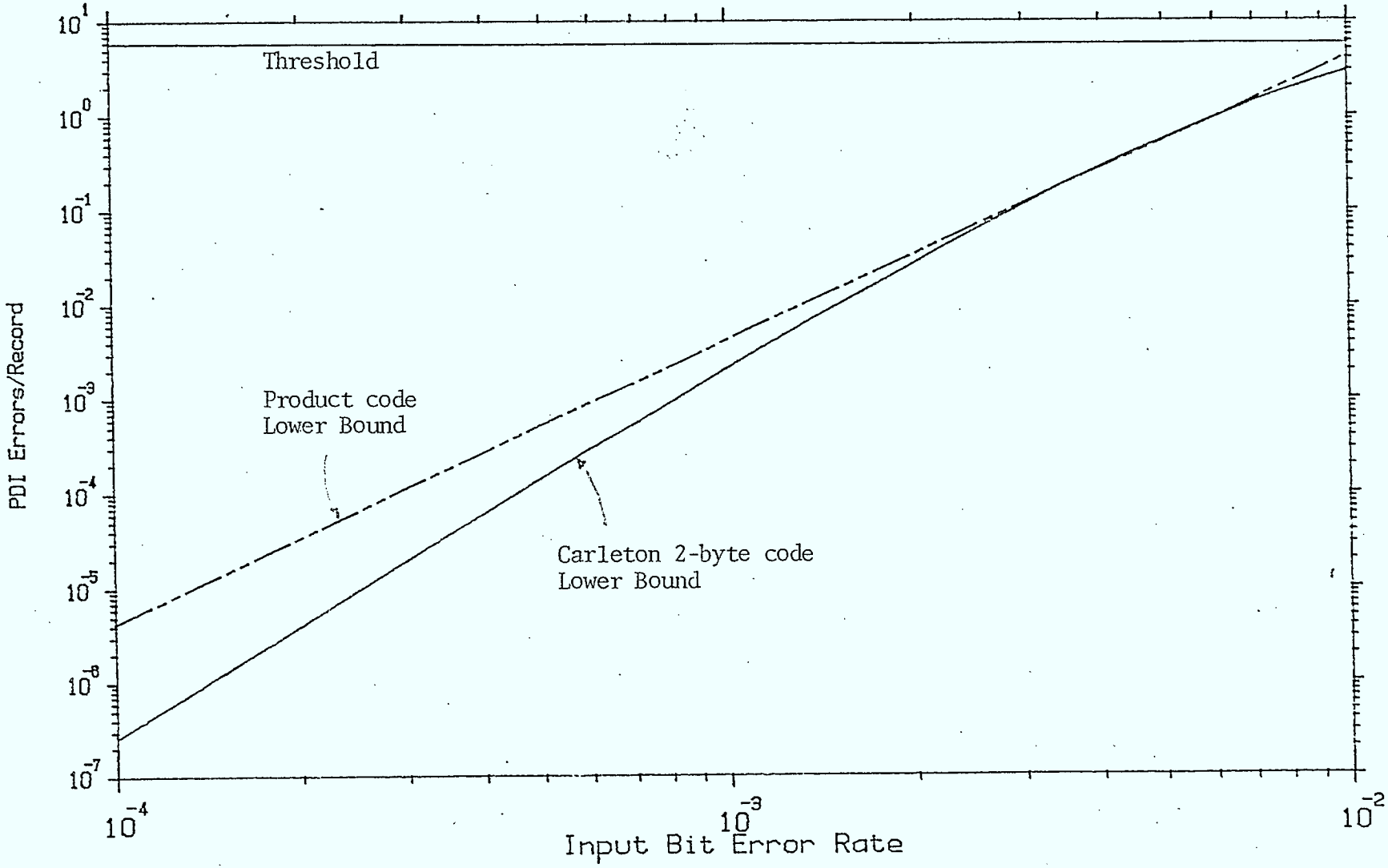

Figure 6.7: Lower bounds on the number of PDI errors/record for the Product and Carleton 2-byte codes assuming a binary symmetric channel.

that a more stringent rejection rate threshold (closer to that of the Japanese system) is required. The rejection and corruption rates for the error files generated by the simulation program exhibit this same discrepancy with respect to the required input bit error rate. The effect of the packet wise bursty channel on the corruption degradation, relative to the binary symmetric channel, appears to be consistant with the explanation of the noise process described in the previous section. Graphs of the PDI errors as a function of input bit error rate are not provided as the data base available was not large enough to provide results with sufficient confidence (in many cases, no corrupting errors were found).

To illustrate the significance of this discrepancy, consider the decision between the Carleton 1-byte code and the Product code. The rejection rate of the two codes are almost identical, however, the Carleton 1-byte code has a lower corruption rate. (It should be noted that both codes have the same correction capabilities. Hence from Equation (5) the decreased corruption rate of the Carleton 1-byte code is at the expense of the rejection rate). As the rejection rate is the limiting factor in terms of the system performance, no advantage is gained in using the Carleton 1-byte code over the Product code.

This misbalance in rejection/corruption rates often forces the choice of a code which is too powerful for the Telidon system. What is meant by too powerful is that the correction capability of the required code, P_{CD}, when added to the required failure and error rates is less than 1 (recall Equation (6.5)).

6.2.3 Proposed Modification

The dominance of the rejection rate over the corruption rate (with respect to the Telidon performance indices) leads one to seek ways to balance these parameters. A couple of approaches come to mind. Firstly, new codes could be designed in light of the required rejection/corruption trade-off. This alternative would require a good deal more research and does not appear practical. A more suitable approach is outlined in this section.

The proposed approach is very simple and effects the decoder not the coding strategy. What is suggested is simply that for a specified set of rejection conditions, the decoder should accept the packet. By doing this the decoder is trading rejections for corruption in a direct manner. For example, for the Product code, if two byte parity errors are detected, the packet is rejected by the conventional decoder. In a modified decoder this condition could be ignored and the packet accepted. This would make the rejection rate of the single error correcting Product code closer to that of the Carleton 2-byte code. At all times it must be remembered that the rejections are being traded for corruptions, the 'strength' of the code is constant. The selection of rejection conditioning which could be made into corruption conditions is greatly dependent upon the distribution of the channel error process. In the limit, a decoder could operate as error correction system, with no rejections (with the exception of those generated by prefix decoding). A further observation is that the set of rejection conditions need not be fixed in a decoder. It is possible to envisage a

decoder which has a switch or dial to select the delay/distortion of the information received. The switch might be set for 'minimum delay' by the user for earlier menus where a correct picture is not vital. When the final screen of information has been located, the user could switch to the 'minimum distortion' mode.

Another approach might be to have the Telidon data packet select the rejection/corruption operating point of the system for a particular page of information. This could be accomplished by specifying one or two bits in the prefix of the first packet in a page as 'decoder selection' bit or bits. The decoder selection bit or bits could be based on the same system which accesses the impact of an error on the page. In it's simplest form, the system might have a single bit which when set specifies full rejection capabilities and when reset selects no rejection capabilities. A possible threshold between the two modes could be based on the length of the page. If say 50 or less packets make up the page the bit might be set to invoke full decoding. When greater than 50 packets make up a page the bit could be reset as the information/packet is less for this case and hence errors might not be as perceptable. The actual threshold would have to be the subject of further study.

From an implementation standpoint, the required modifications to the decoders are minimal. All that is necessary is for an inhibit line to be coupled to the rejection flag, with a small amount of logic to select the set of acceptable error conditions.

6.2.4 Performance with Modification

The limited size of the data base under examination does not enable a firm recommendation to be made as to which set

of detectable errors should be traded for corruptions. Instead results are presented for the two extreme cases - rejection of all detectable errors and no rejection. Figure 6.8 shows the rejection rate of the various codes when all detectable errors cause rejections. (The PDI errors/record are at least an order of magnitude below the acceptable threshold in the range of the Telidon rejection rate threshold). From this figure, we can see the importance of determining the actual threshold for the rejection rate. The weaker Telidon threshold of 2.5×10^{-2} implies that a packet is rejected for just about every record. If this is found to be acceptable all of the codes can meet the threshold at an input bit error rate of approximately 10^{-3}. As there is very little difference in the performance between the codes in this input error rate region, the Product code would probably be the most suitable contender. On the other hand, if the Japanese threshold is found to be a more suitable threshold, the Product code would require an input bit error rate 3 to 4 times lower than the Bundle or Carleton 2-byte codes.

Figure 6.9 shows the corruption rate of the packet when no packet rejections are allowed by the decoder. The threshold of 6.2 PDI errors/record, where a record is defined to be 50 packets is also marked on the graph. Again we find that the input bit error rate must be about 10^{-3} for the decoders to meet the threshold. The relatively small difference in the performance of the codes in the vicinity of 10^{-3} again lends support for the selection of the Product code, which is the simplest to implement. Again a similar trend (with respect to the full decoder) can be observed with regard to the location of the threshold and the code selection. The trend indicates that as the threshold is tightened, the performance of the codes separate and the more powerful codes become attractive.

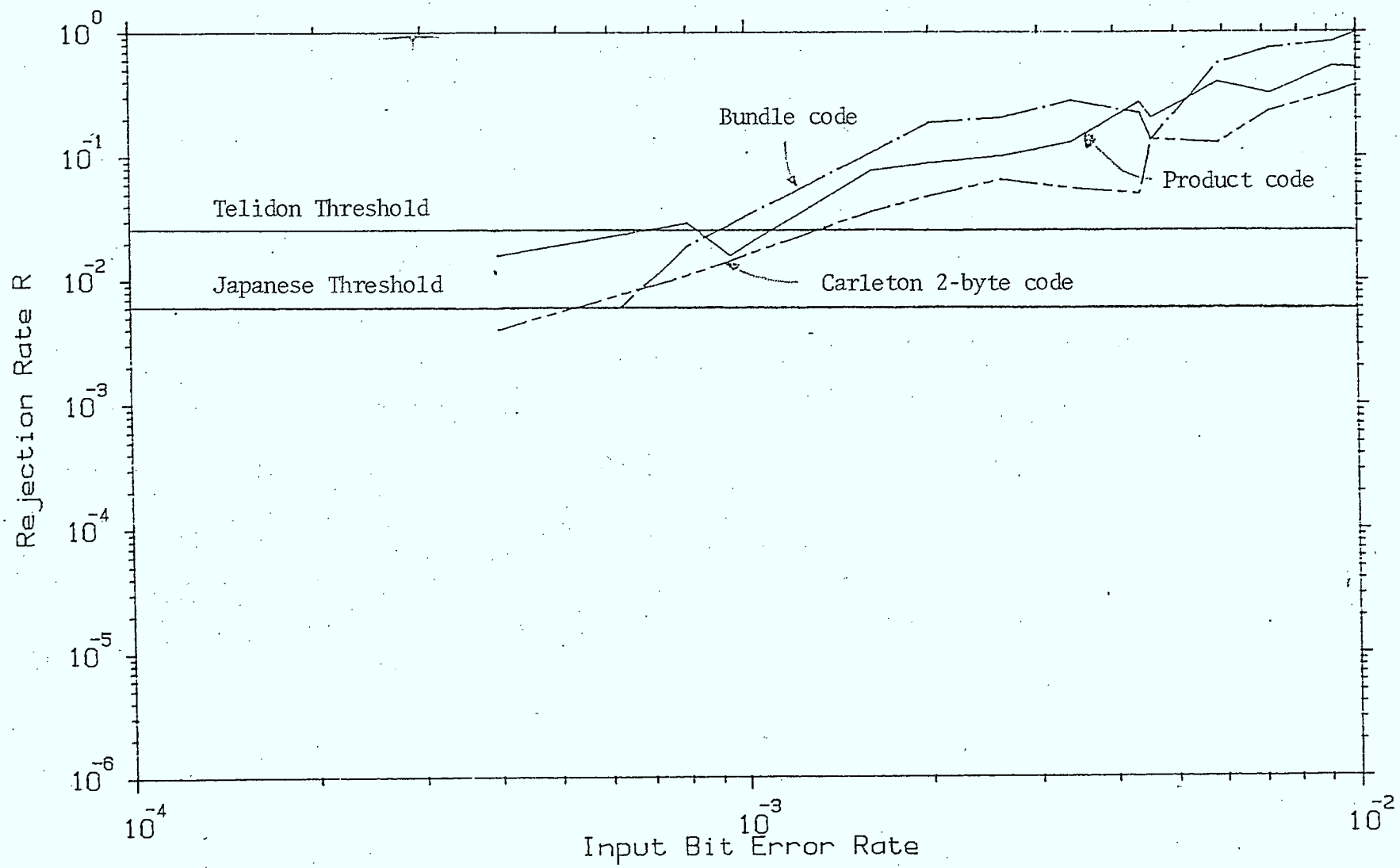

Figure 6.8: Performance of the conventional decoding scheme (full rejection capabilities).(TELSIM error files for an ideal channel corrupted by white gaussian noise).

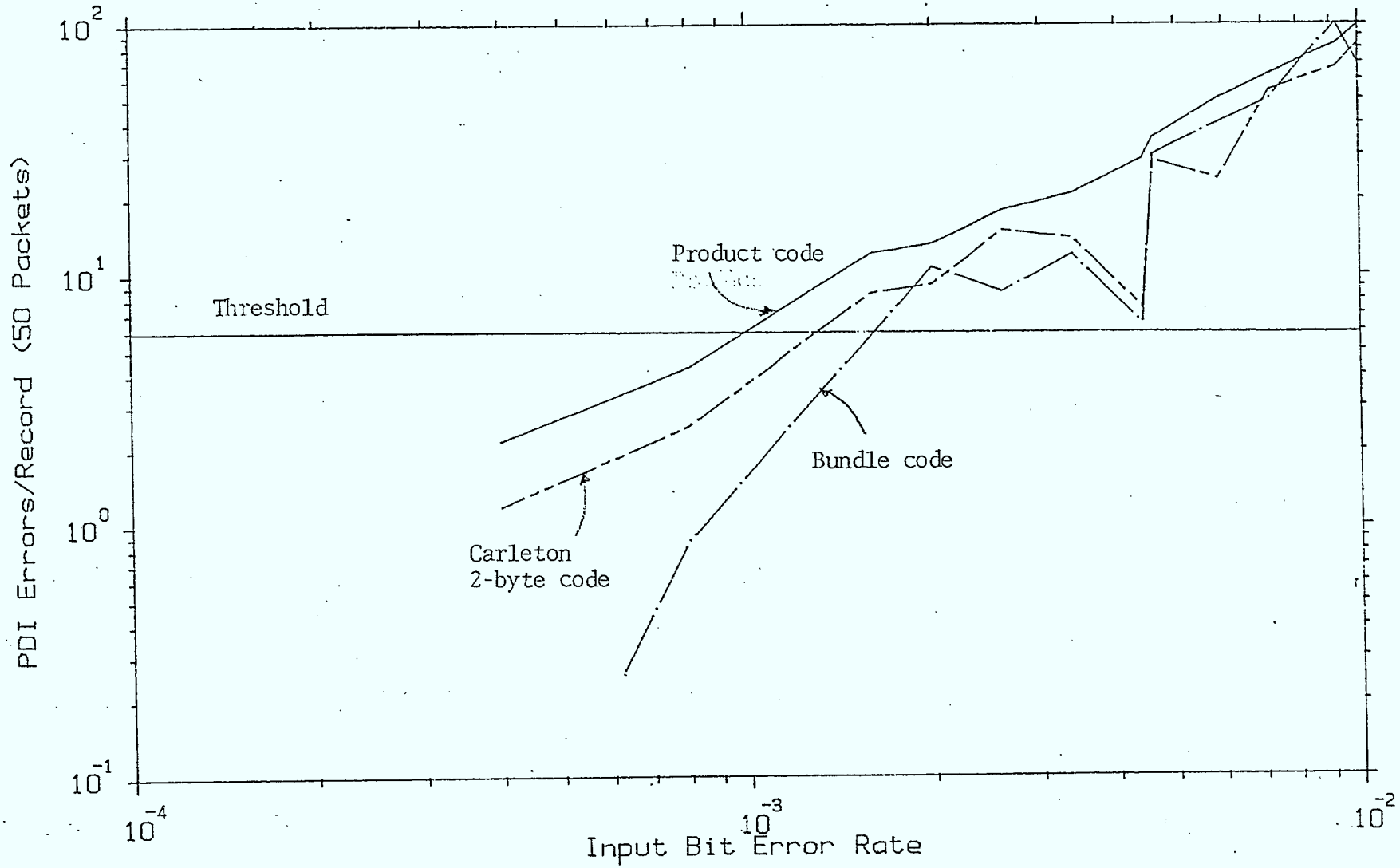

Figure 6.9: Performance of a modified decoding scheme where no packets are rejected. (TELSIM error files for an ideal channel corrupted by white gaussian noise).

An interesting observation between the two decoding techniques can be seen by examining the performance of the Bundle code. In the case of the full decoder (Figure 6.8), the Bundle code exhibits the poorest performance of all of the codes until the input bit error rate is about 6×10^{-4}. The problem appears to stem from the fact that if one 'vertical' packet is rejected by the decoder, all 14 packets in the bundle are rejected. The Telidon channel which exhibits 'dips' in the probability of error on a packet-wise basis, as alluded to earlier, tends to increase the probability of rejection and hence increase the minimum operating point of the code. On the other hand the Bundle decoder which performs error correction only, does not experience this severe degradation in performance as the input bit error rate increases.

6.3 Coding vs Equalization

This section examines the trade-off between coding and equalization. The 'trade-off' can be described as follows:

1) should an equalizer be employed to improve the performance of the system over multipath channels and thus allow a relatively simple coding technique to be employed, or

2) should a code be selected which is powerful enough to improve the performance of the multipath channels to an acceptable level in the absence of an equalizer.

The issue appears to hinge on a number of factors. The first deals with the desired performance of the system. If an equalizer is employed, the effect of multipath is

reduced to the point where most of the channels exhibit equal performance. Then by adding a code powerful enough to reduce the performance indices to the acceptable standards, the system will have uniform acceptable performance for all users. On the other hand, if a powerful code is selected to overcome the problems of multipath, a great range of system performance will be experienced by different users. (The users in severe multipath environments would obtain marginally acceptable performance whereas the user in more ideal channel conditions could expect excellent system response). A first look tends to support the use of an equalizer, as there appears to be no reason from the users standpoint to have the performance of the system a function of the channel severity (users in multipath environments are expected to have the same requirements as the other system users). However, as well as system performance, cost must also be considered. For the broadcast teletext application, equalizers are relatively expensive to design and construct. Also if a nesting of codes is employed as proposed in [56], the user could acquire a decoder which meets the needs of the individual channel.

All of these factors appear to make the decision between coding and equalization a difficult one. The solution to the problem, however, is not at all difficult. The reason for this is that none of the codes are powerful enough to overcome the influence of multipath. The severe degradation of multipath on the Telidon signal format results in an input bit error rate (to the decoder) in the neighbourhood of 3×10^{-2} for relatively good video signal to noise ratio. In some cases it is lower than this figure; however, it is strongly dependent upon the phases of the dominate echoes of the multipath channel. The echo phasing is a very volatile parameter that is extremely

sensitive to antenna location and motion (sway). From Figures 6.8 and 6.9 it can be seen that this input bit error rate is well above the effective operating point of the codes. The TELSIM error files for the multipath channel support this observation placing the rejection rate at about .3 to .5 (30 to 50 percent of the packets would be rejected) for relatively good video channels at reasonable video signal to noise ratios.

The conclusion that is reached is that equalization is required in the broadcast teletext operating environment. The question then becomes which code is acceptable given the presence of an equalizer. The answer to this question hinges on two factors.

1) What is the operating video signal to noise ratio of the system (hence the input bit error rate to the decoder)?

2) What values for rejection rate and picture corruption are acceptable?

Neither one of these questions has a firm answer at this stage of the Telidon system evaluation. In order to gain some information with regard to the most suitable code, the rough thresholds specified in Appendix A will be used. As to the operating TV SNR of the system, the problem will be assessed at two reasonable values, 28 and 30 dB. Figure 6.10 shows the rejection rates of the various decoders as a function of TV SNR for error files generated by the simulation with an averaging slicer and a linear equalizer, when full decoding (all detected rejection conditions result in rejections) is employed. From this figure it is clear that for a video signal to noise ratio of 30 dB any

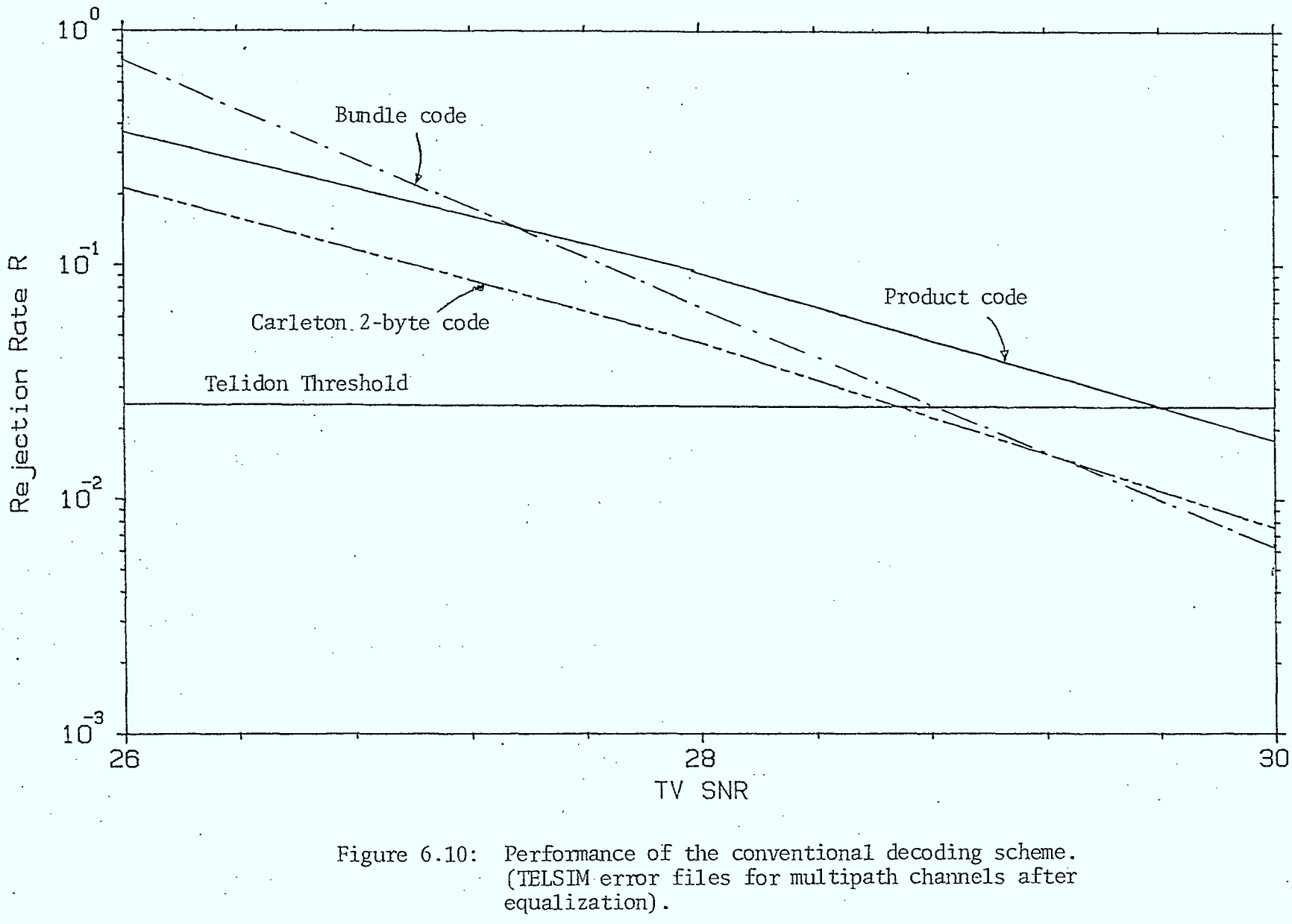

Figure 6.10: Performance of the conventional decoding scheme. (TELSIM error files for multipath channels after equalization).

one of the coding techniques could be employed, with the Bundle and Carleton 2-byte codes offering a rejection rate improvement of a factor of two over the product code. Unfortunately at a video signal to noise ratio of 28 dB, none of the codes meet the rejection threshold. Figure 6.11 shows the PDI errors of the modified system (error correction only) for the same error files. In this case, the results are similar for the video signal to noise ratio of 30 dB. However, the performance is improved at the 28 dB operating point. At 28 dB, the modified Bundle decoder is below the corruption theshold while the Carleton 2-byte and Product codes are not. Thus, it may be concluded that if the system is required to operate with a video signal to noise ratio of 28 dB, the Bundle decoder with error correction only, is the only decoder that can meet the threshold.

6.4 Coding Conclusions

The Telidon channel has been found to be bursty in a packet-wise sense. This burstiness tends to degrade the performance (relative to the binary symmetric channel) of the Bundle and Carleton 2-byte codes more that the Product code. The degradation causes all of the codes to have about the same performance for an input bit error rate of 10^{-3}. As the input bit error rate decreases, the gap in the performance of the codes widens and the Bundle and Carleton 2-byte codes exhibit far superior performance over the Product code. The question as to which code should be selected balances on the problem of determining accurate performance indices. The present estimates for the performance indices indicate that the input bit error rate must be about 10^{-3}. This input bit error rate implies that the Product code should be selected as the gains in going to more powerful coding strategies are minimal. However,

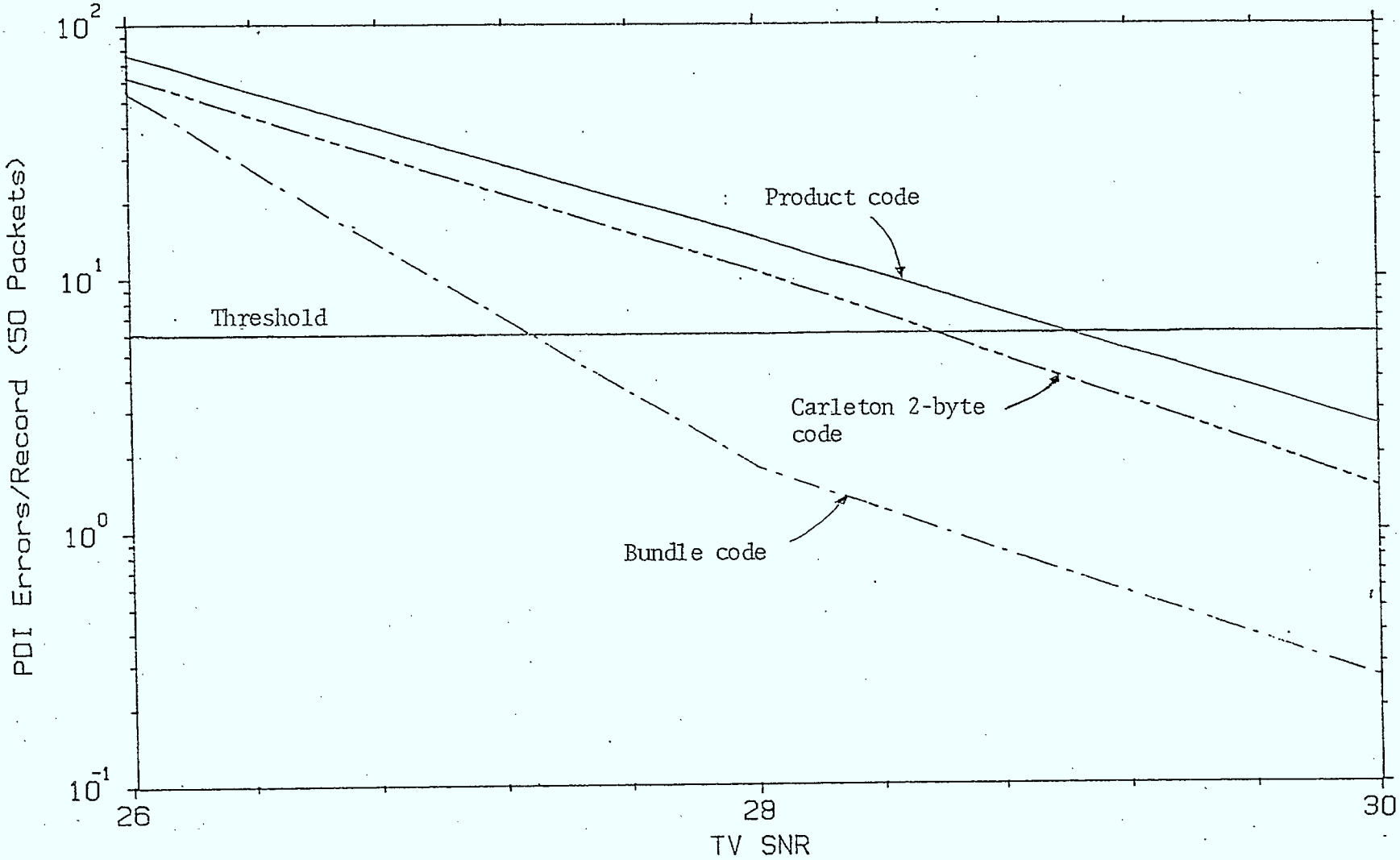

Figure 6.11: Performance of a modified decoding scheme where no packets are rejected. (TELSIM error files for multipath channels after equalization).

if it is found that the estimated thresholds are too high, it is probable that one of the stronger decoding strategies would have to be selected. The strong dependence of the performance thresholds on the coding choise emphasises the importance of establishing firm estimates of these figures. This task should receive high priority in further work on coding.

It was observed that for all of the codes, the rejection rate was the limiting parameter as opposed to the corruption rate. A modified approach to decoding was discussed which is aimed at reducing this inbalance. The extreme case where no packet rejections are permitted (the decoder performs error-correction only) was examined. This approach to decoding appears to have a number of advantages over the full decoding case. One advantage is that the performance of the Bundle code degrades less rapidly as the input bit error rate increases.

The issue of coding vs equalization was also considered. It was found that the input bit error rates, on typical multipath channels are too high to allow any coding strategy to be useful. It is therefore suggested that an equalizer be incorporated for the broadcast television operating environment.

7.0 CONCLUSIONS

It is clear that acceptable system performance cannot be obtained with the current Telidon system in typical broadcast television multipath environments. Improvements to the current system have been proposed in the following areas:

1) Pulse Shaping
(currently a truncated 100% raised cosine pulse shape);

2) Slicing level circuitry
(currently uses a peak detector slicing level decoder);

3) Bit timing recovery
(currently coupled to the slicing level circuitry); and

4) Coding
(currently the product code)

Along with the proposed improvements to the existing system components, additional measures have been outlined and areas for further work highlighted, which should bring the system more in line with desired performance.

7.1 Improvements to Existing System

Given the clear superiority of the averaging slicing level decoder over the current peak detector slicing level decoder, all future teletext decoders should employ the averaging principle. Schemes for improving the peak detector approach (i.e. symmetric reference voltage settings, longer observation window) should only be regarded as interim or temporary solutions.

The slicing level estimation and clock recovery procedures should be decoupled. Furthermore, a more optimal clock recovery scheme (based on using a bank of binary correlators and threshold detectors (appendix I of [II]) should be derived. The current scheme of using a single zero crossing is too sensitive to noise and other interference. In Figure 2.16, the degradation that can be attributed to the present timing recovery scheme is approximately 1 dB. Given the potential performance gain, this item should be given high priority.

The use of the pulse shape which provides an overall nominal transfer function similar to equation 3.1 (Figure 3.3) should be given consideration. The decreased peak sensitivity and reduced intersymbol interference provides approximately a 0.5 dB improvement over the current pulse shape (truncated 100% raised cosine).

The sensitivity of the current Telidon system to multipath propagation has been demonstrated. The major culprit is the format of the teletext signal, which has TV synchronizing signals preceding the clock sync signal used for the slicing level estimation and clock recovery. Clearly, multipath introduces significant slicing level bias errors which impose a significant performance degradation. There are a number of potential mitigatory techniques, viz:

a) Adaptive slicing level estimation

b) Linear equalization

c) Modifications to the teletext signal format

An adaptive slicing level estimator tracks the slicing level over the entire burst. The major problem with this approach is that the estimator must be decision directed to remove offsets introduced by the data signal. There is no protection against a long string of bits with the same polarity. This approach would probably be relatively expensive to implement and further analysis would be required.

Linear equalization is definitely an effective technique to reduce the effects of multipath in thermal noise environments. It was found that even for multipath channels near the video quality acceptability threshold, the average input bit error rate, with the equalizer is less than 1×10^{-3} for video SNR's $\geq$30 dB. In very strong impulse noise environments (arrival rate 30,000 per sec with impulse amplitudes Rayleigh distributed) linear equalization provides a marginal improvement at high SNR's. However, at very low SNR's, performance is in fact degraded by linear equalization. The reason for this performance degradation is that the equalizer smears the impulses, prolonging their duration, and hence corrupting more bits. The major drawback with linear equalization is its implementation complexity and cost.

A final alternative for reducing the effects of multipath involves modifying the teletext signal format so that clock sync and byte sync signals are in the middle of the burst. A half line video delay line (which is commercially available) could be used for data detection after the slicing level and clock phase have been extracted. The major problems with this approach are that the standard teletext format must be changed, and modifications to the way data is presented to the inserter must be made. The

potential gain is that reasonable teletext performance may be achieved in multipath environments without the added expense of a teletext equalizer. This conjecture would have to be substantiated by further simulation effort. The conjecture is based on the fact that the major degradation is caused by slicing level errors and not intersymbol interference. Acceptable video grade channels are not extreme channels with in band nulls or near nulls in the channel frequency response.

The results of the coding evaluation indicate that the error process is dominated by the bit timing and slicing level errors. This results in the errors being packet-wise bursty. This packet-wise bursting inflicts greater degradation (relative to the binary symmetric channel model) as the 'strength' of the code increases. This tends to narrow the gap between the weaker and stronger codes.

The performance of the codes was assessed in terms of their rejection and corruption rates relative to estimated threshold values. In all cases the rejection rate was found to be the limiting factor. The corruption rate was well below its threshold before the rejection rate reached the desired value. To counter this inbalance, a modification to the decoding algorithm was proposed. The approach is to allow a subset of the rejected packets to be accepted. The limiting case, where no packets are rejected, was examined and it was found to be a good alternative under various operating conditions. The possibility of employing a decoder with a variable rejection/corruption selector was also discussed and appears to merit further study.

The problem of coding vs equalization was also examined. It was found that an equalizer (or perhaps one of the other systems proposed to reduce the effect of multipath) is

mandatory for the Telidon system to function in broadcast television operating environment. Without an equalizer, the error rate into the decoder (approximately 5×10^{-3} for good video SNR's) is too great. None of the codes examined are capable of reducing the errors to an acceptable level from this high input bit error rate. (The input bit error rate where the decoders start to meet the performance requirements is approximately 1×10^{-3}).

The analysis of the codes was performed for a relatively small data base and with only rough estimates as to acceptable performance thresholds. Thus, no firm recommendation as to which code should be employed can be made. At the thresholds examined in this report, the Product code performs about as well as the more powerful codes. If the thresholds are tightened, the Bundle code becomes quite attractive. It was found, though, that the Bundle code's performance degrades severely if the input bit error rate becomes too high when full decoding is employed. Therefore, it is recommended that if the Bundle code is selected, one of the modified decoding schemes should be employed. (Error correction only (no rejections) appears to be a good choice).

7.2 Areas For Further Work

Before sound recommendations concerning the teletext receiver can be made, realistic subjective field tests must be made to find acceptable limits on rejection rate and the number of PDI errors per record that can be tolerated. Typical operating conditions must be identified (i.e. video SNR's and noise environment). Furthermore, in field trial measurements, typical noise environments must be monitored.

Digitized records could be used to characterize performance with the simulation program. The data could also be used to validate a noise model (such as the existing mix of impulse and gaussian noise used in the simulation) which could be used to more realistically characterize performance in environments where impulse noise is present.

One area where further work should be done is in coding evaluation. Error sequences generated during the field trial measurements would be best because:

(a) they are representative of errors in typical multipath and noise environments and

(b) the error sequence lengths are much longer than can be realistically generated with the simulation program. Consequently, better statistics on rejection rate and number of corrupting errors can be generated.

The coding evaluation program, CODING is a useful tool for the analysis, and is compatible with the compressed field trial error files.

The development of an error model for the Telidon system might also be the subject of further work. Given the simulated error sequences, one should be able to develop a realistic error model (incorporating slicing level errors, timing recovery errors, etc.) for the purpose of coding evaluation.

Further investigation into modified decoding algorithms (trading rejections for corruptions) would probably be fruitful. The coding analysis program could be used for this with only minor modifications.

7.3 Comments on Field Trial Measurements

To properly characterize system performance complex baseband impulse responses are required. This is true for any bandpass system where the frequency response is not conjugate symmetric about the carrier frequency. It is extremely important for characterizing the performance of carrier recovery systems, as the Nyquist slope region of the receiver IF has a significant impact (generates incidental phase modulation). With real baseband impulse responses, information about the Nyquist slope region is destroyed. Along the same vein, characterizing the performance with quasi-synchronous detection is not possible when only real impulse responses are gathered.

As alluded to earlier, the noise environment should be monitored. This would provide the input data necessary for characterising the broadcast television noise environment and developing reasonable noise models. Given the lack of data available in this area, such measurement data would be extremely valuable for researchers in other fields. A more accurate picture of the noise environment would allow one to make realistic predictions of the performance improvements provided by system enhancements (adaptive linear equalizers for example).

Field trial measurements also give one the opportunity to index television video quality and teletext quality to specific channel environments. This can be particularly useful information for developing subjective classification algorithms (either for television or teletext).

REFERENCE LIST

[1] L.I. Bluestein, "Envelope Detection of Vestigial Sideband Signals with Application to Television Reception", IEEE Trans. on Consumer Electronics, Vol. CE-21. No. 4, November 1975.

[2] T. Rzeszewski, "A System Approach to Synchronous Detection", IEEE Trans. on Consumer Electronics, May 1976.

[3] M. Long, M. Wilcox, and R. Baker, "An Integrated Video IF Amplifier and PLL Detection System", IEEE Trans. on Consumer Electronics, Vol. CE-28, No. 3, August 1982.

[4] A.R. Hamade, "Phase-Lock Television IF Amplifier-Video Detector", IEEE Trans. on Consumer Electronics, Vol CE-21, No. 4, November 1975.

[5] E. Breeze, " A New Design Technique for Digital PLL Synthesizers", IEEE Trans. on Consumer Electronics, Vol. CE-24, No. 1, February 1978,

[6] M. Sasaki et. al., "One-Chip-Controlled Voltage Synthesizer TV Tuning Systems", Vol. CE-24, No. 1, February 1978.

[7] P. Fockens and C.G. Eilers, "Intercarrier Buzz Phenomena Analysis and Cures", IEEE Trans. on Consumer Electronics, Vol. CE-27, No. 3, August 1981.

[8] W.L. Behrend, "Effects of Incidental Phase Modulation of TV Transmitters, or other Circuits, on TV Signals", IEEE Trans. on Broadcasting, Vol. BC-19, No. 3, September 1973.

[9] F.M. Gardner, "Phaselock Techniques: 2nd Edition", John Wiley & Sons, New York, 1979.

[10] A. Blanchard, "Phase-Locked Loops: Application to Coherent Receiver Design", John Wiley & Sons, New York, 1976.

[11] K.W. Moreland and J.H. Lodge, "Telidon System Study, 3rd Interim Report", Miller Communications Systems Ltd. Report, DSS File No. DSS 21ST.36100-2-4380, MCS File No. 8342, September 1983.

[12] C.H. Knapp and G.C. Carter, "The Generalized Correlation Method for Estimation of Time Delay", IEEE Trans. Acoust., Speech, Signal Processing, Vol. ASSP-24, pp. 320-327, August 1976.

[13] M. Sablatash, "Principles of Modelling and Pulse Shaping and Filter Optimization of Broadcast Teletext", CRC Technical Memorandum, June 8, 1983.

[14] E.S. Sousa and S. Pasupathy, "Transmitter-Receiver Design for Teletext Data Transmission", Communications Technical Report, Dept. of Electrical Engineering, The University of Toronto, May 1982.

[15] E.S. Sousa and S. Pasupathy, "Pulse Shape Design for Teletext Data Transmission", IEEE Trans. Commun., Vol. COM-31, pp. 871-878, July 1983.

[16] M. Sablatash, "A Short Essay on Pulse Shaping for Broadcast Teletext", Communications Research Centre, 1983.

[17] C. Eilers and P. Fockens, "Teletext Transmission Pulse Shape Optimization", IEEE Trans. Consumer Electron, Vol. CE-27, pp. 551-554, Aug. 1981.

[18] S.B. Ng, "Pulse Shape Optimization and Channel Equalization for Teletext Transmission over Multipath Channels", M.Sc Thesis, Department of Electrical Engineering and Computer Science, Massachusetts Institute of Technology, February, 1983.

[19] "Broadcast Specifications BS-14", Department of Communications, Government of Canada, Ottawa, Ontario, Issue 1, June 1981.

[20] E.S. Sousa and S. Pasupathy, "Enhanced Receivers for Nonoptimally Allocated Filtering", IEEE Trans. Commun., Vol. COM-31, pp. 879-885, July 1983.

[21] E.S. Sousa and S. Pasupathy, "Filtering Allocation in Teletext Data Transmission Under Power and Peak Constraints", IEEE Trans. Commun., Vol. COM-31, pp. 933-935.

[22] A.V. Oppenheim and R.W. Schafer, "Digital Signal Processing", Prentice-Hall, Inc., Englewood Cliffs, New Jersey, 1975.

[23] "Radio Standards Specification: Television Broadcasting Transmitters Operating in the 54-88 MHz, 174-216 Mhz and 470-806 MHz Frequency Bands", Department of Communications, Government of Canada, Ottawa, Ontario, Issue 2, September 1980.

[24] D. Falconer, "Course Notes for Advanced Digital Communication", Carleton University, Ottawa, January 1983.

[25] J. H. Lodge and S. T. Craig, "Telidon System Study, 4th Interim Report", Miller Communications Systems Ltd. Report, DSS File No. DSS21ST.36100-2-4380, MCS File No. 8342, January 1984.

[26] B. Mazur et.al., "Monitoring and Equaliztion of In-Service QPSK/TDMA Links by Means of Burst-Mode Channel Impulse Response Measurements", Sixth International Conference on Digital Satellite Communications, pp. I-A-18 - I-A-25, Phoenix, September 1983.

[27] P. Monson, "Feedback Equalization For Fading Dispersive Channels", IEEE Trans. Inform. Theory, pp. 56-64, January 1971.

[28] M. Obara et. al., "A TV Ghost Cancellor Using a CCD Transversal Filter", IEEE Trans. on Broadcasting, Vo. BC-29, pp. 60-71, June 1983.

[29] J. O. Voorman et. al., "One-Chip Automatic Equalizer for Echo Reduction in Teletext", IEEE Trans. on Consumer Electronics, Vol. CE-27, No. 3, August 1981.

[30] M. Schetzen, "Nonlinear System Modeling Based on Wiener Theory", Proc. of the IEEE, Vol. 69, pp. 1557-1573, December 1981.

[31] J. G. Proakis, 'Digital Communications', McGraw-Hill Book Company, New York, 1983.

[32] K. W. Moreland, "Automatic Classification And Identification of Radio Emissions, Phase II Report", Miller Communications Systems Ltd. Report, MCS File No. 8101, March 1982.

[33] G. M. Woodruff, "A Study of Impulse Response Estimation From a Sampled Digital Communications Signal", Master's Thesis, Dept. of Electrical Engineering, Queen's University, Kingston, Ontario., April 1982.

[34] S. L. Marple, Jr., "Efficient Least Squares FIR System Identification", IEEE Trans. Acoust., Speech, and Signal Proc., Vol. ASSP-29, pp. 62-73, February 1981.

[35] D. L. Duttweiler et. al., "Error Propagation in Decision Feedback Equalizers", IEEE Trans. Information Theory, July 1974.

[36] K. W. Moreland et.al., "Telidon System Study, 2nd Interim Report", Miller Communications Systems Ltd. Report, DSS File No. DSS21ST.36100-2-4380, MCS File No. 8342, June 1983.

[37] "North American Broadcast Teletext Specification", September 20, 1983.

[38] J. D. Maines and E. G. G. Paige, "Surface-Acoustic-Wave Devices For Signal Processing Applications", Proc. of the IEEE, May 1976.

[39] L. B. Milstein and P. K. Das, "Surface Acoustic Wave Devices", IEEE Communications Magazine, September 1979.

[40] R. A. Haken et. al., "A General Purpose 1024-Stage Electronically Programmable Tranversal Filter", IEEE Journal of Solid State Circuits, Vol. SC-15, pp. 984-996, December 1980.

[41] F. Williams, "Video-Speed Filtering Gets Its Own Digital IC", Electronics, pp. 148-151, October 20, 1983.

[42] E. R. Caudel and R. K. Hester, "A Chip Set For Audio Frequency Digital Signal Processing", International Conference on Acoustic, Speech, and Signal Processing, pp. 1065-1068, April 1982.

[43] T. Nishitani et. al., "LSI Signal Processor Development For Communications Equipment", International Conference on Acoustics, Speech, and Signal Processing, pp. 386-389, April 1980.

[44] W. L. Behrend, "Performance Comparison of TV Transmitters, RF Demodulators and the Home Receivers", IEEE Trans. on Broadcasting, Vol. BC-17, No. 1, March 1971.

[45] A. Vincent, "A Simulation Study of Teletext Transmission", CRC, DOC, Ottawa, February 1983.

[46] K. W. Moreland and R. K. Tiedemann, "Telidon System Study, 1st Interim Report", Miller Communications Systems Ltd. Report, DSS File No. DSS 21ST.36100-2-4380, MCS File No. 8342, March 1983.

[47] R. K. Tiedemann, "Simulation of VHF Multipath Propagation Model for Telidon", Miller Communications Systems Ltd., Technical Memorandum, 29 April, 1983.

[48] R. K. Tiedemann, "Intuitive Confirmation of Far Field Approximation for VHF Multipath Reflections", Miller Communications Systems Ltd. Technical Memorandum, 5 May, 1983.

[49] S. Yamazaki and Y. Endo, "A Quantitative Measurement of Subjective Effects of TV Multiple-Ghost Images by "Perceived DU Ratio", IEEE Trans. on Broadcasting, Vol. BC-26, No. 3, September 1980.

[50] S. K. Goyal, C. B. Neal, and E. R. Bowerman, "Television Transcient Response Computations Using a New Simulation Program", IEEE Trans. on Broadcasting, Vol. BC-23, No. 2, June 1977.

[51] W. C. Treurniet and P. J. Hearty, "Qualitative and Quantitative Measures of Users Responses to Errors In Teletext Transmissions .... Draft", Presented at CVCC/TS/WGB Meeting, January 1983.

[52] J. R. Storey, "Distribution of Errors in Japanese Teletext", 20 July, 1983.

[53] V. K. Bhargava et.al., "Realization, Economic and Performance Analysis of Error Correcting Codes and ARQ Systems for Broadcast Telidon and other Videotex Transmission", Concordia University, Montreal, Quebec, 15 June 1981.

[54] J. M. Wozencraft and I. M. Jacobs, "Principles of Communication Engineering", John Wiley and Sons, New York, 1965.

[55] W. F. McGee, "Coding, Equalization, and Feedback of Digital Cable Pair Signals", Canadian Elect. Eng. Journal, Vol. 7, No. 1, 1982.

[56] B. Mortimer, M. Moore, "More Powerful Error-Correction Scheme for the Broadcast Telidon System", DSS Contract OSU82-00164, March 1983.

[57] K. Hari et al, "Further Results on High Rate Codes for Byte-Oriented Information Systems", Concordia University, Montreal, February 1983.

[58] E. Séguin et al, "A Class of High Rate Codes for Byte-Oriented Information Systems", IEEE Trans. on Communications, Vol. COM-31, No. 3, March 1983.

[59] M. Sablatash, J. Storey, "Determination of Throughputs, Efficiencies and Optimal Block Lengths for an Error-Correcting Scheme for the Canadian Broadcast Telidon System", Can. Elect. Eng. J., Vol. 5, No. 4, 1979.

[60] B. Mortimer, "A Study of the Use of Error-Correcting Codes in Broadcast Telidon", DSS Contract OSU801-00095, February 1982.

APPENDIX A

PERFORMANCE DEGRADATION ESTIMATES

APPENDIX A

PERFORMANCE DEGRADATION ESTIMATES

1.0 INTRODUCTION

The error process affecting a digital communication system is strongly dependent on the type of interference influencing the system. For example, in thermal noise environments, errors tend to be randomly distributed. In this case, the average bit error rate essentially characterizes the error process. However, for impulsive interference, errors tend to occur in bursts. To characterize a burst error process, second order statistics (such as the error autocorrelation function) are required. The burstiness of errors has a significant impact on the choice of an appropriate error detection/correction code. Consequently, for the Telidon system, the average bit error rate will not necessarily provide an accurate gauge of system performance.

The ultimate gauge of system performance would require subjective evaluation by a sample of users. This is not a very reasonable or practical approach, especially during the design phase, when a number of computing alternatives are being contemplated. What is required is a nominal subjective index which can be evaluated from system parameters that can be estimated (either by purely analytical means and/or computer simulation). Unfortunately, no procedure is presently available for establishing subjective performance indices for the Telidon system. One can, however, estimate performance degradation parameters (corruption and delay) that are closely related to subjective performance.

One really requires a method of determining the information loss due to errors, and some procedure for relating this loss to a subjective degradation. A direct measure of the information loss for given channel conditions could be obtained if it were practical to simulate an entire decoder and simulate the transmission of numerous Telidon pages. Unfortunately, such a simulation would a formidable task and would also be computationally unattractive. Therefore, what is needed is a means of relating error statistics to subjective performance without explicit knowledge of the page being transmitted. This problem is complicated by the variability and compact form of Telidon data. For instance, one page may be entirely textual, while another may be a mix of text and graphics, implying different severities of errors in the PDI regions of the two pages. This is due to the fact that for graphical images, the severity of an error in a PDI instruction is strongly dependent on its location. Also, one page may require 100 records and corresponding headers, while another page may require a single (perhaps long) record. This variability problem will be treated by defining an average 'record' in terms of packet structure. The implication of errors within the regions of these typical pages will be categorized. A brief review of the packet structure will now be given.

A packet always contains the three sync bytes, and a Prefix. It optionally contains a Header (Data Group and Record Headers always occur together), and/or a Data Field. Synchronization bytes are considered part of the Telidon

'channel' and will not be dealt with here. These sections may be grouped under Hamming encoded (Prefix and Headers), and block encoded (PDI's) groups. Such a grouping is logical because it has been assumed that all types of errors are equally likely to occur at any position within the packet (ergodic and stationary); hence, statistics on the entire packet can be applied proportionately to the different sections of a transmission, with the appropriate error protection capabilities accounted for. What is required then is a measure of the relative importance of the Hamming encoded bytes to the block encoded bytes in order to allow determination of the best tradeoff between channel and decoder enhancements.

2.0 DEVELOPMENT OF EXPRESSIONS FOR REJECTION RATE AND PDI CORRUPTION

Errors can either corrected, detected, or missed. If an error is detected within a packet of interest (i.e. correct channel, address, etc.) the packet is discarded and the user will experience a delay as the decoder waits for the packet to be rebroadcast on the next cycle. Such errors will be referred to as delaying errors. Another component of the delaying errors are missed errors that result in packet rejection due to an incorrect sequence number, address, etc. Missed errors that do not result in packet rejection will be referred to as corrupting errors because they will result in errors in the displayed page. When deciding whether a missed error is a delaying or corrupting error it is assumed that the probability of accepting a packet as the correct one, due to errors in an undesired packet, is negligible. This assumption is made because there are 131,000 possible single missed errors in the P1, P2, P3, CI, PS prefix bytes, only one of which would be accepted as a "mid-record"

packet. (Note that, if the packet were the first of a record, all channel, address, sequence counter, and link counter bytes would have to correspond to those requested, further reducing the possibility of packet acceptance.) Another way of stating the above assumption is that all packets will be assumed to be currently requested by the user and the errors in each packet are independent of those in other packets.

The contribution, of each packet section, to the total delaying error rate and the corrupting error rate must be determined. The sections that will be considered are the Prefix, Header, and Data Field (PDI's). Error detection in any of the three sections has approximately equal delay consequences (packet rejected). Corrupting errors in the Header potentially affect the entire record. Corrupting errors in the Prefix affect the packet and in some cases may affect the entire record. Undetected errors in the PDI's will minimally affect that one PDI or possible effect all PDI's that follow. Differentiating between the PDI's is not feasible due to the variety of possible pages. The basic unit of corrupting error severity will be the number of incorrect PDI bytes that are passed onto the display.

A Data Block contains 25 to 28 data bytes. Using 25 bytes/block, the fact that the maximum record is 2 kbytes, and letting L = the length in packets of a record, then $L_{max} = 82$.

A short record might be half a screen of ASCII encoded text (20 rows of 40 columns/screen), giving $L_{min} \simeq 16$ packets, $L_{ave} \simeq 50$. Now, for

P_{HC} = Prob. (Header corrupting error situation in a packet),

P_H = Prob. (above situation occurs within a Header or single packet).

then,

$$P_H \cong \frac{P_{HC}}{L_{ave}+1}$$

and the number of PDI bytes affected, N_H is

$$N_H = P_H L_{ave} * 25$$

$$= P_{HC} \frac{L_{ave}}{L_{ave}+1} * 25$$

$$N_H \cong P_{HC} * 24.5 \qquad (A.1)$$

Similarily, effects of Prefix error situations, N_P, excluding Prefixes followed by Headers, is

$$N_P \cong P_{PC} * 24.5 \qquad (A.2)$$

where P_{PC} = Prob. (prefix corrupting error situation in a packet)

P_H and P_P will be approximated by measuring the average occurances of missed error, then adjusting these 'probabilities' by the proportion of errors that would result in delay and the proportion that would result in corruption. This is only a first order approximation because, in the event of multiple missed errors within a Header, any error resulting in packet rejection will throw out the associated corrupting errors.

In order to predict the split between corrupting and delaying errors, of undetected errors, a byte by byte breakdown of the Prefix and Header is given in Table A.1. From the Table it can be seen that the only way that a missed error within the Prefix can result in picture corruption is if the PS byte is in error alone. Then for

$$P_{PC} = \text{Prob. (packet corruption due to missed errors in Prefix)}$$

$$= 0.2 * P_{HAM}(1, 5), \qquad \text{(A.3)}$$

where

$$P_{HAM}(m,n) = \text{Prob. (m missed byte errors in n bytes, with no error detections, after Hamming decoding).}$$

Letting

$$P_{PD} = \text{Prob. (packet rejected due to prefix)}$$

$$= 0.8*P_{HAM}(1,5) + \sum_{m=2}^{5} P_{HAM}(m,5) + D_{HAM}(5), \qquad \text{(A.4)}$$

$$D_{HAM}(n) = \text{Prob (Hamming decoding will detect an error in n bytes).}$$

Similarity, for the Prefix followed by a Header,

$$P_{HC} \cong \sum_{\ell=1}^{L_H} P_{HAM}(\ell, L_H)*C, \text{ where} \qquad \text{(A.5)}$$

TABLE A.1
DELAY/CORRUPTION CLASSIFICATION OF UNDETECTED HAMMING (8,4) ENCODED SECTIONS

Byte(s)	Delay/ Corruption	Comments Prefix (undetected errors)
P1-P3	delay	packet identifier
CI	delay	
PS	corruption	incorrect use of suffix can result in packet corruption
		HEADER
TG	--	not yet sufficiently defined
C	delay	record identifier
R	corruption	appears to have applications in non-cyclic applications only
S1,S2	corruption	data will be incomplete, or contain portions of other records
F1,F2	corruption	as S1, S2 except to a lesser extent
N	--	not used by the decoder
TR	corruption	
RHD	corruption	indicates format of any extension
A1-A3	delay	record identifier
A4-A9		
L1,L2	delay	record identifier
Yxx	corruption	affects display options, may represent many bytes
EI, ES	corruption	indicates record identity for cross references

TOTALS:	delay	corruption	total bytes
Prefix	4	1	5
Prefix and Header	16	≈15	≈31

L_H = average length of Header, for simplicity, taken as one Data Block = 33 bytes.

C = fraction of missed errors that result in corruption

$\simeq$ .5 (from Table A.1),

$$P_{HD} \cong \sum_{\ell=1}^{L_H} P_{HAM}(\ell, L_H)*(1-C) + D_{HAM}(L_H) \ . \qquad (A.6)$$

An approximate measure of packet rejection and data corruption, due to the Prefix and Header, can be obtained by using equations (1) to (6). The following five measurements are needed in order to use these equations:

(a) $\alpha_1 = P_{HAM}(1,5)$ = the probability of 1 missed byte error in 5 bytes (not detected)

(b) $\alpha_2 = \sum_{\ell=2}^{5} P_{HAM}(\ell,5)$ = the probability of more than 1 missed byte error in 5 bytes (no error detection)

(c) $\alpha_3 = \sum_{\ell=1}^{33} P_{HAM}(\ell,33)$ = the probability of at least 1 missed byte error in 33 bytes (no error detection)

(d) $\beta_1 = D_{HAM}(5)$ = the probability that at least one error 1 error is detected in 5 bytes

(e) $\beta_2 = D_{HAM}(33)$ = the probability that at least 1 error is detected in 33 bytes

Instead of actually Hamming encoding/decoding packets in the simulation, the following simple rules may be used:

(a) any even number of bit errors/byte will be detected, but not corrected,

(b) any odd number of bit errors/byte ≥ 3 will result in a missed error.

Use of these rules ignores the unlikely occurance of three errors occurring in only the parity check bits.

Within the simulation, all packets should be encoded/decoded by a block code under test. The post decoding packet rejection rate and PDI failure (missed error) rate can be measured in order to approximate:

P_{DD} = the probability that the packet is rejected due to PDI error detection (post-decoding PDI rejection rate with selected block code)

N_D = Average number of post decoder PDI errors that were not detected per packet.

Combining all seven measurements, an overall packet rejection rate, R, and PDI error rate, N_C, can be approximated:

$$R \cong \frac{P_{HD}}{L+1} + \frac{L}{L+1}\,(P_{PD} + P_{DD} - P_{PD}P_{DD}) \quad \text{Packet rejection/Packet} \qquad (A.7)$$

$$N_C \cong \underset{\text{PDI errors/Record}}{\left(P_{HC}+P_{PC}(1-P_{DD})\right)*24.5} + N_D*L\left(1-(P_{PC}+P_{PD})\right) \qquad (A.8)$$

where a pessimistic assumption that Prefix and PDI rejections are independent is used. The average record length in packets is ≈50; therefore,

$$R \simeq \frac{P_{HD}}{51} + 0.98(P_{PD}+P_{DD} - P_{PD}P_{DD}), \qquad (A.9)$$

$$N_C \simeq (P_{HC}+P_{PC}(1-P_{DD}))24.5+N_D*50(1-P_{PC}-P_{PD}) \qquad (A.10)$$

The R and N_C values represent an attempt to map certain error statistics into measures of delay, and displayed errors.

3.0 ESTABLISHING REALISTIC BOUNDS FOR ACCEPTABLE PACKET REJECTION RATES AND NUMBER OF PDI ERRORS PER RECORD

Ideally, acceptable limits on R and Nc should be established by subjective testing, as the values are likely to be highly variable due to differing personal opinions. However we must establish realistic bounds without the benefit of the results of such subjective tests.

In [36], a rough bound on the packet rejection rate was established. It was based on the results of an MCS study "Comparison of Error Correction", where it was found that the mean waiting time increased dramatically for bit error rates greater than 10^{-4}. This was based on random error statistics and a similar block length to that used in Telidon (i.e. 256 bits). Assuming that essentially all errors can be detected, the packet rejection rate is given by:

$$R \simeq 1 - (1-p_e)^{256}$$

$$\simeq 256\ p_e = 2.5 \times 10^{-2} \qquad \text{(A.11)}$$

To get a better feel for the average amount of time between retransmissions, we can compute the mean number of records between retransmissions, N_{RR}, which is given by:

$$N_{RR} = \frac{(1-R)}{RL} * \qquad \text{(A.12)}$$

where L = the number of packets per record (assumed to be 50).

Using $R = 2.5 \times 10^{-2}$ and L = 50, the average number of records between retransmissions is 0.78, which is not very good performance. Consequently, when R exceeds 2.5×10^{-2}, it is safe to classify this as unacceptable performance. In fact, some limited subjective testing should be conducted to either support or contradict this bound, and if the latter, provide data that could be used to derive a reasonably tight bound.

In [36], a maximum number of byte errors per picture (15.5) is derived based on the maximum bit error rate of 5.5×10^{-4} quoted in Treurniet's subjective tests [51] and the average number of bits per picture (page) which was 28,228 [51]. Assuming 50 data packets per record, with 28 data bytes per packet, the average number of records per picture is approximately 2.5. Therefore a reasonable bound on the number of PDI errors per record is:

$$N_C(\max) = 6.2 \qquad \text{(A.13)}$$

*In [53], there are obvious errors on page 28, equations (2.17) and (2.18).

It must be emphasized that subjective quality in [51] was established using pictures (maps) as opposed to textual information. Because the subjective tests were based on only one specific type of graphical image, one must be cautious of the above figure. Clearly subjective tests, with a variety of pictures and mixes of graphical and textual information, should be performed to ensure realistic limits on PDI error rate and the tolerance to delay. However without the benefit of such information, we will use $R_{(max)} = 2.5 \times 10^{-2}$ and N_c (max) = 6.2.

It is interesting to examine some of the requirements of the Japanese Teletext system presented in [52]. Their major objective was achieving a page error rate of 5×10^{-2}, and they make no distinction between errors that can be detected (which result in retransmission) and missed errors (which result in corruption). It is remarked in [52] that the above page error rate is considered to be rather severe compared to those for other systems developed in other countries.

In the Japanese system, a page consists of 8 packets of 34 bytes each (total of 272 data & control bytes). Consequently, one of our records, composed of packets with 33 control & data bytes, corresponds to roughly 6 Japanese pages. First let us assume that the majority of errors can be detected, in which case the page rejection rate (P_R) is 5×10^{-2}. The average number of pages between retransmissions is $\frac{1-P_R}{P_R} = 19$. Converting this to our standard record, we obtain:

Average Number of Records Between Retransmission ≈ 3.2

which is significantly better than what was obtained using R (max). In fact the above corresponds to a equivalent packet rejection rate, R_{eq}, of 6.2×10^{-3}, which is a factor of 4 better than R (max). Since this is supposed to be a stringent requirement, one should be able to find a reasonable value between 2.5×10^{-2} and 6.2×10^{-3}.

The page error definition used in the Japanese calculations [52] is somewhat bizarre. If a packet has more than 2 error bits it is regarded as an error block. If there are two or more error blocks in the page of eight blocks, the page is referred to as an error page. Note that these errors could be detectable errors. Acceptable pages can be guaranteed if the upper limit on the number of errors per line is one, which corresponds to one byte error per packet. The threshold bit error rate for the Japanese system was 5×10^{-3}. At this error rate, the probability of error detection is much greater than data corruption (by at least an order of magnitude) for most codes. On page 22 of [53], the validity of the above assumption for the SAB and S&S codes for bit error rates exceeding 4.96×10^{-3} is clearly demonstrated. Consequently we can take $\frac{1}{10}$ byte errors per packet as an upper limit on the number corrupting errors (undetected). This translates into

$$N_c = \frac{1}{10} * 8 \text{ packets/Jap. page} * 6 \text{ Jap. pages/MCS record}$$

$$= 4.8 \text{ PDI errors/record.}$$

This upper limit is in reasonably close agreement with the limit of 6 PDI errors/record extrapolated from the subjective tests conducted by Treurniet [51]. The only major question mark is whether or not the bound on R is tight enough.

APPENDIX B

CHANNEL CLASSIFICATION PROCEDURE

APPENDIX B - CHANNEL CLASSIFICATION PROCEDURE

1.0 INTRODUCTION

Measurements of complex impulse responses performed by CRC personnel, for television channels in the 200 MHz region, have provided results that tend to support rather than contradict the Telidon RF multipath propagation model simulation results [36], [47]. Consequently, the Telidon propagation simulation can be used to generate realistic multipath channels for evaluating Telidon system performance. Because attention should be restricted to the subset of channels which provide acceptable video signals, a prescreening procedure for discarding channels not providing usable television signals is required.

Until recently, the examination of the effects of echoes on the subjective quality of television pictures has received little attention. Some work was done in the early 70's by Lessman [49], [50]. However, only the restrictive cases of positive (in-phase) and negative (out-of-phase) single echoes were studied. A procedure for weighting multiple ghosts to obtain an estimate of the subjective picture quality is proposed in [49] and will be summarized later.

The subjective effect of long echoes on television pictures was studied by Allnatt (1965) [49]. The major observation was that there is almost no difference in the degree of degradation of picture quality for delay times between 5-15 μsec. Lessman's pioneering work is still useful and is often referenced. Lessman used a seven point comment scale, shown in Table B.1, for accessing the subjective quality of the picture. In [50], the effects on picture quality of transmitter amplitude and group delay responses which satisfy the FCC tolerances (fit inside amplitude and

group delay masks) are discussed. The amplitude and group delay tolerances are shown in Figure B.1. In [50], an arbitrary amplitude response varying ±2 dB in the frequency range (-1.0 MHz to 4.0 MHz) at a rate of 1 cycle per MHz and a constant group delay response were assigned to the transmitter characteristic. In evaluating the effects of this transmit characteristic, an ideal VSB receiver characteristic with constant group delay was used. The output signal exhibited paired echoes (11.5% of the main signal) displaced from both sides of the main response by 1 μsec. It is claimed in [50] that this echo level and delay corresponds to a cumulative comment class 4 or better by at least 50% of the audience. As is apparent from Table B.1, this corresponds to fairly good picture quality (not at the threshold of acceptability).

Also in [50], computations were performed with an ideal transmitter amplitude response, but with group delay varying sinusoidally with peak amplitude of 100 nsec between 0-3 MHz, and 50 nsec between 3.0 - 4.2 MHz. The output for the above transmitter and an ideal receiver revealed a negative echo pair that was 5% of the main signal. According to [50], this corresponds to 60% comment 2 or better. It is evident that amplitude and group delay tolerances for transmit and receiver characteristics provide good quality pictures and cannot be used for prescreening multipath channel responses. In fact, in [50] it is claimed that a transmission system (incorporating an ideal receiver) should be capable of producing a picture of at least 80% comment 2 or better. This is a very high quality picture.

The echo strength versus echo delay for 80% comment 2 or better performance is shown in Figure B.2. One can see that for 100 nsec ripples in the group delay response, the

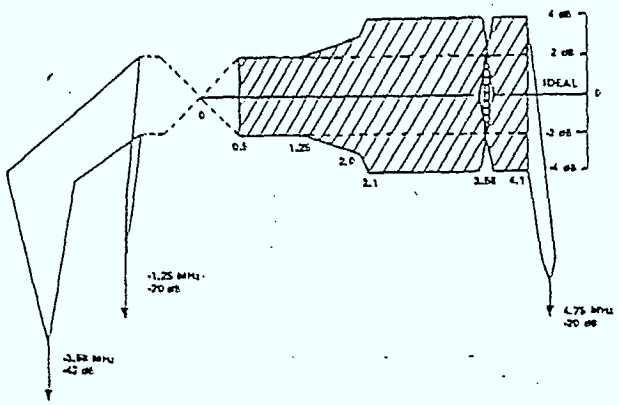

a) FCC Amplitude Response Mask

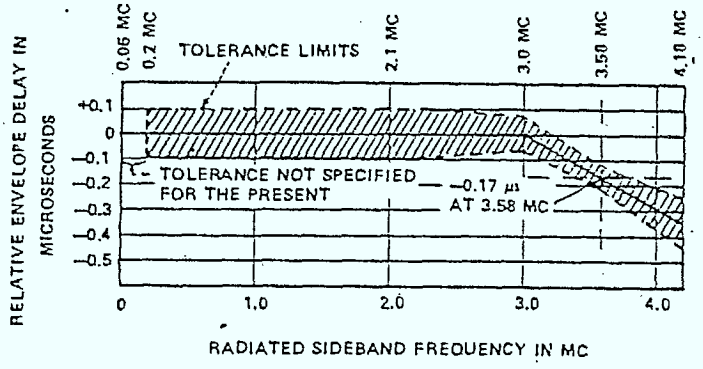

b) FCC Group Delay Mask

Figure B.1 : Transmitter amplitude and group delay tolerance specifications (FCC) [50].

Comment Number	Comment Description
1	Not Perceptible
2	Just Perceptible
3	Definitely Perceptible, But Only Slight Impairment to Picture
4	Impairment To Picture, But Not Objectionable
5	Somewhat Objectionable
6	Definitely Objectionable
7	Extremely Objectionable

Table B.1: Lessman's Seven Point Comment Scale (after [50])

echo delay must be greater than 2 μsec (undulation frequency less than 0.5 cycles per MHz) for acceptable colour TV performance. It is quite clear from Figure B.2 that strong close-in echoes are not as objectionable as those with longer delays. Shorter echoes are subjectively masked by the main signal. Many people even appreciate some occurence of short echoes, as they accentuate contours in the picture [29]. Curves, presented in Figure B.3 [29], indicate the subjective influence on a television picture of a single (in-phase) echo as a function of relative level and echo delay. It is evident that close-in echoes are significantly less annoying than far out echoes. These short echoes, however, can seriously disturb Teletext transmission.

The curves of Figure B.3 are more useful than the curves of Figure B.2, as they allow us to approximately establish the threshold of acceptability. The major deficiency, however, is that the above curves are restricted to the single, positive echo case. This deficiency is addressed in the next section.

2.0 CHANNEL CLASSIFICATION

A procedure for weighting multiple ghosts to obtain an estimate of subjective picture qulaity, proposed in [49], was adopted for channel classification. To estimate the subjective quality of a television picture, a "perceived DU (desired to undesired) ratio", denoted by PDUR, is computed. It is essentially the ratio of the power of the desired signal to the power sum of individual ghost images (Signal to Clutter Ratio), with appropriate weighting applied to each echo to account for the effects of echo delay, τ, and phase, ψ.

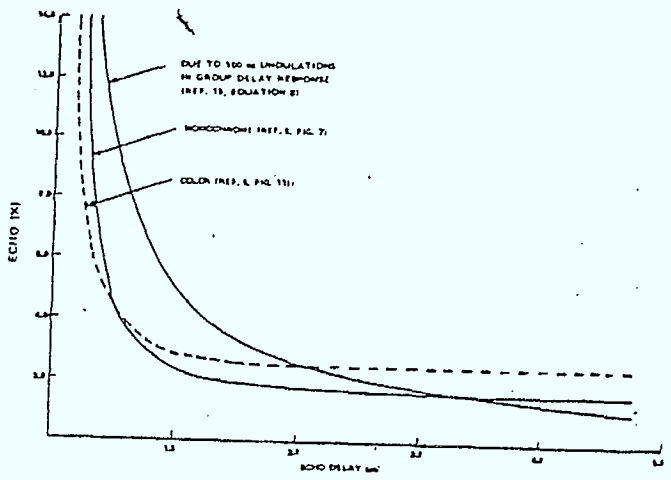

Figure B.2 : Echo due to 100 nsec group delay undulations compared with subjective perceptibility data

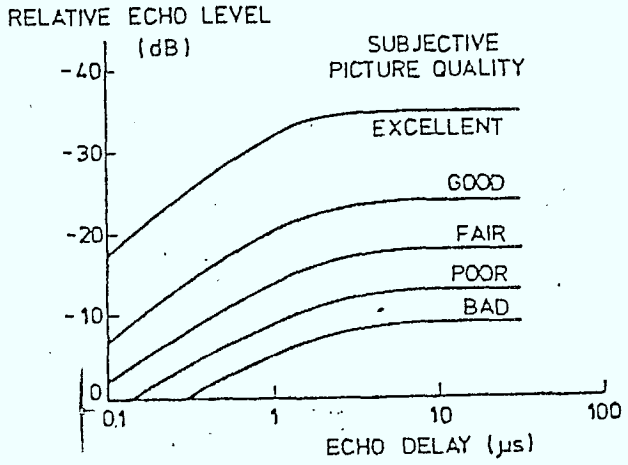

Figure B.3 : Subjective quality of TV pictures for a single (in-phase) echo as a function of relative level and echo delay (after [29])

The degree of quality degradation is dependent on the phase, ψ, and delay, τ, of the ghost. The perceived DU ratio of a particular individual ghost with delay, τ, and phase, ψ, is the DU ratio of a positive ghost with standard delay (5 μsec) which provides equivalent subjective degradation.

The perceived DU ratio of the i-th ghost is given by:

$$P_{i[dB]} = \frac{D}{U}(i) + W_{\psi}(i) + W_{\tau}(i)_{[dB]} \qquad (B.1)$$

where

$\frac{D}{U}(i)$ is the DU ratio of the ghost

W_{ψ} is the phase weighting function (see Figure B.4)

W_{τ} is the delay weighting function. (see Figure B.5)

In [49], the standard delay for a ghost is 5 μsec.

The perceived DU ratio, which provides an indication of the degree of quality degradation of a picture impaired by multiple ghosts, is:

$$PDUR = -10 \log_{10} \sum_{i=1}^{n} 10^{-P_i/10} \ [dB] \qquad (B.2)$$

where

n = the number of ghosts.

The relationship between PDUR and subjective picture quality is shown graphically in Figure B.6. The

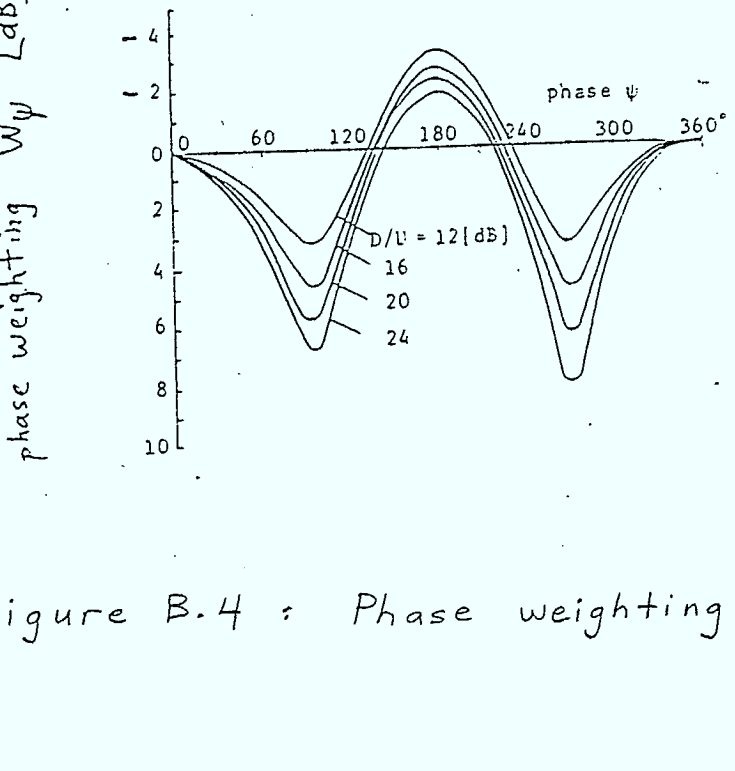

Figure B.4 : Phase weighting curve

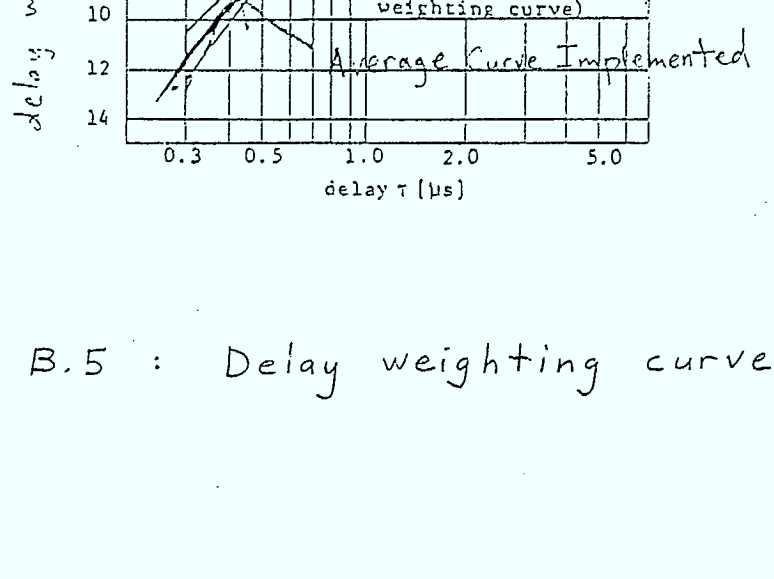

Figure B.5 : Delay weighting curve

subjective picture evaluation was made using the 5 point comment scale shown in Table B.2. In fact, experiments conducted by the authors of [49] indicate that the correlation coefficient between the numerical PDUR and subjective quality assessment is very high. In fact, the PDUR is probably the best gauge of subjective picture quality available at present.

Using Figure B.6 and the comment scale of Table B.2, the following thresholds were selected for acceptable and good video channels:

PICTURE QUALITY	COMMENT SCALE THRESHOLD	PDUR THRESHOLD
Unacceptable	≤ 1.5	≤ 11 dB
Good	≥ 3.5	≥ 24 dB

3.0 DEVELOPING CHANNEL STATISTICS USING THE SIMULATION PROGRAM

The VHF propagation model simulation program can be used to generate realistic multipath channels to use for establishing Telidon system performance. To do so, one must establish the number of echo paths, N, comprising the channel impulse response. This parameter is strongly dependent on the density of buildings and extent of the urban area. In the simulation, one simply has to combine N Monte Carlo cycles into an impulse response, specifying the delay, magnitude, and a uniform phase angle on the interval $[-\pi, \pi]$ for each component path. The channel can then be classified using the PDUR classification scheme discussed

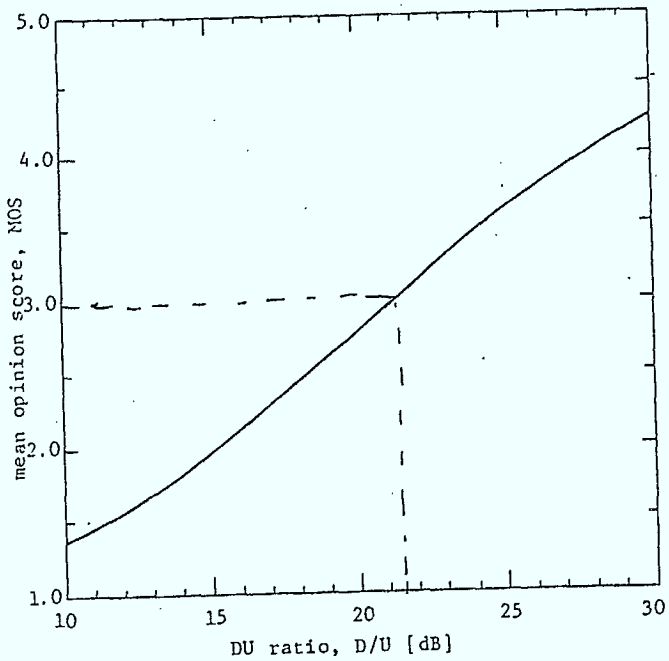

Figure B.6 : Relationship between PDUR and mean opinion score for picture quality [49].

Comment Number	Description
5	imperceptible
4	perceptible but not annoying
3	somewhat annoying
2	severely annoying
1	unusable

Table B.2: 5-point comment scale used in [49] for subjective picture evaluation

in the previous section. Only acceptable channels are retained, and statistical analysis performed on the acceptable and the good channels. The PDUR, and consequently, the classification procedure will be a function of the number of echo paths comprising a channel impulse response. The sensitivity of this parameter must be investigated. With the simulation program, the generation of impulse responses of acceptable video channels is relatively easy. For example, one can even collect impulse responses that have PDUR's between specific limits (i.e. '13 - 15 dB', '19 - 20 dB', etc). This allows one to easily exercise control over the quality of the channel under investigation. However, it must be emphasized that good video quality does not necessarily imply good teletext performance.

3.1 Generating CDF Contours With The Simulation Program

Generating and classifying channels to use for evaluating system performance is relatively straight-forward. An extremely important parameter is the number of echoes (reflectors), N. Phase weighting is also important, as the subjective effect of an echo does depend on the phase of the echo. To statistically characterize channels with acceptable video, we would like to develop cdf contours of magnitude versus delay. Consequently we would like to decondition with respect to phase.

Originally, the proposed channel characterization procedure involved assigning a uniform phase [0°, 360°] to each path, estimating the phase weighting from implementations of the phase weighting curves (see Figure B.4), estimating the delay weighting (see Figure B.5), and determining the PDUR ratio. The average delay weighting function can be approximated as follows:

$$W_{\tau[dB]} = \begin{cases} 11.5 - 15.78 \log_{10}(\tau/0.3) & \text{for } \tau \leq 0.5\mu\text{sec} \\ 8 - 13.29 \log_{10}(2\tau) & \text{for } 0.5\mu\text{sec} \leq \tau \leq 1\mu\text{sec} \\ 4 - 8.3 \log_{10}(\tau) & \text{for } 1\mu\text{sec} \leq \tau \leq 2\mu\text{sec} \\ 1.5 - 5.68 \log_{10}(\tau/2) & \text{for } 2\mu\text{sec} \leq \tau \leq 3\mu\text{sec} \\ 0.5 - 4 \log_{10}(\tau/3) & \text{for } 3\mu\text{sec} \leq \tau \leq 4\mu\text{sec} \\ 0 & \text{for } \tau \geq 4.0\ \mu\text{sec} \end{cases} \quad \text{(B.3)}$$

Implementing the phase weighting curves, which are indexed according to DU ratio, is more involved. Consequently, a simpler procedure has been adopted.

3.2 Phase Weighting

The subjective effect of a ghost depends on its r.f. phase. However, the r.f. phase is a volatile parameter that can change dramatically with small perturbations in the position of the antenna. A channel that is classified as acceptable may be so only because of fortunate phases on dominate echoes. Perturbations in these phases would provide a channel that does not give acceptable video quality. Channels that are certain to provide acceptable video quality can be guaranteed by assuming worst case phases (ψ=180°) for each path.

It must be emphasized that the mean opinion score of '1.5' (which corresponds to a PDUR of 11 dB) was established as a conservative estimate of the threshold of acceptability. Variations of ±2 dB about the PDUR threshold, do not

greatly improve or degrade mean opinion scores on subjective quality. For example increasing the threshold by 2.5 dB translates into an increase of only 0.25 on the comment scale. As a result, there does not really exist a clear cut threshold, and the choice is rather arbitrary.

For an impulse response defined by a number of echo paths with delays, τ_i, and magnitudes, u_i, an infinite number of potential channels can be defined by assigning uniform phases to each path. One could classify the channel based on an average phase weighting, worst case phase assumption, or assuming zero phase (positive) echoes. The PDUR's computed using these assumptions are related as follows:

$$PDUR_{(ave)} \simeq PDUR_{(zero\ phase)} + 0.46\ dB$$

$$PDUR_{(worst\ case)} \simeq PDUR_{(zero\ phase)} - 2\ dB$$

The average phase weighting was evaluated assuming the phase weighting curve for a DU ratio of 12 dB, and the mean worst case weighting is approximately 2 dB.

The difference between average and worst case phase weighting is 2.5 dB, which translates ito only a 0.25 change in the quality comment scale in the neighbourhood of the threshold. Consequently, we will require that each channel have a PDUR exceeding 11 dB, for worst case phase weighting. This can be evaluated assuming positive echoes (avoiding the need for considering phase weighting) by increasing the thresholds by 2 dB, i.e.

Channel Classification	PDUR Threshold
Unacceptable	$\leq$13 dB
Good	$\geq$26 dB

3.3 Statistics Gathering and Sensitivity Versus 'N'

A scatter table for acceptable channels (this includes good channels) and a scatter table for good channels are maintained. When an impulse response is classified, the magnitude and delay for each path comprising that impulse response is entered into the appropriate scatter table. The scatter tables are then analyzed to generate cumulative distribution functions of magnitude versus delay. The cdf contours of the ensemble of paths belonging to acceptble channels are generated to obtain an indication of the delay spread that an adaptive equalizer must content with, and to allow a comparison with channel measurements. One could select channel responses from the cdf contours. However, there is no guarantee that the channel response selected would in fact be a channel providing acceptable picture quality. One would have to compute the PDUR to be certain. Since channels are generated and classified during the statistics gathering process, storing these (and indexing them according to PDUR value) for future use is much better than generating channels from the cdf contours.

The PDUR is dependent on the number of echoes, N. As N increases, the background clutter level increases. This tends to reduce the PDUR ratio, resulting in a higher percentage of rejected channels.

3.4 Simulation Runs And Results

The major purpose of these preliminary runs was to establish the sensitivity of the cdf contours with respect to the number of echoes in the channel impulse response. Furthermore, one can establish the effect of the acceptability criterion on the cdf contours by comparing the results with those previously obtained [36], [47]. The model that was used was the same as that specified in [47], i.e.

frequency	selectable
ϵ_r	3.0
σ	3×10^{-4} mho/m
T	randomly selected between 10-30 cm
W, H	randomly selected between 7.6m and 30m
Occupational Domain	6 km x 6 km, centered on the receiver
Transmitter Height, h_1	60m
Receiver Height, h_2	8.3m
Path Length	16 km
Reflector Orientation	Randomized

Table B.3 contains a summary of the simulation results, and the corresponding figure numbers of the appropriate CDF contours. As expected, as the number of impulse response components increases, the percentage of channels rejected increases and the percentage of good channels decreases. This is simply due to the increased background clutter level. As indicated in Table B.3, when the number of significant reflectors in the 6 km x 6 km occupational domain is dense (800) for channel 13, over 50% of the channels are rejected (PDUR's less than 13 dB). The number of reflectors in the occupational domain can be related to the frontage density [47] of significant reflectors (as seen from the street) as follows:

Frequency (MHz)	Number of Channels Classified	Number of Paths Per Channel	Percentage Rejected	Percentage Accepted	Percentage Good
211.25 (channel 13)	5,000	100	5.1	94.9	54.9
	2,000	200	10.8	89.2	18.6
	2,000	400	22.6	77.4	0.45
	1,000	800	51.8	48.2	0.0
55.25 (channel 2)	10,000	100	0.0	100	98
	2,500	400	0.0	100	91
201 (corresponds to frequency used in CRC measurements)	10,000	100	4.5	95.5	57.5
	5,000	200	9.58	90.42	21.5

Table B.3: Preliminary Simulation Results

N (number of reflectors)	FRONTAGE DENSITY
100	3.13%
200	4.43%
400	6.27%
800	8.87%

The CDF contours for acceptable and good channels for a carrier frequency of 201 MHz, which corresponds to the frequency used in the CRC measurements, are presented in Figures B.7 - B.10. As the number of rejected channels increases with increasing N, the general trend is a reduction in the magnitude contours for acceptable channels. However, the changes are not that dramatic, and it is safe to conclude that the magntitude versus delay contours are not very sensitive to the number of reflectors (echo paths).

In examining the contours for good channels it is not surprising to find that significant multipath components can arise for short delays (≤ 0.5 μsec). Such close in echoes, while not troublesome for video, can be troublesome for teletext. For longer delays, the echo magnitudes are below -26 dB.

By adjusting simulation programs parameters, it was found that the simulation results could be made agree quite

ANALYSIS OF SCATTER DIAGRAM PAR1000 - ACCEPTABLE CHANNELS

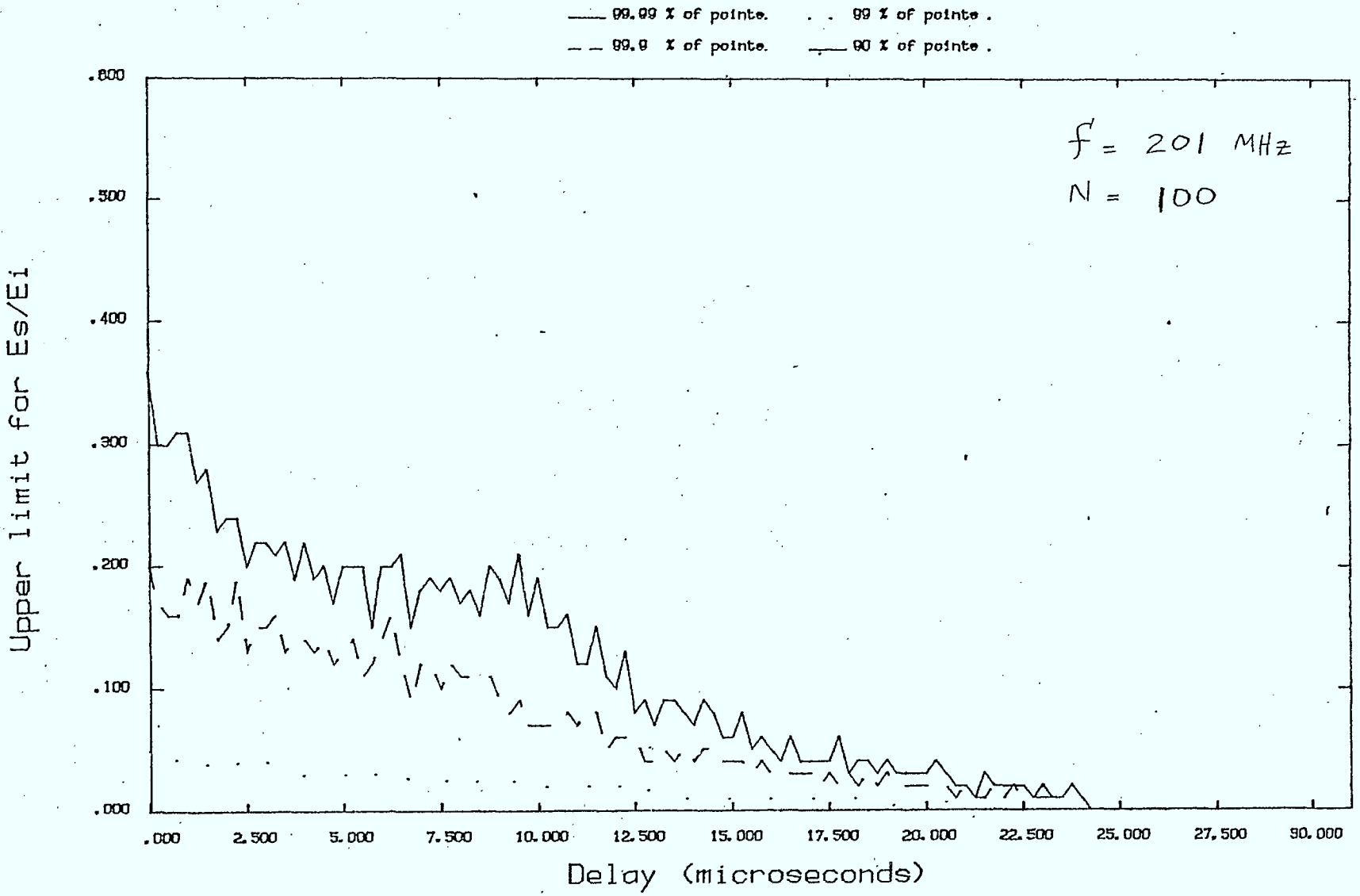

Figure B.7

ANALYSIS OF SCATTER DIAGRAM PAR1000 - GOOD CHANNELS

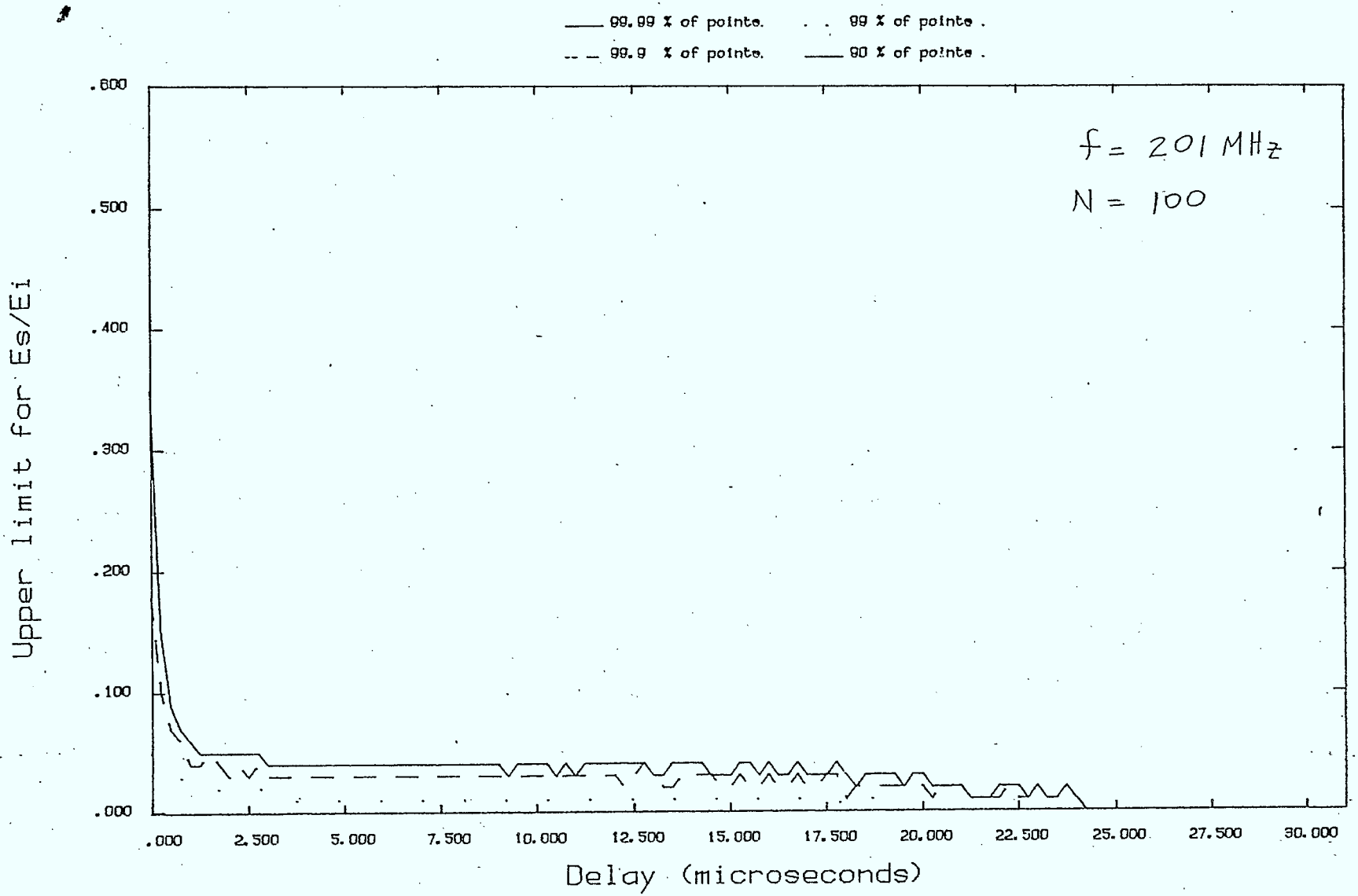

Figure B.8

ANALYSIS OF SCATTER DIAGRAM PAR1001 - ACCEPTABLE CHANNELS

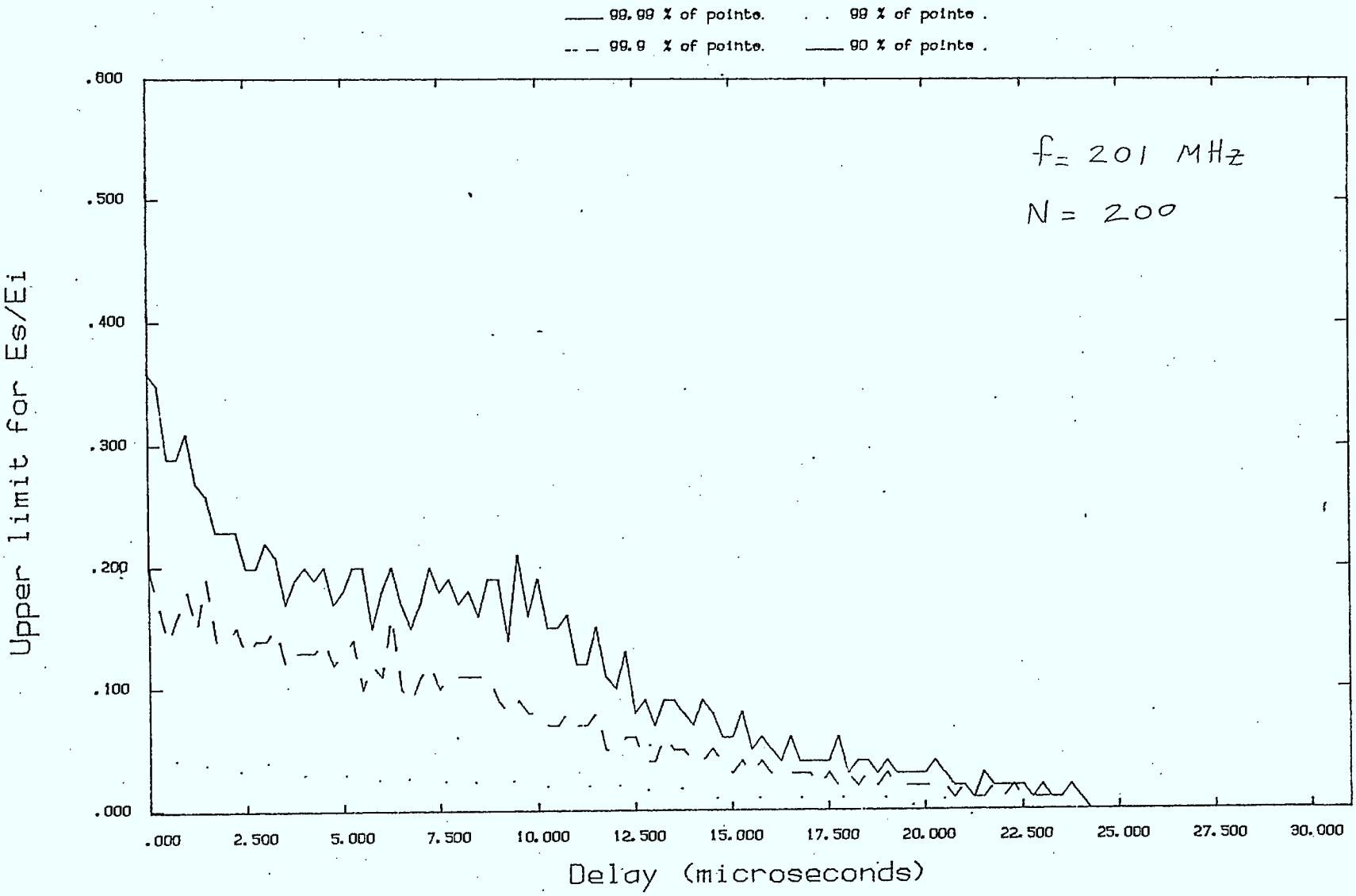

Figure B.9

ANALYSIS OF SCATTER DIAGRAM PAR1001 - GOOD CHANNELS

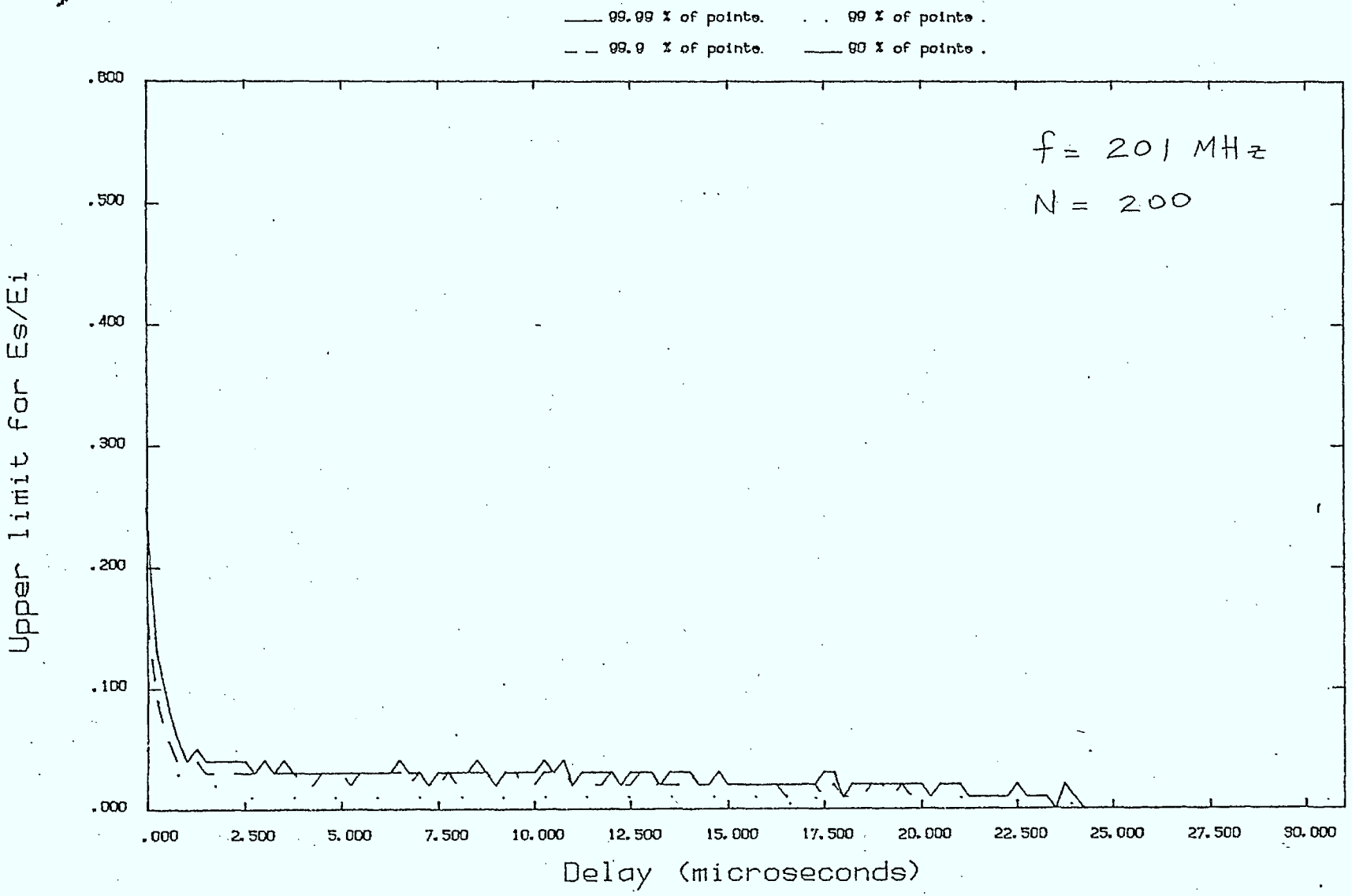

Figure B.10

well with the CRC channel measurement results. Consequently, the simulation program is a good working model. It's major advantage is its flexability, allowing one to characterize multipath channels in other frequency bands, and with reflector dimensions and densities characteristic of other metropolitan areas.

APPENDIX C

MODELLING THE QUASI-SYNCHRONOUS CARRIER RECOVERY ERROR

TABLE OF CONTENTS

1.0 INTRODUCTION

2.0 QUASI-SYNCHRONOUS RECOVERY TECHNIQUES

3.0 QUADRATURE DISTORTION INTRODUCED BY THE SYNCHRONIZATION SIGNALS

3.1 Determining the Baseband Spectral Components of the Synchronization Signals

3.2 Carrier Stripping Approach with an ideal Bandpass Filter

3.3 Phase Locked Loop Model

3.4 Second Order Phase Locked Loop Results

4.0 INCORPORATING THE EFFECTS OF LOW FREQUENCY VIDEO CONTENT

4.1 Video Random Process Models

4.2 Analysis of Phase Locked Loop Performance

5.0 POSSIBLE IMPROVEMENTS TO TELEVISION CARRIER RECOVERY SYSTEMS

6.0 CONCLUSIONS

APPENDIX C

MODELLING THE QUASI-SYNCHRONOUS CARRIER RECOVERY ERROR

1.0 INTRODUCTION

The purpose of this appendix is primarily to present the details of an attempt to develop a model for the phase error process of a quasi-synchronous carrier recovery system. Such a model could simplify the evaluation of television video and teletext system performance. The action of a quasi-synchronous detector is illustrated in Figure C.1. The output of the complex equivalent baseband model (of a synchronous detection system) is complex demodulated by $\exp\{-j\ \phi_e(t)\}$, and the real component taken as the detector output. The reduced computational requirements possible with the random process phase error model is the major advantage. This advantage is derived from the fact that effort does not have to be expended to extract the actual phase error of the carrier recovery system. The difficulty, however, is developing a phase error model that is valid over the wide range of possible quasi-synchronous carrier recovery techniques, which include the traditional carrier stripping approach and PLL recovery systems. It seems clear that separate models would have to be developed for each class of carrier recovery system.

A block diagram of a broadcast television based teletext system is provided in Figure C.2. The asymmetric (vestigial) sideband nature of the transmission system results in the generation of a quadrature component signal. The most crucial filtering in the system is performed at the receiver. The linear Nyquist slope region is shaped in such a fashion that when perfect synchronous detection is employed, the inphase component is a replica of the

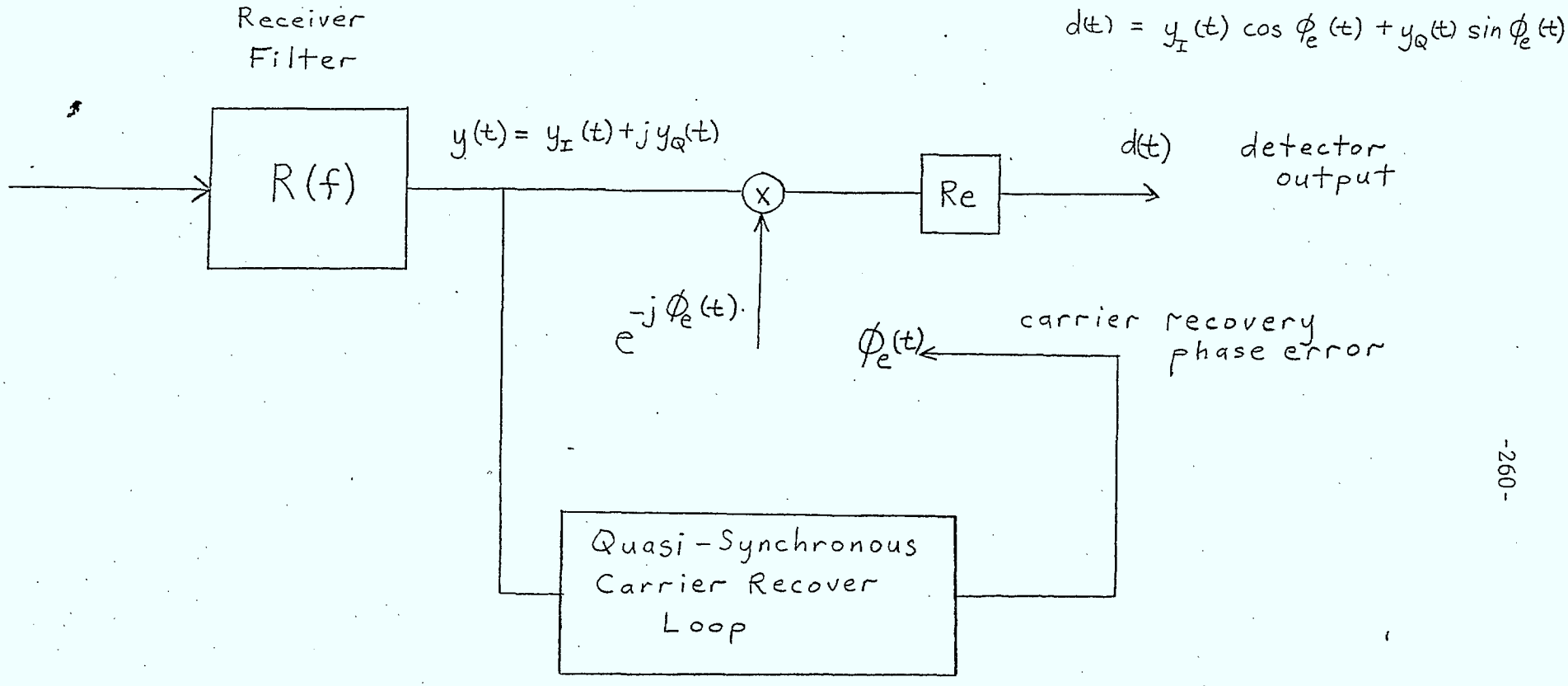

Figure C-1 : Quasi-synchronous detection

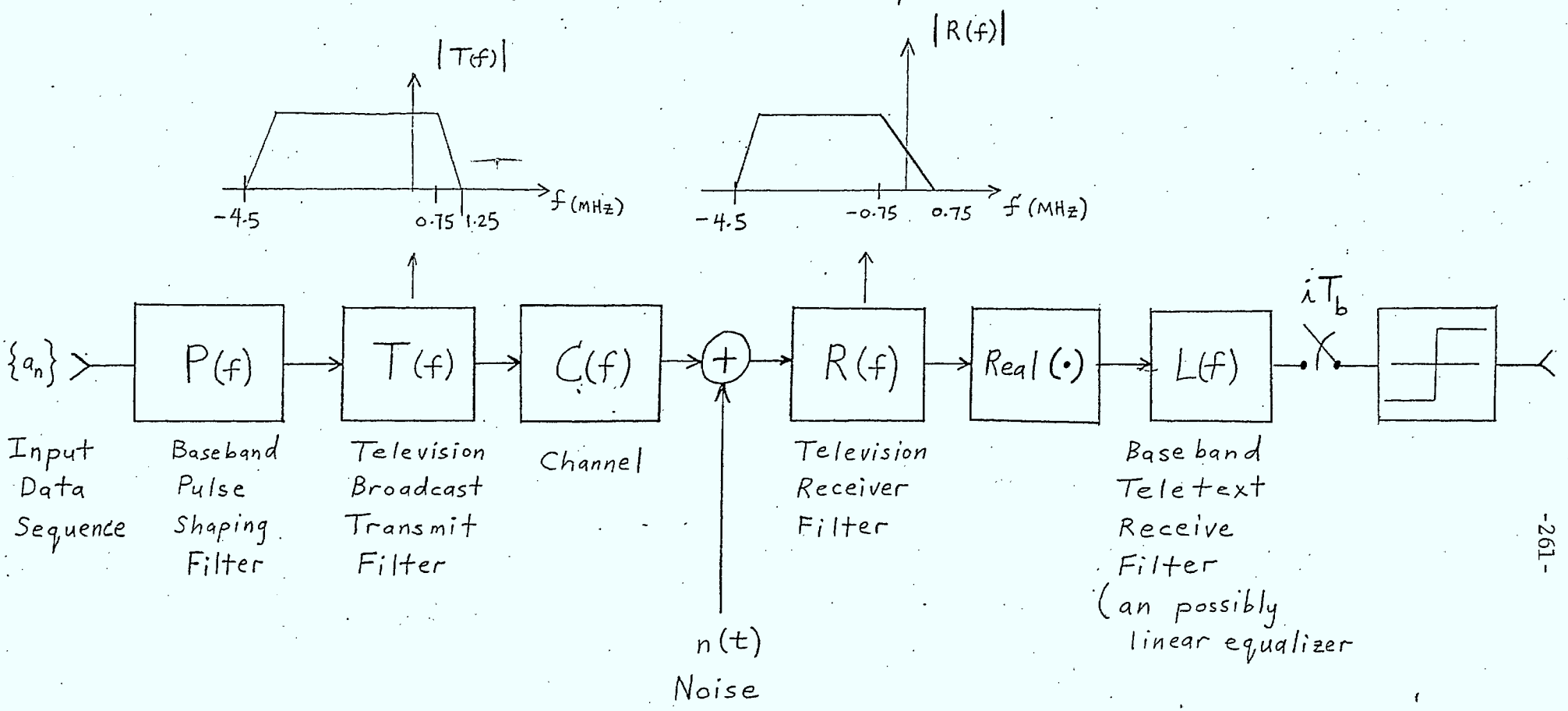

Figure C.2 : Baseband model for broadcast television based teletext transmission

transmitted baseband video signal. Ideally, $R_I(f) = \frac{R(f) + R(-f)^*}{2}$ should be constant over roughly a 4 MHz bandwidth. In practice, finite tolerances in the amplitude and group delay response in the Nyquist region result in departures from the ideal requirement and therefore distortion in demodulated output.

The quadrature component generated by the filtering at the receiver gives rise to non-linear distortion in an envelope detector. Another major concern with envelope detection is the 920 kHz beat that results because of the intermodulation between the colour subcarrier signal and the sound signal. This quadrature distortion can be completely eliminated from the video output if the receiver employs a synchronous demodulator; provided that the carrier frequency and the phase are correctly regenerated in the receiver. The asymmetrical nature of the receiver response about the picture carrier frequency (45.75 MHz) introduces phase modulation (due to the generation of a quadrature component) in the resultant output signal. In commerically available television receivers, the carrier recovery circuitry follows the receiver IF. Consequently, the phase modulation introduced by the quadrature component makes carrier recovery more difficult. Inevitably, some residual phase modulation persists, introducing a form of quadrature distortion. This can be minimized by reducing the bandwidth of the recovery loop. Narrowband recovery loops can be employed with receivers with closed loop frequency synthesizer tuning systems with quartz crystal stability and accuracy. Systems of such sophistication are synchronous detectors. To date, commerically available television receivers employ relatively wideband reference channels, and are referred to as quasi-synchronous detectors.

Rzeszewski's paper [2], published in May 1976, claims that all tuning systems to date produce an IF signal whose

picture carrier frequency is dependent on picture content. It is also quite clear that the dc level of the received video signal (which has significant impact on the input SNR of a phase locked loop recovery system) is strongly dependent on picture content. Rzeszewski also claims that in conventional tuning systems, there can be rapid frequency excursions as a function of picture content. Such tuning changes are small enough that they pose no real problem to envelope or quasi-synchronous detection (with a wide bandwidth reference channel). They are, however, especially troublesome for narrowband PLL carrier recovery systems. In particular, narrow reference channel recovery systems can suffer long transcients when subjected with such signals. Under extreme conditions the loop may even unlock, resulting in complete loss of sync until the loop reacquires. The major problem with wideband reference channels is that there will be chroma and video signal distortion in the reference channel.

2.0 QUASI-SYNCHRONOUS RECOVERY TECHNIQUES

A simple block diagram of two common quasi-synchronous recovery systems is provided in Figure C.3. The first method is commonly referred to as the carrier stripping approach [1]. The carrier is estimated by passing the receiver IF output through a bandpass limiter. The bandpass limiter consists of a bandpass pre-filter (typically a tuned circuit such as an L-C tank circuit) followed by a hardlimiter and a zonal filter for removing unwanted harmonics. Typically the tank circuit bandwidth is roughly 1.5 MHz (covering the linear skirt region of the IF filter).

An analysis of the carrier stripping approach has been conducted by Bluestein [1]. In this analysis, the complex baseband frequency response of the tank circuit is a simple first order filter $T_c(f) = \frac{\alpha}{jf + \alpha}$, where '$\alpha$' is the corner frequency.

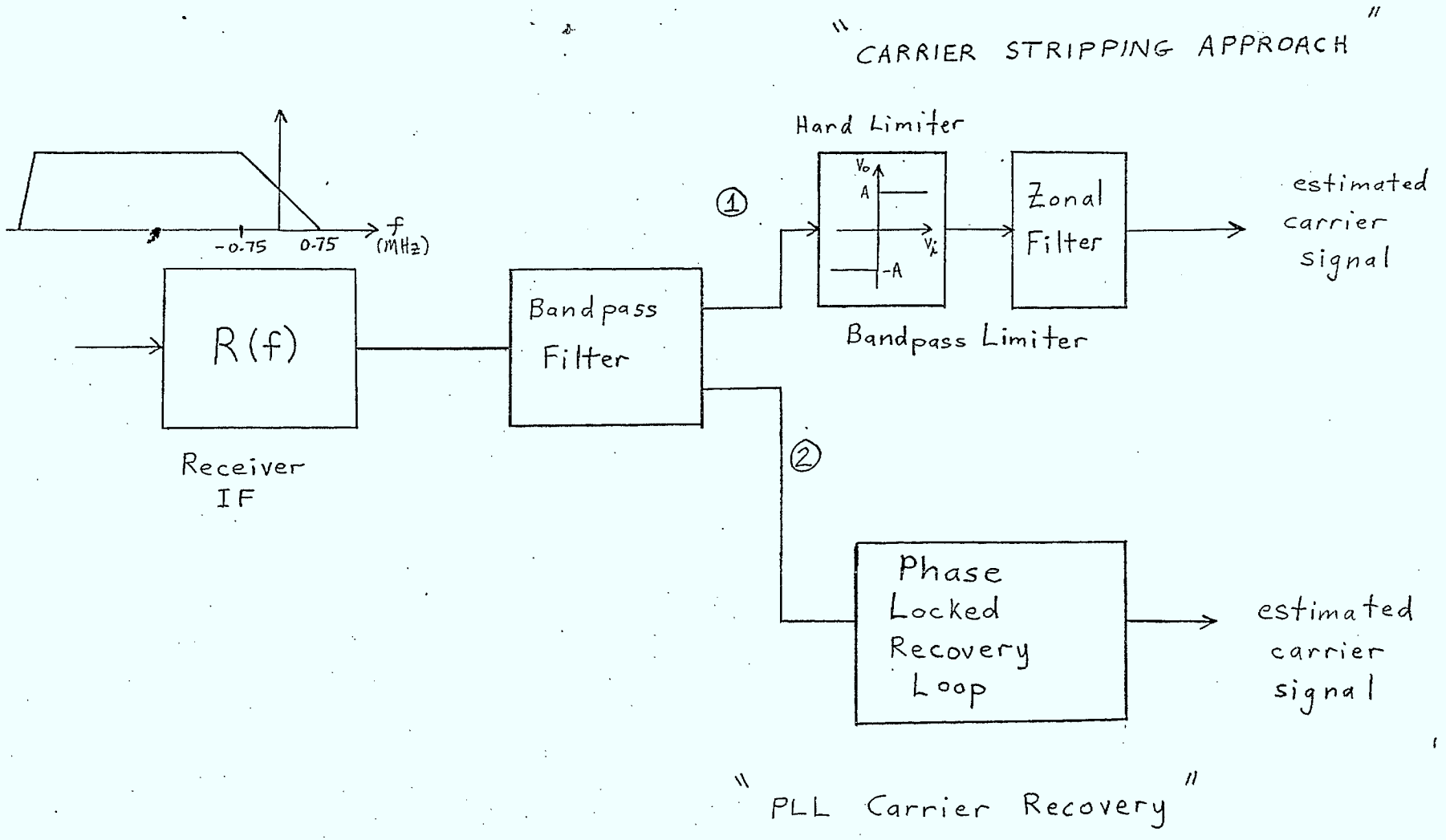

Figure C.3 : Two common quasi-synchronous recovery systems.

The phase error versus time is considered for a step in the video input going from peak white (12.5% modulation) to the blanking level (75% modulation), as a function of "α". The format of a TV line is provided in Figure C.4. It is clearly demonstrated that to reduce the peak phase error at the beginning of the step, making 'α' small is the appropriate solution. The problem with this solution is that as 'α' becomes smaller, the transcient lasts longer and the subjective effect is more discernable. Note that for a teletext signal, which will have numerous transitions from low to high signal levels, the transcients would be the problem with small 'α' and the higher peak phase errors the problem with large 'α'. There is a clear performance tradeoff, with the optimal choice somewhere between the two extremes. Another major factor which discourages the choice of small pre-filter bandwidth is the effect of mistuning. Clearly one must choose 'α' larger than the mistuning offset, to ensure that there will be sufficient carrier produced for product detection. As indicated in [1], for mistuning, it is the steady state phase error which is of primary importance. Bluestein's analysis indicates that this is reduced by making 'α' as large as practicable (i.e. roughly equal to the bandwidth of the linear skirt (Nyquist) region of the receiver IF).

The second method indicated in Figure C.3 is the PLL approach. In this case the majority of the filtering is performed by the PLL loop filters. As a result, the bandpass filter can be relatively crude. It's major purpose is to limit the amount of noise power subjected to the phase locked loop input. In some cases the phase locked loop may be preceeded by a hardlimiter-zonal filter combination to strip off the amplitude modulation from the signal. Provided that the amplitude modulation has a DC component, the loop will be able to lock. As indicated in [9], for an amplitude modulated signal (with no phase modulation), the

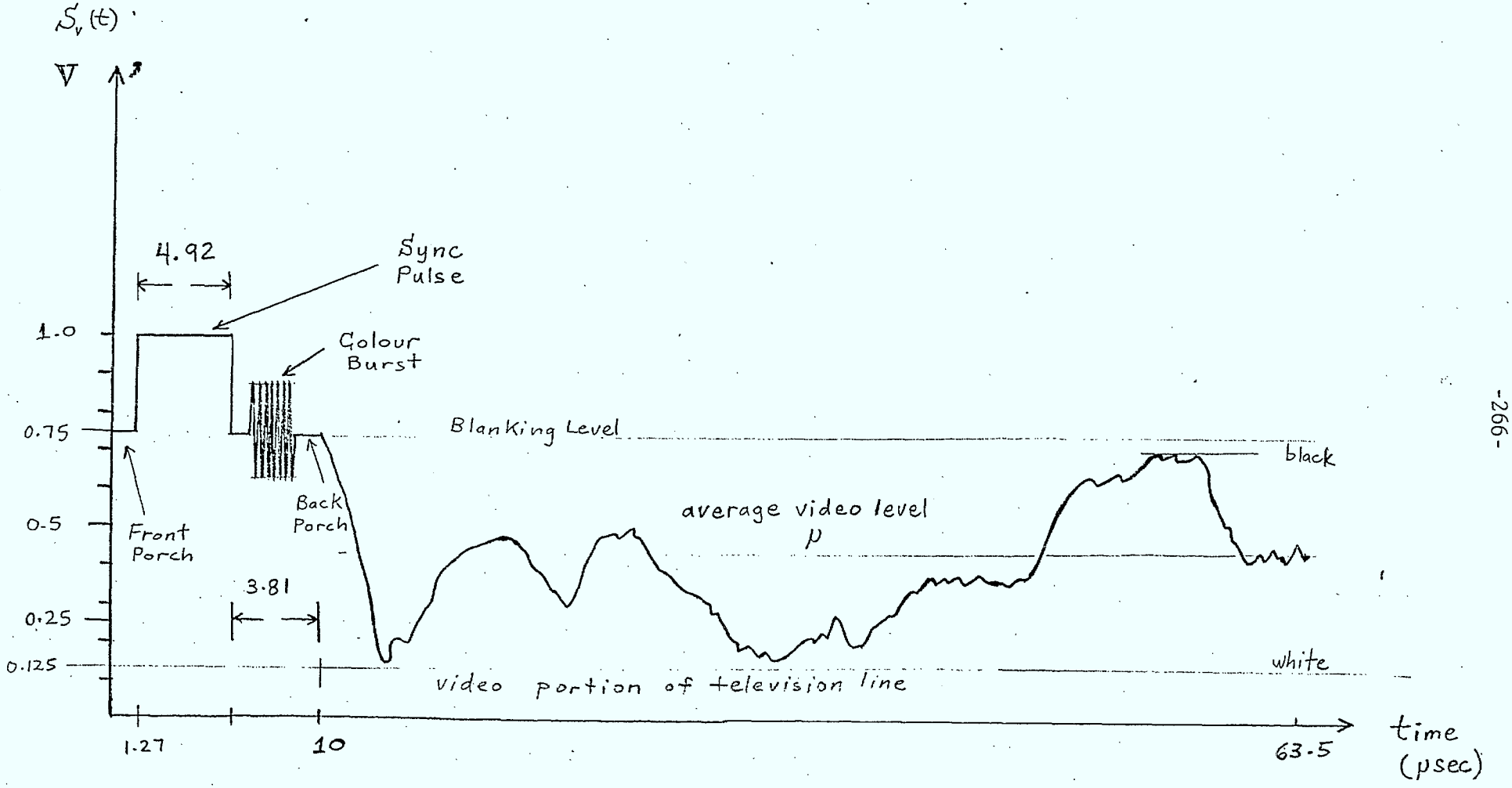

Figure C.4 : Television Line Format (negative modulation, 87.5% modulation index)

steady state (equilibrium) performance is not altered by the presence of amplitude modulation. The situation is complicated somewhat by the presence of incidental phase modulation produced by the receiver IF. It is also pointed out in [9], that considering the PLL output to be insensitive to amplitude modulation is only a first order approximation. When one recognizes that the loop gain is proportional to input signal amplitude, it is apparent that amplitude modulation results in an instantaneous reduction of gain during certain time periods. Consequently, the tracking ability of the PLL is impaired and the loop is less capable of tracking modulation excursions such as transmitter induced and tuning system incidental phase modulation. To prevent distortion in the demodulated video output, the system should track such incidental phase modulation. Consequently many systems employ bandpass limiters prior to the PLL recovery circuit [2], [3].

Unfortunately, limiters introduce performance degradations. Since the output power from a limiter is constant, irrespective of the input signal to noise ratio, noise suppresses the signal in a limiter. Because the signal suppression is a function of input signal to noise ratio (see [9] p. 126), the loop gain and bandwidth are functions of input signal to noise ratio. Furthermore, the non-linear nature of the limiting action complicates the characterization of the output noise (introduces spectral spreading of the input noise spectrum, tending to increase the spectral density of the tails, and lowering it in the center of the spectrum). Also, the limiter suppresses the AM component of the noise, and the output SNR of the limiter in the region about the fundamental can in fact be enhanced for high input SNR. One should not confuse this with improved PLL performance, because the PLL jitter depends only the phase noise (suppression of AM noise does not improve performance). The true degradation imposed by a

limiter depends on the nature of the input signal, the limiter pre-filter, the zonal output filter, and the phase detector of the PLL. An analytical treatment is far too involved to be persued here.

One should not get the impression that all systems employ limiters in the phase recovery process. The system discussed in [4] and illustrated in Figure C.5 for convenience does not employ limiters. In this system, the AFC function of the TV receiver is also performed. When the system is first turned on (or when the channel is changed) the L.O. and IF input signals are at different frequencies. The difference frequency at the phase detector output is used by the search oscillator to speed up acquisition and guarantee a wide pull-in range. The search signal varies the VCO frequency until the negative feedback PLL acquires lock, at which point the search signal is quenched. The system does employ AGC to adjust the signal to the appropriate operation level, and similar to the limiter action, this controls the phase locked loop bandwidth. Hamades paper [4] is primarily concerned with implementation details rather than performance analysis. It is claimed that the hold-in range of the loop is in excess of 1 MHz for VHF channels, thereby adequately performing the AFC function.

3.0 QUADRATURE DISTORTION INTRODUCED BY THE SYNCHRONIZATION SIGNALS

The periodic nature of the synchronization signals results in a discrete line spectrum about the picture carrier. It is no surprise that the spectrum of a television signal tends to concentrate at multiples of the horizontal (H) and vertical (V) scan rates. These clusters consist of the exact horizontal multiple (15.75 kHz) with multiples of V (60 Hz) around it. Since the synchronization signals provide a major contribution to the low frequency video

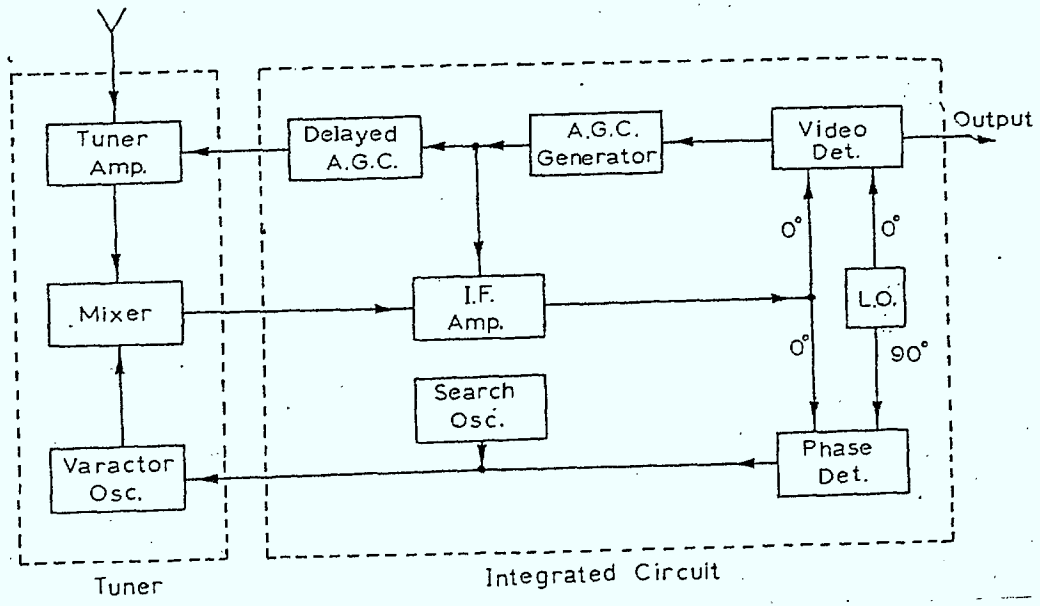

Low Frequency Output When Incoming And L.O. Frequencies Are Mismatched

Figure C.5 : System block diagram of the PLL carrier recovery system presented in [4].

spectrum, they can have a significant impact on carrier recovery. This portion of the spectrum is reasonably consistent from scene to scene. One can accurately consider the synchronization signal to be composed of a carrier and sideband pairs at multiples of the horizontal scan rate (H). There are a large number of these spectral components in the Nyquist slope (linear skirt) region of the receiver IF filter. The receiver IF unbalances the sidebands, thereby introducing phase modulation. In this section, effort is concentrated on establishing the influence of the phase modulation introduced on the discrete synchronizing signals for various average video levels. The video signal occupies a 53.5 μsec time slot in the TV line, and the average video level, denoted by av% = μ, is a random quantity which varies with picture content.

An analysis of the unbalancing effect due to one sideband pair is presented in [2]. This analysis is extended in this section.

3.1 Determining the Baseband Spectral Components of the Synchronization Signals

The synchronizing signal and average video level of the television line is depicted in Figure C.6. The high frequency colour burst has been omitted because it will have little influence in the crucial Nyquist slope region of the receiver IF. Negative modulation, with a modulation index of 87.5%, with the peak baseband signal normalized to 1 V is assumed. The synchronizion signal, g(t), can be expressed as:

$$g(t) = p_1(t) + p_2(t) + p_3(t) \qquad \text{(C.1)}$$

where

$$p_1(t) = \begin{cases} \mu & t \in [0, T_o] \\ 0 & \text{elsewhere} \end{cases}$$

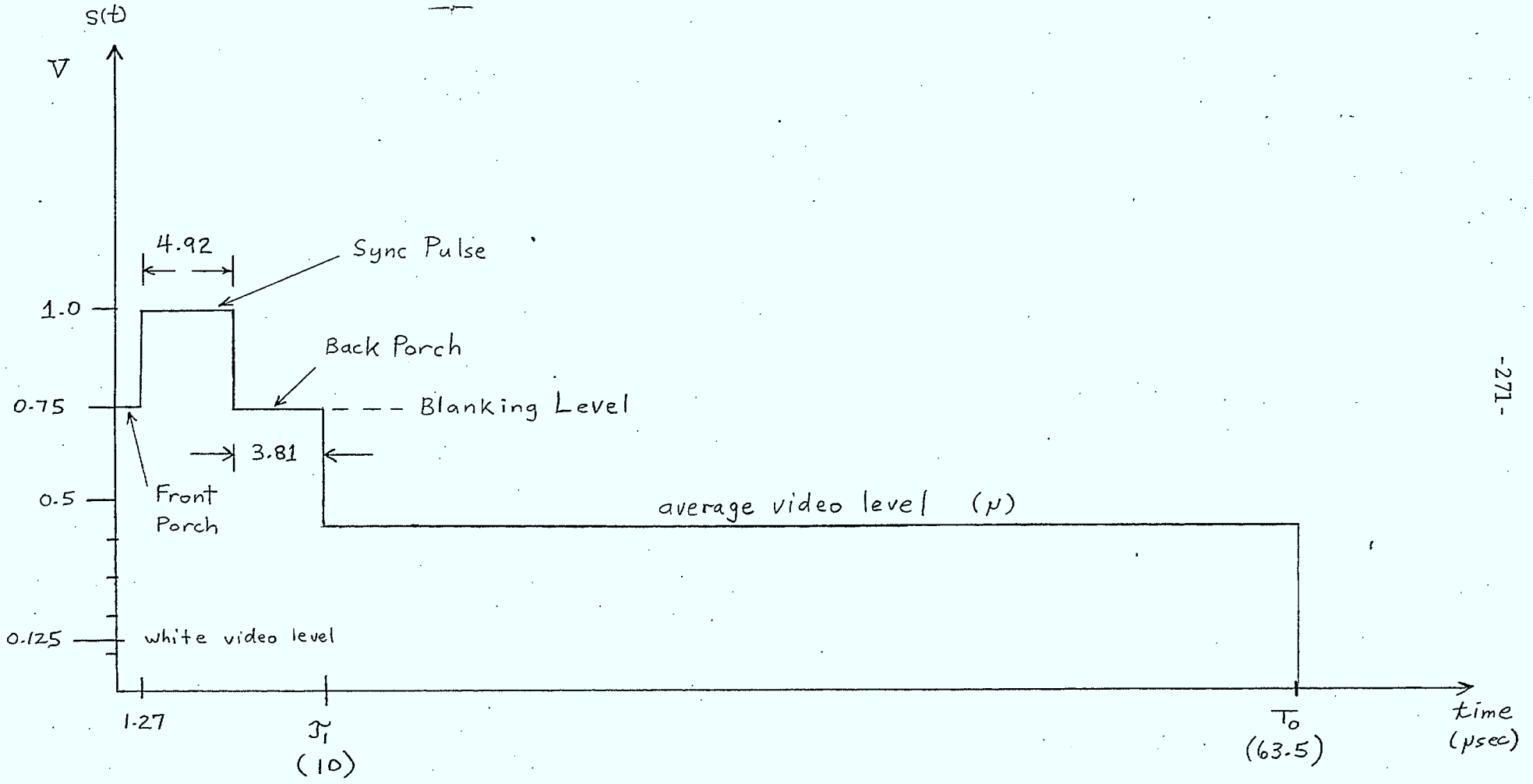

Figure C.6 : Synchronization signal approximation for analysis

$$p_2(t) = \begin{cases} A_1 & t \in [0,\ \tau_1] \\ 0 & \text{elsewhere} \end{cases}$$

$$p_3(t) = \begin{cases} A_2 & t \in [1.27_{\mu sec},\ 6.19_{\mu sec}] \\ 0 & \end{cases}$$

$A_1 = 0.75 - \mu$

$A_2 = 0.25$ V

$T_o = 63.5$ μsec

$\tau_1 = 10$ μsec .

The periodic time function $g_p(t) = \sum_n g(t-nT_o)$,

can be expressed in a Fourier series:

$$g_p(t) = \sum_n c_n \exp\{j\frac{2\pi nt}{T_o}\} \qquad (C.2)$$

where $c_n = \frac{1}{T_o} \int_o^{T_o} g(t) \exp\{-j\frac{2\pi nt}{T_o}\}\, dt$

$$= \frac{1}{T_o} \mathcal{F}\{g(t)\}\Big|_{f=n/T_o} .$$

Therefore, $c_n = \frac{1}{T_o} \mathcal{F}\{p_1(t)\}\Big|_{f=n/T_o} + \frac{1}{T_o} \mathcal{F}\{p_2(t)\}\Big|_{f=n/T_o}$

$$+ \frac{1}{T_o} \mathcal{F}\{p_3(t)\}\Big|_{f=nT_o} .$$

The frequency responses of the pulses $p_1(t)$, $p_2(t)$ and $p_3(t)$ are given by:

$$\mathcal{F}\{p_1(t)\} = [\mu\ T_o\ \text{sinc}\ (f\ T_o)]e^{-j\pi fT_o} \qquad (C.3)$$

$$\mathcal{F}\{p_2(t)\} = \{A_1\ \tau_1\ \text{sinc}\ (f\ \tau_1)\}e^{-j2\pi fD_1}$$

$$\mathcal{F}\{p_3(t)\} = \{A_2\ \tau_2\ \text{sinc}\ (f\ \tau_2)\}e^{-j2\pi fD_2}$$

where $\text{sinc}\ x = \dfrac{\sin \pi x}{\pi x}$.

$A_1 = [0.75 - \mu]$ V, $A_2 = 0.25$ V, $\tau_1 = 10$ μsec, $\tau_2 = 4.92$ μsec, $D_1 = 5$ μsec, and $D_2 = 3.73$ μsec.

Therefore,

$$c_n = \mu\ \text{sinc}\ (n)\ e^{-j\pi n} + \frac{A_1\ \tau_1}{T_o}\ \text{sinc}\left(\frac{n\tau_1}{T_o}\right)\ \exp\left\{\frac{-j2\pi nD_1}{T_o}\right\} + \frac{A_2\ \tau_2}{T_o}\ \text{sinc}\left(\frac{n\tau_2}{T_o}\right)\ \exp\left\{\frac{-j2\pi nD_2}{T_o}\right\} \qquad (C.4)$$

The average carrier level (apℓ) is given by:

$$c_o = \mu + \frac{A_1\ \tau_1}{T_o} + \frac{A_2\ \tau_2}{T_o}\ , \qquad (C.5)$$

and for $n > 1$,

$$c_n = \frac{A_1\ \tau_1}{T_o}\ \text{sinc}\left(\frac{n\tau_1}{T_o}\right)\ \exp\left\{\frac{-j2\pi nD_1}{T_o}\right\} + \frac{A_2\ \tau_2}{T_o}\ \text{sinc}\left(\frac{n\tau_2}{T_o}\right)\ \exp\left\{\frac{-j2\pi nD_2}{T_o}\right\}\ . \qquad (C.6)$$

The Fourier coefficients, c_n, are complex quantities that are often expressed in terms of amplitude, a_n, and phase, ϕ_n. These values for n = 0, 1, 2, .. 39 are supplied in Table C.1.

3.2 Carrier Stripping Approach with an Ideal Bandpass Filter

This situation is depicted in Figure C.7. Note that the orientation of the receive filter is flipped by the tuner. For the following analysis, the Fourier coefficients will be normalized by $ap\ell$, $\tilde{c}_n = \frac{c_n}{ap\ell}$, which results in $\tilde{a}_n = \frac{a_n}{ap\ell}$. The number of Fourier coeffients pairs passed by the IF - BPF combination is $J = INT[\frac{\alpha}{1/T_o}]$ where $1/T_o = 15.748$ kHz.

The IF signal at the input to the receiver filter can be expressed as:

$$r_i(t) = \cos 2\pi f_c t + \sum_n \tilde{a}_n \cos\{2\pi(f_c + \frac{n}{T_o})\, t + \phi_n\} \,. \tag{C.7}$$

The output of the receiver - bandpass filter combination (using the notation presented in [2]) is given by:

$$r_o(t) = \frac{1}{2}\cos 2\pi f_c t + \sum_{n=1}^{J} (h_n + k_n)\tilde{a}_n \cos\{2\pi f_c t - \frac{2\pi n}{T_o} t - \phi_n\}$$

$$+ \sum_{n=1}^{J} h_n \tilde{a}_n \cos\{2\pi f_c t + \frac{2\pi n}{T_o} t + \phi_n\} \tag{C.8}$$

where $h_n = \frac{1}{2} - \frac{15.748\ n}{1500}$

AVℓ = μ = 0.4375

COEFF #	AMPLITUDE	PHASE (radians)
0	.50608	0.0000
1	.66301E-01	-.45848
2	.59775E-01	-.91196
3	.49911E-01	-1.3533
4	.38076E-01	-1.7693
5	.25930E-01	-2.1284
6	.15389E-01	-2.3419
7	.90894E-02	-2.1929
8	.88226E-02	-1.9034
9	.10021E-01	-2.0184
10	.94556E-02	-2.3529
11	.69090E-02	-2.7789
12	.30839E-02	2.9989
13	.11487E-02	-.26974
14	.47729E-02	-.95594
15	.72500E-02	-1.4843
16	.82488E-02	-2.0150
17	.78134E-02	-2.5660
18	.62952E-02	3.1239
19	.42676E-02	2.4331
20	.24896E-02	1.4825
21	.18772E-02	.14591
22	.20930E-02	-.92514
23	.19681E-02	-1.6741
24	.12542E-02	-2.3070
25	.15645E-03	-2.9437
26	.98106E-03	-.31464
27	.18198E-02	-.90660
28	.21357E-02	-1.5376
29	.19100E-02	-2.2870
30	.15000E-02	2.9203
31	.17854E-02	1.5874
32	.27420E-02	.64799
33	.36235E-02	-.32504E-01
34	.40274E-02	-.61284
35	.37953E-02	-1.1432
36	.29547E-02	-1.6340
37	.16895E-02	-2.0548
38	.37944E-03	-1.8059
39	.10811E-02	-.31845

Table C.1 : Fourier coefficients of sychronization signals

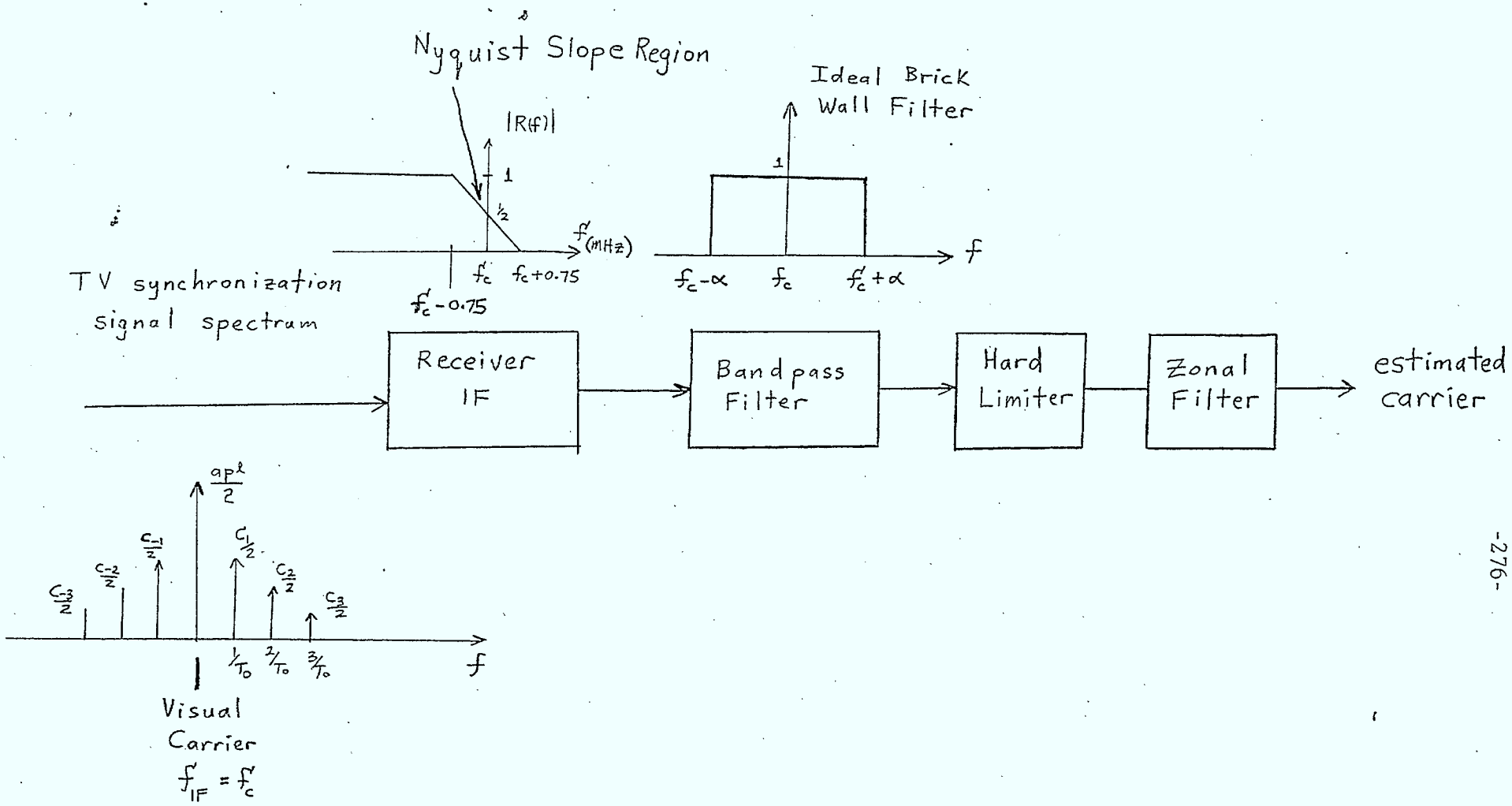

Figure C.7 : Carrier stripping model for analyzing effect of television synchronization signals.

$$k_n = \frac{2(15.748)n}{1500} .$$

This can be simplified to give:

$$r_o(t) = \cos 2\pi f_c t \left[\frac{1}{2} + \sum_{n=1}^{J} (2h_n+k_n)\, \tilde{a}_n \cos\left[\frac{2\pi n}{T_o} t + \phi_n\right]\right]$$

$$+ \sin 2\pi f_c t \left[\sum_{n=1}^{J} k_n \tilde{a}_n \sin\left(\frac{2\pi n}{T_o} t + \phi_n\right)\right]$$

Since $2h_n + k_n = 1$ for all n,

$$r_o(t) = \left(\frac{1}{2} + \sum_{n=1}^{J} \tilde{a}_n \cos\left[\frac{2\pi n}{T_o} t + \phi_n\right]\right) \cos 2\pi f_c t$$

$$+ \left(\sum_{n=1}^{J} k_n \tilde{a}_n \sin\left[\frac{2\pi n}{T_o} t + \phi_n\right]\right) \sin 2\pi f_c t. \qquad (C.9)$$

The phase error at the output of the bandpass limiter is given by:

$$\phi(t) = -\tan^{-1}\left[\frac{\sum_{n=1}^{J} k_n \tilde{a}_n \left\{\sin\left[\frac{2\pi n}{T_o} t + \phi_n\right]\right\}}{\frac{1}{2} + \sum_{n=1}^{J} \tilde{a}_n \cos\left[\frac{2\pi n}{T_o} t + \phi_n\right]}\right] \qquad (C.10)$$

It is interesting to note that the denominator of the argument of the arctangent function is simply a lowpass filtered version of the synchronization signal (scaled by a factor of $\frac{1}{2}$). Since this signal is always positive, the phase function will always between $\pm \frac{\pi}{2}$. This clearly

simplifies the extraction of the phase signal as no phase unwrapping is required. If one isolates attention to a single sideband pair, one obtains an expression similar to that derived by Rzeszewski [2, equation 6]. Similarly, for sidebands close to the picture carrier, the argument of the arctangent function is small, and the phase unbalance is given by:

$$\phi_n(t) \approx \frac{k_n \tilde{a}_n \sin[\frac{2\pi n}{T_o} t + \phi_n]}{\frac{1}{2} + \tilde{a}_n \cos[\frac{2\pi n}{T_o} t + \phi_n]} \approx k_n \tilde{a}_n \sin[\frac{2\pi n t}{T_o} + \phi_n] \qquad (C.11)$$

The major observation here is that for a narrowband reference channel, the amount of phase distortion caused by the synchronization signals will be relatively minor. If we consider an average video level half way between the blanking level (0.75 V) and the white level (0.125 V), $\mu = 0.4375$ V and the average picture level is 0.5064 V. The Fourier coefficients for this case are illustrated in Table C.1. The normalized coefficient $\tilde{a}_1 = \frac{a_1}{ap\ell} \approx \frac{1}{7.63}$, which is somewhat higher than the ratio of the first sidelobe to carrier ratio of $(\frac{1}{10})$ quoted in [2]. At any rate, the peak phase distortion introduced by the first sidelobe pairs is:

$$\phi_e(1) \leq \frac{1}{363.5} \text{ rad} \approx 0.158°.$$

Similarly, the peak phase distortion introduced by the second sidelobe pair is:

$$\phi_e(2) \leq \frac{1}{201.6} \text{ rad} \approx 0.284°.$$

It is apparent that the first and second sideband pairs introduce insignificant distortion. Consequently, that a phase locked loop bandwidth can be on the order of 2 times the horizontal scan rate (31.5 kHz) with no appreciable distortion introduced by the synchronization signals. This analysis cannot be extended to quasi-synchronous detection. For this reason, a computer simulation of the model of Figure C.7 has been implemented. The phase error, given by equation (C.10), is computed for various average video levels and bandpass filter bandwidths.

The results are summarized in Figures C.8(a), (b), (c), (d), (e). In Figure C.8(a), the results for an α=750 kHz (bandpass filter bandwidth of 1.5 MHz) are presented. As anticipated, the peak phase errors are a strong function of the average video level and thus the average carrier level. The reason for this is probably most apparent in Figure C.6. The higher the average video level, the smaller the video step from blanking level to the average video level. The phase error is a function of the size of a video step, as evidenced from the phase error expression derived in [1]. For an avℓ = 0.3375V, the peak phase error is 15°. During the clock run-in sequence the peak phase error is in the neighbourhood of 2.5°, and is in the neighbourhood of 1° - 1.5° over the majority of the teletext burst.

The results for an α=500 kHz, presented in Figure C.8(b), demonstrate an considerable reduction (5°) in peak phase error (relative to α=750 kHz). Over the majority of the teletext burst, the peak phase error is only 0.5°. The bandwidth reduction to an α = 500 kHz has introduced a noticeable increase in the transient duration, although at this bandwidth transients are not troublesome. The results for an α=250 kHz, presented in Figure C.8(c), demonstrate the trend of reduced peak phase error and increased phase transient duration as the pre-filter bandwidth is reduced.

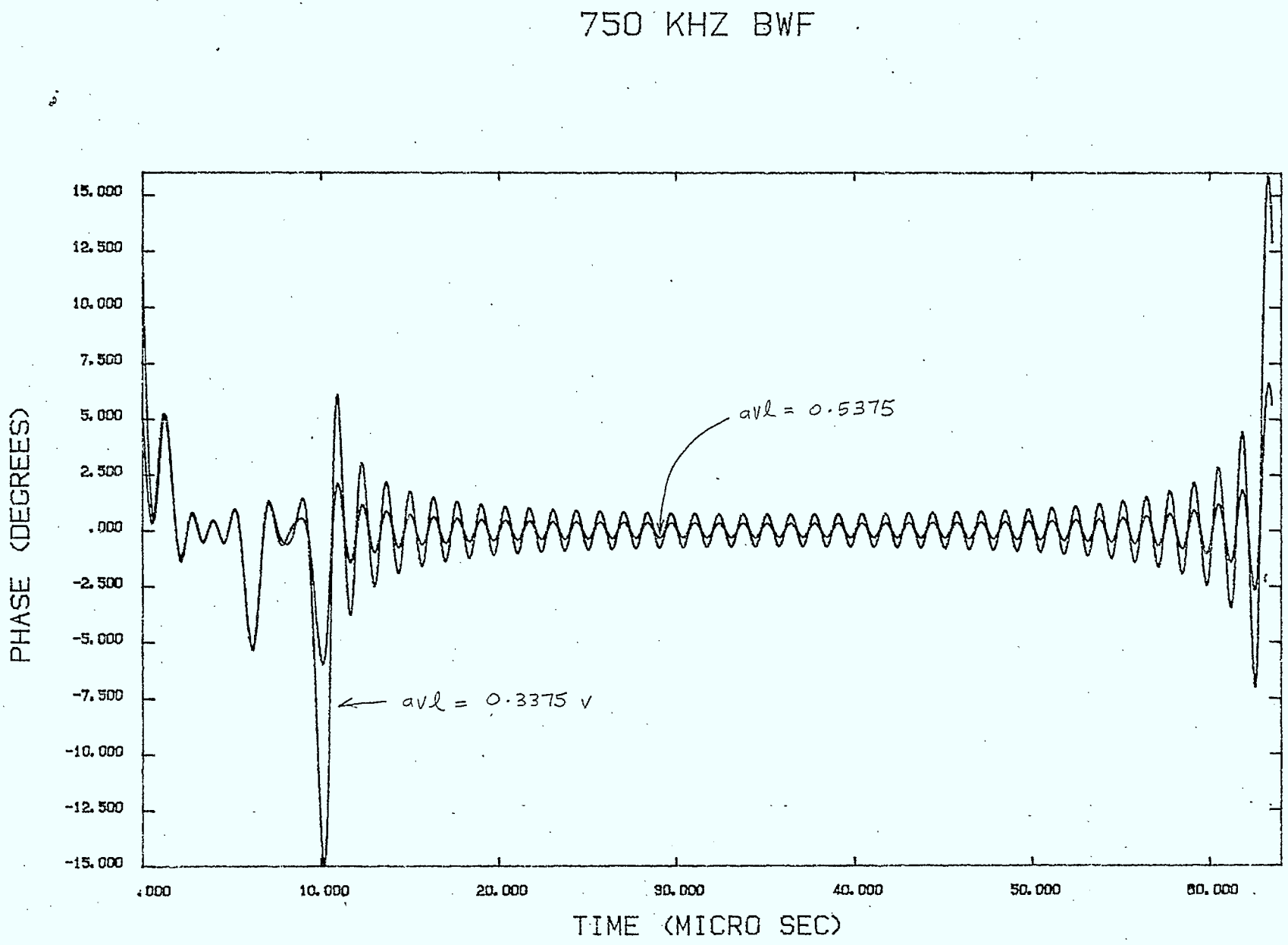

Figure C.8(a): Carrier stripping phase error due to synchronization signals for [redacted] filter [redacted] to [redacted].

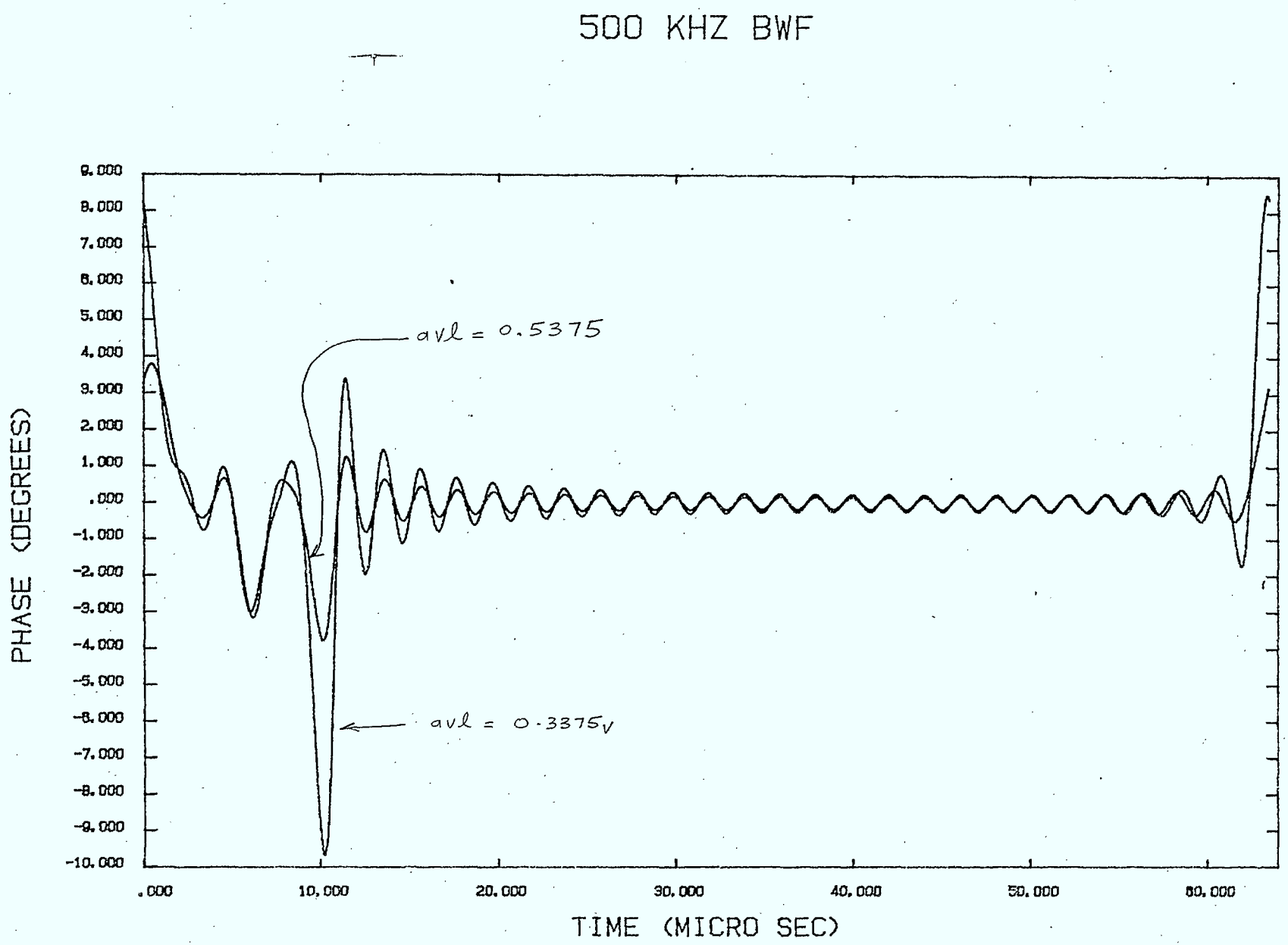

Figure C.8 (b): Carrier stripping phase error due to synchronization signals for a pre-filter α = 500 KHz

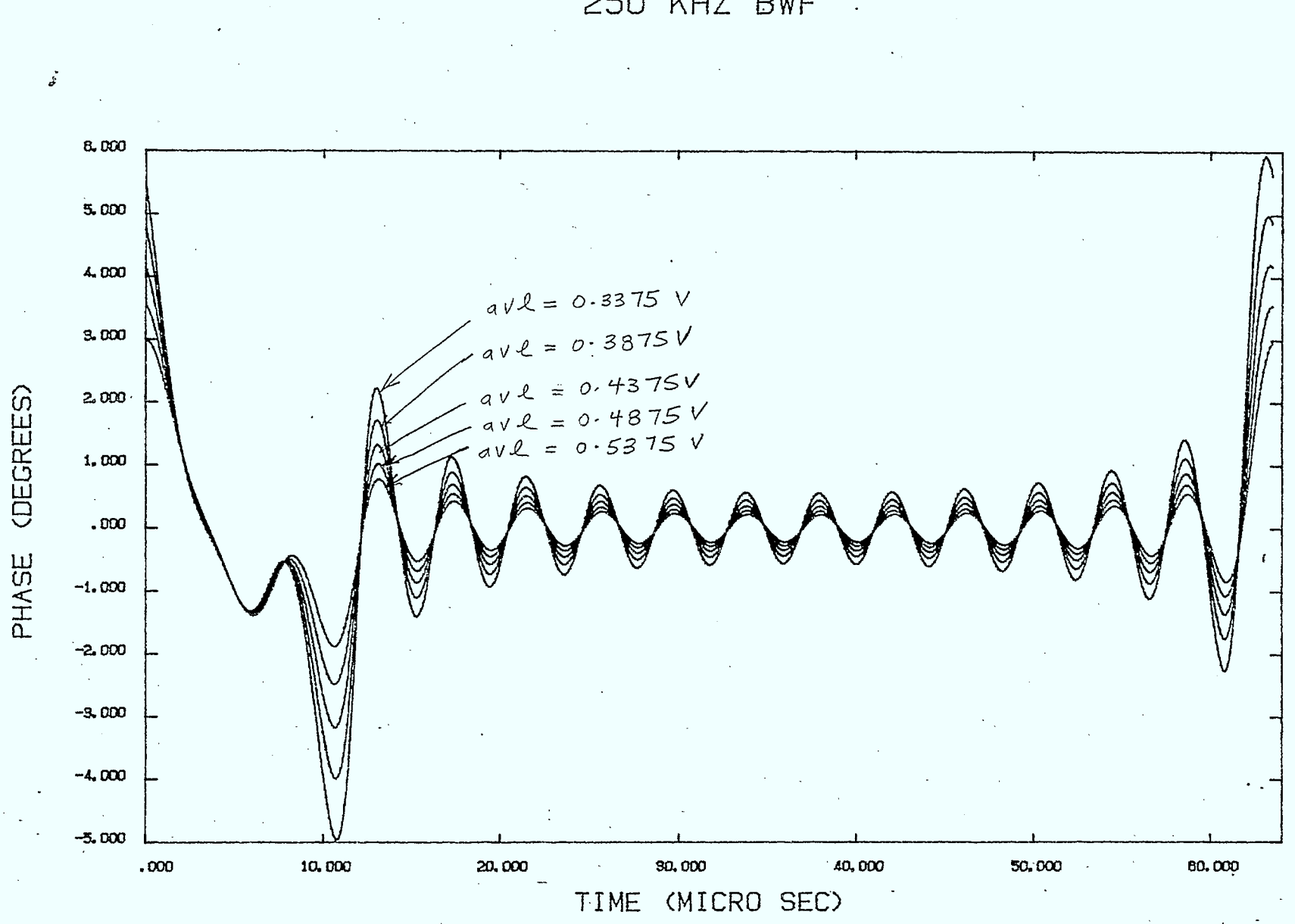

Figure C-8 (c): Carrier stripping phase error due to synchronization signals for a pre-filter α = 250 KHz.

The peak phase error relevant over the teletext portion of the line is in the neighbourhood of 0.5°. The phase variations are noticeably slower than they were for the wider bandwidth pre-filters. The basic trend continues for an α=100 kHz. As indicated in Figure C.8(d), the peak phase error over the teletext portion of the burst is reduced to approximately 0.25°.

The results for a narrowband pre-filter (α=50 kHz) are illustrated in Figure C.8(e). In this case, the phase error is a much more sensitive function of the average video level primarily because of the increased transient duration. Although the peak error is reduced (relative to α=100 kHz), the increased transients result in worse phase errors over the teletext portion of the line. This concurs with the bandwidth trade off mentioned by Bluestein [1] that was presented earlier in Section 2 of this appendix. Optimization of the bandwidth to reduce the carrier recovery phase error is typically not performed, as the problem of mistuning tends to force the selection of a wideband loop (i.e. $\alpha \simeq$ 750 kHz).

This analysis with a periodic approximation to the synchronization signals has been useful for validating the quasi-synchronous carrier recovery procedure used in the Telidon simulation. In the simulation program the phase is extracted on a burst by burst basis. By zeroing the data in the teletext portion of the line, and selecting a prefilter bandwidth of 750 kHz, the phase error at the output of a bandpass limiter due to the synchronization signals can be extracted. The only differences between the isolated synchronization pulse and the periodic approximation are:

(1) The periodic approximation does not include the colour burst, which should have little influence on the carrier recovery loop.

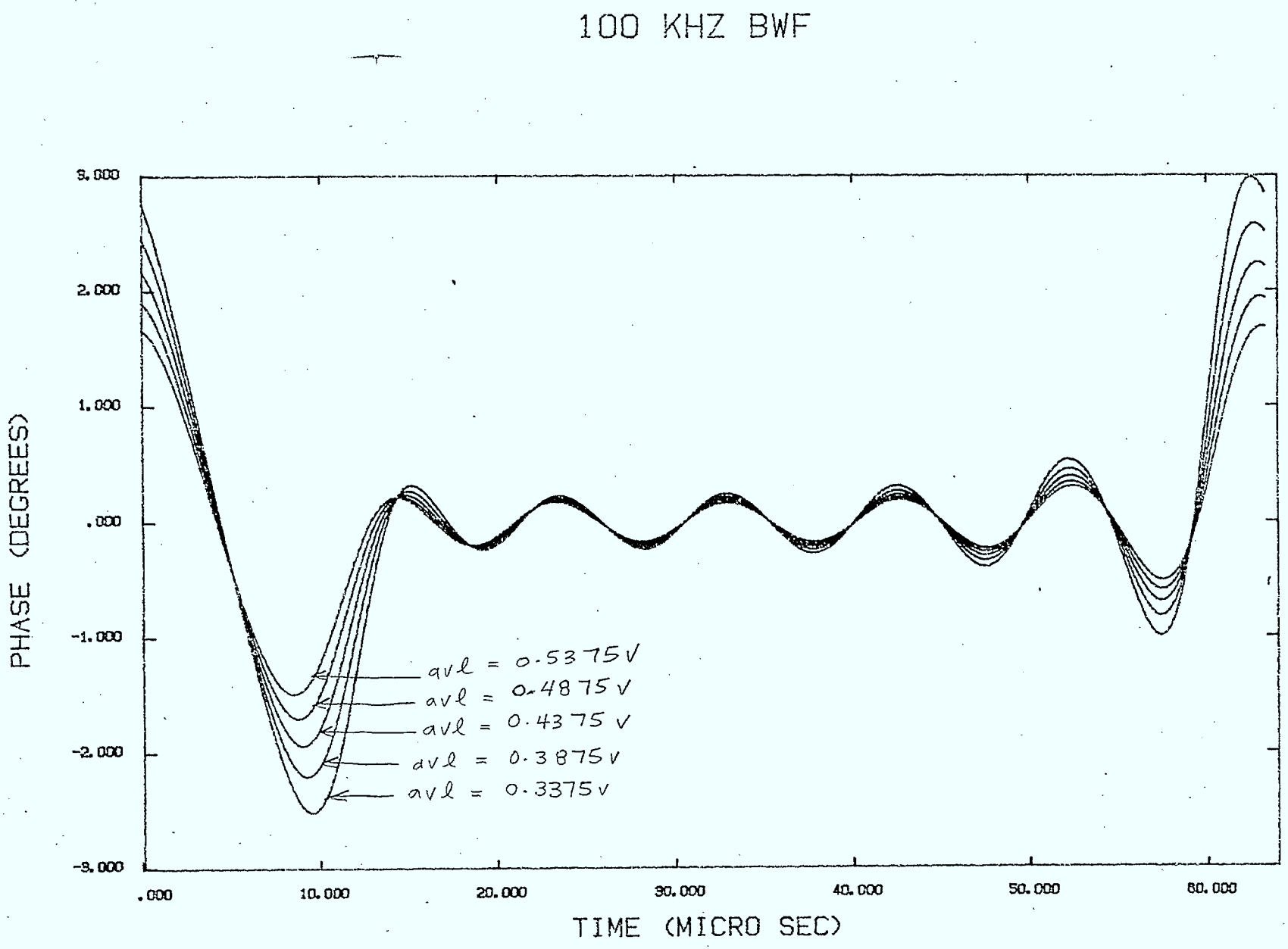

Figure C.8(d): Carrier stripping phase error due to synchronization signals for a Pre-filter α = 100 KHz.

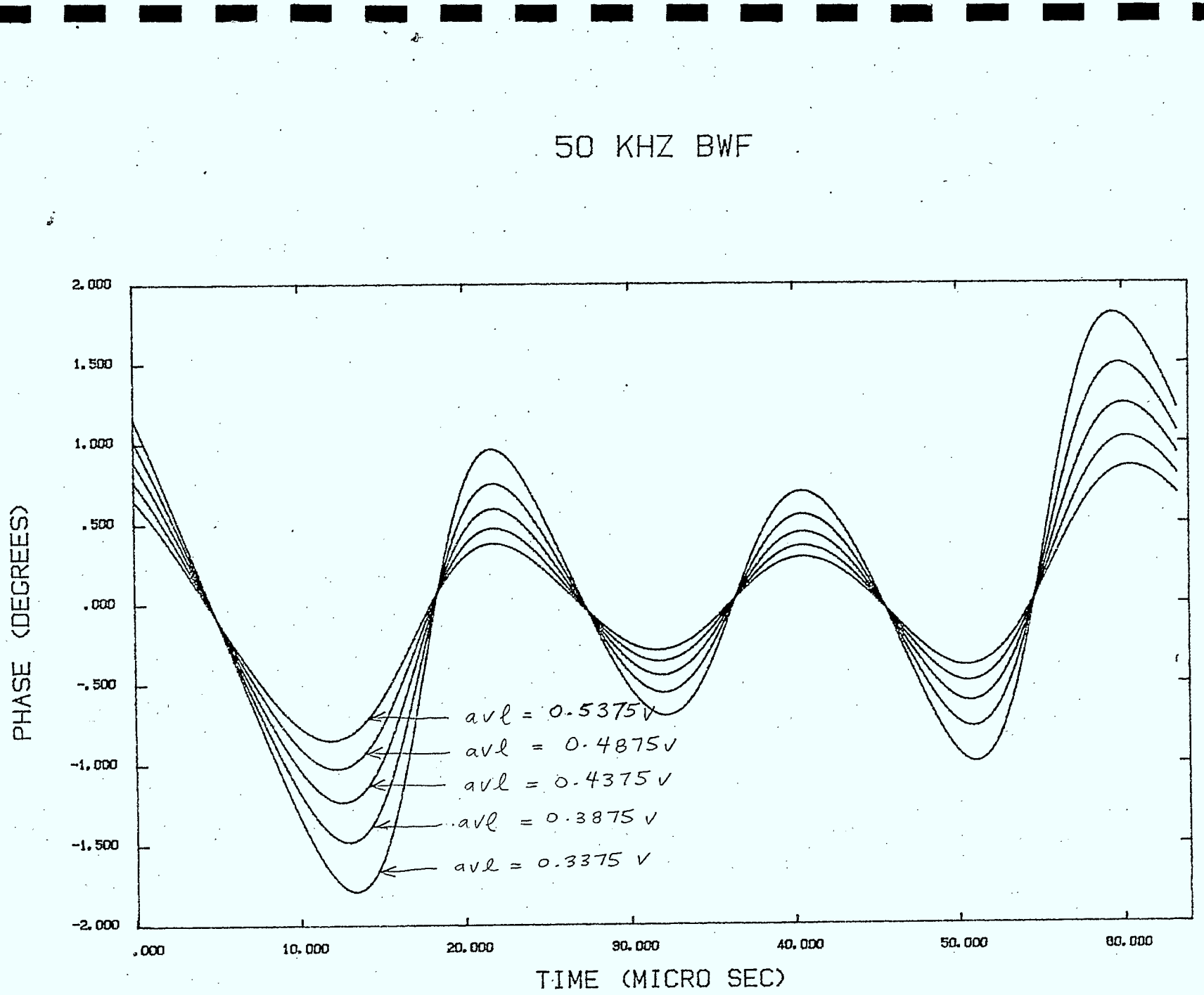

Figure C.8(e): Carrier stripping phase error due to synchronization signals for a pre-filter $\alpha = 50$ KHz.

(2) There are minor differences at the beginning and end of the line due to the periodic extension of the analytical model.

Despite these minor differences (which will give rise to different transient behaviour at the beginning and end of the burst), over the majority of the line the analytical and simulation models should exhibit similar behaviour. In Figure C.8(f), the analytical results for α=750 kHz and μ = 0.525 V are presented. The corresponding run with the simulation program is presented in Figure C.8(g). With the exception of differences in the transient behaviour at the beginning and end of the burst, the analytical and simulation results are in excellent agreement.

Because of the lack of tracking capability, the carrier stripping approach is clearly suboptimal to a PLL recovery system. Consequently, the steady state phase error introduced by the synchronization signals for a phase locked loop recovery system have been investigated. The next section is devoted to defining a realistic phase locked loop model.

3.3 Phase Locked Loop Model

A generalized model of a phase locked loop is provided in Figure C.9. The essential components are a phase detector (mixer, zonal filter to remove the second harmonic, and amplification), a loop filter, and a voltage controlled oscillator (VCO). The output frequency of the VCO is proportional to the VCO input control voltage. Stated another way, the output phase function of the VCO is proportional to the integral of the input control voltage.

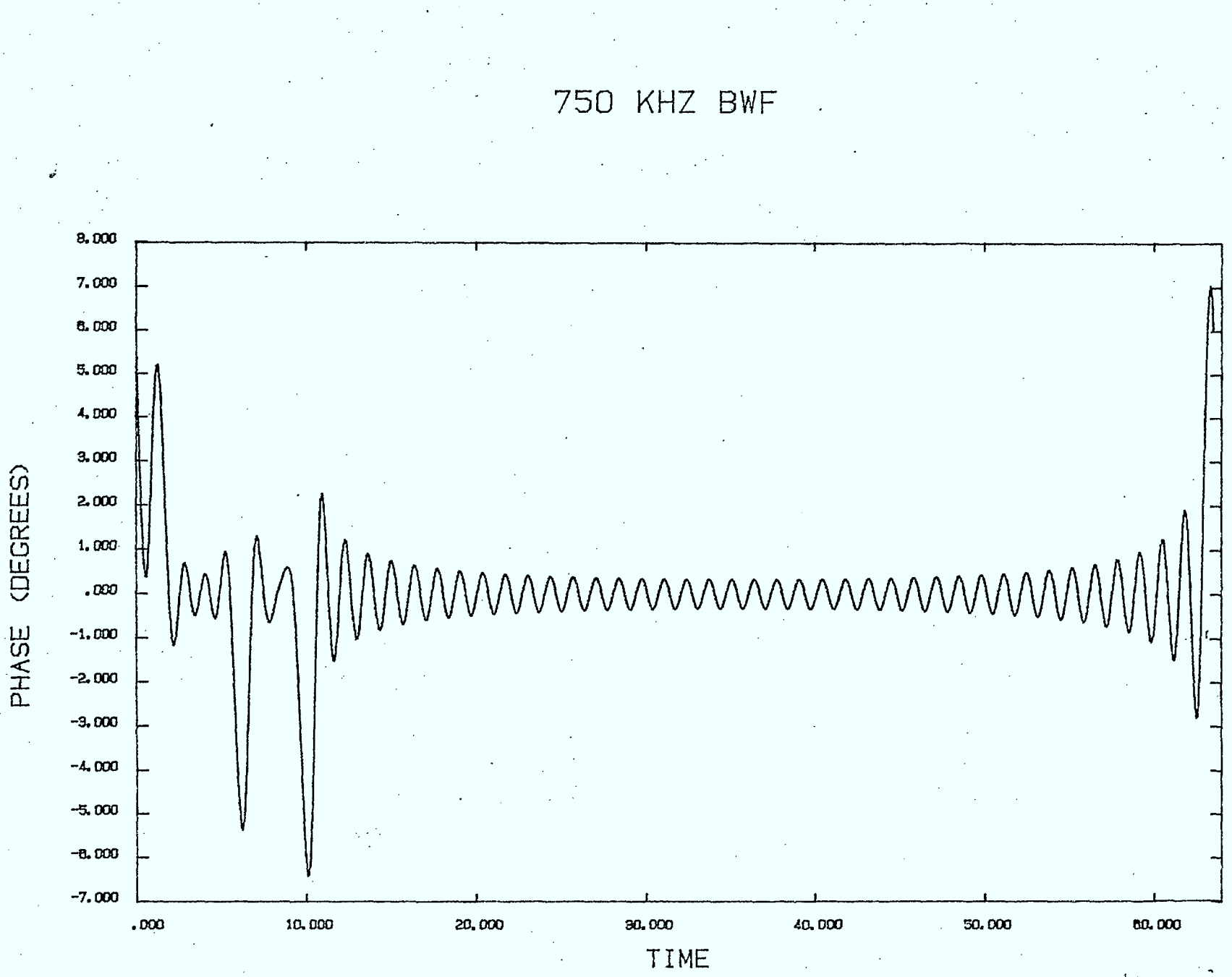

Figure C.8(f): Carrier stripping phase error due to synchronization signals for a prefilter α = 750 KHz and avl = 0.525V

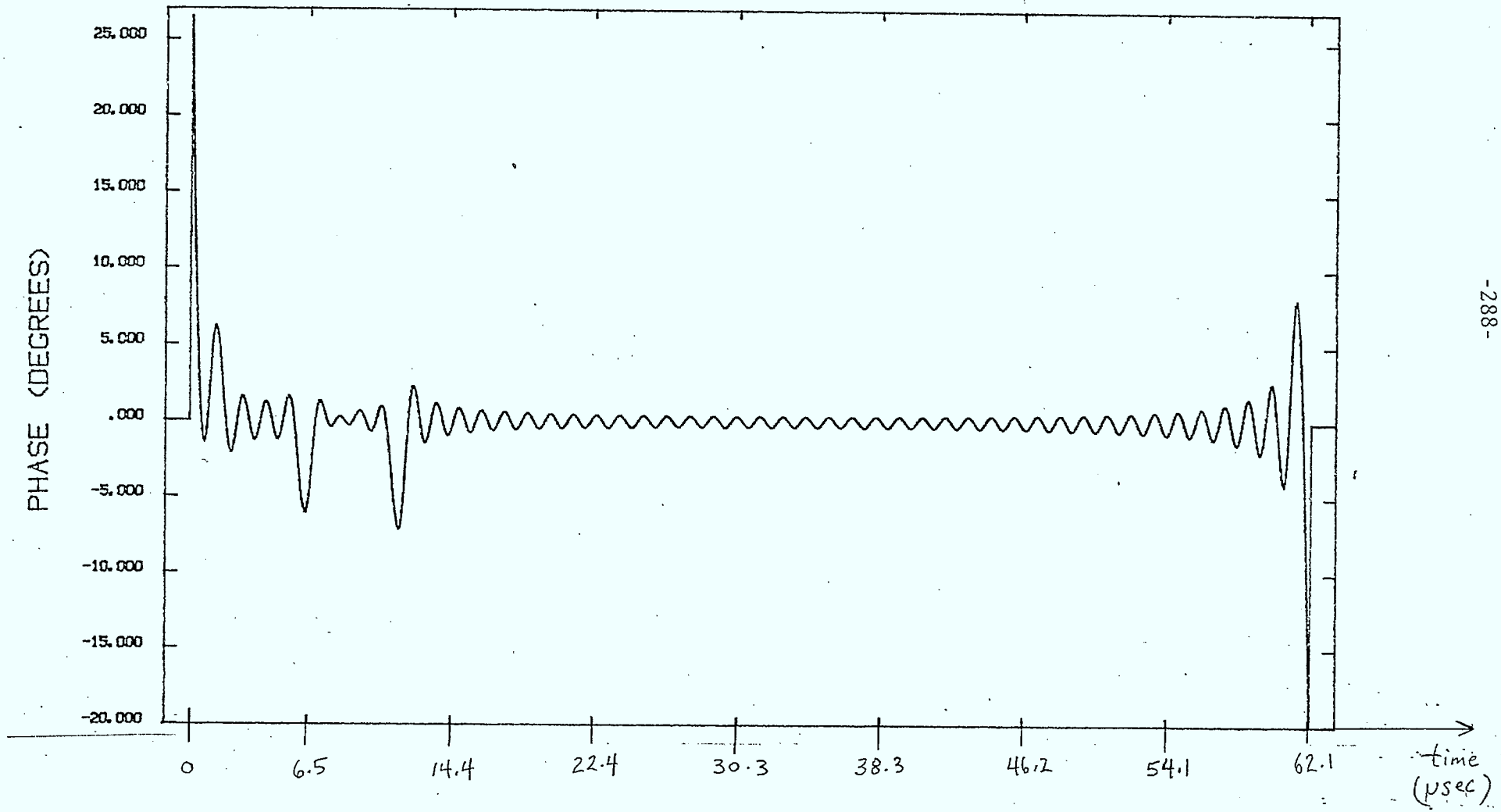

Figure C.8 (g): Carrier stripping phase error for zeroed data impulse amplitude in the simulation program.

The linearized model of a phase locked loop is provided in Figure C.10. It is an example of a negative feedback control system. The closed loop transfer function is given by:

$$H(s) = \frac{K\ F(s)}{s + K\ F(s)} \qquad (C.12)$$

where $K = K_D\ K_v$ (dc loop gain).

With a second order loop, the steady state error resulting from a step change in input signal frequency can be made arbitrarily small with an active loop filter, F(s). Since the signal frequency is invariably unequal to the frequency of the free-running VCO, a non-zero control voltage is needed to tune the VCO and hold the loop in lock. The integrator in the loop filter permits a small phase error while still generating the necessary control voltage. In addition, the large integrator gain can be achieved with relatively small noise bandwidth.

A common loop filter for a second order phase locked loop is the active filter illustrated in Figure C.11. For high gain operational amplifiers,

$$F(s) = \frac{1 + s\tau_2}{s\ \tau_1} \qquad (C.13)$$

where $\tau_1 = R_1C$, $\tau_2 = R_2C$

With this loop filter, the closed loop response is:

$$H(s) = \frac{K\ \tau_2\ s + K}{\tau_1\left(s^2 + \frac{K\ \tau_2}{\tau_1}\ s + \frac{K}{\tau_1}\right)}$$

$$= \frac{2\zeta\ w_n s + w_n^2}{s^2 + 2\zeta\ w_n s + w_n^2} \qquad (C.14)$$

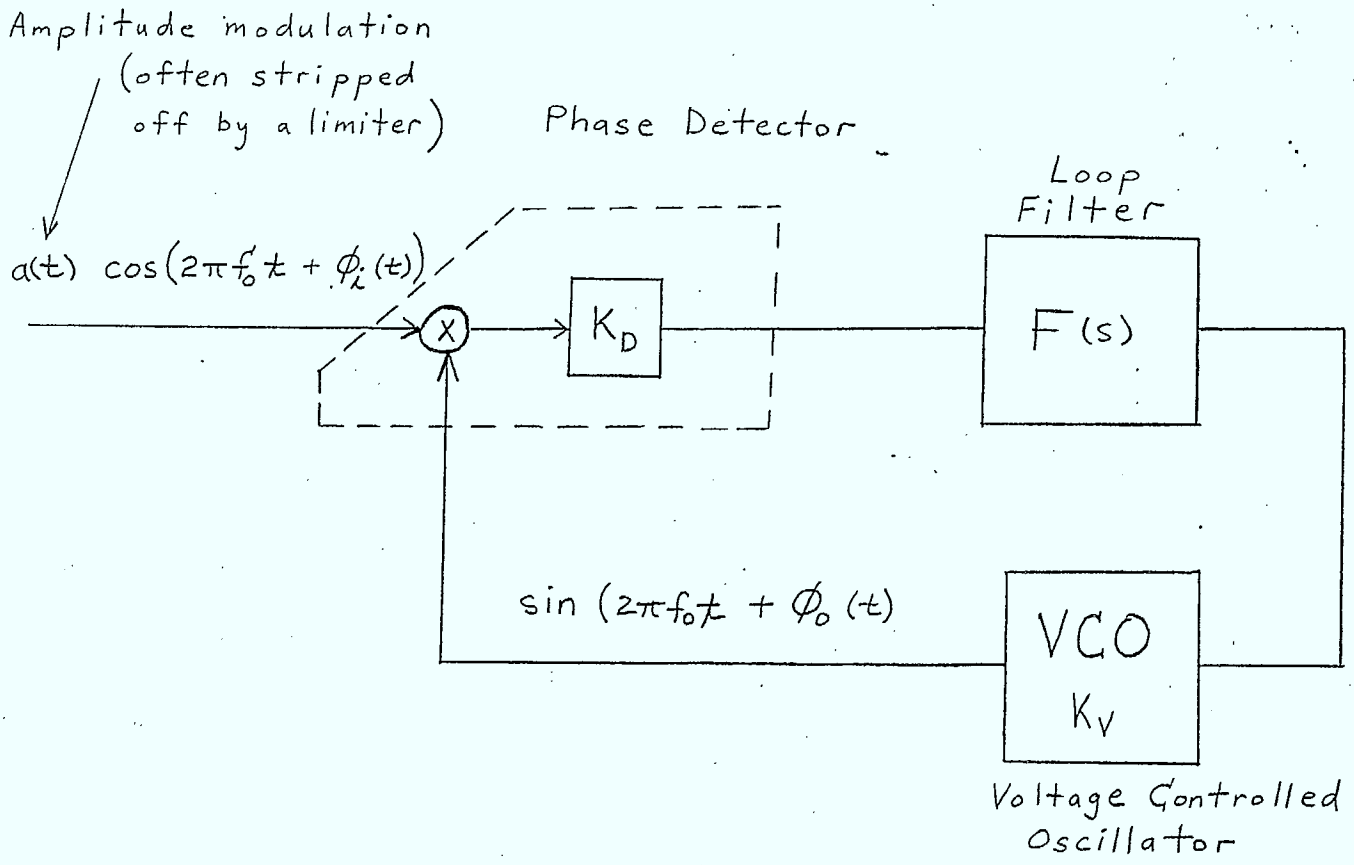

Figure C.9 : Phase Locked Loop Model

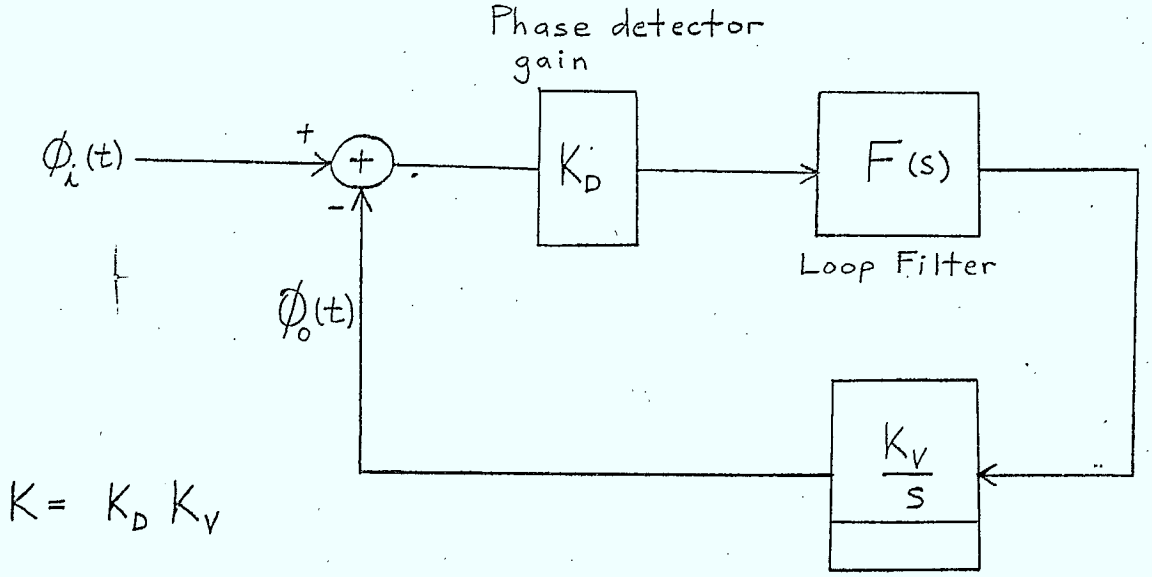

$K = K_D K_V$

Transfer Function $\frac{\phi_o(s)}{\phi_i(s)} = H(s) = \frac{K\ F(s)}{s + K\ F(s)}$

Figure C.10 : Linearized phase locked loop model

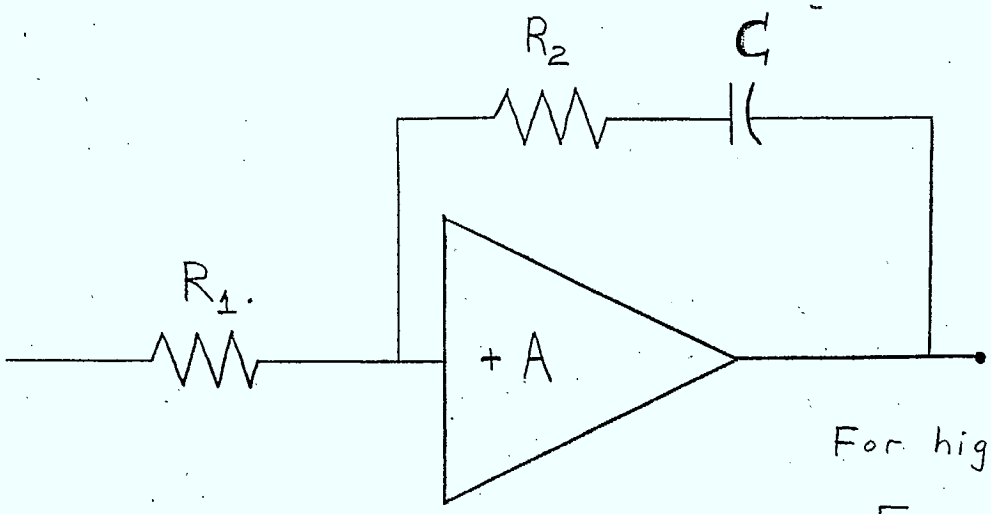

For high gain $A \gg 1$

$$F(s) = \frac{1 + s\tau_2}{s\tau_1}$$

$$\tau_1 = R_1 C \qquad \tau_2 = R_2 C$$

Figure C.11 : Common active lag – lead loop filter

where $w_n = \sqrt{\frac{K}{\tau_1}}$, $\zeta = \frac{\tau_2 w_n}{2}$.

The one sided noise equivalent bandwidth of the above mentioned second order loop is evaluated in [9], [10]. The result is:

$$B_L = \frac{w_n}{2}\left(\zeta + \frac{1}{4\zeta}\right) . \qquad (C.15)$$

As noted in [9], [10], the loop bandwidth dimension is Hz even though w_n is expressed in radians per second.

The statement in [10] that the noise equivalent bandwidth of this loop is independent of loop gain is clearly not correct. It is true that one can make B_L a less sensitive function of loop gain by appropriate choice of the time constants τ_1 and τ_2 (i.e. $B_L = \frac{1}{2\tau_2} + \frac{1}{2}\frac{\tau_2}{\tau_1} K$). Considering the loop with minimum noise equivalent bandwidth ($\zeta = \frac{1}{2}$),

$$B_L = \frac{w_n}{2} , \quad \tau_2 = \frac{1}{w_n} .$$

If we select $\tau_1 = \tau_2$, the loop gain, K, is given by $K = (2B_L)$ rad/sec and $\tau_1 = \frac{1}{K}$. Note that the constant K has dimensions rad/sec despite the fact that B_L is in Hz [9]. The closed loop transfer function is given by:

$$H(s) = \frac{K(s + K)}{s^2 + Ks + K^2} \qquad (C.16)$$

where $K = 2B_L$.

With negative feedback control systems, there is always the question of stability. The open loop transfer function is given by:

$$G(s) = \frac{K}{s}\left(\frac{1 + s\tau_2}{s\tau_1}\right)$$

$$= w_n^2 \frac{\left(1 + \frac{s}{w_n}\right)}{\left(\frac{2\zeta}{s^2}\right)} \qquad \text{(C.17)}$$

The Bode plot of this transfer function is provided in Figure C.12. For $\zeta > \frac{1}{2}$, w_n is greater than corner frequency of the numerator zero. For $\zeta = \frac{1}{2}$, there is a 45° phase margin and 40 dB gain margin. The phase and gain margins improve further with increasing damping factor. Clearly there are no stability problems with this loop.

A second order loop with a high gain active loop filter is attractive because it has a good steady state frequency hold in range. What this means is that it is difficult for such a loop to lose lock permanently. However if a large frequency step is applied, the loop unlocks, skips cycles for while, and then locks up again. There is a frequency step limit, $\Delta\omega_{po}$, below which the loop does not skip cycles and remains in lock. The emperical relation [9, p. 57]:

$$\Delta\omega_{po} = 1.8\, w_n\, (1 + \zeta) \qquad 0.5 \leq \zeta \leq 1.4. \qquad \text{(C.18)}$$

This is maximized by increasing the damping factor and natural frequency, w_n, which will degrade the noise bandwidth of the loop.

The transcient response of a loop is often of considerable importance. In [9, p. 49], the transcient phase error due a frequency step is presented. A dampling factor between $1/\sqrt{2}$ and unity results in a transcients which persist for

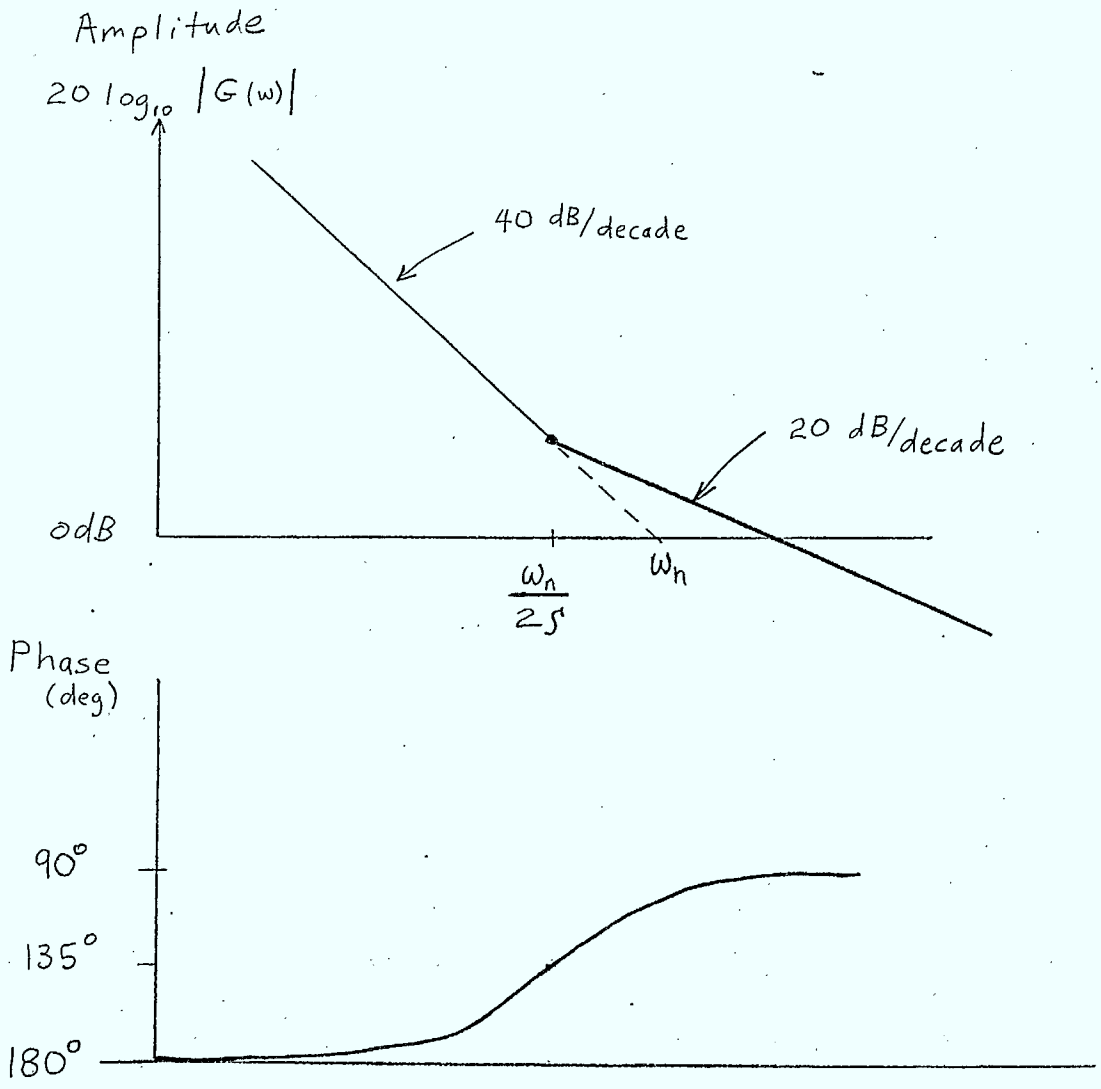

Figure C.12 : Bode plot of open loop response with active lag-lead filter

approximately $\frac{4}{w_n}$ seconds. It is apparent that to minimize the transcient duration, one must sacrifice noise bandwidth.

In the above discussion it was assumed that the loop was initially in lock. A few comments about acquisition will now be provided. Phase acquisition is considerably simpler than frequency acquisition. For phase acquisition, if the signal frequency is close enough to the VCO frequency, the PLL locks up with just a phase transcient and no cycle skipping occurs. This lock in range is typically approximated by:

$$\Delta\omega_L \approx \pm K_D K_V F(\infty). \qquad (C.19)$$

For the active second order loop, $\Delta\omega_L \approx 2\zeta w_n$. Self acquisition of frequency, or frequency pull-in, by a PLL tends to be slow and often unreliable, especially for narrowband loops. An example from [9] clearly demonstrates this. For a second order loop with $\zeta = \frac{1}{\sqrt{2}}$, the acquisition time is $T_{ACQ} \approx \frac{4.2\ (\Delta f)^2}{B_L^3}$ sec, where B_L is the one sided noise equivalent bandwidth. For Δf = 1 kHz and B_L = 60 Hz, the acquisition time is 1 hr, 10 minutes. Consequently, some form of aided frequency acquisition is often necessary. The system presented in Hamades, paper [4] discussed earlier employed the sweeping of the VCO frequency technique. When the VCO frequency and incoming frequency are in coincidence, the loop locks up, inhibiting further change of the VCO frequency.

3.4 Second Order Phase Locked Loop Results

The phase error at the output of a second order phase locked loop, with closed loop transfer function given by Equation (C.16), has been investigated for various one sided noise equivalent bandwidths. The superiority of a phase locked loop with noise equivalent bandwidth of 400 kHz over a carrier stripping phase extraction process (with a bandpass pre-filter with α=750 kHz) is clearly illustrated in Figure C.13(a). In Figure C.13(b), the phase error for B_L = 400 kHz, 100 kHz, and 25 kHz are presented on the same graph. As expected, the peak phase error is reduced as the loop bandwidth is reduced at the expense of increasing the transient duration. The phase error introduced by the synchronization signals is relatively minor over the majority of the teletext burst. Consequently, the teletext data signal will be the major source of error in the recovered carrier. The much more frequent transitions (from high to low and low to high signal level) of the data signal must be kept in mind when trading off peak phase error and transient duration. However, as was the case for the carrier stripping approach, bandwidth optimization must also account for non-standard signal impairments such as transmitter and tuner generated incidental phase modulation. In practice, it is these signal impairments which have the major influence on the choice of the phase locked loop bandwidth.

4.0 INCORPORATING THE EFFECTS OF LOW FREQUENCY VIDEO CONTENT

In addition to the synchronization signals, the video content can have a significant impact on the input phase function of the carrier recovery system. The average video level (which is a strong function of picture content) influences the level of the carrier component. Furthermore,

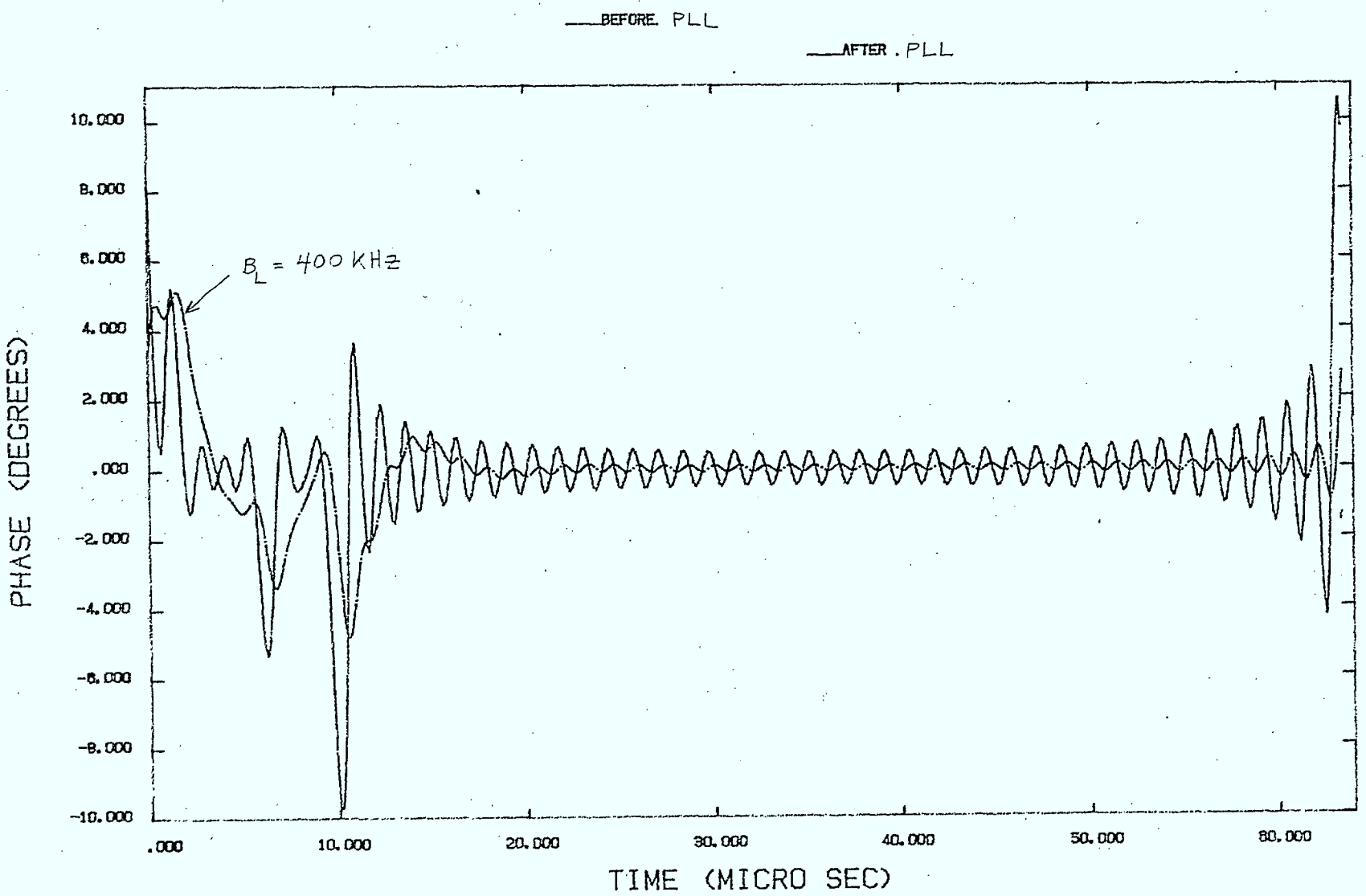

Figure C.13(a): Carrier stripping versus second order PLL phase recovery error.

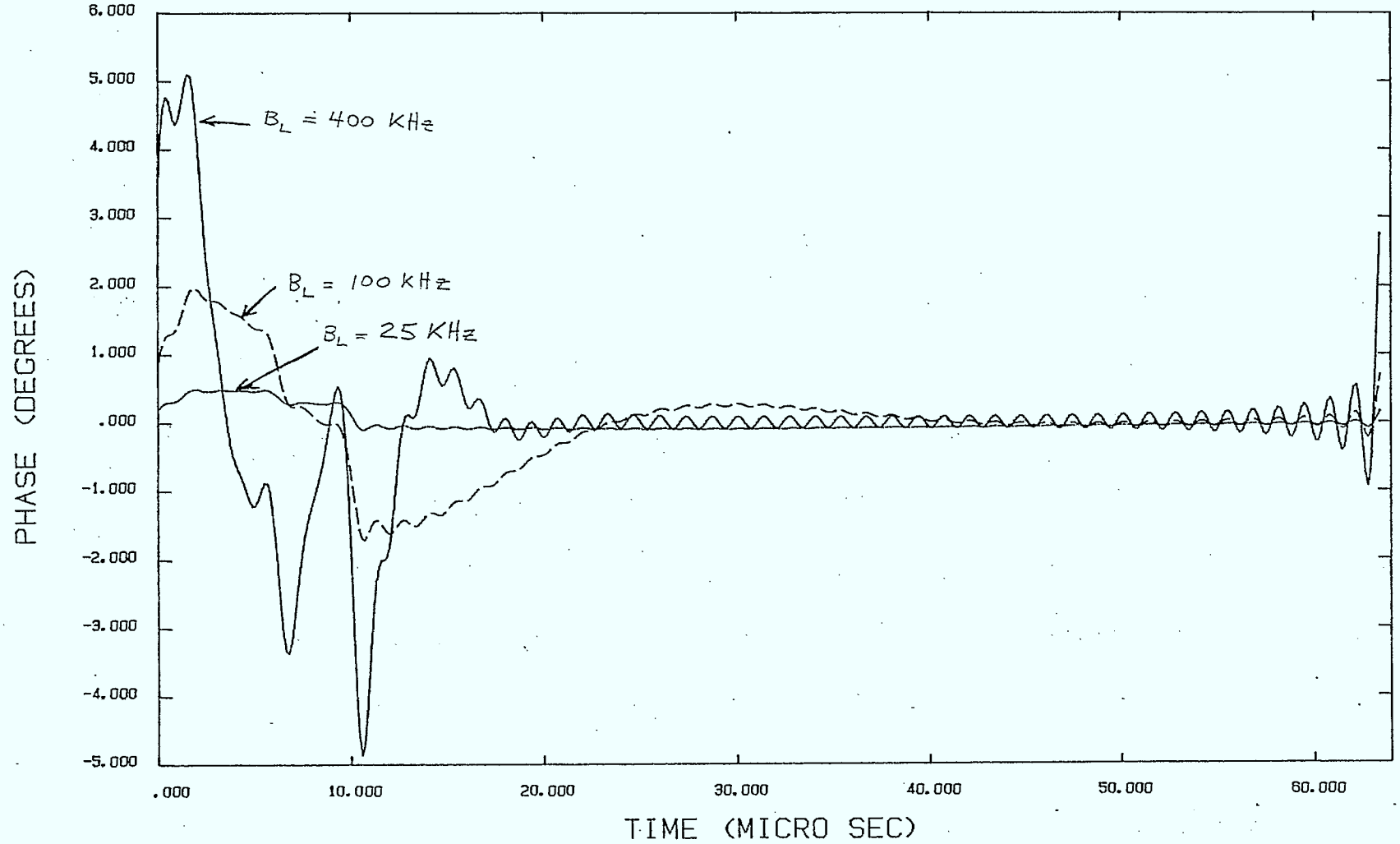

Figure C.13 (b): Phase error introduced by the synchronization signals for a second order PLL with various noise equivalent

low frequency spectral content of the video signal is unbalanced by the linear skirt of the receiver IF, thereby introducing phase modulation. The corrupting influence of the low frequency video content is really deterministic in nature. For a given field of video information, the resulting output phase function of the carrier recovery loop could be evaluated. The major drawback is that a significant amount of computation is required to characterize the output phase error function. To realistically simulate actual operation, a significant number of fields or pictures would have to be processed. The use of a random video process model does permit the evaluation of the standard deviation of the steady state phase error of a phase locked loop recovery system. The only difficulty is the choice of realistic model for the video process. Two models will be discussed in the next section.

4.1 Video Random Process Models

Gaussian random process are excellent candidates for mathematical analysis. With this in mind, the candidate model for the video process is a gaussian random process with a dc component (the average video level), denoted by μ. The autocovariance function will be assumed to be gaussian, giving rise to a gaussian power spectrum with a discrete spectral component. The a.c. power of the video signal is denoted by σ_v^2. When the modulation index is 87.5%, the voltage difference between the blanking level and white signal level is 0.625 V. Appropriate a.c. video power levels can be obtained by selecting:

(i) $3\,\sigma_v = \frac{0.625}{2} \rightarrow \sigma_v^2 = 0.01085$

(ii) $2.5\,\sigma_v = \frac{0.625}{2} \quad \rightarrow \sigma_v^2 = 0.015625$

(iii) $2\sigma_v = \frac{0.625}{2} \quad \rightarrow \sigma_v^2 = 0.024414$.

The video signal autocovariance function is:

$$C_{vv}(\tau) = \sigma_v^2 \exp\{-\frac{1}{2}(\frac{\tau}{\tau_c})^2\}, \tag{C.20}$$

and the power spectrum is:

$$G_{vv}(f) = \mu^2 \delta(f) + \frac{\sigma_v^2}{\sqrt{2\pi}\,\sigma_c} \exp\{-\frac{1}{2}(\frac{f}{\sigma_c})^2\} \tag{C.21}$$

where τ_c is the correlation time of the process, and

$$\sigma_c = \frac{1}{2\pi\,\tau_c} .$$

An example correlation time, τ_c, is $\frac{1}{5}$ of a video line (i.e. 10.7 μsec) and $\sigma_c \simeq 14.87$ kHz and the 40 dB bandwidth ($\simeq \sqrt{8\,\ell n\,10}\;\sigma_c$) is approximately 63.84 kHz.

The first video model considered assumes that each line is repeated with the same video content. This signal can be thought of as a windowed version of a periodic video process as illustrated in Figure C.14. The time windowed signal will be denoted by y(t). It will be assumed that the dc component has been removed and incorporated in the average carrier level. The periodic random process can be expanded in a Fourier series as follows:

$$y(t) = \sum_k Y(k)\exp\{j\frac{2\pi kt}{T_o}\} \tag{C.22}$$

where $Y(k) = \frac{1}{T_o}\int_o^{T_o} y(t)\exp\{-j\frac{2\pi kt}{T_o}\}\,dt$.

Periodic Video Random Process

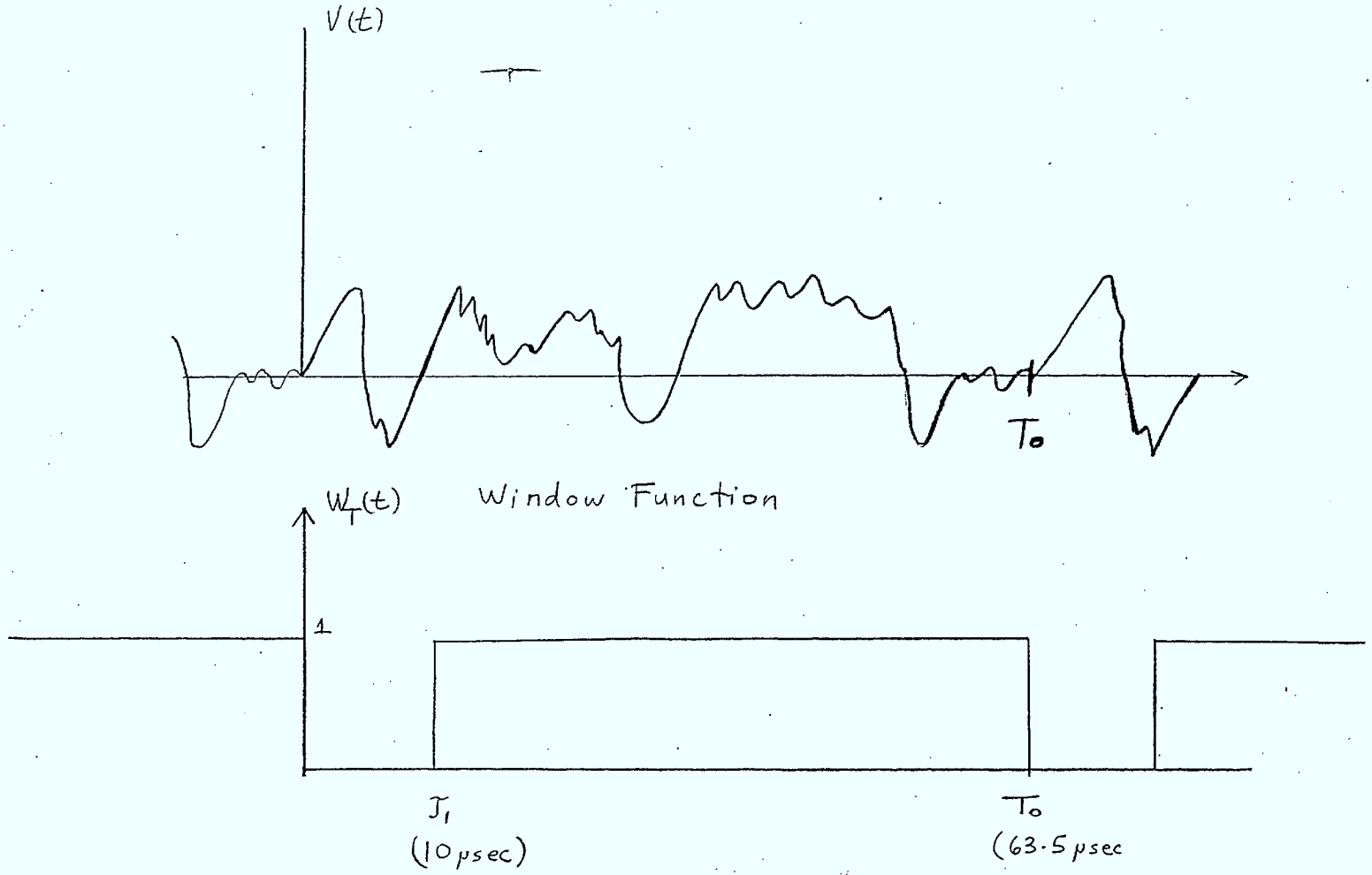

$$y(t) = V(t) \cdot W_T(t)$$

Figure C.14 : Windowing The Random Video Signal.

Each Fourier coefficient is a complex gaussian random variable. From the Knapp and Carter paper [12],

$$E\{Y(k)\ Y(\ell)^*\} \approx \frac{1}{T_o} G_{yy}(f)\Big|_{f=k/T_o} \delta_{k\ell}\ , \qquad (C.23)$$

when T_o is large compared to the correlation time of the process. $\delta_{k\ell}$ is the Kroeneker delta function which equals unity if $k=\ell$, and is zero otherwise. It is easily shown that:

$$G_{yy}(\frac{k}{T_o}) = (1-\frac{\alpha_1}{T_o})\ \tilde{G}_{vv}(\frac{k}{T_o}) \qquad (C.24)$$

where α_1 = 10 μsec (sync signal portion of the television line),

T_o = 63.5,

$\tilde{G}_{vv}(f) = G_{vv}(f) - \mu^2\ \delta(f)$.

The spectral components of the synchronization signals were normalized by the average picture level. Performing the same in this case,

$$\tilde{y}(t) = \sum_k \tilde{Y}(k)\ \exp\{+j\frac{2\pi k}{T_o}\ t\}$$

and

$$E[\tilde{Y}(k)\tilde{Y}(\ell)^*] = \frac{1}{T_o\ (ap\ell)^2}\ G_{yy}(\frac{k}{T_o})\ \delta_{k\ell}\ . \qquad (C.25)$$

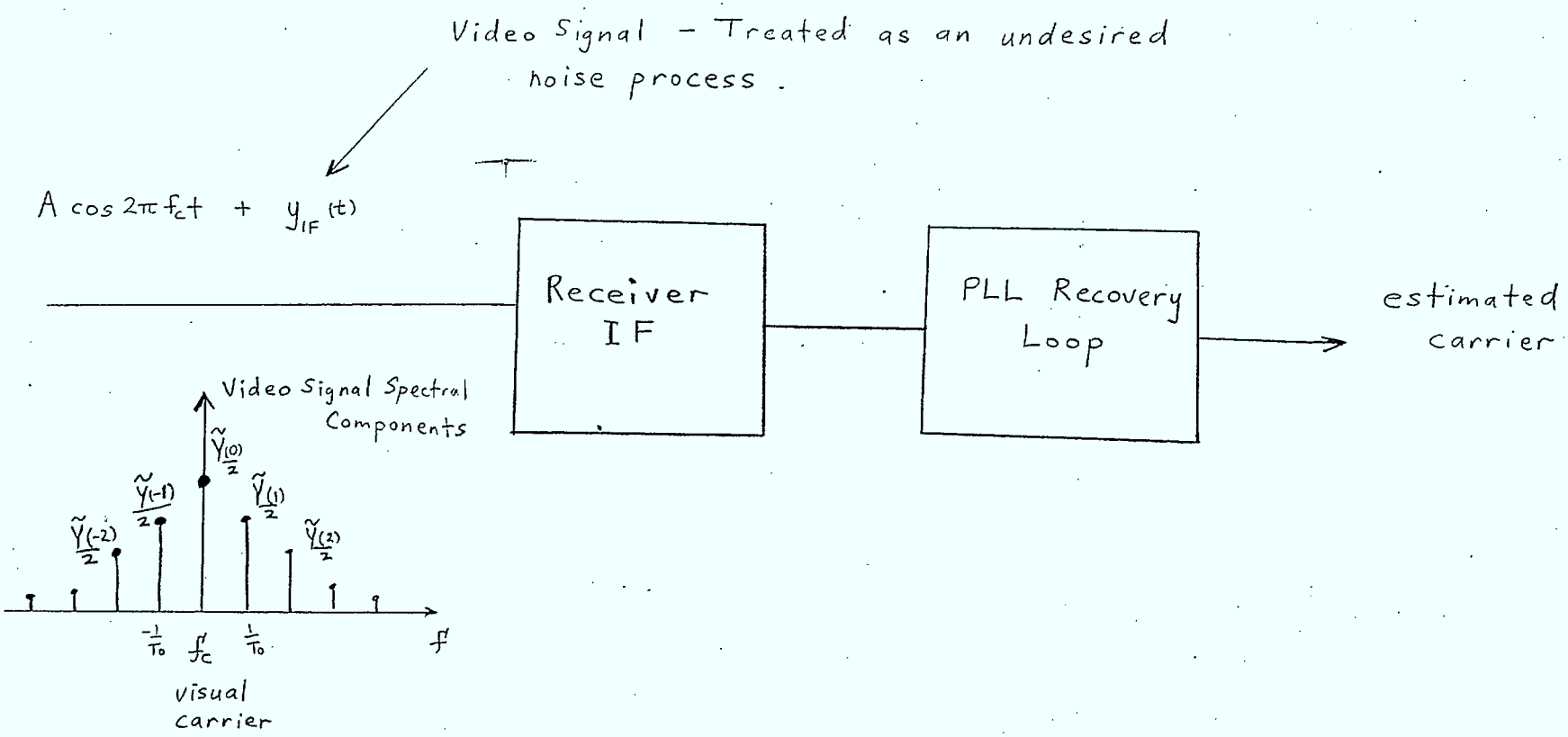

Figure C-15 : Model for analyzing distortion caused by low frequency video components

The modulated IF signal can be represented by

$$\tilde{y}_{IF}(t) = R_e \{ \sum_k \tilde{Y}(k) \exp\{+j\ 2\pi (f_c + \frac{k}{T_o})t\} \qquad (C.26)$$

and the spectrum at the input to the receiver filter is as shown in Figure C.15.

Another reasonable model is to simply treat the video signal as a time windowed version of a continuous gaussian process, v(t), with a gaussian autocovariance function. Ignoring the dc component,

$$\tilde{G}_{vv}(f) = \frac{\sigma_v^2}{\sqrt{2\pi}\ \sigma_c} \exp\{-\frac{1}{2}(\frac{f}{\sigma_c})^2\}$$

where $\sigma_c = \frac{1}{2\pi\ \tau_c}$

and τ_c is the correlation time of the video random process.

The random process, y(t), is given by:

$$y(t) = v(t)\ w_T(t)$$

where the window function is illustrated in Figure C.14. The autocorrelation function, $R_{yy}(\tau)$, is given by:

$$R_{yy}(\tau) = \lim_{T\to\infty} \frac{1}{2T} \int_{-T}^{T} y(t+\tau)\ y(t)\ dt \qquad (C.27)$$

$$\simeq R_{vv}(\tau)\ (1 - \frac{\alpha_1}{T_o}) \qquad \text{(converges to its expected value)}$$

where $\alpha_1 = 10\ \mu\text{sec}$ and $T_o = 63.5\ \mu\text{sec}$.

Using the approximation of (C.27), the spectrum of the time windowed video signal is approximately:

$$G_{yy}(f) \simeq (1 - \frac{\alpha_1}{T_o})\ \tilde{G}_{vv}(f). \qquad \text{(C.28)}$$

This is an approximation because time windowing, strictly speaking, destroys stationarity. With normalization one obtains:

$$\tilde{G}_{yy}(f) = (1 - \frac{\alpha_1}{T_o})\ \frac{\tilde{G}_{vv}(f)}{(ap\ell)^2}\ . \qquad \text{(C.29)}$$

4.2 Analysis of Phase Locked Loop Performance

It is quite realistic to assume that the random video signal and deterministic synchronization signals are independent. Consequently, one could treat the video signal corruption as an equivalent noise process and establish output variance bounds. The standard bandpass "white" noise process is not applicable because the receiver IF filter colours the noise.

The phase recovery system model is illustrated in Figure C.15. The random process at the output of the receiver IF filter is most easily determined at complex baseband (see Figure C.16. For the periodic video signal model, the autocorrelation function of the signal $y_B(t)$ is determined below:

$$R_I(f) = \frac{R(f) + R(-f)^*}{2}$$

$$R_Q(f) = \frac{R(f) - R(-f)^*}{2}$$

where $R(f)$ is complex baseband representation of receiver IF.

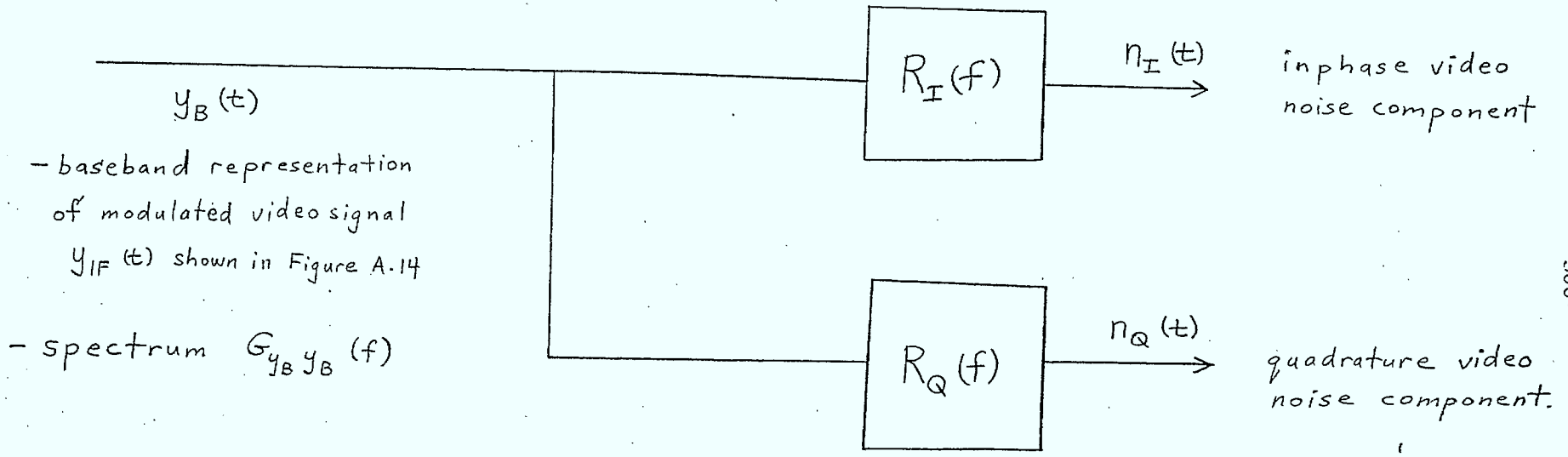

IF Noise Process $n(t) = 2n_I(t)\cos 2\pi f_c t - 2n_Q(t)\sin 2\pi f_c t$

Figure C.16 : Video noise process evaluation at complex baseband

$$R_{y_B y_B}(\tau) = E[y_B(t+\tau)\, y_B^*(t)]$$

$$= E \sum_k \sum_\ell \frac{\tilde{Y}(k)}{2} \frac{\tilde{Y}(\ell)^*}{2} e^{+j\frac{2\pi k(t+\tau)}{T_o}} e^{-j\frac{2\pi \ell t}{T_o}}$$

$$= \frac{1}{4} \sum_k \sum_\ell E[\tilde{Y}(k)\, \tilde{Y}(\ell)^*]\, e^{+j\frac{2\pi (k-\ell)t}{T_o}} e^{+j\frac{2\pi kt}{T_o}}$$

$$= \frac{1}{4T_o\,(ap\ell)^2} \sum_k G_{yy}(\tfrac{k}{T_o})\, e^{j\frac{2\pi k\tau}{T_o}} \qquad \text{(C.30)}$$

It is apparent that the spectrum of $y_B(t)$ has discrete spectral components:

$$G_{y_B y_B}(f) = \frac{1}{4T_o\,(ap\ell)^2} \sum_k G_{yy}(\tfrac{k}{T_o})\, \delta(f + \tfrac{k}{T_o}) \,. \qquad \text{(C.31)}$$

The inphase and quadrature components of the equivalent noise process have power spectral densities given by:

$$G_{n_I n_I}(f) = G_{y_B y_B}(f)\, \left|R_I(f)\right|^2 \qquad \text{(C.32)}$$

$$G_{n_Q n_Q}(f) = G_{y_B y_B}(f)\, \left|R_Q(f)\right|^2 \,.$$

For the idealized receiver response, $\left|R_I(f)\right|^2$ and $\left|R_Q(f)\right|^2$ are as shown in Figure C.17, and $G_{n_I n_Q}(f) = - G_{n_Q n_I}(f)$, which implies that $R_{n_I n_Q}(\tau) = - R_{n_Q n_I}(\tau)$.

The bandpass filter of the recovery system simply limits the number of spectral components of $G_{y_B y_B}(f)$ which effect the phase recovery loop. (i.e. $J = \text{INT}(\alpha T_o)$ where α = one sided prefilter bandwidth and $T_o = 63.5\ \mu\text{sec}$).

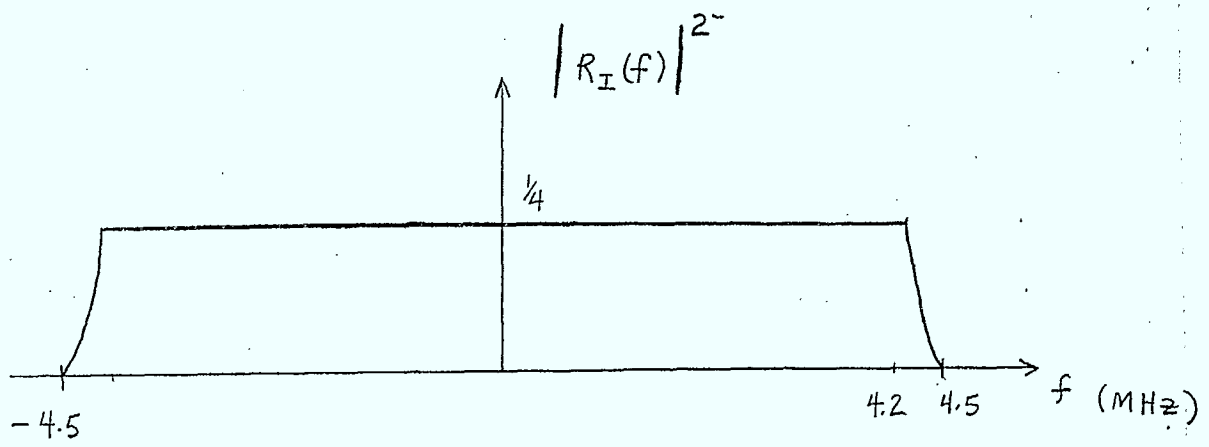

$$G_{n_I n_I}(f) = G_{y_B y_B}(f) \left| R_I(f) \right|^2$$

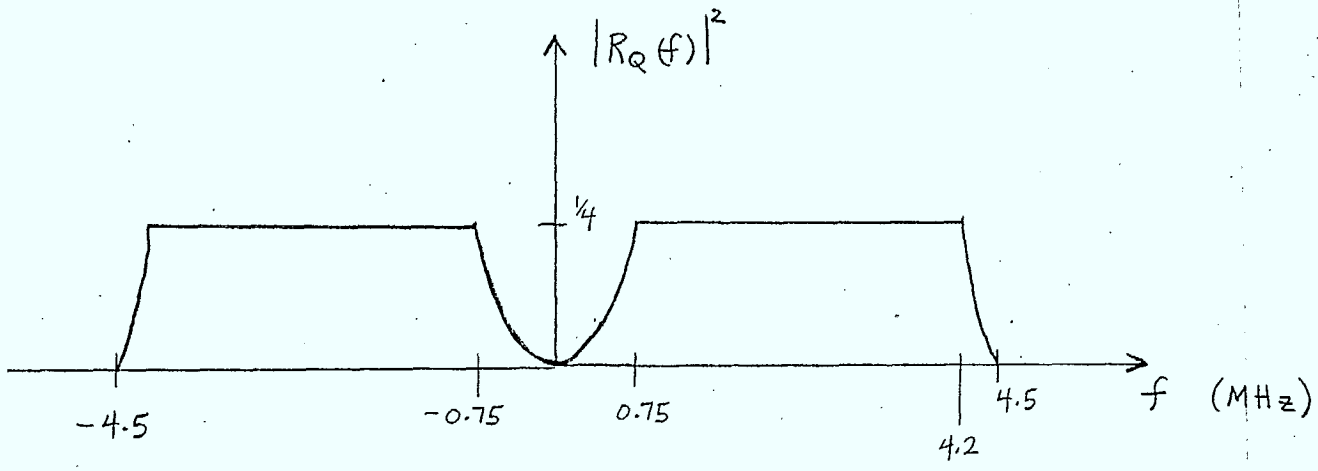

$$G_{n_Q n_Q}(f) = G_{y_B y_B}(f) \left| R_Q(f) \right|^2$$

Figure C.17 : In phase and quadrature responses for idealized receiver characteristic.

The phase locked loop model is illustrated in Figure C.18. The purpose of this section is to determine the effects of the video signal corruption, which is treated as an undesired noise process. The phase detector output is given by:

$$p(t) = K_D \sin[\phi_i(t) - \phi_o(t)] + \frac{K_D}{A}(2n_I(t) \sin \phi_o(t)) + \frac{K_D}{A}(2n_Q(t) \cos \phi_o(t)).$$

$$= K_D(\sin[\phi_i(t) - \phi_o(t)] + n'(t)) \qquad (C.33)$$

where $n'(t) = N_I(t) \sin \phi_o(t) + N_Q(t) \cos \phi_o(t)$

$$N_I(t) = \frac{2\, n_I(t)}{A}$$

$$N_Q(t) = \frac{2\, n_Q t}{A}$$

A represents the average carrier level.

Consequently, the linearized model is as shown in Figure C.19. The autocorrelation properties of n'(t) are examined below:

$$E\{n'(t_2)\, n'(t_1)\} = E(N_I(t_2)N_I(t_1))\, E(\sin \phi_o(t_2)\sin \phi_o(t_1)) + E(N_Q(t_2)N_Q(t_1))\, E(\cos \phi_o(t_2)\cos \phi_o(t_1)) + E(N_I(t_2)N_Q(t_1))\, E(\sin \phi_o(t_2)\cos \phi_o(t_1)) + E(N_Q(t_2)N_I(t_1))\, E(\cos \phi_o(t_2)\sin \phi_o(t_1)). \qquad (C.34)$$

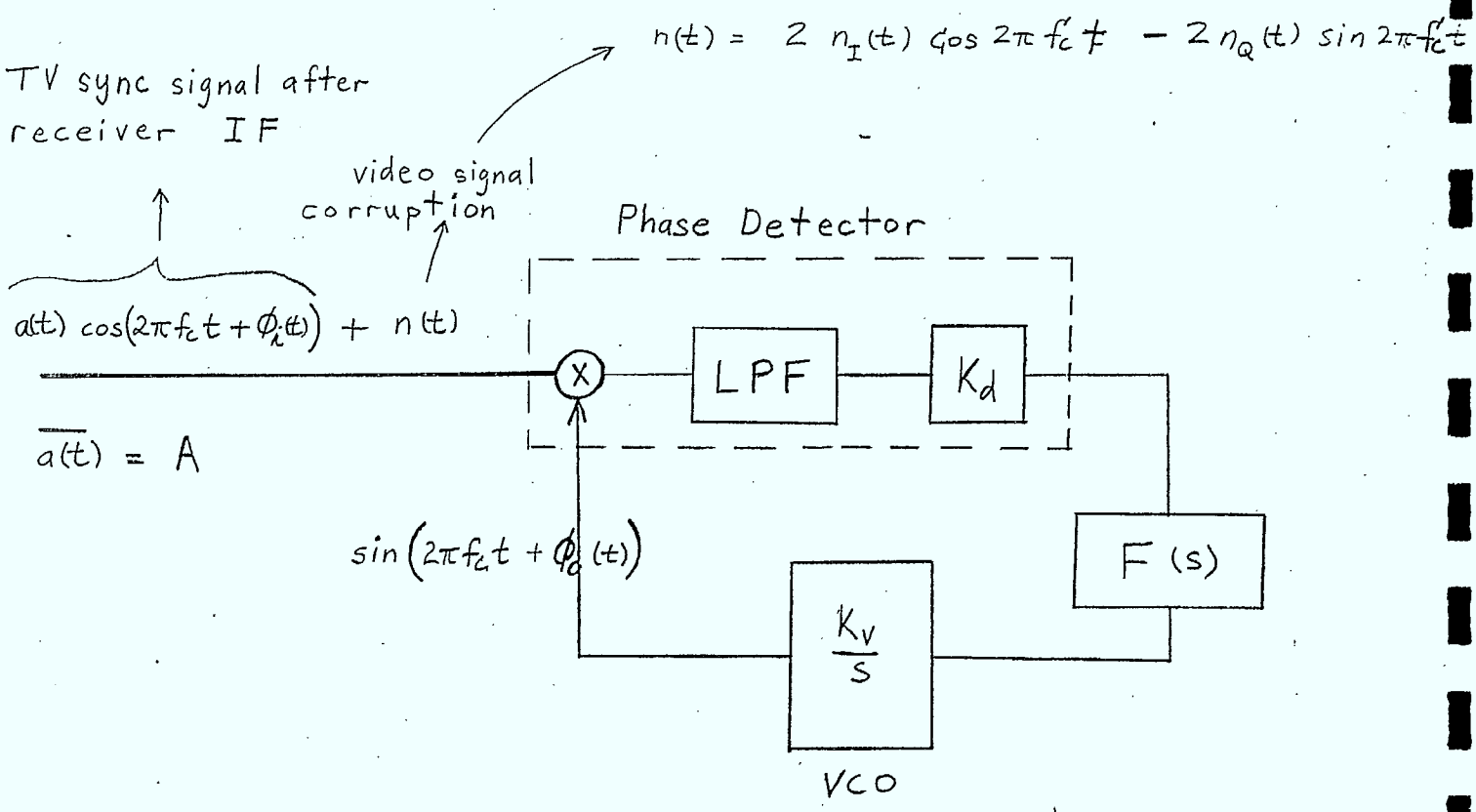

Figure C.18 : Detailed phase locked loop model

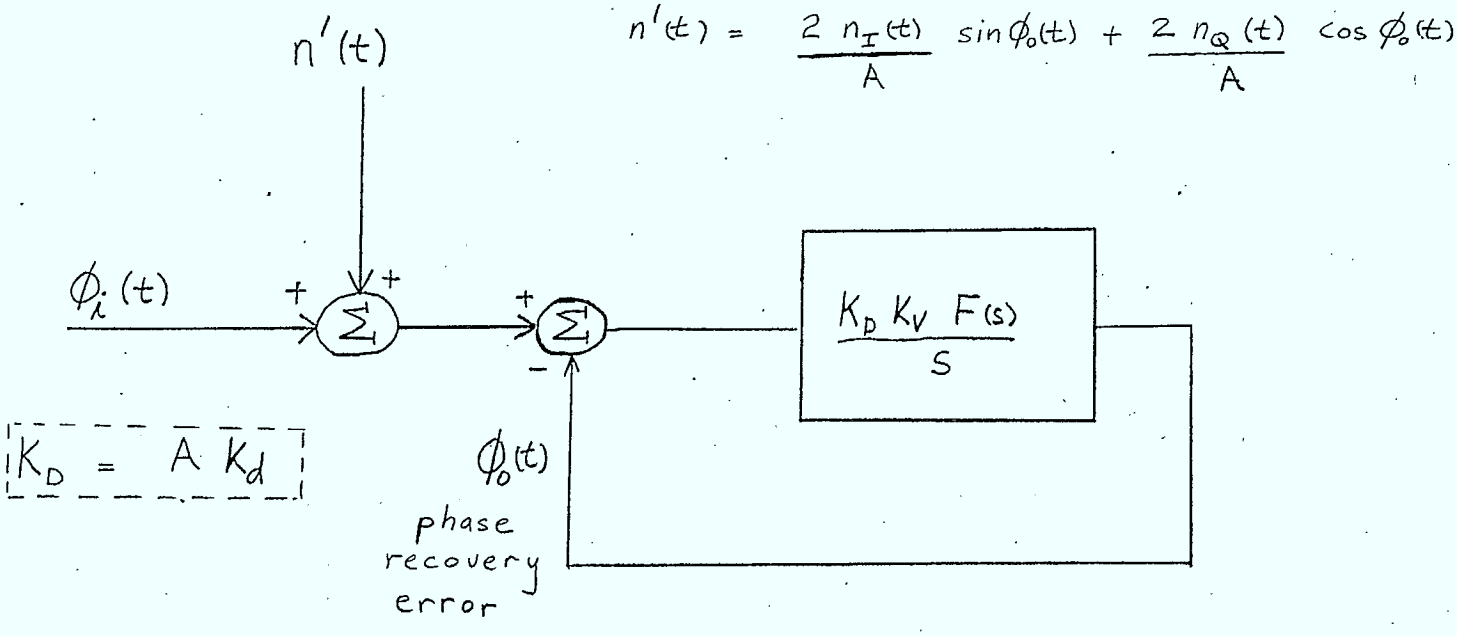

Figure C.19 : Linearized PLL recovery model with video corruption modelled as noise

An often made assumption when analyzing loops with bandpass Gaussian noise at the input, is that the change in $\phi_o(t)$ is negligible over the correlation time of the input noise process. This assumption is valid when the loop bandwidth is much smaller than the bandwidth of the input noise process. This assumption will not be completely valid for wideband loops. However, the assumption does simplify the analysis, and in this case:

$$R_{n'n'}(\tau) \simeq R_{N_I N_I}(\tau) \sin^2 \phi_o(t) + R_{N_Q N_Q}(\tau) \cos^2 \phi_o(t). \tag{C.35}$$

From equations C.31 and C.32 and Figure C.17, it is apparent that $G_{N_I N_I}(f) \neq G_{N_Q N_Q}(f)$. Consequently, the autocorrelation function of n'(t) will not be independent of time (process is non-stationary). Since $G_{N_Q N_Q}(f) \leq G_{N_I N_I}(f)$ for all frequencies, one can define a bounding spectrum:

$$G_{n'n'}(f) \leq G_{N_I N_I}(f). \tag{C.36}$$

Consequently, the output phase variance due to periodic video effects is bounded by:

$$\sigma_o^2 \leq \int_{-\infty}^{\infty} G_{N_I N_I}(f) \, |H(f)|^2 \, df \tag{C.37}$$

where $G_{N_I N_I}(f) = (1 - \frac{\alpha_1}{T_o}) \frac{1}{4T_o A^2 (ap\ell)^2} \sum_{k=-J}^{J} G_{vv}(\frac{k}{T_o}) \, \delta(f - \frac{k}{T_o})$

$$G_{vv}(\frac{k}{T_o}) = \sigma_v^2 (\sqrt{2\pi}\, \tau_c) \exp\{-\frac{1}{2}(\frac{2\pi \tau_c k}{T_o})^2\}$$

τ_c = correlation time of video process

σ_v^2 = a.c. video power

$H(f)$ = phase locked loop transfer function.

With normalization of the spectral components, the carrier level at the input to the receiver is unity, and at the output of the receiver filter $A = \frac{1}{2}$. The above expression for output phase variance, σ_o^2, can be simplified to yield:

$$\sigma_o^2 \leq \frac{2}{T_o (ap\ell)^2} \left(1 - \frac{\alpha_1}{T_o}\right) \sum_{k=0}^{J} G_{vv}\left(\frac{k}{T_o}\right) \left|H\left(\frac{k}{T_o}\right)\right|^2 . \tag{C.38}$$

where $\alpha_1 = 10$ μsec and $T_o = 63.5$ μsec.

A lower bound can be easily fabricated as well. Clearly $G_{n'n'}(f) \geq \frac{G_{n_I n_I}}{2}(f)$, which implies that the lower bound is simply one-half the upper bound value.

For the non-periodic gaussian video random process, a similar analysis yields the following bound on the output phase error variance:

$$\sigma_o^2 \leq \frac{2\left(1 - \frac{\alpha_1}{T_o}\right)}{(ap\ell)^2} \int_o^{\alpha} \tilde{G}_{vv}(f) \left|H(f)\right|^2 df \tag{C.39}$$

where $\left|H(f)\right|^2$ is the energy spectrum of the closed loop response of the second order loop, and

α is the pre-filter bandwidth parameter.

As was the case for the periodic gaussian video random process, a lower bound on the output phase variance is given by one-half the upper bound value.

It is believed that the periodic video random process model, with its discrete spectrum, is the worst case model. The phase error bounds (given by equations (C.38) and (C.39)) where evaluated for various values of σ_v^2, τ_c, apℓ, B_L (one sided noise equivalent bandwidth of the phase locked loop). The phase locked loop considered was a second order loop with minimum noise equivalent bandwidth ($\zeta = \frac{1}{2}$), whose transfer function is given by equation (C.16). The volume of results obtained by individually varying each parameter over a range of possible values is too extensive to be presented here. As one would expect, the phase error becomes worse as the apℓ is decreased and the a.c. video power is increased. The results for an apℓ = 0.4375 V and $2\sigma_v = (\frac{0.625}{2})$ are summarized in Table C.2. When the correlation time of the gaussian random process is 10.7 μsec, ($\frac{1}{5}$ video line), the video spectrum is narrowband. From the results in Table C.2 it is apparent that the phase variance actually degrades as the loop bandwidth is decreased. Noting the low frequency peaking of the closed loop transfer function (see Figure C.20 with $\zeta = \frac{1}{2}$), this is not at all surprising. As indicated earlier, the periodic video random process is clearly worst case. The phase error bound for the periodic video process is in the neighbourhood of 23° for quasi-synchronous detection. It is quite apparent that the video signal can introduce an appreciable phase error. When the correlation time is reduced to 2.675 μsec ($\frac{1}{20}$ of the video line), performance improves with narrowband loops. However, for the worst case periodic video random process, the bound on the phase error standard deviation is on the order of 16° for a 25 kHz loop bandwidth. When the a.c. video power is

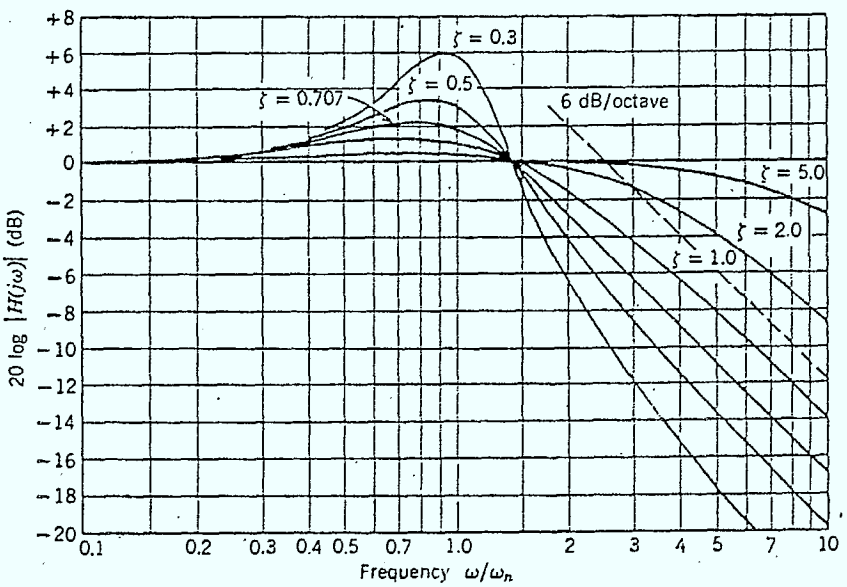

Figure C.20: Amplitude response of high gain lag-lead filter second order loop (after [9]).

Correlation Time of Video Process, τ_c (μsec)	Phase Locked Loop Noise Equivalent BW BL (kHz)	Bound on the Standard Deviation of Phase Error Process in Degrees for	
		Periodic Video Model	Continuous Video Model
10.7	400	22.5	18.8
	300	22.5	18.9
	200	22.6	19.0
	100	23.3	19.8
	50	25	21.8
	25	25.6	22.2
2.675	400	20.7	19.8
	300	21.4	20.5
	200	22.7	21.8
	100	22.9	22.1
	50	19.8	18.8
	25	16.1	14.5

$2\sigma_v = [\frac{0.625}{2}]$ V apℓ = 0.4375 V

σ_v = standard deviation of a.c. video power

apℓ = average carrier level

Table C.2: Bounds on the Phase Error Standard Deviation Introduced by a Gaussian Video Random Process Model

reduced ($3\sigma_v = \frac{(0.625}{2}$)), the bound on the phase error standard deviation for a 100 kHz noise equivalent loop bandwidth is roughly 15.5° for the periodic video model and 13.2° for the continuous random process model when $\tau_c = \frac{1}{5}$ of a video line.

This analysis on the influence of the corrupting low frequency components of video signal clearly indicates that the effects are non-negligible for systems which extract the carrier after the television receiver IF.

5.0 POSSIBLE IMPROVEMENTS TO TELEVISION CARRIER RECOVERY SYSTEMS

A major source of degradation in conventional television carrier recovery systems is the incidental phase modulation caused by the linear skirt of the receiver IF filter. This can be eliminated by routing the reference channel around the receiver IF. This requires an extra amplifier for the reference channel and one must accurately maintain the phase balance between the two paths. The increased cost of this solution is primarily the reason why it is not used in commercial television systems. Rzeszewski, [2], presents an approach which re-establishes the double sideband integrity of the received signal over the linear skirt region of the receiver IF, before amplitude limiting the signal. The technique basically inverts the frequency sence of the signal around the picture carrier and adds this to the original signal before amplitude limiting. The major deterent of this approach is complexity and cost (two phase locked loops, two product detectors, and a frequency doubler are required).

For the television systems of the future, which are likely to predominately have surface acoustic wave (SAW) IF filters (which have fairly linear phase response around the carrier frequency), the bandpass filter of the carrier recovery system can be tailored to compensate for the Nyquist slope. Eliminating the incidental phase modulation introduced by the receiver IF would improve considerably the performance of quasi-synchronous detectors. Given that most television sets currently being produced employ more accurate and stable tuning systems than in the past, tuning is usually independent of picture content. Consequently narrower bandwidth recovery systems are now practical. However, very narrow bandwidth systems (synchronous detectors) require precision components and probably eliminate or at least reduce Nyquist slope incidental phase modulation in some fashion. For complexity and economic reasons, the phase recovery systems of current commercial carrier recovery systems must contend with receiver generated phase modulation. They typically have 3 dB bandwidths on the order of 100 kHz to 300 kHz to contend with commonly occurring signal impairments (transmitter incidental phase modulation) [3].

6.0 CONCLUSIONS

Bounds on the standard deviation of the phase error introduced by a random Gaussian video signal have been presented in this appendix. It is clearly evident that the video signal can have a significant influence on quasi-synchronous carrier recovery systems. The nature of the phase error is strongly dependent on the characteristics of the video signal. The phase error model development is complicated by the need for several different accepted video process models. Furthermore, for characterizing the performance of teletext systems which transmit information during the vertical blanking interval and use quasi-synchronous carrier recovery, the influence of the past

picture is relatively minor. For very narrowband recovery loops, past picture information can have some influence. For quasi-synchronous systems, the teletext signal will have the major impact on the carrier recovery system. For such systems, one can extract a reasonably accurate characterization of the phase error (when the PLL is in equilibrium) by filtering the phase signal at the output of a bandpass limiter by the closed loop PLL transfer function. This approach will definitely not work for narrowband recovery systems as past lines will have an important influence. Since the above mentioned approach avoids the difficult problems of developing and validating a random process model, and properly takes account of the effects of multipath channel impairments and noise, this approach is proposed for characterizing the performance of teletext systems using quasi-synchronous detection.

APPENDIX D

IMPLEMENTATION CONSIDERATIONS FOR TELETEXT EQUALIZATION

APPENDIX D

IMPLEMENTATION CONSIDERATIONS FOR TELETEXT EQUALIZATION

1.0 INTRODUCTION

In this appendix, some considerations regarding the implementation of an equalizer for the off-air reception of broadcast teletext are discussed. Delving into implementation details is beyond the scope of the present study. Instead, several hardware components that are potentially useful for implementing a teletext equalizer are described. A possible equalizer structure is then proposed.

Both advanced coding schemes and equalization are techniques that can be employed to improve the performance over poor channels. Thus, in a sense, equalization can be viewed as an alternative to advanced coding schemes. Of course, we are not precluding the possibility of using both equalization and an advanced coding scheme simultaneously. Typically, the advanced coding schemes assume that the Hamming-encoded prefix is adequately protected and therefore the advanced coding scheme is the applied only to the data block. This assumption has the practical advantage that the decoder can decode the prefix "on the fly" and then decode the data block only for the lines that are requested by the user (i.e. from a given channel). Since a large number of channels are time-division multiplied, there is a reasonable amount of time for the decoder to decode a line from a given channel before the next line from that channel arrives. A minimum time separation of 4 ms is given in [19]. Thus the decoder has at least 4 ms to decode a line before the next line to be decoded is received. If a truly fair comparison is to be

made between coding and equalization, then a mode of equalization where only the data block is equalized should be considered as a possible option. Here, this option will be referred to as "data-only equalization". In this mode, the average data rate that the equalizer must contend with is no greater than 72 kbits/s. Note that the prefix must be passed through the equalizer's filter, even though only the data blocks will benefit from the equalization. This is necessary because the presence of the prefix will affect the data block due to multipath propagation. Clearly, data-only equalization represents one approach to non-real-time equalization.

The assumption that the Hamming-encoded prefix is adequately protected cannot be justified for multipath environments where the eye is closed (i.e. detection errors can occur due to intersymbol interference even when there is no noise present). For example, consider a case where the signal-to-noise ratio is very high but the eye is closed. Suppose that the customer requests a packet address for which the intersymbol interference causes multiple errors. That is that one or more of the prefix bytes is rejected. Assuming that the channel is stationary, lines bearing the desired packet address will continue to be rejected. This is in contrast to the case of noise induced errors, in which case the line would typically be properly received after a small number of retransmissions, for reasonable signal-to-noise ratios. It is for the above reason that equalization (and advanced coding) strategies that can operate on the prefix are desirable.

For vertical blanking interval transmission, up to 12 lines per field can be used for broadcast teletext transmission. Assuming that 288 bits are transmitted on a line, the maximum average bit rate that an equalizer must be capable

of handling is 207.36 kbits/s. This observation suggests a second mode of non-real-time equalizer. Clearly this mode is only appropriate for vertical blanking interval transmission, and not for full-field transmission. Here, we will refer to this option as "VBI-only equalization".

Another possibility exists which allows for the non-real-time equalization of the entire line for either vertical blanking interval or full field transmission, and will be referred to here as "scheduled equalization". For this scheme, it is assumed that packets on a given channel are always transmitted on a particular line of a particular field. For example, packets on channel 836 are always transmitted on line 16 of field 1. Thus the equalizer (and decoder) need only operate on one line per frame, which results in an average bit rate of 8.64 kbits/s. This is encouraging because this bit rate is in the range of that for high-rate data transmission over a voice grade channel, which is an application where both adaptive equalization and coding have been used extensively. The disadvantage of this approach is that it places a restriction on the format of the transmissions, that is not included in any of the current specifications for broadcast teletext [19], [37].

The fourth option considered here is real-time equalization. For this option, a discrete-time transversal filter should be capable of operating at a sampling rate of 11.4545 MHz (i.e. T/2 sampling). Although the equalization of the television video signal will not be discussed in this section, it should be kept in mind that this fourth option is the only one for which the same equalizer can be used to equalize both the video and the teletext signals.

Before proceding with the description of a possible equalization strategy, a brief survey of some useful hardware components will be provided. This survey is intended to be representative of the available components rather than be comprehensive in nature.

2.0 POSSIBLE BUILDING BLOCKS FOR TELETEXT EQUALIZATION

Most of the devices that will be discussed here are devices that are capable of performing convolution (i.e. the programmable linear filtering function) on wideband signals. However, the first device that is discussed is not a convolver. It is a device that can be used for "time expansion" for non-real-time processing.

Not discussed here are the Philips teletext equalizer [29] and SAW wideband convolvers [38], [39]. The Philips equalizer is not considered here because it has already been discussed in detail in Section 5.1 and it was concluded that this device is not appropriate for the equalization of off-air signals in an urban environment. SAW convolvers are not discussed because it is unlikely that these devices will provide a cost-effective means of equalizing the teletext signals.

2.1 CCD Video Analog Shift Registers

Several manufacturers make video-rate CCD analog shift registers (e.g. the Fairchild CCD321A and the Reticon R5103). Typically these devices are designed to store one full line of the video signal at a sampling rate of four times the colour subcarrier frequency (i.e. 14.318 MHz). The length of these shift registers is therefore usually 910 samples. Clearly one of these shift registers is capable of storing more than a full video line at the 2/T rate of 11.4545 MHz. Once a line has been stored, it can be clocked out of the shift register at a much lower rate for A/D conversion* or some other processing operation.

*Video-rate sample-and-hold and analog-to-digital devices are commercially available, but they are very expensive. Furthermore, high speed digital memory is required to store the outputs of these devices.

2.2 CCD Analog-Analog Convolvers

Convolvers can be constructed using CCD registers and analog multipliers. A block diagram illustrating this type of convolver can be seen in Figure D.1. Reticon manufactures a 32-tap CCD analog-analog convolver that is capable of operating at sampling rates up to 2 MHz. The length of this device is only marginal for the given application. (Recall that in Section 5.2, it was suggested that 35 taps is the minimum number of taps for the equalization of off-air signals in downtown Ottawa.) Also, the maximum sampling rate is not high enough for real-time equalization. However, the maximum sampling rate is more than adequate for VBI-only equalization.

A very promising CCD analog-analog correlator has been developed in Japan [28]. This device has 128 taps and was designed to operate at a sampling rate of 10.7 MHz, which is three times the colour subcarrier frequency. Thus it could probably operate at the 2/T rate of 11.4545 Hz. This device has been successfully tested for the equalization of the video signal, but to the best of the author's knowledge it has not been tested for teletext. Thus the author does not know if it possesses sufficient bandwidth and linearity for the teletext application. However, this device does provide some encouragement that a CCD convolver is capable of providing cost-effective real-time equalization of teletext.

2.3 CCD Digital-Analog Convolvers

CCD techniques can also be used to realize digital-analog convolvers. A block diagram illustrating the structure of a digital-analog correlator can be seen in Figure D.2. Digital-analog convolvers have the advantage over analog-

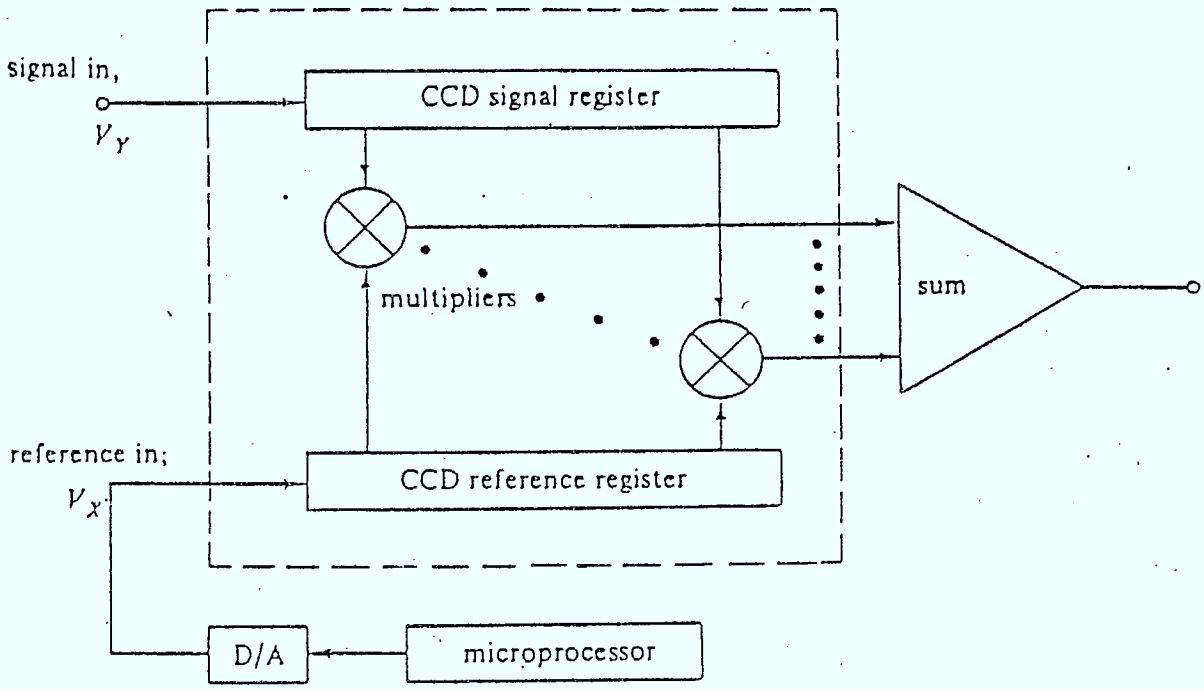

Figure D.1: A conceptual block diagram illustrating the structure of a CCD analog-analog convolver

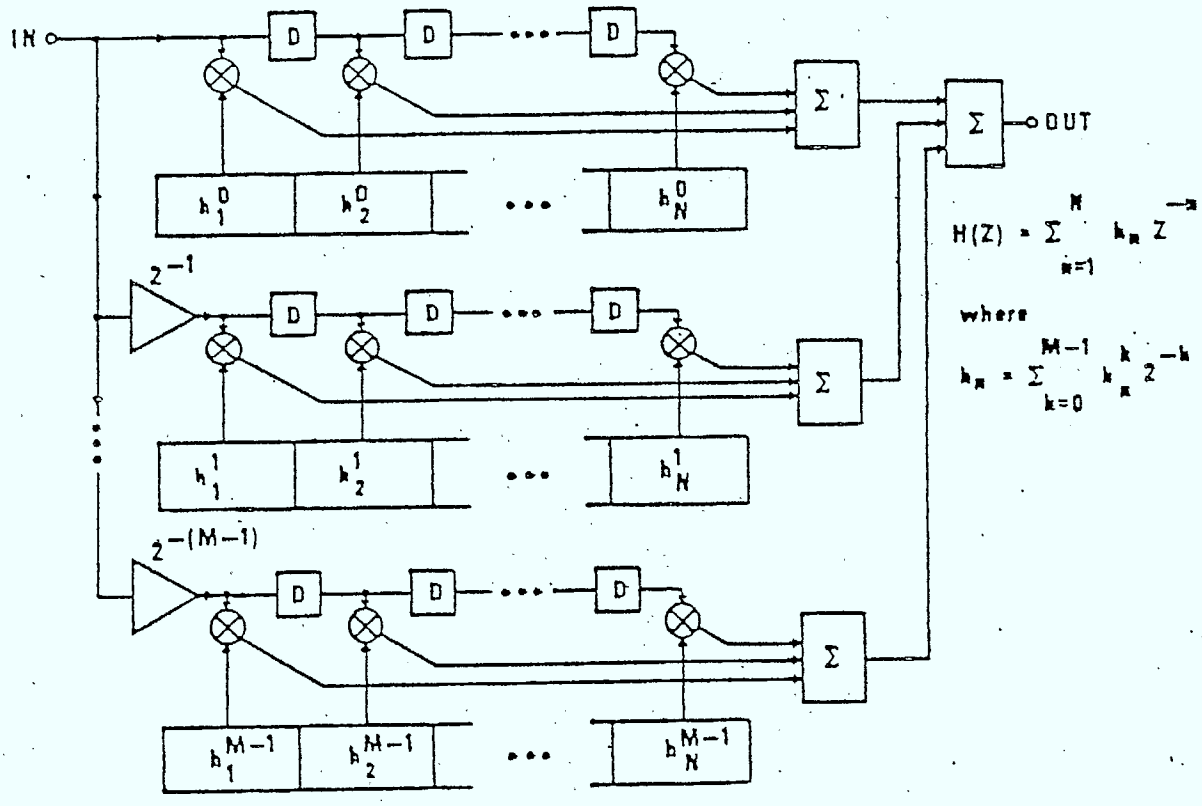

Figure D.2: A block diagram of a digital-analog correlator [40]

analog convolvers that the filter coefficients are stored statically on the chip in digital form. A digital-analog convolver has been built at Texas Instruments Inc. [40], that can be configured so that it has 128 taps with 8-bit coefficients. However, the maximum sampling rate for this device is 1 MHz. Thus, it is not fast enough to be used for the real-time equalization of teletext signals. However, it is fast enough for all of the other equalization options.

2.4 Components for Digital Filtering

TRW has recently begun to manufacture an FIR digital filter building block that can operate at sampling rates of up to 20 MHz [41] and is therefore capable of providing real-time teletext equalization. This building block is essentially an 8-tap FIR digital filter, with 4-bit coefficients and a 4-bit wide input signal path, which has been configured so that multiple devices can easily be paralleled and cascaded in order to construct a filter with a longer word length and more taps. Although this device has some interesting possibilities, it is felt that a programmable filter with enough taps and a long enough word length for the teletext application, would be too expensive to represent a practical solution at this time.

High-speed digital signal processing components (e.g. hardware multiplier and multiplier-accumulator chips) can be used to construct a high-speed programmable digital filter. An example of this type of filter is the ADF-16 digital FIR filter board that is produced by the Ottawa-based company Interactive Circuits and Systems Limited. This is a 16-bit programmable FIR filter that is capable of operating at 10/N MHz, where N is the number of filter taps. Thus this device could be used for either the data-

only equalization strategy or the scheduled equalization strategy. At present this filter board is sold for approximately one thousand 1983 Canadian dollars. However, it must be considered as a specialty device (i.e. low quantity). If it were manufactured for the consumer market, its cost would probably drop to a couple hundred dollars. Even at this lower cost, it must be considered a relatively high cost solution.

If a strategy such as the scheduled equalization strategy is adopted, then a LSI digital signal processor chip (or chip set) may represent an economical solution to the equalizer realization problem. Examples of this type of device include the Texas Instruments TMS320 [42] and the Nippon Electric NEC μPD7720 [43]. The TMS320 contains a hardware multiplier that will perform a multiplication in 200 ns. The TMS320 signal processing chip has been successfully used in speech processing applications with sampling rates in excess of 10 kHz. In large quantities the TMS320 chip price range should be between 20-30 dollars. In addition to performing the programmable filtering, the above mentioned devices would be able to perform the parameter adaptation on a time-shared basis, as they are very similar to general purpose microcomputers.

3.0 A POSSIBLE STRUCTURE FOR THE LINEAR EQUALIZATION OF TELETEXT

A conceptual block diagram illustrating a possible structure for the linear equalization of teletext can be seen in Figure D.3. This diagram is at the conceptual level in that only the signal paths are shown. The many timing and control lines that would be necessary are not included in this illustration. Several points about this structure should be mentioned. Note that both the input signal to the equalizer and the error signal (i.e. the difference

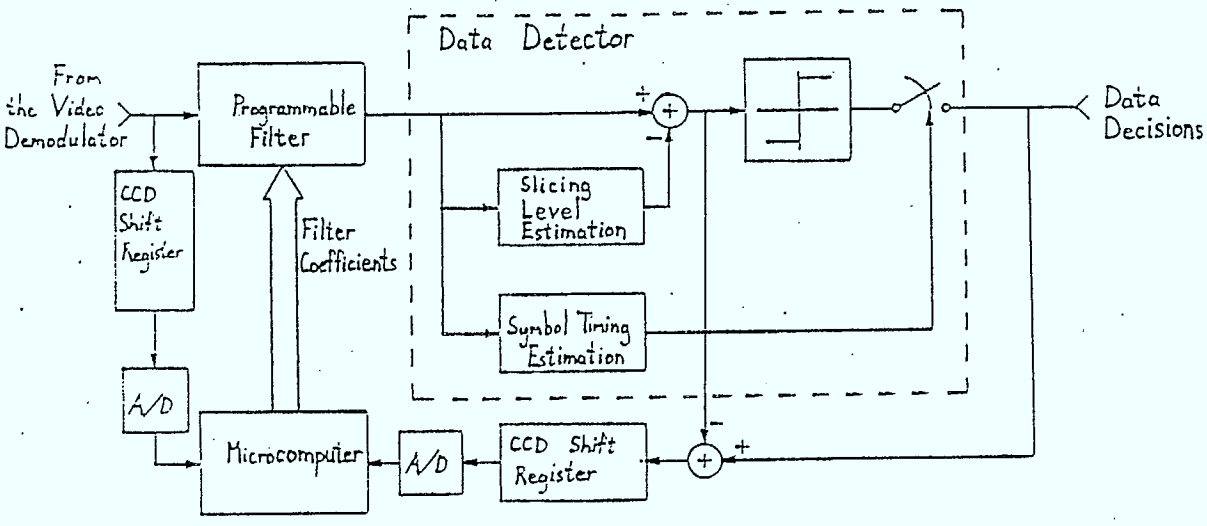

Figure D.3: A conceptual block diagram illustrating the structure of the linear equalization concept.

between the signals prior to and following the detector) are stored in the microcomputer's random-access memory. Thus the microcomputer has access to all of the information it needs to perform a closed-loop iterative coefficient adaptation algorithm.

An important point to note is that the slicing level estimation and the symbol timing estimation (i.e. bit clock phase recovery) are implemented after the programmable filter. This is a highly desirable arrangement because multipath propagation can severely degrade the performance of these synchronization circuits.

The microcomputer must aid in the various synchronization and control tasks as well as being responsible for the coefficient adaptation. It may be advantageous to speed up the microcomputer by including a hardware multiplier. One candidate, for the hardware multiplier, is the RCA CDP1855. This CMOS device has a lower cost and a lower power consumption than the faster bipolar multipliers that are manufactured by companies such as TRW and Advanced Micro Devices Inc. Another realistic choice is the previously mentioned TMS320 microcomputer which has a built in hardware multiplier and a highly pipelined architecture.

With the coefficient adaptation being implemented on a microcomputer, the adaptation strategy can be made somewhat more intelligent than a direct software implementation of LMS gradient adaptation algorithm of Widrow and Hoff. For example a given line might only be used for the coefficient adaptation if no errors are detected by the coding scheme.

The structure illustrated in Figure D.3 is for real-time equalization. However, with minor modifications it can be applied to the other equalization options. The required modification, to the equalization structure, for VBI-only

equalization, is shown in Figure D.4. Note that a bank of multiplexed CCD shift registers are required at the input. A shift register is required for each teletext-bearing line in a field. Thus the number of shift registers is given by the maximum number of lines in a field that can be used for teletext (e.g. 12 in [19]). For the data-only equalization strategy and the scheduled equalization strategy the bank of multiplexed shift registers can be replaced by a single shift register.

In Figure D.3, no reference is made as to which portions of the structure are implemented in the digital domain and which portions of the structure are implemented in the analog domain. The reason for this is that the choice of which portions of the structure should be implemented in the given domains is highly technology dependent. Since the candidate technologies are still dynamically evolving a detailed specification of the equalizer is both difficult and undesirable.

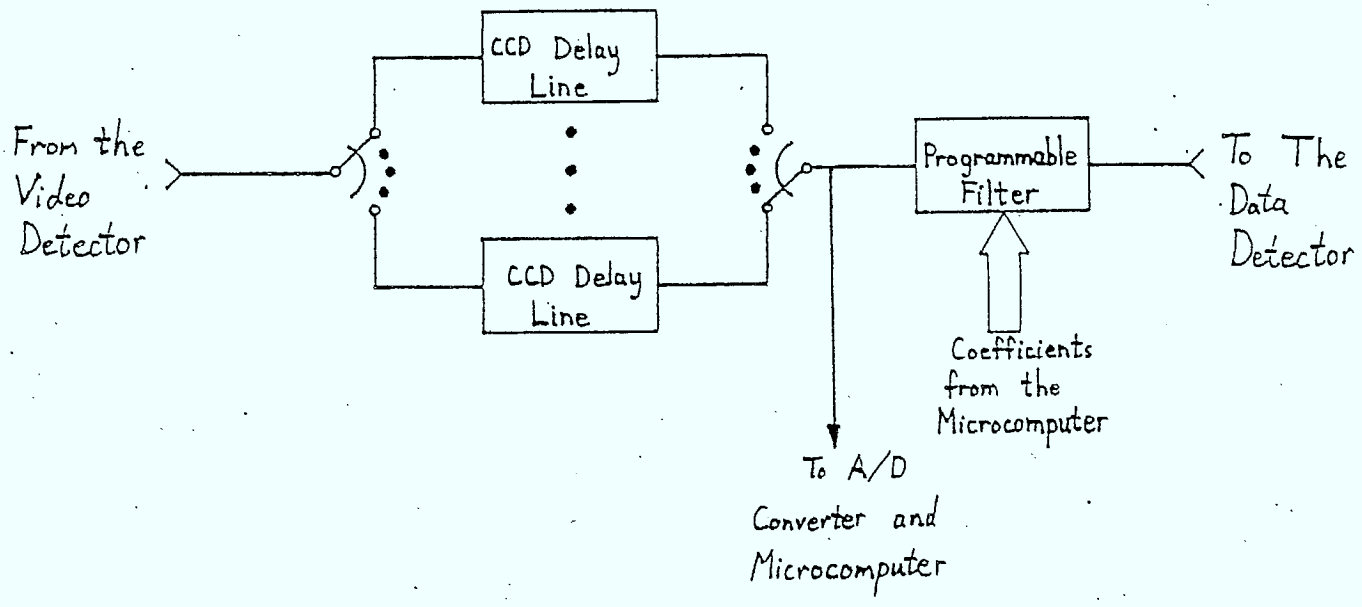

Figure D.4: An illustration of the modification, to the equalization structure, for VBI-only equalization

APPENDIX E

DETAILS OF THE SIMULATION PROGRAM EQUALIZER

APPENDIX E

DETAILS OF THE SIMULATION PROGRAM EQUALIZER

The transfer function of the optimal linear equalizer, constrained such that the overall channel response satisfies Nyquist's first criterion for no intersymbol interference (ISI), is given by:

$$E_{opt}(f) = \left(K \frac{H_I^*(f)}{W(f)}\right) \cdot \left(\frac{1}{\sum_n \frac{|H_I(f + \frac{n}{T_b})|^2}{W(f + \frac{n}{T_b})}}\right) \qquad (E.1)$$

where $H_I(f)$ is the overall inphase channel response,

$W(f)$ is the shape of the input noise spectrum,

T_b is the bit period, and

K is an arbitrary constant.

The first factor in equation (E.1) is a noise whitened matched filter and the second term is a transversal filter, with tap spacings of T_b, the baud interval. The transversal filter response has zero phase, which implies that its impulse response is symmetric about the origin ($g(-t) = g(t)$) and is clearly non-causal.

In the case where one of the components of the overall channel is a multipath channel, the overall response will exhibit ripping in its amplitide response. The denominator of the transversal filter response is composed of baud rate aliased versions of the frequency response of the channel

autocorrelation function normalized by the noise spectrum shape. The overall equalizer impulse response is given by the convolution of the transversal filter with the time reversed version of the overall channel response (the impulse response of the matched filter is $h_I(-t)$). It is apparent that, in general, the equalizer impulse response does not have to be causal. It is informative to consider a few special cases to gather better insight into the characteristics of the optimum equalizer.

For the following special cases, consider a multipath channel with a single "inphase" echo with impulse response:

$$c(t) = 1 + a\,\delta(t-d) \qquad \text{(E.2)}$$

where a is the echo amplitude, and

d is the echo delay.

As a first special case consider an overall channel, $H_I(f)$, that is bandlimited at "$\frac{1}{2T_b}$". In this case there is no overlap of bit rate aliased versions of the channel, and

$$E_{opt}(f) = \frac{K}{H_I(f)}$$

$$= \frac{1}{H_p(f)\ C(f)}$$

where $H_p(f)$ is the overall channel response in the absence of multipath.

The most important component is $J(f) = \frac{1}{C(f)}$, which has an impulse response:

$$j(t) = \sum_{n=0}^{\infty} (-a)^n \delta(t-nd) \quad . \qquad (E.3)$$

This impulse response is illustrated in Figure E.1. For strong echoes, the effective duration will be several times the original channel spread. The regions where impulse response energy is concentrated is harmonically related to the original echo delay, d.

Next let us consider a channel with an overall channel response in the absence of multipath, $H_p(f)$, which has a sampled response as in Figure E.2(a). For the purposes of this discussion, let us also assume that the noise spectrum is white. Consider an echo with a delay that is an integer multiple of the bit period, T_b, as illustrated in Figure E.2(b). The bit rate sampled version of this channel is illustrated in Figure E.2(c), and the autocorrelation function in Figure E.2(d).

For weak echoes, an approximation for the transversal filter impulse response is given in Figure E.2(e). The equalizer impulse response is formed by convolving the time reversed version of the channel response with the transversal filter impulse response. This convolution process is illustrated in Figure E.3. The basic result is a cancellation of the negative time response, giving rise to a causal impulse response (when second order effects are ignored).

To demonstrate that the above is not true in general consider the case where the echo delay is not an integer multiple of the bit period (see Figure E.4(a)). In this case, the bit rate sampled channel autocorrelation function is given in Figure E.4(b). For small echoes, a reasonable

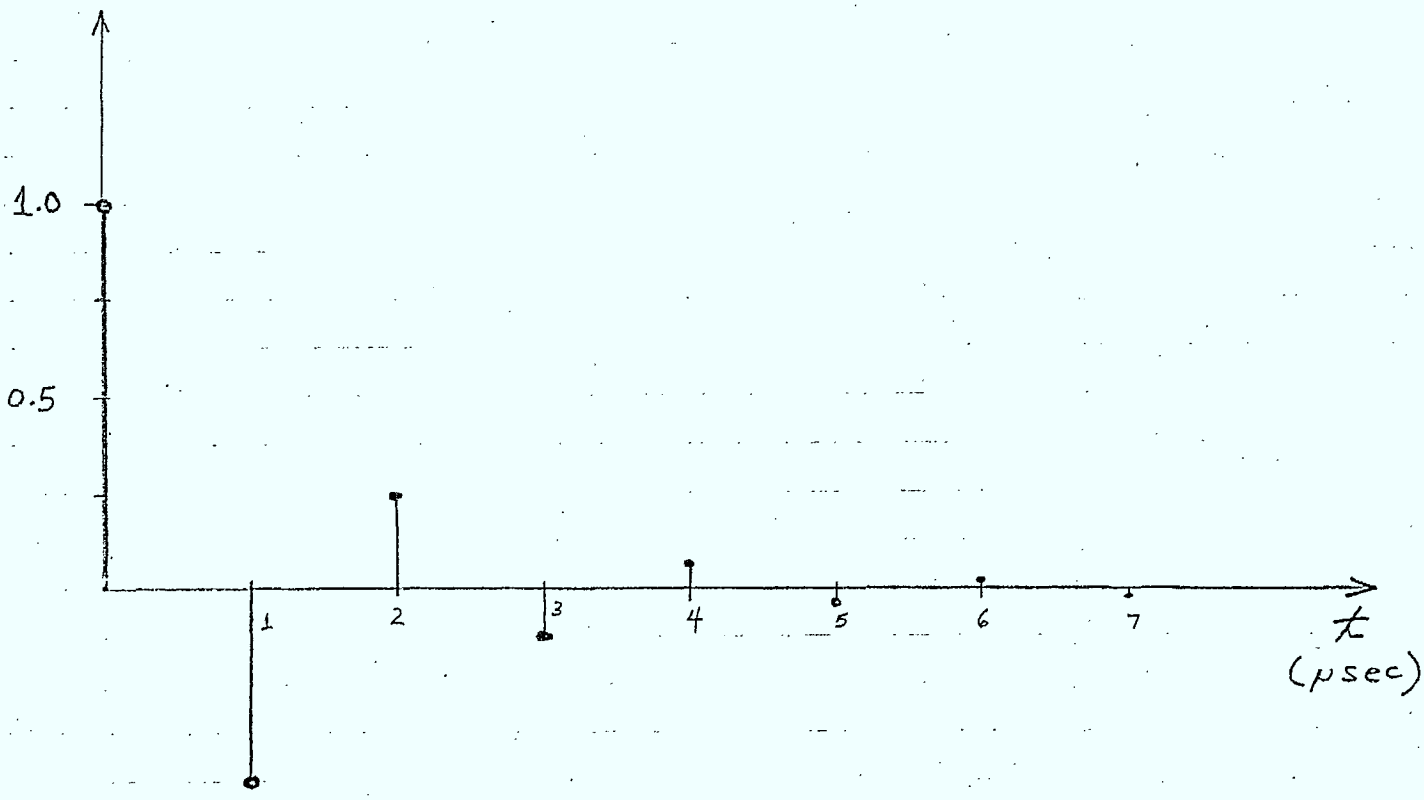

Figure E.1 : Impulse response of channel inverting filter for a -6 dB echo with 1 μsec delay.

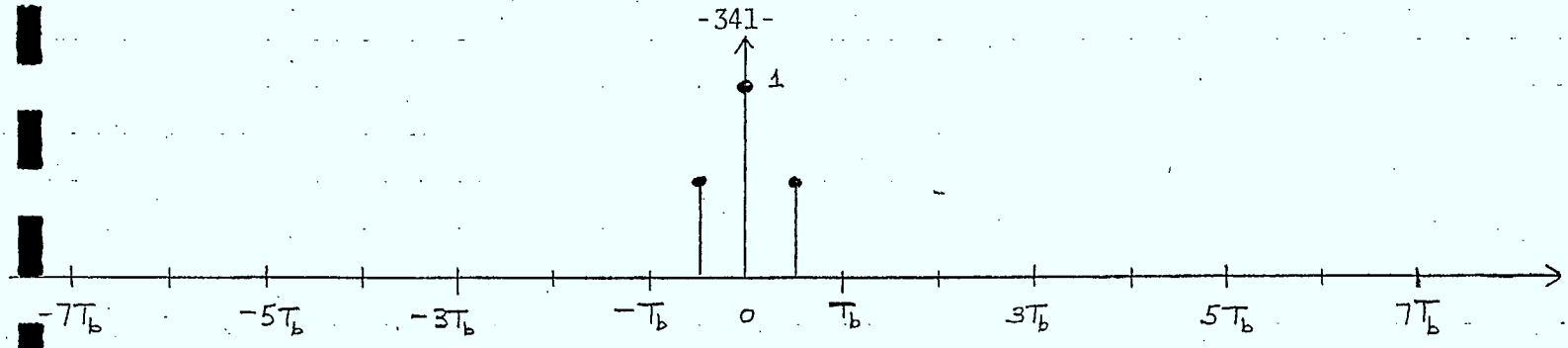

a) Sampled channel response in the absence of multipath

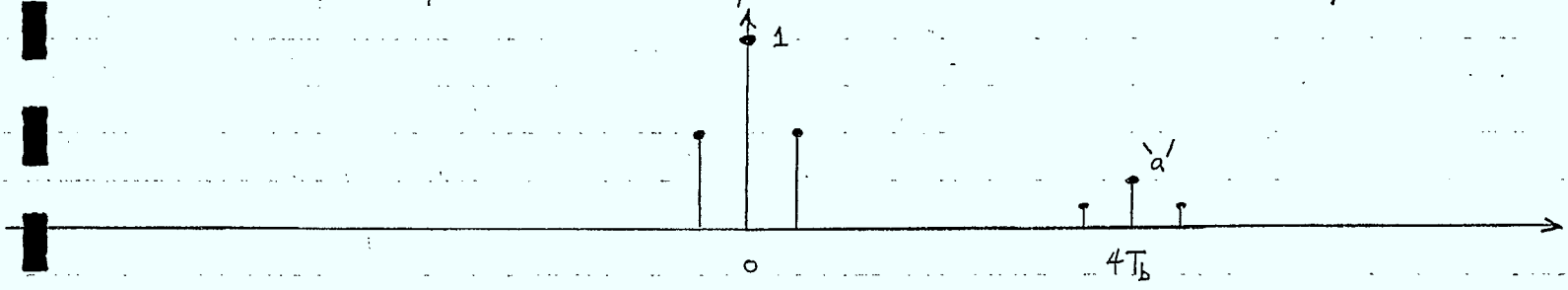

b) Overall channel response when echo delay is a multiple of the bit period

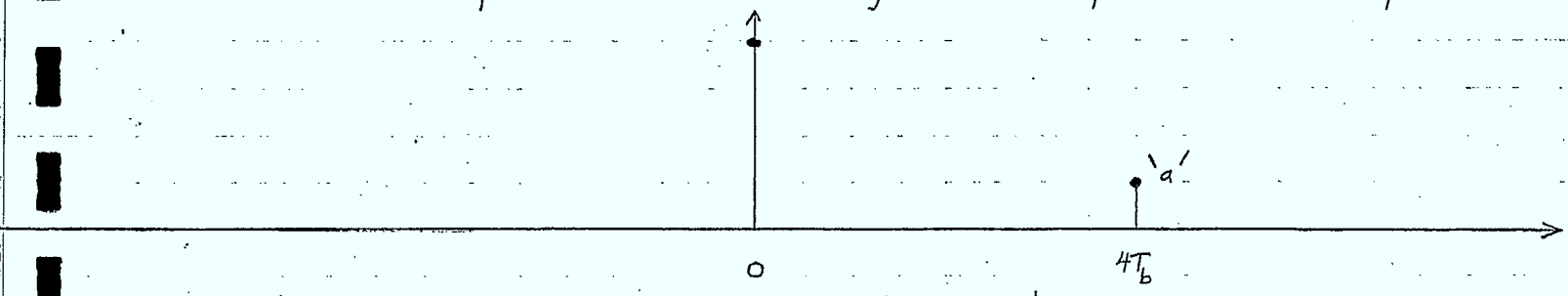

c) Bit rate sampled version of overall channel

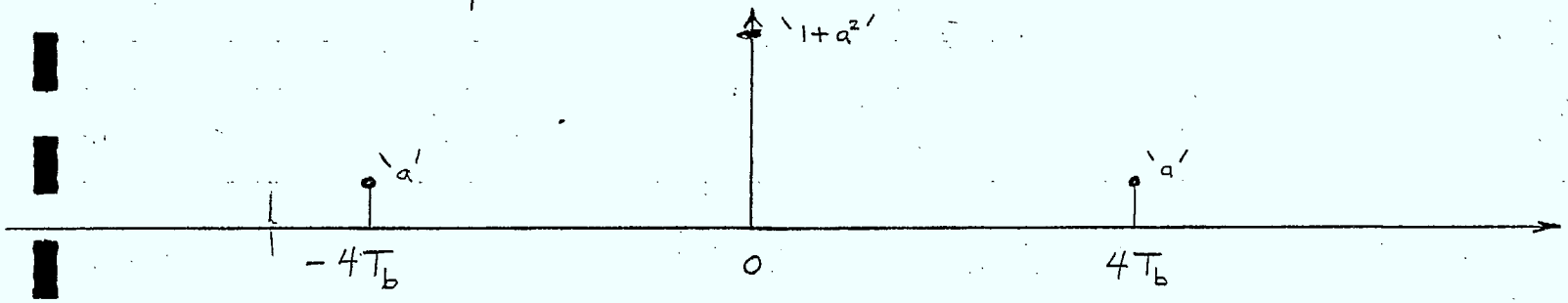

d) Channel autocorrelation function (sampled at bit rate)

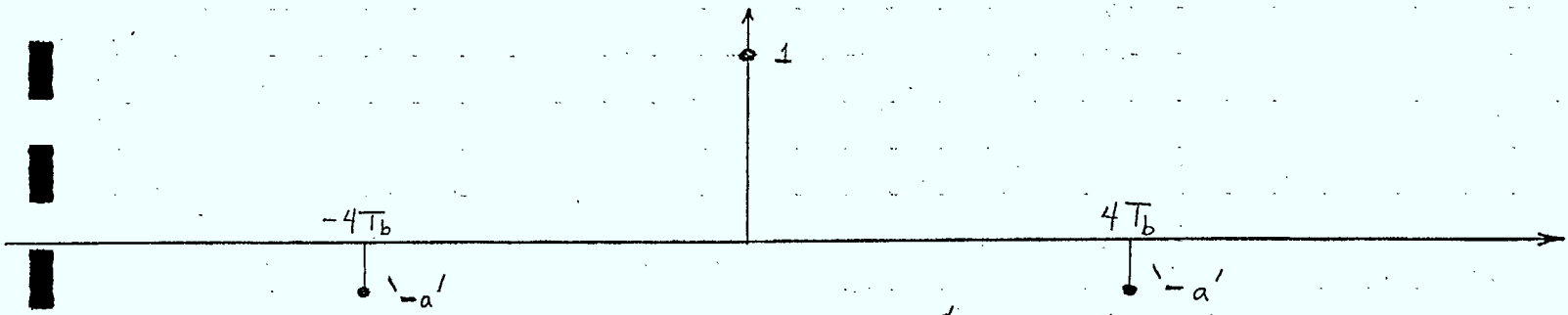

e) approximate transversal filter for weak echoes

Figure E.2

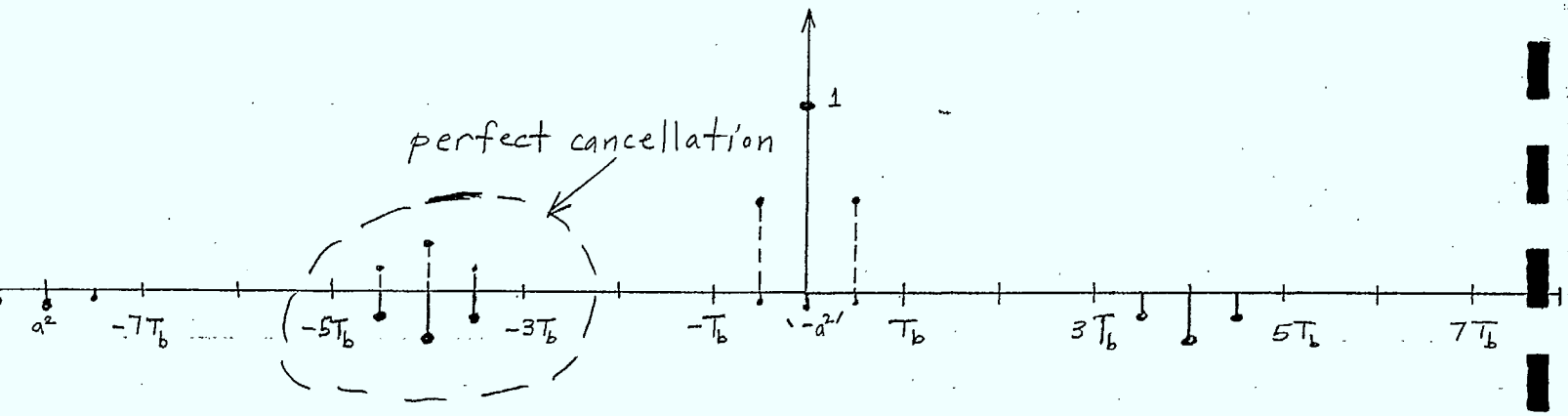

a) Performing the convolution of a time reversed version of Figure 2(b) with the impulse response in Figure 2(e).

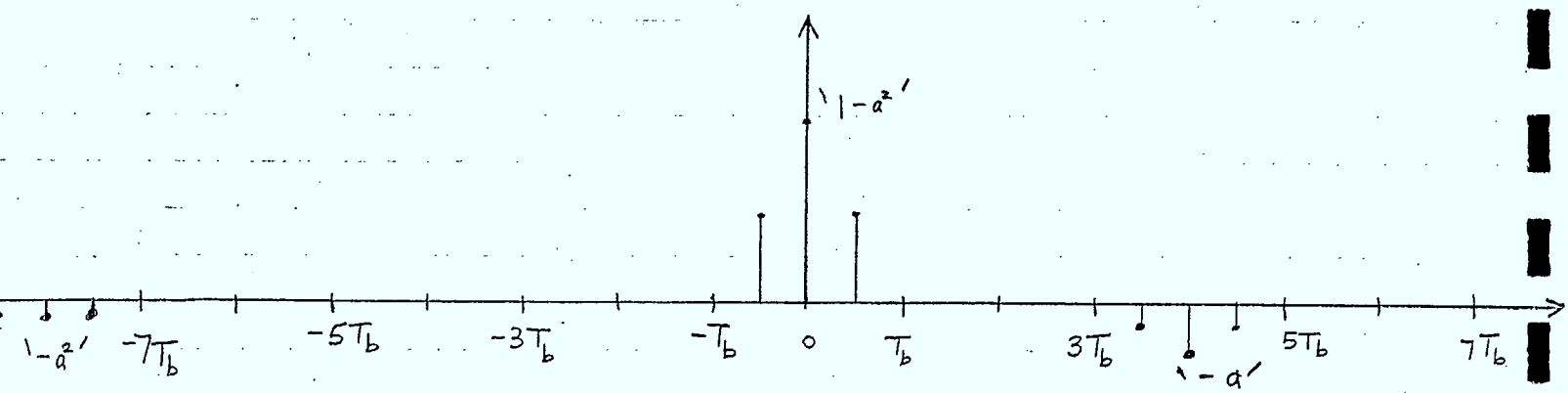

b) Linear equalizer response

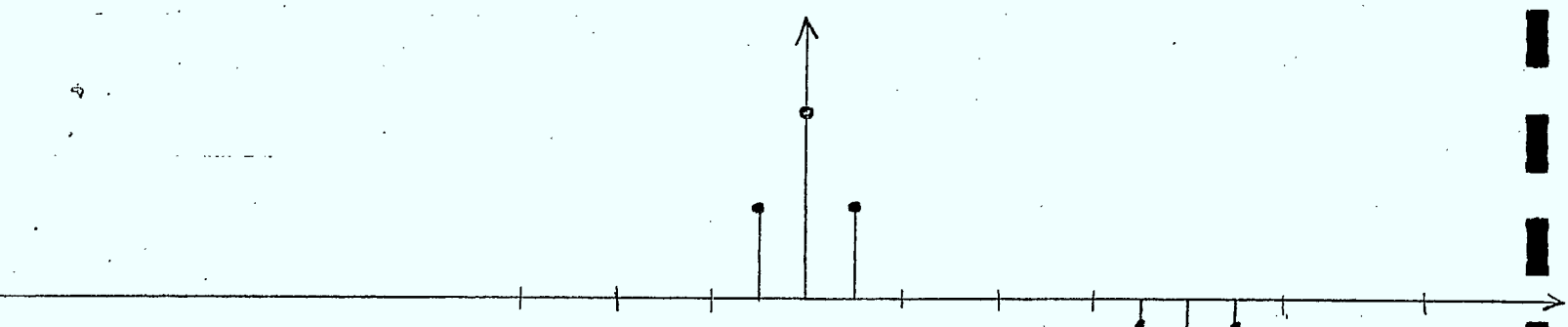

c) Linear equalizer response ignoring second order effects.

Figure E.3: Establishing the linear equalizer impulse response

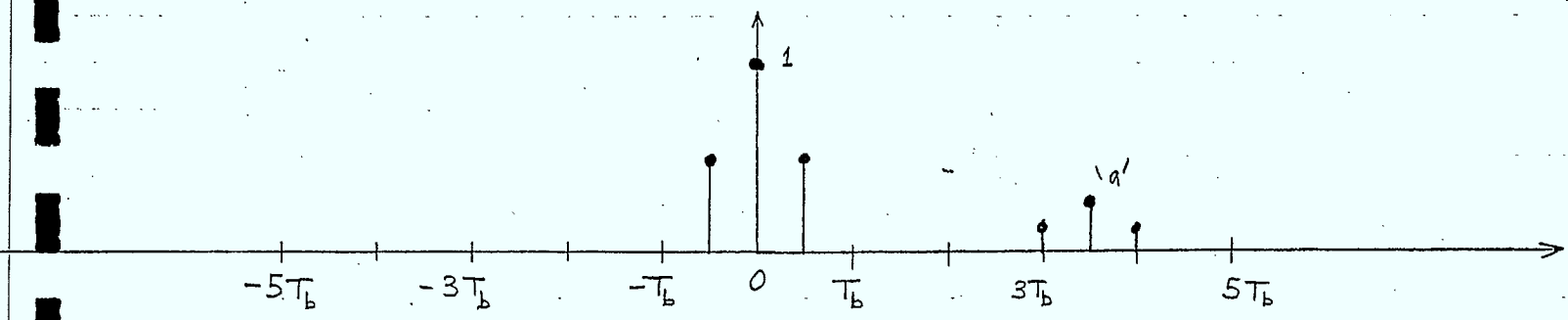

a) Overall sampled channel response

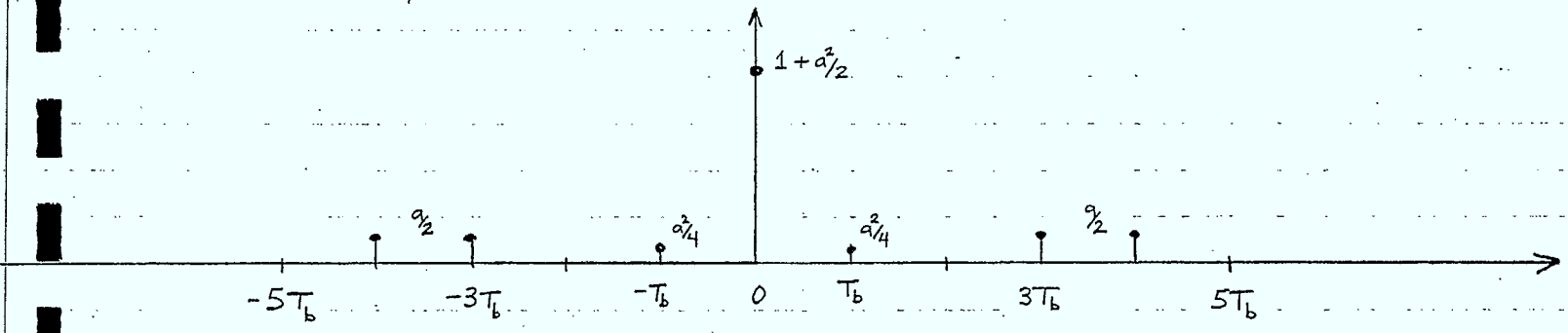

b) Channel autocorrelation function (sampled at bit rate)

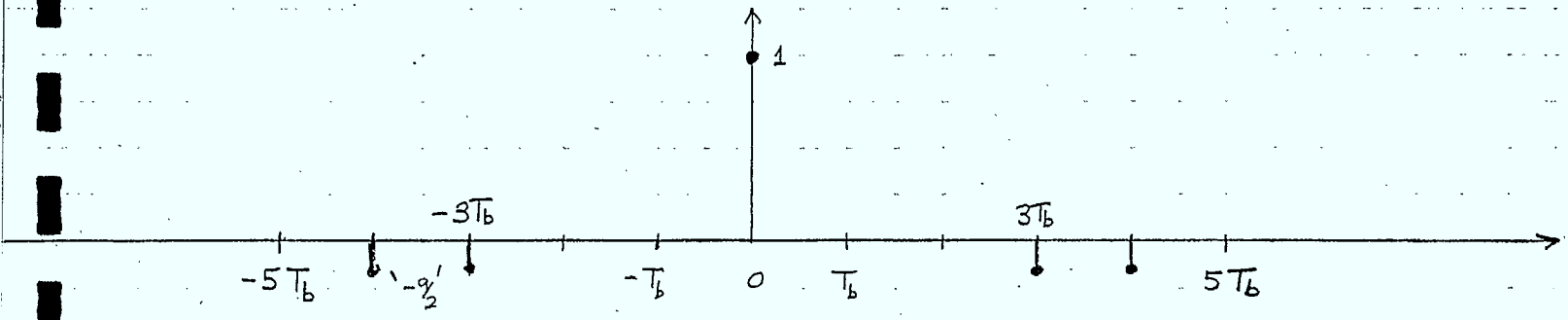

c) Approximate transversal filter response (for small echoes)

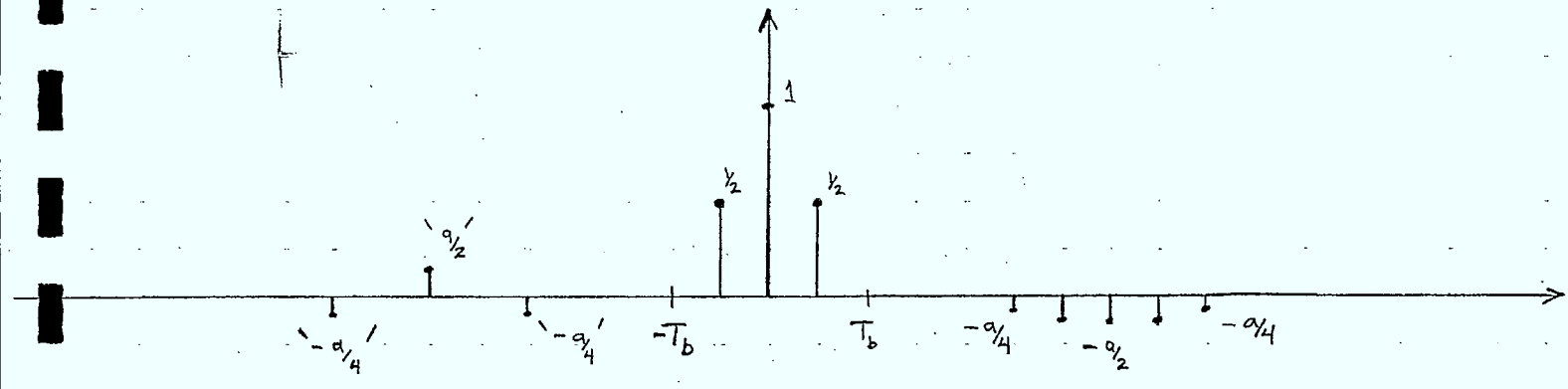

d) Approximate linear equalizer impulse response (ignoring second order effects)

Figure E.4

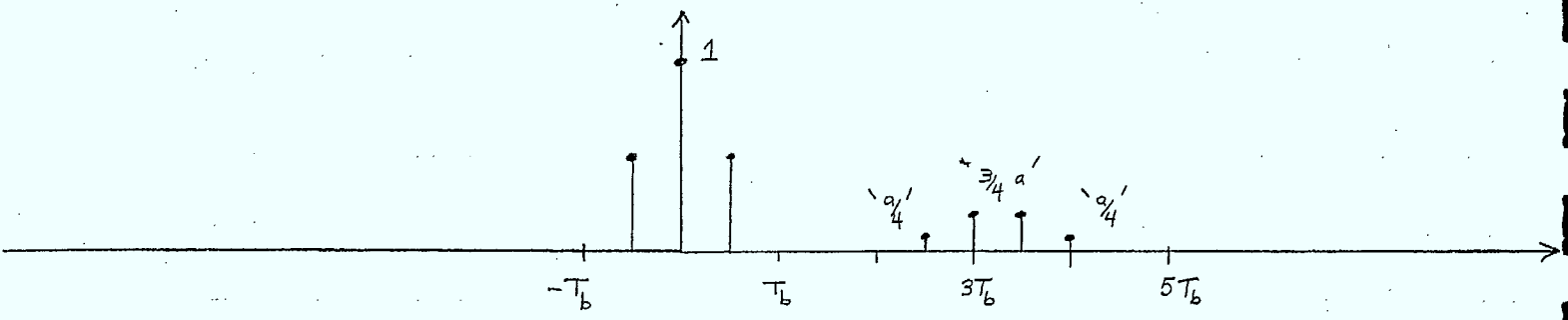

a) Sampled channel response

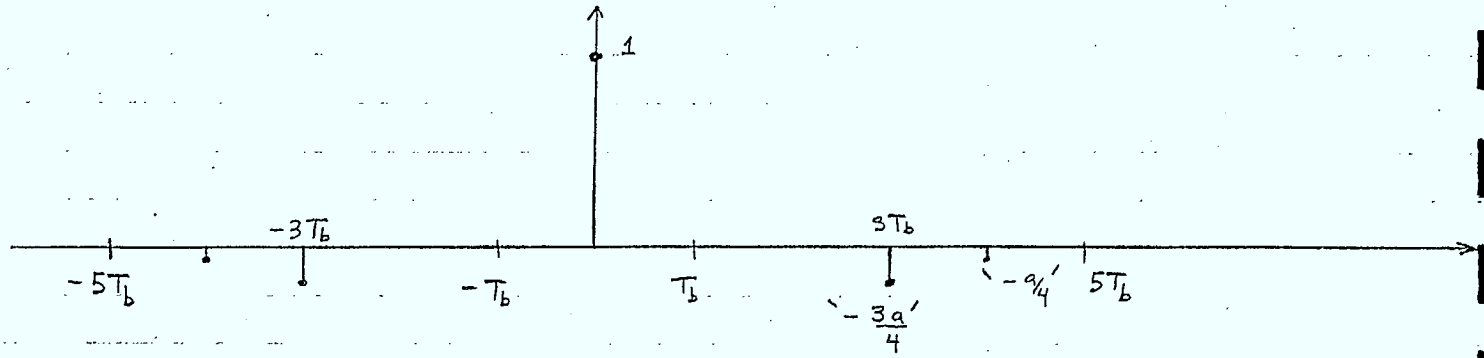

b) Approximate transversal filter response (for small echoes)

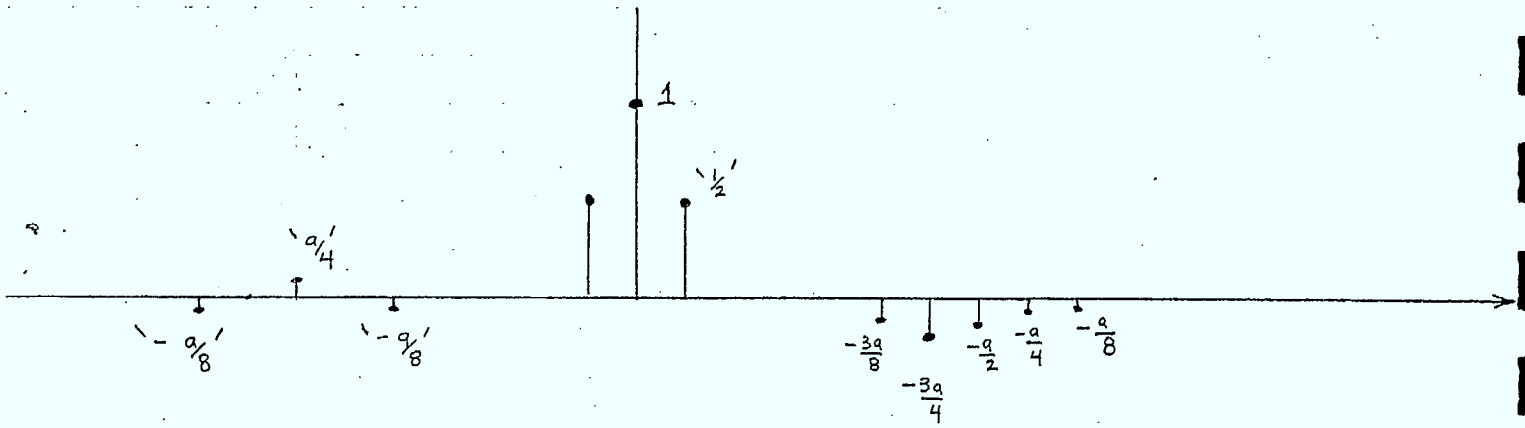

c) Approximate linear equalizer impulse response (ignoring second order effects)

Figure E.5

approximation for the transversal filter impulse response is given in Figure E.4(c). The resulting equalizer impulse response formed by convolving the time reversed channel impulse response and the transversal filter response (ignoring second order effects) is provided in Figure E.4(d). The resulting equalizer impulse response is non-causal. An example when the delay is $\frac{1}{4}$ of a bit period away from being an integer multiple of the bit period is illustrated in Figure E.5. The resulting equalizer impulse response is once again non-causal. There is evidence of the predominence of the causal region in this example, however.

The transfer function that is being implemented in the simulation program is

$$E_{opt}(f) = \frac{0.5\, H_I^*(f)/\, W(f)}{\frac{|H_I(f)|^2}{W(f)} + \frac{|H_I(f - \frac{1}{T_b})|^2}{W(f - \frac{1}{T_b})}} \quad 0 \leq f \leq \frac{1}{T_b} \tag{E.4}$$

The values of $E_{opt}(f)$ for $(\frac{-1}{T_b} \leq f \leq 0)$ can be easily determined from conjugate symmetry. The equalizer impulse responses shown in Figures E.6 and E.7 were derived by sampling this optimal equalizer frequency response and inverse transforming to the time domain via an FFT. In deriving the impulse response seen in Figure E.6, a multipath channel with a -20 dB echo at 4.76 μsec was used in the simulation program. This equalizer impulse response has a cluster of energy at 4.76 μsec as expected. Small second order distortion is apparent at 9.52 μsec. Some

distortion is present at -4.76 μsec because the echo delay is not an integer multiple of the bit period. In deriving the impulse response of Figure E.7, a multipath channel with a -8 dB echo at 4.76 μsec was used in the simulation program. In this case the importance of extending the equalizer impulse response beyond the spread of the channel response is evident. The non-causality of the impulse response is also evident. Although the response for negative time is less important than the response for positive time, it is not really insignificant. The "harmonic" nature of the equalizer impulse response is clearly evident with this more pronounced echo in the channel response.

In the simulation program, the equalizer impulse response is truncated to more realistically simulate a practical, implementable equalizer. An equalizer with 128 taps at a T/2 - spacing has been simulated. This number was chosen because some of the more promising hardware approaches to realizing a programmable teletext equalizer are capable of realizing 128-tap equalizers.

In the simulation program, this is handled by using a 704 sample window for the equalizer impulse response sampled at the high sampling rate used in the simulation. The only major issue is the placement of the window. One fairly realistic approach is to center it about the origin as illustrated in Figure E.8. However, there is the possibility of improving the multipath channel spread which can be effectively equalized slightly by sliding the window to include more of the positive time axis. However, with the window centred, one should be able to effectively equalize 5.6 μsec echoes. Since the majority of echoes should be below 3.0 μsec for the Ottawa area, the above equalizer should be sufficient for downtown Ottawa. We will not bother delving into the issue of optimizing the window, because it will be of little interest in practice.

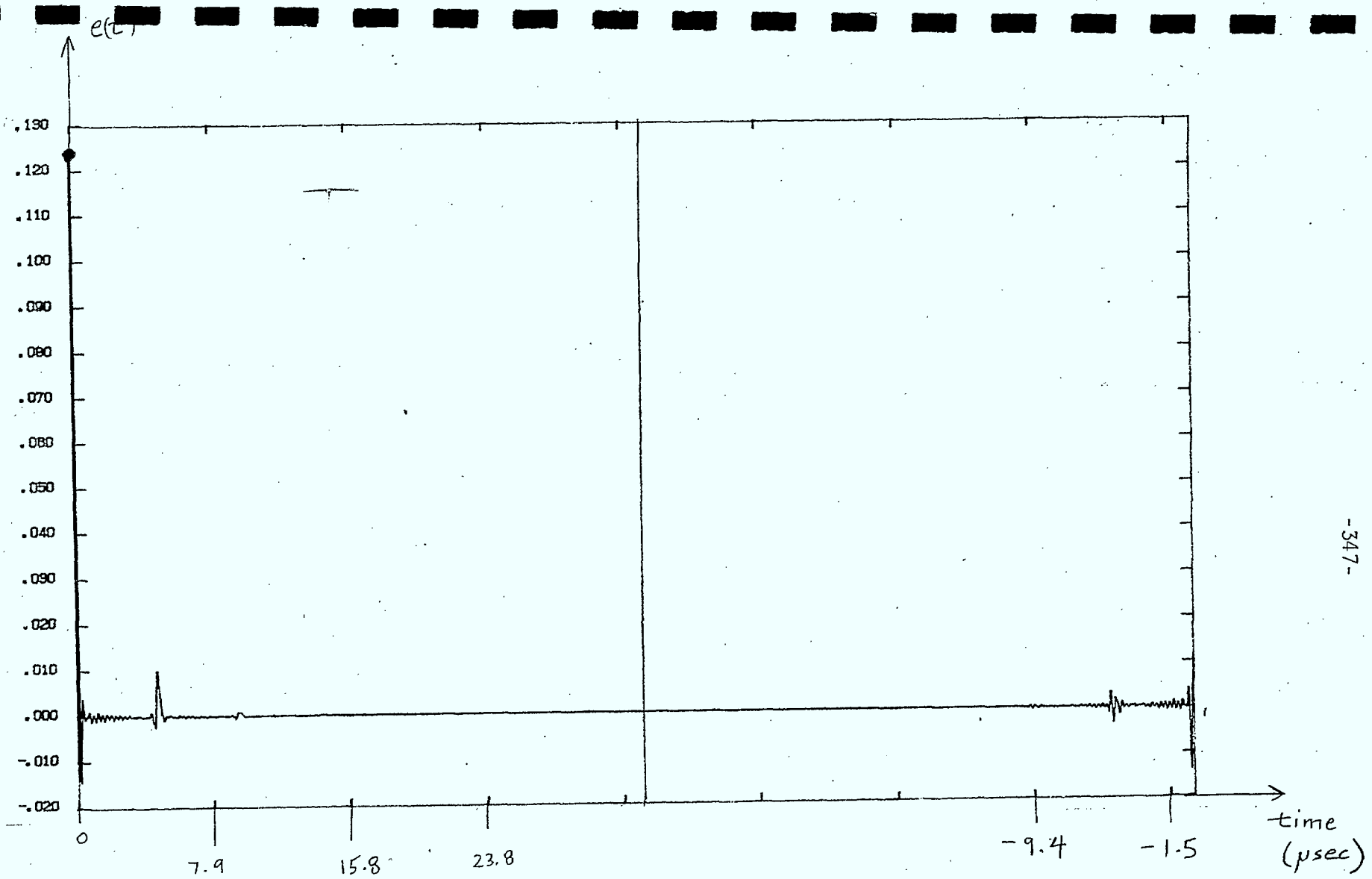

Figure E.6: Equalizer impulse response for a -20dB echo at 4.76 μsec.

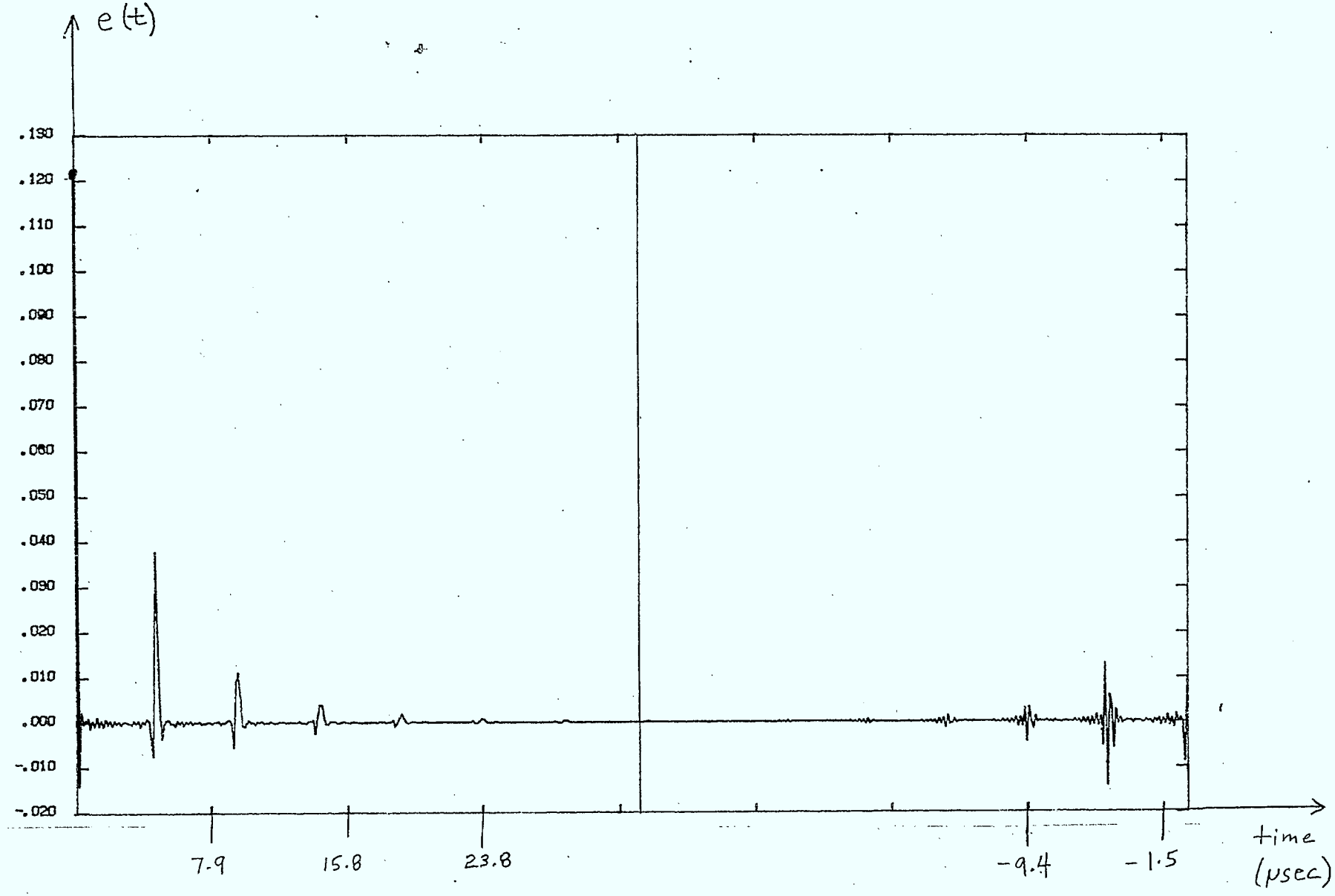

Figure E.7 : Equalizer impulse response for a -8 dB echo at 4.76 μsec.

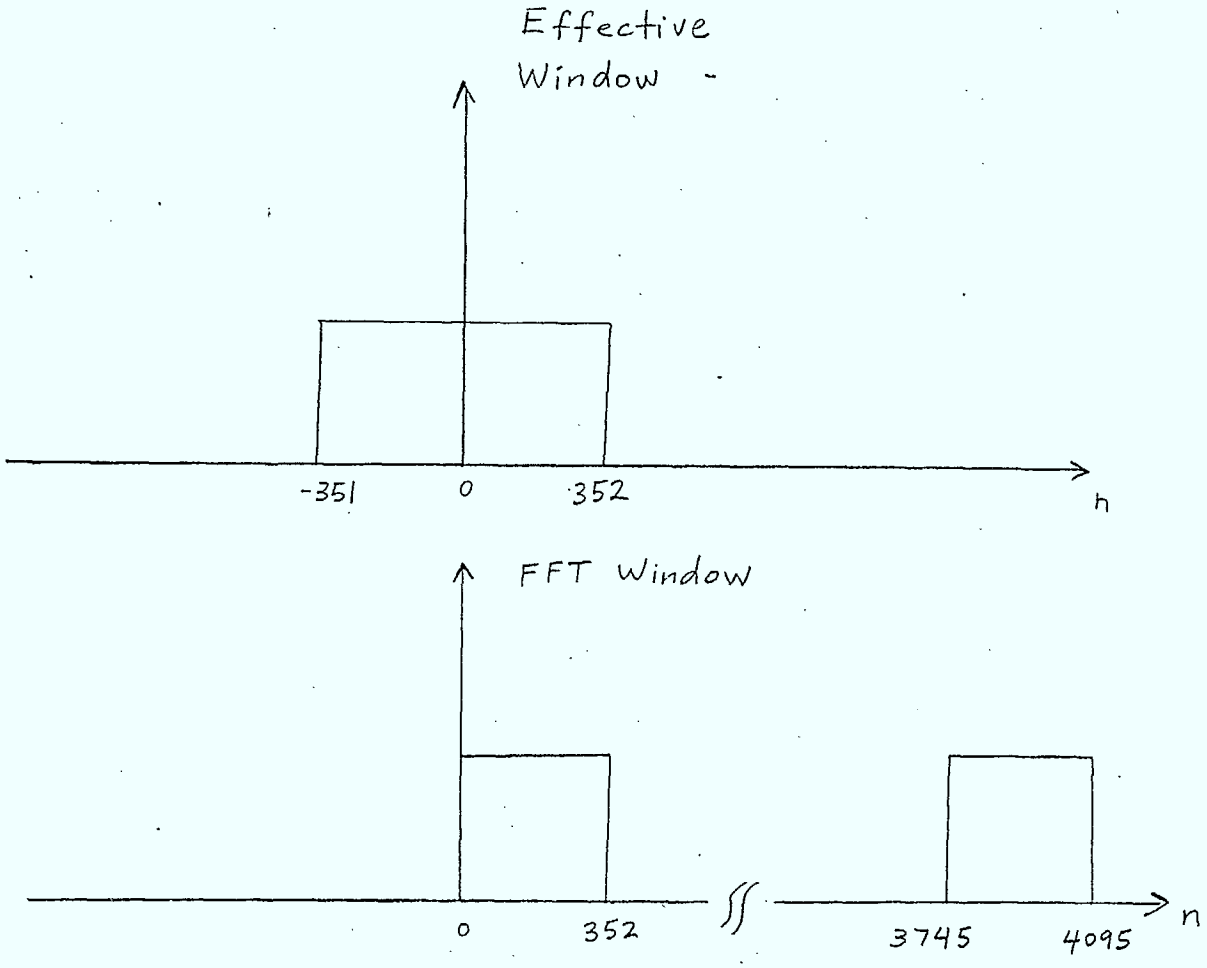

Figure E.8 : Windowing applied for a 128-tap, $T_{b/2}$ equalizer

In practice, the filter impulse responses will all be causal, and the equalizer will have a causal impulse response where the tap coefficients are adjusted adaptively to minimize the mean square error between the equalizer output and desired output.

CACC / CCAC
38684

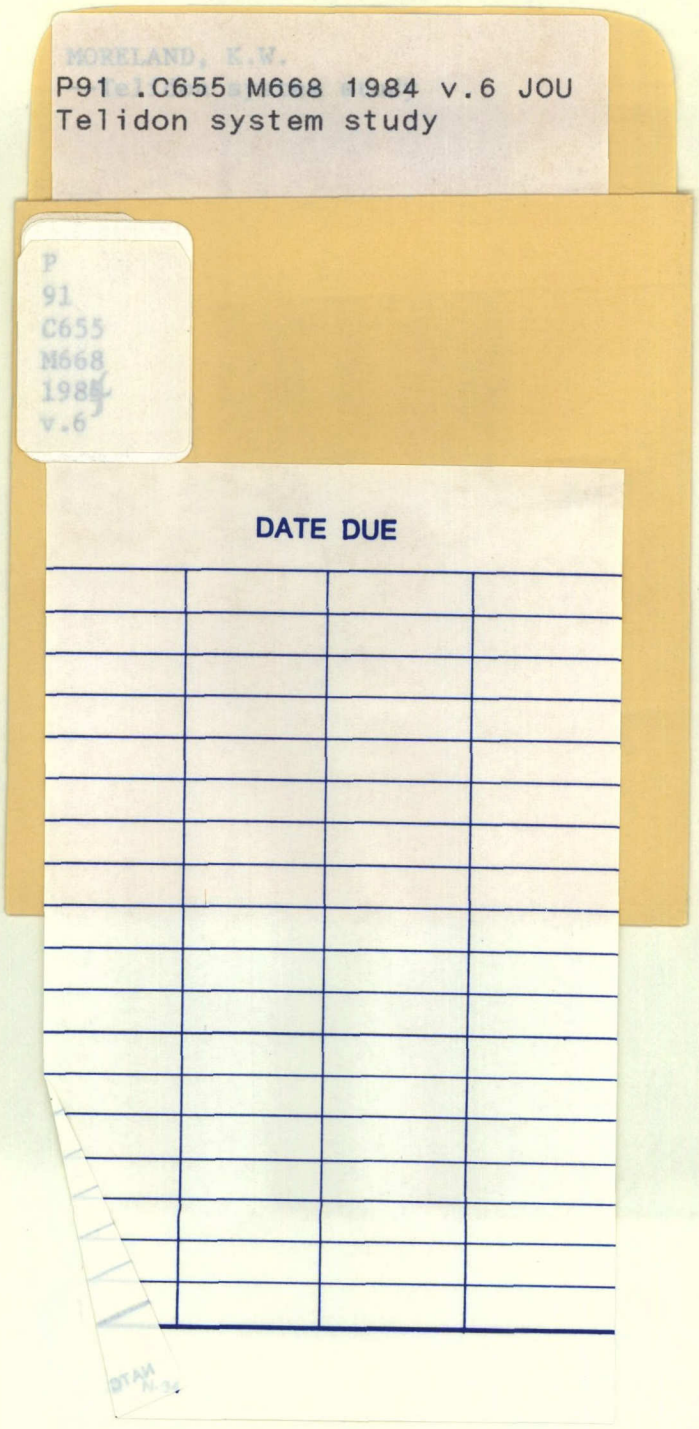
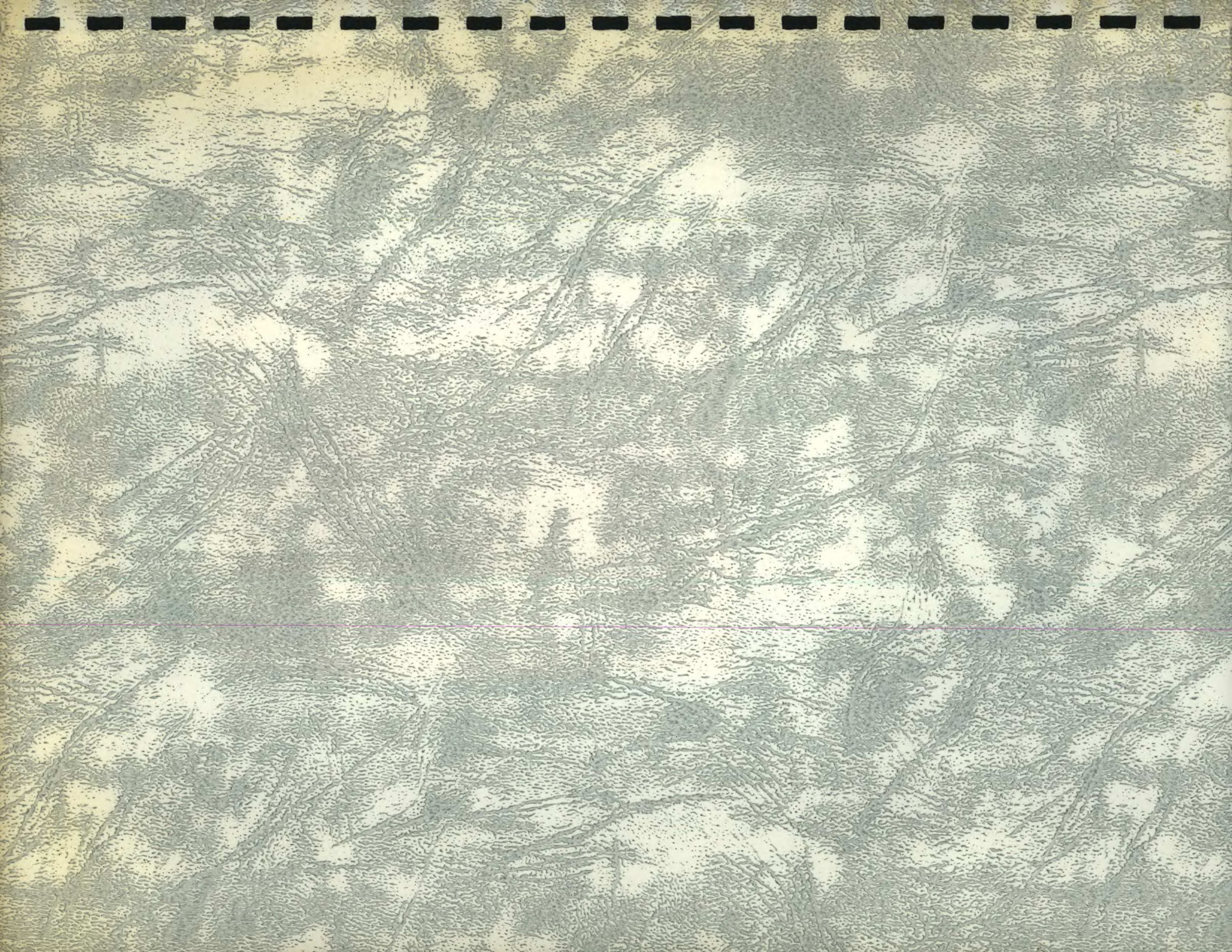
QUEEN P 91 .C655 M668 1984 v
Moreland, K. W. 1956- (Kenne
Telidon system study